

**DENSIFICATION BEHAVIOUR  
OF  
IRON AND IRON BASED ALLOY POWDER  
PREFORMS DURING HOT FORGING**

A THESIS

*submitted in fulfilment of the  
requirement for the award of the degree  
of*

**DOCTOR OF PHILOSOPHY**

University of Roorkee, Roorkee

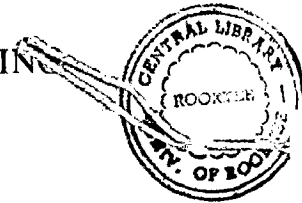
*in*

Certified that the **METALLURGICAL ENGINEERING**

Dissertation has been accepted for the  
award of Degree of Doctor of  
Philosophy / Master of Engineering

*Met. Engrg.* ...  
No. *111/P-65-191*

(Degree) dated *25-11-1983*



By

**KRISHNA SHANKAR PANDEY**

*Signature*

*Asstt. Registrar (Exam)*

*177777*

*19-5-84*

*17-7-84*



**DEPARTMENT OF METALLURGICAL ENGINEERING  
UNIVERSITY OF ROORKEE  
ROORKEE 247 667 (India)**

August, 1982

## CANDIDATE'S DECLARATION

*I hereby certify that the work which is being presented in the thesis entitled "Densification Behaviour of Iron and Iron Based Alloy Powder Preforms During Hot Forging" in fulfilment of the requirement for the award of the degree of DOCTOR OF PHILOSOPHY submitted in the Department of Metallurgical Engineering of the University is an authentic record of my own work carried out during a period from July 30, 1979 to August 16, 1982 under the supervision of Dr. M.L. Mehta and Dr. P.S. Misra.*

*The matter embodied in this thesis has not been submitted by me for the award of any other degree.*

*K.S. Pandey*

(KRISHNA SHANKAR PANDEY)

*This is to certify that the above statement made by the candidate is correct to the best of our knowledge.*

*P. S. Misra*

(P. S. MISRA)

Reader,

Department of Metallurgical Engineering  
University of Roorkee,  
Roorkee, U.P., India

*M. L. Mehta*

(M. L. MEHTA)

Professor

Department of Metallurgical Engineering  
University of Roorkee,  
Roorkee, U.P., India

August 25, 1982

dedicated to  
the everlasting memory  
of my father

## ACKNOWLEDGEMENTS

Author expresses his deep sense of gratitude and indebtedness to Dr. M.L. Mehta, Professor and Dr. P.S. Misra, Reader, both from the Department of Metallurgical Engineering, University of Roorkee, Roorkee, for their excellent piece of guidance, lasting encouragement and wholehearted co-operation throughout the course of this work. Their efforts in going through the manuscript and suggestions for its improvement are gratefully acknowledged.

The author deeply appreciates the constant encouragement, help and technical discussions at various stages of the work with his wife, Mrs. Shashi Krishna Pandey, Research Scholar under Quality Improvement Programme in Department of Chemical Engineering, University of Roorkee, Roorkee.

The author acknowledges with special thanks to Dr. M.L. Kapoor, Professor and Head, Department of Metallurgical Engineering, University of Roorkee, Roorkee for his help in providing facilities for conducting the present work successfully.

The author expresses his deep sense of appreciation and thankfulness to his colleagues Shri K.C. Sharma and Shri Shahab Prasad for their help and co-operation in bringing down this thesis to ultimate reality.

Author is also thankful to Dr. A.K. Patwardhan, Dr. Satya Prakash, Dr. V.K. Tewari, Readers, Metallurgical Engineering Department for their keen interest in the work which encouraged the author from time to time. Their constructive criticism and valuable suggestions for the improvement of the various aspects of the present work is highly appreciated.



The author is extremely grateful, to Professor F. Fischmister, Hognaes Corporation, Sweden; Professor H.A. Kuhn, Department of Metallurgical and Materials Engineering, University of Pittsburgh, Pittsburgh, Pennsylvania, U.S.A.; Professor W.J. Huppmann, Max-Planck-Institut, West Germany; Dr. G.T. Brown, GKN Group, U.K. ; Dr. S. Mocarski, Mech. Engg. Department, Office Ford Motor Co., Dearbon Mich. and Dr. H.M. Skelly, Metal Forming Section, Physical Metallurgy Research Laboratories for their generosity and timely response in sending their valuable research reprints.

Special thanks are due to :

- Quality Improvement Programme, a scheme run by Government of India to provide facilities for higher studies to Engineering Faculty.
- Department of Atomic Energy, Trombay, Bombay, India for financing this project.
- Thiru C. Arangnayagam, Education Minister, Tamil-Nadu and Chairman, Regional Engineering College, Tiruchirapalli - 620015, for sponsorship under Quality Improvement Programme.
- Prof. P.S. Manisundaram, Formerly Principal, Regional Engineering College, Tiruchirapalli, presently Vice-Chancellor, University of Tiruchirapalli, Tamil-Nadu for sponsorship and help.
- Miss Jyoti Lata Pandey, Research Scholar, Department of Metallurgy, University of Roorkee, Roorkee, for her help and co-operation rendered during experimentation.
- Shri N.C. Jain and Shri S.S. Singh, for their useful discussions.

- S/Sri J.P. Sharma, S.N. Kaushik, Hari Chand, Ajmer Singh, Shamsheer Singh, Karan Singh, T.K. Sharma and Inder Lal, for their assistance during experimental work.
- S/Shri S.P. Kush, S.K. Seth, R.M. Mangal, S.C. Kaushik, S.S. Gupta, B.D. Sharma, S.P. Anand, M. Pandey, Vidya Prakash, Madhu, Mohd. Youinish and Abdul Ghaphoor, M.M. Singhal, S.B. Sharma, A.P. Nautiyal, Rajender Pal, RamGopal, Rakesh Mishra for their unconditional help and co-operation during the entire course of this work.
- Shri Atam Prakash for his neat draftsmanship and Sri V.P. Kaushish, for typing the manuscript excellently.
- Shri M.C. Vaish for taking out Ammonia prints.
- To my mother Shrimati Rajmati Devi and youngest brother Shri V.S. Pandey for their help and encouragement

Lastly to my sons 'SUNIL' and 'SIDDHARTHA' for having co-operated extremely well during the course of the present investigation.

KRISHNA SHANKAR PANDEY

## CONTENTS

	<u>Page</u>
CERTIFICATE	
ACKNOWLEDGEMENT	
ABSTRACT	i
NOTATIONS	v
LIST OF TABLES	vii
LIST OF FIGURES	ix-xxiii
CHAPTER - 1 INTRODUCTION	1- 6
CHAPTER - 2 LITERATURE REVIEW	7-53
2.1 Definition of Powder Forging	9
2.2 Necessity of Powder Forging	10
2.3 Materials Forged	12
2.4 Process Variables	14
2.5 Forging Parameters	16
2.6 Material Variables	17
2.7 Deformation of Porous Materials	18
2.8 Products Produced Through Powder Metallurgy Route	48
CHAPTER - 3 FORMULATION OF THE PROBLEM	54-67
3.1 Statement of the Problem	55
3.2 Selection and Alloy Compositions	56
3.3 Applications of Carbon and Phosphorous Steels	57
3.4 Poisson Ratio	59
3.5 Pore Structure	60
3.6 Extrusion Forging	61
3.7 Closed Dies	62
3.8 Experimental Approach	62

	Page
CHAPTER - 4      DESIGN CONSIDERATION IN POWDER PREFORM FORGING	68-79
4.1      Press Consideration	68
4.2      Upsetting Dies	70
4.3      Partially Open Dies	70
4.4      Closed Dies	73
 CHAPTER - 5      EXPERIMENTAL PROCEDURE	 80-98
5.1      Materials and Their Characterisation	80
5.2      Structure of Iron and Iron- Phosphorous Alloy Powder	83
5.3      Cold Compaction	85
5.4      Ceramic Coating	85
5.5      Sintering	86
5.6      Soaking Treatment	86
5.7      Forging	87
5.8      Removal of Ceramic Coating	89
5.9      Dimensional Measurements	89
5.10     Density Measurements	90
5.11     Hardness Measurements	91
5.12     Tensile Test	91
5.13     Impact Tests	91
5.14     Chemical Analysis	92
5.15     Metallographic Studies	92
 CHAPTER - 6      RESULTS AND DISCUSSION	 99-284
6.1      Upsetting of Iron, Iron-Carbon and Iron-Phosphorous Powder Preforms	100
6.2      Partially Open Dies	133
6.3      Metallographic Studies on Forged Products Obtained Through the Partially Open Dies	153

	Page	
6.4	Closed Die Forgings	171
6.5	Mechanical Properties of Upset Forged Samples (Square Section Bars)	176
6.6	Kinetics of Pore Closure	180
CHAPTER - 7	CONCLUSIONS	285-289
APPENDICES		
Appendix A	Compressibility and Mixing Data for Iron, and Iron Based Alloy Powders	290-295
Appendix B	Data of Upset Forging of Iron and Iron Based Alloy Powder Preforms at Different Tempera- tures and H/D Ratios	296-350
Appendix C	Data on Forgings of Iron and Iron Based Alloy Powder Preforms Through Partially Open Dies at H/D = 1.18	351-360
Appendix D	Ceramic Coating	361
Appendix E	Model Calculation for Deformation and Densification	362-369
REFERENCES		370-390

## A B S T R A C T

The present investigation deals with hot upsetting, partially open die forgings and closed die forgings of sintered iron, iron-carbon alloys (carbon varying from 0.35 to 1.36 %) and 0.45 % phosphorus steel powder preforms which were sintered at 1120°C for a period of one hour. Forging temperature was varied in the range of 800-1120°C for hot upsetting of iron and iron-carbon preforms with varying initial aspect ratio (0.57 to 1.17) whereas, iron-phosphorus alloy powder preforms were upset forged at 960°C at the initial aspect ratio of 0.59. Height strains at which fine to heavy cracking at the circumference of the forged component occurred were employed in the design of partially open and closed dies.

Partially open (step down cylindrical and hemispherical) dies were designed with an aim to study the characteristics of pore flow. This study has helped to understand metal flow, existence of dead metal zone (hydrostatic zone) and mechanism by which pore closure takes place. Design of closed dies was based on introduction of circumferential constraints such that the preform experiences these constraints after varying degree of deformation under upset forged condition. Different height strain values were set such that a preform experiences limited degree of upset

(ii)

forging condition before being subjected to circumferential die constraints. One of the height strain was corresponding to a limit of cracking.

Partially open and closed die forgings were performed on sintered preforms ( $H/D = 1.18$ ) of iron and iron-carbon alloys at  $1120^{\circ}\text{C}$  while 0.45 % phosphorus steel preforms ( $H/D = 1.18$ ) were forged at  $960^{\circ}\text{C}$  at various density levels.

Major findings of the present investigation are as follows :

- (i) Per cent theoretical density with respect to height strain expressed in ' $\lambda_n$ ' terms for iron and all other alloys studied during hot upsetting at different temperatures of forgings and at different initial aspect ratio can be expressed by a second order polynomial of the form :

$$\left(\frac{\rho_f}{\rho_{Th}}\right) = a_0 + a_1 \lambda_n \left(\frac{H_0}{H_t}\right) + a_2 \left[\lambda_n \left(\frac{H_0}{H_t}\right)\right]^2$$

where,  $a_0$ ,  $a_1$  and  $a_2$  are temperature and material composition dependent constants.

- (ii) Lower initial aspect ratio at all forging temperatures studied showed better densification as compared to higher initial aspect ratio at the same temperature for all compositions.

(iii)

- (iii) Carbon as an alloying additive improves densification upto 0.83 % while beyond this limit densification drops.
- (iv) Theoretical density could not be achieved in hot upsetting.
- (v)  $\nu$  versus per cent theoretical density plots for all pure iron and alloy compositions exhibit three distinct stages : - a sharp rise in  $\nu$  with little change in per cent theoretical density (87-90 %), a steady state region in which an extremely gradual rise in  $\nu$  in the density range of 90 to 96 %, whereas, beyond 96 % to as close as 100 % density,  $\nu$  fast approaches to 0.5.
- (vi) Linear variation of hardness of forgings is observed with density. Carbon addition improves the hardness.
- (vii) Circumferential cracks are delayed as carbon content is increased upto 0.83 % whereas further increase in carbon content, 1.36 % circumferential cracks occur quickly.
- (viii) Densification behaviour of iron, iron carbon alloys at 1120°C and iron - 0.45 % phosphorus at 960°C can be expressed with a dimensionless parameter '  $\Phi$  ' by the following general expression :



(iv)

$$\left( \frac{\rho_f}{\rho_{Th}} \right) = c \phi^n$$

where 'C' and 'n' are constants. The die used was partially open type (step down cylindrical and hemi-spherical cavities).

- (ix) In partially open die forgings, pore shape, size and its orientation indicates the mode of metal flow at various regions of the powder preform.
- (x) Flow of grains, recrystallization and shearing of pores exhibit combined beneficial effect on densification.
- (xi) In partially open die forgings lower order of fractional horizontal constraints are required compared to vertical fractional constraints in order to obtain same level of densification.

NOTATIONS

$L$	=	length, mm
$e$	=	engineering strain
$e_t$	=	true strain
$\gamma$	=	shear strain
$E'$	=	Deviator component of the strain
$E''$	=	Hydrostatic component of the strain
$e_{t,m}$	=	true mean strain
$\sigma$	=	average stress
$A$	=	area of the cross section
$\tau_{xy}, \tau_{yx}, \tau_{xz}, \tau_{zx}, \tau_{yz}$ and $\tau_{zy}$	=	shear stress
$\sigma_1, \sigma_2$ and $\sigma_3$	=	Principal stresses
$S$	=	Principal stress tensor
$S'$	=	deviator part of the stress tensor
$S''$	=	spherical part of the stress tensor
$I_1, I_2$ and $I_3$	=	invariants
$G$	=	shear modulus
$K$	=	bulk modulus
$\nu$	=	Poisson's Ratio
$\nu_p$	=	Poisson's Ratio for porous body
$H_o$	=	initial height of the preform (mm)
$D_o$	=	initial diameter of the preform (mm)
$H_t$	=	forged height of the component (mm)
$D_t$	=	forged diameter of the component (mm)
$\nu$	=	Poisson's Ratio
$\rho_f$	=	forged density gm/cm <sup>3</sup>
$\rho_{fc}$	=	corrected density gm/cm <sup>3</sup>
$\rho_{Th}$	=	Theoretical density gm/cm <sup>3</sup>
VPN	=	Vicker's Pyramid Number
$h$	=	height unconfined (mm)

- $D_t$  = forged diameter (mm)
- $h_c$  = horizontal surface area of the deformed compact which was in contact with the die cavity
- $v_c$  = vertical surface area of the deformed compact which was in contact with the die cavity
- $f_{hc}$  = fractional horizontal constraint
- $f_{vc}$  = fractional vertical constraint
- $\phi$  = ratio of the horizontal fractional constraint with that of vertical constraint
- $\rho_{fc}$  = corrected density of the deformed component
- $C_{1,n}$  are constants.

LIST OF TABLES

	Page
2.1 Values of n and K for Metals at Room Temperature	35
2.2 Work Hardening Exponents ( $n_p$ ) and $K_p$ Values From Log-Log Plots of $\sigma$ vs $\epsilon$ For Iron-Carbon Alloys	37
2.3 Work Hardening Exponents ( $n_p$ ) and ' $K_p$ ' Values For Low Alloy Steels	38
5.1 Characterization of Iron Powder	81
5.2 Characterization of Iron - 0.45 % P Alloy Powder	83
5.3 Chemical Analysis For Carbon	92
6.1 Coefficients of Parabolic Curves of the Form : $y = a_0 + a_1x + a_2x^2$	109
6.2 Coefficients of Parabolic Curves of the Form : $y = a_0 + a_1x + a_2x^2$ for 0.35 % C-Steel Sintered Preforms During Hot Upsetting	110
6.3 Coefficients of Parabolic Curves of the Form : $y = a_0 + a_1x + a_2x^2$ for 0.83 % C-Steel Sintered Preforms During Hot Upsetting	111
6.4 Coefficients of Parabolic Curves of the Form : $y = a_0 + a_1x + a_2x^2$ for 1.36 % C-Steel Sintered Preforms During Hot Upsetting	112
6.5 Coefficients of Parabolic Curve of the Form : $y = a_0 + a_1x + a_2x^2$ for 0.45 % P-Fe Alloy Powder Sintered Preform (H/D=0.59) During Hot Upsetting	113
6.6 Variation of $a_1/a_2$ with Composition, Forging Temperature and H/D Ratio	114

6.7	Per cent Deformation with respect to the Relative Position of the Coarse Pores	129
6.8	Values of $f_{hc}$ , $f_{vc}$ at Different Density Levels for Iron, Iron-Carbon Steels and a Phosphorous Steel for Partially Open Step-down Cylindrical Die Cavity Forgings	139
6.9	Values of $f_{hc}$ , $f_{vc}$ at Different Density Levels for Iron, Iron-Carbon Steels and a Phosphorous Steel for Partially Open Hemi-Spherical Die Cavity Forgings	145
6.10	Coefficients and Exponents of $\Phi$	148
6.11	Empirical Relations for Different Geometries of the Partially Open Dies	150
6.12	Data on Closed Die Forgings	173
6.13	Mechanical Properties of Iron and Iron-Based Powder Forged Products	177
6.14	Relative Pore Diameter with respect to Per Cent Deformation	181

LIST OF FIGURES

FIG.		<u>Page</u>
1.1	Influence of porosity on mechanical properties of hot repressed pure iron	6
2.1	Total stress $S$ , its normal component $\sigma$ and its shear component $\tau$	51
2.2	Components of total stress of a point relative to an $x, y, z$ orthogonal system	51
2.3	Effect of hydrostatic pressure (mean stress, $\sigma_m$ ) on tensile ductility	52
2.4	Comparison between maximum-shear-stress theory and vonMises Distortion Energy theory	52
2.5	Deformation of Pores	53
2.6	Deformation of Inclusions	53
3.1	Phase diagram of iron-phosphorous	66
3.2	Relationship between Poisson ratio and density of forging of 601 AB preforms (preform density 83 %)	67
4.1	Friction screw press	74
4.2	Upsetting Die	75
4.3	Partially open step-down cylindrical die cavity	76
4.4	Partially open hemi-spherical die cavity	77
4.5	(a) Closed die	78
4.5	(b) Die rings	79
5.1	Compressibility plots of iron and graphite Admixed iron powder	94
5.2	Apparent density vs time of mixing of graphite powder in iron powder	95
5.3	Plot of flow rate vs. mixing time of graphite powder in iron powder	96
5.4	Compressibility plot of iron and iron phosphorous alloy powder	97

FIG.		<u>Page</u>
5.5	Particle/s structure/s of iron powder	98
5.6	Particle/s structure/s of 0.45 % phosphorous steel powder	98
6.1	(a) Effect of height strain on per cent theoretical density for sintered iron powder preform (H/D=0.57 and 0.99)	182
6.1	(b) Effect of height strain on per cent theoretical density for sintered iron powder preforms (H/D=1.17)	183
6.2	Effect of H/D ratio on per cent theoretical density for sintered iron powder preforms	184
6.3	Effect of height strain on per cent theoretical density for 0.43 % graphite admixed iron powder sintered preform (% C <sub>a</sub> = 0.35), H/D = 0.58	185
6.4	Effect of Height strain on per cent theore- tical density for 0.43 % graphite admixed iron powder sintered preform (%C <sub>a</sub> =0.35), H/D = 0.99	186
6.5	Effect of Height strain on per cent theoretical density for 1.14 % graphite admixed iron powder sintered preform (%C <sub>a</sub> = 0.83), H/D = 0.58	187
6.6	Effect of height strain on percent theore- tical density for 1.14 % Graphite admixed iron powder sintered preform (%C <sub>a</sub> =0.83), H/D = 0.99	188
6.7	Effect of height strain on per cent theoretical density for 1.86 % graphite admixed iron powder sintered preform (%C <sub>a</sub> =1.34), H/D = 0.58 and 0.99	189

FIG.		<u>Page</u>
6.8	Effect of carbon on densification behaviour for $H/D = 0.57 - 0.58$ , and temperature of forging $1120^{\circ}\text{C}$	190
6.9	Plot of per cent theoretical density with respect to % carbon in the alloy at height strain of 0.50 at $1120^{\circ}\text{C}$	191
6.10	Densification behaviour of iron -0.45 % phosphorous alloy powder sintered preform ( $H/D = 0.59$ ) upset forged at $960^{\circ}\text{C}$	192
6.11	Density variation in forged components at $900^{\circ}\text{C}$ for sintered iron powder preforms ( $H/D = 0.57$ and $0.97$ )	193
6.12	Relationship between reduction in height and forging temperature with respect to cracking for pure iron	194
6.13	Relationship between reduction in height and forging temperature with respect to cracking during hot upset forging for different iron-carbon alloys	195
6.14	Effect of forging temperature upon densification for a fixed amount of deformation with different $H/D$ ratios for iron powder sintered preforms	196
6.15	Effect of forging temperature on densification for a fixed amount of height strain for different $H/D$ ratios for 0.35 % carbon steel	197
6.16	Effect of forging temperature on densification for a fixed amount of height strain for different $H/D$ ratio for 0.83 % carbon steel	198
6.17	Effect of forging temperature on densification for a fixed amount of height strain for different $H/D$ ratios for 1.36% carbon steel	199



FIG.		<u>Page</u>
6.18	Relationship between diameter strain and height strain for iron powder sintered preform (H/D=0.57) during hot upsetting	200
6.19	Relationship between diameter strain and height strain for iron powder sintered preform (H/D=0.99) during hot upsetting	201
6.20	Relationship between diameter strain and height strain for iron powder sintered preform (H/D=1.17) during hot upsetting	202
6.21	Relationship between diameter strain and height strain for 0.35 %C-Fe preform (H/D=0.58) during hot upsetting	203
6.22	Relationship between diameter strain and height strain for 0.35 %C-Fe preform (H/D=0.98) during hot upsetting	204
6.23	Relationship between diameter strain and height strain for 0.83 %C-Fe preform (H/D=0.57) during hot upsetting	205
6.24	Relationship between diameter strain and height strain for 0.83%C-Fe preform (H/D=0.98) during hot upsetting	206
6.25	Relationship between diameter strain and height strain for 1.36 %C-Fe preform (H/D=0.58) during hot upsetting	207
6.26	Relationship between diameter strain and height strain for 1.36%C-Fe preform (H/D=0.99) during hot upsetting	208
6.27	Relationship between diameter strain and height strain for 0.45%P-Fe preform (H/D=0.59) during hot upsetting	209
6.28	Plot of diameter strain vs height strain for carbon steels(0.00-1.36 %C) with different H/D ratios	210

FIG.		<u>Page</u>
6.29	Plot of diameter strain vs height strain for iron and 0.45 %P-steel sintered preforms during hot upsetting	211
6.30	Variation of Poisson ratio with increasing density in hot upsetting of sintered iron powder preforms (H/D=0.57)	212
6.31	Variation of Poisson ratio with increasing density in hot upsetting of sintered iron powder preforms (H/D=0.97)	213
6.32	Variation of Poisson ratio with increasing density in hot upsetting of sintered iron powder preforms (H/D=1.17)	214
6.33	Variation of Poisson ratio with increasing density in hot upsetting of 0.35%C-steel sintered preform (H/D=0.57)	215
6.34	Variation of Poisson ratio with increasing density in hot upsetting of 0.35%C-steel sintered preforms (H/D=0.99)	216
6.35	Variation of Poisson ratio with increasing density in hot upsetting of 0.83 %C-steel sintered preform (H/D=0.57)	217
6.36	Variation of Poisson ratio with increasing density in hot upsetting of 0.83 %C steel sintered preforms (H/D=0.99)	218
6.37	(a) Variation of Poisson Ratio with increasing density in hot upsetting of 1.36%C-steel sintered preforms (H/D=0.58)	219
6.37	(b) Variation of Poisson ratio with increasing density in hot upsetting of 1.36 %C steel sintered preforms (H/D=0.99)	220

FIG.		<u>Page</u>
6.38	Variation of Poisson ratio with increasing density in hot upsetting of 0.45%P steel sintered preforms (H/D=0.59) at 960°C	221
6.39	Effect of H/D on Poisson ratio for hot upset forging of iron powder preforms, (sintered)	222
6.40	Effect of H/D on Poisson ratio for hot upsetting of 0.35 %C steel preforms (sintered)	223
6.41	Effect of H/D on Poisson ratio for hot upsetting of 0.83 %C steel preforms (sintered)	224
6.42	Effect of H/D on Poisson ratio for hot upsetting of 1.36 %C steel preforms (sintered)	225
6.43	Comparison of Poisson ratio for hot upsetting of iron preforms and 0.45% P-steel preforms (H/D=0.57)(H/D=0.59) sintered	226
6.44	Plot of hardness vs per cent theoretical density for sintered iron powder preforms of H/D = 0.57	227
6.45	Plot of hardness vs per cent theoretical density of preform hot upset forging of H/D = 0.99	228
6.46	Hardness vs per cent theoretical density for sintered iron powder preforms upset forged, H/D = 1.17	229
6.47	Variation of hardness with respect to per cent theoretical density for 0.35 % carbon steel, H/D = 0.58 during hot upset forging	230

FIG.		<u>Page</u>
6.48	Relationship between hardness and percent theoretical density for 0.35 % carbon steel, H/D = 0.99 during hot upset forging	231
6.49	Relationship between hardness and per cent theoretical density for 0.83 % carbon steel, H/D = 0.58 during hot upset forging	232
6.50	Relationship between hardness and per cent theoretical density for 0.83 % carbon steel, H/D = 0.99 during hot upset forging	233
6.51	Relationship between hardness and per cent theoretical density for 1.36 % carbon steel, H/D = 0.58 during hot upset forging	234
6.52	Plot of hardness vs per cent theoretical density of 1.36 % carbon steel, H/D=0.99 during hot upset forging	235
6.53	Variation of hardness with respect to theoretical density for 0.45 % phosphorous steel, H/D = 0.59 during hot upset forging	236
6.54	Pore morphology of iron powder sintered preform (H/D=0.99) upset forged at 900°C	237
6.55	Relationship between per cent deformation with coarse pores relative position	238
6.56	Etched structure of iron powder sintered preform (H/D=0.99) upset forged at 900°C.	239
6.57	Etched structure of 0.35 % C-Iron powder sintered preform (H/D=0.99) upset forged at 900°C	240

FIG.		<u>Page</u>
6.58	Morphology of 0.83 % C-iron powder sintered preform (H/D=0.99) upset forged at 900°C	241
6.59	Etched structure of 1.36 %C-Iron powder sintered preform (H/D=0.99) upset forged at 900°C	241
6.60	Morphology - 0.45 % phosphorous powder sintered preform (H/D=0.59) upset forged at 960°C	242
6.61	Relationship between per cent theoretical density and fractional constraints (horizontal and vertical) in forging sintered iron powder preform (H/D=1.18) through partially open step-down cylindrical die cavity at 1120°C	243
6.62	Relationship between per cent theoretical density and fractional constraints (horizontal and vertical) in forging sintered 0.35% carbon steel preform (H/D=1.18) through partially open step-down cylindrical die cavity at 1120°C	244
6.63	Relationship between per cent theoretical density and fractional constraints (horizontal and vertical) in forging sintered 0.83 % carbon steel preform (H/D=1.18) through partially open step-down cylindrical die cavity at 1120°C	245
6.64	Relationship between per cent theoretical density and fractional constraints (horizontal and vertical) in forging sintered 1.36% carbon steel preform (H/D=1.18) through partially open step-down cylindrical die cavity	246

FIG.	<u>Page</u>
6.65 Relationship between per cent theoretical density and fractional constraints (horizontal and vertical) in forging sintered 0.45 % phosphorous steel through partially open step-down cylindrical die cavity at 960°C	247
6.66 Plot of per cent theoretical density against die constraint ( $\Phi$ ) in forging sintered preforms (H/D=1.18) through partially open step-down cylindrical die cavity	248
6.67 Relationship between per cent theoretical density and $\Phi$	249
6.68 Plot of per cent theoretical density against fractional constraints in forging sintered iron powder preforms (H/D=1.18) through partially open Hemi-spherical die cavity at 1120°C	250
6.69 Plot of per cent theoretical density against fractional constraints ( $f_{hc}$ and $f_{vc}$ ) in forging sintered 0.35 % carbon steel preforms (H/D=1.18) through partially open step-down cylindrical die cavity at 1120°C	251
6.70 Relationship between per cent theoretical density and fractional constraint ( $f_{hc}$ and $f_{vc}$ ) in forging sintered 0.83 % C-steel preforms (H/D=1.18) through partially open Hemi-spherical die cavity at 1120°C	252
6.71 Relationship between per cent theoretical density and fractional constraint ( $f_{hc}$ and $f_{vc}$ ) in forging sintered 1.36 % carbon steel preforms (H/D=1.18) through partially open Hemi-spherical die cavity at 1120°C	253

FIG.		<u>Page</u>
6.72	Relationship between per cent theoretical density and fractional constraint ( $f_{hc}$ and $f_{vc}$ ) in forging sintered 0.45 %P steel through partially open Hemi-spherical die cavity at 960°C	254
6.73	Plot of per cent theoretical density against die constraint ( $\bar{\Phi}$ ) in forging sintered preforms (H/D=1.18) through partially open Hemi-spherical die cavity	255
6.74	Relationship between per cent theoretical density and $\bar{\Phi}$	256
6.75	(a) Relationship between $v_c$ and $h_c$ in partially open step down cylindrical die cavity during forging of iron and iron based alloy powder preforms (H/D=1.18)	257
6.75	(b) Relationship between $v_c$ and $h_c$ for partially open Hemi-spherical die cavity during forging of iron and iron based alloy powder preforms (H/D=1.18)	257
6.76	Log-log plot of vertical constraint vs horizontal constraint during forging of iron and iron based alloy powder preforms (H/D=1.18) through two partially open step-down cylindrical and hemi-spherical dies	258
6.77	Log-log plot between $v_c$ and $h_c$ for partially open step-down cylindrical and hemi-spherical dies	259
6.78	Plot of hardness vs per cent theoretical density of partially open die forgings for all compositions of steel	260

FIG.		<u>Page</u>
6.79	Pore morphology iron powder sintered preform (H/D=1.18) forged through hemi-spherical die cavity at 1120°C	261
6.80	Showing flow of pearlite and ferrite in 0.35 % carbon steel sintered powder preform (H/D=1.18), forged through the hemi-spherical die cavity at 1120°C	263
6.81	Pore morphology - 0.83 % carbon steel sintered powder preform (H/D=1.18), forged through the hemi-spherical die cavity at 1120°C, at the centre of the specimen 100X ; enlarged 6 times	263
6.82	Pore morphology - 1.36 % carbon steel sintered powder preform (H/D=1.18), forged through the hemi-spherical die cavity at 1120°C. At the centre of the specimen 100X ; enlarged 6 times	263
6.83	Micro-structure - 0.45% phosphorous steel sintered powder preform (H/D=1.18) forged through hemi-spherical die cavity at 960°C	264
6.84	Microstructure showing different nature at different location of the forged component of pure iron through partially open step-down cylindrical die cavity at 1120°C	265
6.85	Microstructure revealing different modes of pore flattening and grain deformation at different locations of a component forged through partially open step-down cylindrical die cavity at 1120°C	266



FIG.		<u>Page</u>
6 86	Microstructure of 0.83 % carbon steel sintered preform deformed at 1120°C through partially open step-down cylindrical die cavity.	268
6.87	Microstructures taken on the second stage of confinement in a component (1.36 % carbon steel) forged through the partially open step down cylindrical die at 1120°C	269
6.88	Microstructures showing pore morphology and structure details at different locations of the specimen prepared from the component forged through partially open step down cylindrical die cavity at 1120°C for 0.45 % phosphorous steel,	271
6.89	(a) Pore shape changes schematic representation as obtained from metallographic studies	273
6.89	(b) Qualitative flow of metal derived from mode of shearing pore	273
6.90	(a) Pore shape change schematic representation as obtained from metallographic structure	273
6.90	(b) Qualitative flow of metal derived from mode of shearing force	273

FIG.		<u>Page</u>
6.91	Shows the components produced through partially open step-down cylindrical die cavity at 1120°C of iron and iron carbon alloys	274
6.92	Showing components produced through partially open hemi-spherical die cavity at 1120°C of iron and iron carbon alloys	275
6.93	Forged powder products in various shapes of 0.45 % phosphorous steel at 960°C	276
6.94	Microstructure showing iron grains with the mode of pore deformation through closed die forging at 1120°C	277
6.95	Microstructure showing $\approx$ 50 % coarse Pearlite and $\approx$ 50 % ferrite. Forged component through closed die at 1120°C of 0.35 % carbon steel. 100X ; enlarged 6 times.	277
6.96	Microstructure showing very fine eutectoid structure of 0.83 % carbon steel forged through closed die at 1120°C. 500X ; enlarged 6 times.	277
6.97	Microstructure taken at the centre of the polished and etched specimen of 1.36 % carbon forged through closed die at 1120°C.	277

FIG.		<u>Page</u>
6.98	Microstructural details of closed die forging of 0.45 % phosphorous steel at 960°C.	278
6.99 (a) to (e)	Stress versus per unit elongation for various forged steels	279
6.99(f)	Plot of tensile strength vs hardness for carbon steels	280
6.99(g)	Plot of hardness and tensile strength against composition of 90° turned upset forging	281
6.100	Scanning electron micrograph of tensile fracture surface of forged sintered iron	282
6.101(a)	Scanning electron micrograph of tensile fracture surface of forged sintered 0.35 % carbon steel	282
6.101(b)	Scanning electron micrograph of tensile fracture surface of forged sintered 0.35 % carbon steel	282
6.102	Scanning electron micrograph of tensile fracture surface of forged sintered 0.83 % carbon steel	282
6.103	Scanning electron micrograph of tensile fracture surface of forged sintered 1.36 % carbon steel	
6.104	Scanning electron micrograph of tensile fracture surface of forged sintered 0.45 % phosphorous steel	282
6.105	Macrophotographs of Charpy unnotched Impact Specimens of various steels after fracture	283

FIG.

Page

5.106 Plot of relative pore size with  
respect to per cent deformation  
for iron powder sintered preform  
(H/D=0.99) during hot upsetting  
at 900°C

284

## CHAPTER - 1

### INTRODUCTION

Among the many processes for converting metal powders to useful dense products, the hot forging is relatively a new process. It offers better densification coupled with a large amount of deformation in a single operation. Engineering components can be made as dense as 100 % through sintering followed by hot forging. Parts produced by conventional powder metallurgy technique (cold compacting and subsequent sintering under protective atmosphere) are porous. Inherent porosity is used to advantage in the production of filters and bearings, but it is highly disadvantageous in view of the better mechanical properties of structural components.

Powder forging process although had a wide potential for its adoptability in shaping various products, the successful implementation of this process, however, depends upon many complicated factors. Lack of understanding of these factors has, in the past, given rise to unsuccessful performance of the products produced by this process. This has resulted in early setbacks in adopting this process as an industrial venture.

It is well understood that during forging of powder preforms, three predominant stages of deformation are present, namely, upsetting, plane strain and hydrostatic. In these three stages densification as well as shape change occurs simultaneously. It has been suggested that the mechanical properties of the final product depend very much as to how complete densification has been achieved vis-a-vis shape change. Obviously densification should precede the shape change otherwise the final product could remain porous, but the extent to which it should precede is not well understood. Response of material in the three stages of deformation are also not well understood as far as densification is concerned. Due to lack of detailed information on these parameters, the design of preforms and forging dies are still in rudimentary stage and the only guiding factors for such designs are that the final product should be free from mechanical defects such as cracks. Literature, however, indicates that there still exists immense scope for improvement in the product quality by improving these designs.

The mode of variation of mechanical properties with respect to porosity is shown in Fig. 1.1 [1]. From this figure, it can be deduced that in order to develop high load carrying capacity stressed parts, the porosity must be eliminated. Pore elimination in powder forging can be brought down to almost zero level by means of applying adequate pressure at

elevated temperatures. Thus, a metallurgically sound product can be produced by eliminating pores to minimum possible limit. Present investigation, with the above in mind, was undertaken to study the densification behaviour during hot forging of iron and iron based alloys.

Aim of the present investigation is to study in detail the densification aspect during the different stages of deformation and obtain data which could be effectively utilized for designing closed dies suitable for powder forging. The preform geometry has been kept identical whereas die design has been altered to develop different shapes as well as to change the magnitude of deformation. The preforms of these dies vis-a-vis change in material composition as well as other forging parameters have also been studied.

Subject matter embodied in this thesis has been divided into eight chapters. CHAPTER-1, 'introduction' - the running chapter.

CHAPTER - 2 deals with 'literature review'. Hot forging process has been described with respect to forging parameters, nature of process and densification mechanism. Effect of level of deformation, forging temperature, alloy composition and initial aspect ratio on Poisson ratio and on densification with respect to porous products (in case of hot upsetting) of iron and iron based alloy powder sintered

preform forgings have been detailed. Effect of residual porosity on mechanical properties along with microstructural changes, are high-lighted.

CHPATER - 3 deals in detail with the general formulation of the problem with regard to the experimental techniques to be persued and selection of systems for the present study with the aim of their applications.

CHAPTER - 4 deals with the design considerations in powder preform forging. Also, discussed are press consideration, upsetting, partially open and closed dies.

CHAPTER - 5 deals with the experimental details such as mode of cold compaction sintering, protection against oxidation and decarburization, forging, dimensional measurements, and hardness evaluations on suitably prepared surfaces etc.

CHAPTER - 6 deals with the experimental results which are discussed in the light of densification versus height strain, height reduction of cracking with respect to forging temperature, effect of H/D ratios on densification at various temperatures. Microstructural observations are correlated with the mode of densification. Densification results of partially open die forging with various types of constraints have been discussed. A correlation between fractional theoretical density and ' $\phi$ ' has been



developed. Microstructural studies were carried out to establish the mode of pore closure with and without the addition of alloying elements.

Densification results of closed die forgings with changing stages of repressing are presented. Alloying additives and their effect on densification and soundness of the products were evaluated. Microstructures are taken and compared with those of upset and partially open die forgings. Evaluation of mechanical properties such as tensile strength and impact values were carried out.

CHAPTER - 7 deals with the conclusions of the present investigation.

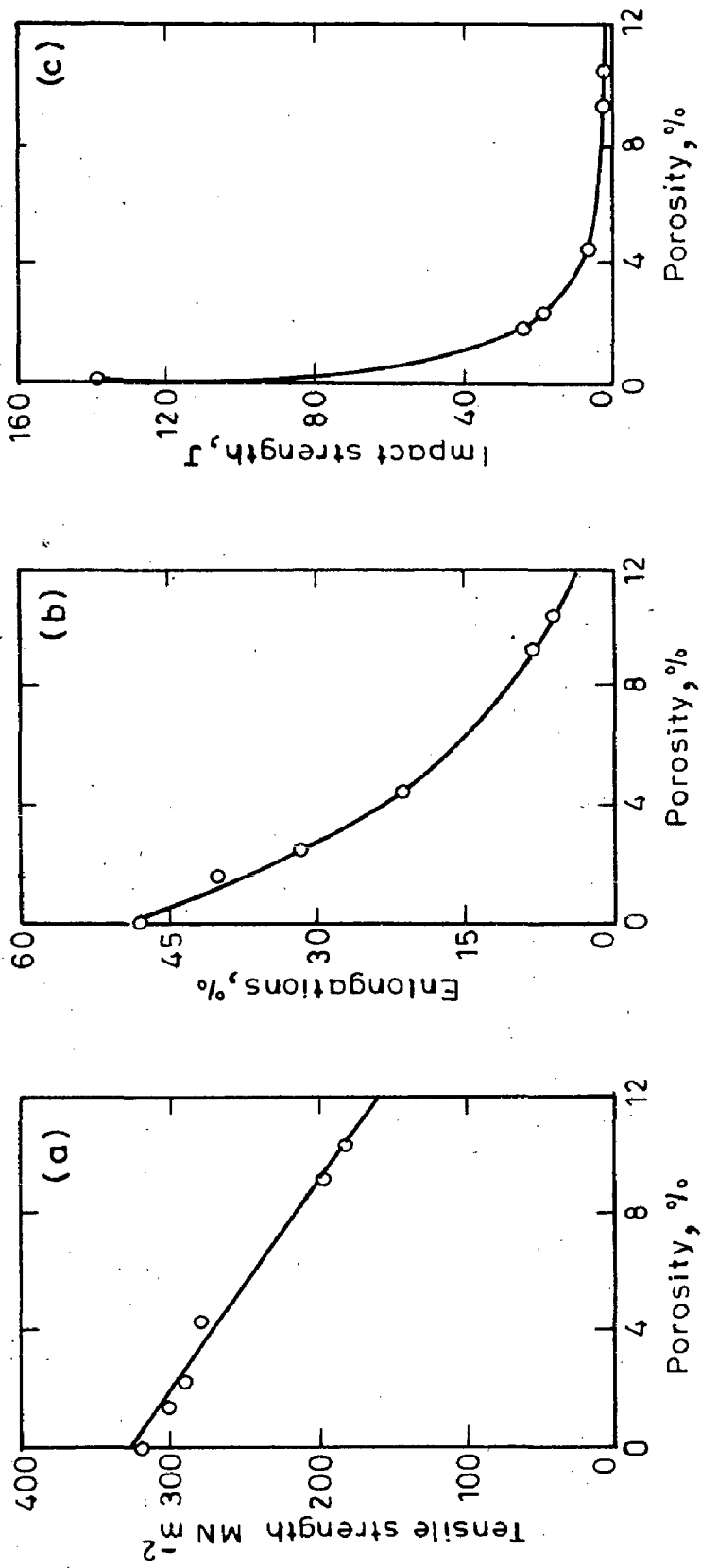


Fig.1.1—Influence of porosity on mechanical properties of hot repressed pure iron (After Backstiegal and Blando) [1]

## CHAPTER - 2

### LITERATURE REVIEW

Conversion of metal powder or granules to dense products was executed at least 5,000 years ago (metal age) when primitive furnaces could not have attained the melting and casting temperatures of metals such as iron and copper, therefore, definitely powder or granules could have been preheated and hammered to various shapes. Famous Iron Pillar of Delhi and large Sword of Wieland the Smith well known in German mythology were made many centuries ago by combining the sintering of iron sponge with a hammering operation [2]. Platinum ingots were first produced by Wollaston in Britain in 1829 by hot pressing [3] and tungsten powder was converted into ductile filament in the early part of this century by Coolidge, in U.S.A., following the above route [3]. However, by employing the above technique a successful attempt was made by Henry and Cordiano in 1944-45 to produce a product of electrolytic iron powder by hot pressing into a heated die for a period of 7.5 minutes at 20 KSI. Properties reported were for superior to those conventionally pressed and sintered specimens [4]. Herman Tormyn who produced preforms from crushed steel turnings in 1941 [5] and, thereafter, Koehring

reported the results of his experimental findings [6] and Wassermann independently proposed the process in 1946 [7]. Though the above technologies were available to the industries, but, the present interest in powder forging developed much later. The development of this interest became obvious when size and density limitations of standard sintering technique became apparent [2]. At that time powder metallurgical industries had found the new area of expansion, i.e., 'powder forging' of sintered metal powder preforms which has emerged out as the most exciting new field within metal working industries. Wide applications of forged steel powder preforms emerged from the investigations conducted during the past few years [8,9]. Further, extensive applications of powder preform forging are anticipated, once the designers and manufacturers accurately predicted and achieve the required properties and attain economic goals [10].

Although in due course of time variety of powder forging techniques were developed, the predominant process utilized was the hot forging of powder metal preforms in closed dies, thereby utilizing the combined advantages of both powder metallurgy and forging [11]. The powder is compacted in a preform shape and sintered in a controlled atmosphere to produce metallurgical bond amongst the powder particles followed by forging within a closed die to achieve the final shape of the

component aimed through a single stroke of the press.

## 2.1 DEFINITION OF POWDER FORGING

The 'powder forging', 'sinter forging' or 'powder preform forging' has been defined differently but, however, conveying the same meaning. The International Standards Organization has proposed the definition of 'powder forging' as 'hot densification by forging of an unsintered, presintered or sintered preform made from powder with an accompanying significant change of shape'. Often the designation 'sinter forging' is used if a separate sintering step is carried out. In U.S.S.R. the designation dynamic hot pressing of powder preforms is used [2].

Irrespective of the types of definitions, proposed, the common point in all is that improved densification coupled with the desired shape is achieved by simultaneous application of the temperature and pressure over unsintered, presintered or sintered preforms made from metal powders. Powder, or preform, forging is the consolidation and densification of metal powders, using forging as one of the steps in the process. Preform forging combines the advantages of conventional powder metallurgy, such as dimensional accuracy and minimal material waste, with the high strength of

forgings. However, conventional forging requires several blows and dies whereas preform forging can usually produce a fully formed component with one blow only.

## 2.2 NECESSITY OF POWDER FORGING

'Powder forged' components can be produced having mechanical and physical properties equivalent to conventional wrought steels, together with the complexity and dimensional accuracy normally associated with sintered parts.

Powder forging appears to be an attractive manufacturing route for many components because of the fact that material utilization is better than in conventional forging; detail and tolerances obtainable can lead to the elimination of much, if not all, finish machining; tight weight tolerances are possible in the 'as forged' condition [12-15]. This process appears to be economical on the ground that lower forging temperatures are required which results in better surface condition ultimately increasing fatigue strength [16]. Added to this powder forging requires one and two blows instead of three or many more as required in the conventional forging of bar stock. Single quality of iron powder can be used to make carbon steels of any desired composition. Less die

wear and simpler die configuration accompanied with the properties required could be tailored to the application. These factors directly govern the economics of the process, favouring ultimately the use of powder forging [16].

Generally powder metallurgy process produces finished products more economically than the established methods of melting, casting, forging and machining. This led to the emergence of sintered engineering components industry, in late thirties of the present century. These days, the powder metallurgy process is used to make a great variety of products from ferrous and non-ferrous metals and alloys, refractory metals, super alloys, and composites. In recent times, there has been an increasing tendency to develop methods of ore treatment that result in the metal being produced in the form of powder. Since the production of metal powders involve less pollution than smelting and casting processes, it is advantageous to produce parts through powder metallurgy route. In the production of iron and steel, the increasing shortage of metallurgical grade coke and heavy atmospheric pollution cause great concern to consider other processes. Powder metallurgy saves materials as well as energy by not generating scrap. It saves materials and energy by recycling scrap of other sources. It does not foul the atmosphere, or dump pollutants into the

streams. Thus, to produce highly dense products, mechanical and physical properties comparable to those produced through conventional techniques, powder forging is a most viable process. Added to what has been stated above powder metallurgy does not require highly skilled personnel [3].

### 2.3 MATERIALS FORGED

Upto 1950 basically powder compacts, pure or alloyed, were sintered and used directly without forging. Various powder blends were prepared, compacted and sintered to produce porous parts for various applications - such as oil impregnated bearings and filters [17]. But, at the advent of powder forging, and the economic involved into the process, the substitution of various parts which were being produced by conventional techniques were shifted to powder forging. In the process of replacing conventionally produced components by P/M technique larger grades of powder varieties were tried and used successfully. Basically, the types of powders used to produce components were iron [18-32], iron based alloy powder [18,32,33-61], iron graphite with and without the addition of other alloying elements [62,63], aluminium and aluminium based alloy powders [32,64-69], titanium and titanium based alloy powders [32,70-80]. Other



powders used were refractory powders and their mixes [81], super alloy powders [32,35,82-89] and Beryllium and its alloys [32,70,90-93] and also the cobalt [94,95] and nickel [96] alloys were forged through this technique. Thus, great variety of metallic and non-metallic powders were forged to produce high density, high strength products for useful applications. The development of CERAMIC GUARD [97-99] to protect the preform surfaces

---

against oxidation and decarburization, during sintering stage, led the powder production line to operate smoothly. This avoided the complications of explosive sintering environments such as hydrogen and cracked ammonia. Added to the above advantages, use of ceramic guard is economical too. Till date, a large number of alloy compositions of ferrous and non-ferrous and their combinations have been forged at elevated temperatures through powder metallurgical route. There exists a large list consisting of number of alloy compositions, standard and non-standard, which were frequently used by investigators because they, at their will, could blend any alloy mixture, sometimes for academic interest only. However, large number of investigators [18-96] have tried to forge mostly the conventionally existing alloys compositions so that mechanical and physical properties of the powder forged product could be directly compared.

## 2.4 PROCESS VARIABLES

The process variables[100], in general consist of preform shape, preform weight control, preform and tooling temperature, materials of toolings and type of lubrication. These parameters had definite effects on tool life as well as the final properties of the components.

### 2.4.1 Preform Shape

It is essential to produce preforms of correct dimensions to achieve desirable flow of material during forging, so as to control the amount of porosity in the finished product.

### 2.4.2 Preform Weight Control

The weight control of the preform is essential when forgings are to be executed in closed dies to obtain reproducible dimensions. This is one of the inherent advantage of powder forging over the conventional forging. Accuracy of weight control can be maintained as close as  $\pm 0.5$  per cent.

### 2.4.3 Preform and Tooling Temperatures

It is necessary to select the proper preform and tooling temperatures so as to obtain the desired part with properties comparable to that of the wrought products. Appropriate tooling temperature provides enhanced life of the toolings.

When the preform temperature is too low the flow of material is restricted resulting in generation of shear cracks in the formed product. Too low a temperature of the preform offers more resistance against deformation which ultimately leaves behind sufficient amount of porosity in the product leading to its failure in service.

Whenever, the difference between tooling temperatures is too large, extensive thermal cycling of the tool is likely to cause fatigue of the die surfaces, resulting in poor lubrication and reduced tooling life. Therefore, an optimization of difference is warranted between these two temperatures for the over all success of the process.

### 2.4.4 Materials of Toolings

Normally hot die steels are used whenever high temperature deformation of preforms is required. It is practical experience that hot die steels be heat treated to Rc 40-45 for forging purposes.

#### 2.4.5 Lubrication of Dies

For the appropriate flow of material during deformation, it is essential to use proper die lubrication. In general, the use of sprayed graphite powder over the die surfaces is recommended and sometimes graphite paste in acetone or in water is used for the purpose of lubricating the dies [101-103] whereas the ceramic coatings [97-99] used for protection of preform surfaces against oxidation and decarburization, at high temperatures acts as self lubricant during deformation of powder preforms.[99].

In addition to the parameters stated above, the purity of the powder, sintering atmosphere and its control, time of exposure of the hot preform to environment (during transfer from the furnace to the press), the degree of distribution of inclusions and the amount as well as distribution of porosity in the finished product affect the properties of the forgings to a greater extent.

#### 2.5 FORGING PARAMETERS

Forging parameters are basically the forging temperature, deformation rate and contact time of the work piece with the tools. In general, at low forging rates, considerably greater portion of the surface regions of the forged product does not densify, whereas, high deformation rates produce comparatively dense products [104]. The difference in densification

level achieved in the above case is because of different degree of die chilling resulting from wide variation in contact times associated with different forging procedures. Whenever chilling is less severe, flow of material is more leading to improved densification. However, surface porosity basically depends upon the tool temperature and lubricant used. Forging temperature and relative amount of shear lead to the interparticle welding occurring as a result of pores elimination. Highly effective inter-particle bonding occurs when shear forces are strong enough to break residual surface oxide layers [105-107]. It can also be said from the property data which, when equal are better than those of wrought materials, are indicative of strong inter-particle bonding [108-109]. High forging temperatures re-close the transient cracks [110]. Thus, an appropriate temperature of forging, adequate die pre-heating and proper lubrication in conjunction with optimum strain rate of deformation results in improved densification and in turn leads to better mechanical properties.

## 2.6 MATERIAL VARIABLES

In general, the optimization of the complete process requires the characterisation of preform material specially the powder characteristics (purity,

size and shape), preform properties (porosity, uniformity, pore structure and its shape) and forging details (die design, lubrication, coating and temperature of forging). All these factors either in combination or indivisually affect the forgeability of the powder preforms [111-112].

## 2.7 DEFORMATION OF POROUS MATERIALS

Existence of pores in powder preforms is due to the irregular shapes of randomly oriented powder particles. This results in reduced area of contact during compaction and may cause localized interlocking. The presence of pores in powder preform can be attributed to the combined effect of inadequate applied pressure, powder size and its distribution, particle geometry, the compaction temperature, the cleanliness of the powder particles and the atmosphere under which the compaction has been performed [100]. Depending upon the above conditions the shape, size and distribution of pores affect the properties of powder compacts (leaving aside the material properties).

In general, the pores must be closed to achieve full density and a sound metallurgical structure. Pores are sites of weaknesses where cracks may initiate during forging [113-114].

In the initial stage of compaction, the sizes of the pores are comparable with that of the powder particles but however, when the compacting pressure is increased the sizes of pores start reducing. A limit of pressure application is reached where no further densification is resulted. During initial stage of compaction, the coarser pores are expected to be closed in preference to the smaller ones. In this process few of them might get closed permanently while few may remain stable with respect to the applied pressure. This is a stage where pore pressure equals the externally applied pressure and consequently chances of pore closure further become very remote, because pore closure is a function of shear stress prevailing around [2,100,114-116] it and the magnitude of the shear stress at any point inside the compact gradually diminishes even when more of the pressure is being applied.

Once the powder preform is subjected to heavy forging (upsetting) under the varying conditions of temperature and initial preform aspect ratio, fast density changes are expected. This is because of the fact that extensive heterogeneous deformation occurs and the pores are subjected to shear as well as compressive forces - a situation more favourable for pore closure. The pore closure in upsetting is also influenced by its position inside the compact e.g.,

pores situated near the free surfaces of the compact might even get opened because of the fact that tensile forces start dominating the shear/compressive forces during upsetting in this region.

The presence of pores anywhere in the component is ought to be closed up during forging. Irrespective, of the mode of forging, pores are generally allowed to collapse under shear strain for improved densification whereas totally repressing mode will result into fairly good amount of porosity inside the repressed component. Therefore, for better densification material movement is required.

Since powder preforms have porosity upto a level of 30 volume per cent, therefore, during deformation of powder preforms, volume changes are associated with the mode of deformation. Hence, yielding, flow and fracture are the major factors considered in evaluating deformation behaviour of porous materials. Principal reasons, for deforming porous material, are to reduce porosity and provide a specific shape. The amount and type of deformation affects mechanical properties due to the presence of residual porosity [117]. Deformation or flow terminates with fracture.

If the material is continuous, homogeneous, isotropic and incompressible, the elastic and plastic behaviour of the material can be simplified. Continuously



fully dense, fine grain size, cubic lattice materials approach these requirements and theories have been developed for predicting their elastic and plastic behaviours as also the yielding. In the elastic range, Hooke's Law can be applied. Yielding can be predicted fairly accurately for any general type of loading by the Von Mises Theory [118]. Plastic flow behaviour can be predicted by slip line Field Theory or by Upper and Lower bounding Theories. In case of fully dense materials, yielding and flow are not affected by the hydrostatic component of the stress, system, because this pressure component of stress is responsible for volume changes only and there is no volume change in fully dense material. However, porous material must yield under the influence of a hydrostatic type of loading because a significant inelastic volume change can be achieved. Therefore, theories of yielding and flow of porous materials must be an extension of current classical theories for fully dense material [117]. The deformation in materials fully dense or porous can be explained either using stress or strain tensors. The important types of strain in deformation are basically of two types :

- (a) normal strain, and
- (b) shear strain.

Strains are generally defined in the following two ways :

(a) engineering strain =  $e$ , and

(b) true strain =  $e_t$

The engineering strain is defined as the change in length per unit original length,

$$e = \frac{\Delta L}{L_0} = \frac{L - L_0}{L_0} \quad \dots(2.1)$$

where:  $L$  = deformed length

$L_0$  = original length of the gauge.

Engineering strain is applicable for small strains (i.e.  $e < 0.1$ ); whereas, for large strains like those encountered in plastic flow and metal working, the change in length,  $\Delta L$  may be very large. If the engineering strain is measured at various stages of deformation process and then all of the individually measured strains added, the sum will not equal the value of 'e' calculated from the beginning and final values of the gauge length. To overcome this problem a concept of true strain was developed and is used in metalworking problems. True strain  $e_t$  is defined as :

$$e_t = \frac{L_1 - L_0}{L_0} + \frac{L_2 - L_1}{L_1} + \frac{L_3 - L_2}{L_2} + \dots$$

$$\text{or, } e_t = \int \frac{dL}{L}$$

$$\text{or, } e_t = \ln\left(\frac{L}{L_0}\right)$$

$$e_t = \ln(1+e) \quad \dots(2.2)$$

Shearing strain,  $\gamma$ , is defined as the change in right angle that occurs during deformation. That is, if a square grid is scribed on the surface of a specimen and if after deformation the angles of the grid have changed from  $90^\circ$ , then during deformation shear occurred.

The total tensor  $E$  may be written in matrix form as tensor :

$$E = \begin{vmatrix} e_{t,x} & \gamma_{xy}/2 & \gamma_{xz}/2 \\ \gamma_{yx}/2 & e_{t,y} & \gamma_{yz}/2 \\ \gamma_{zx}/2 & \gamma_{zy}/2 & e_{t,z} \end{vmatrix} \quad \dots(2.3)$$

Strain,  $E$  may be divided into a deviator component and a spherical or hydrostatic component.

$$E = E' + E'' \quad \dots(2.4)$$

Deviator      Hydrostatic

Where :

$$E'' = \begin{vmatrix} e_{t,m} & 0 & 0 \\ 0 & e_{t,m} & 0 \\ 0 & 0 & e_{t,m} \end{vmatrix} \quad \dots(2.5)$$

$$\text{and } e_{t,m} = \frac{e_{t,x} + e_{t,y} + e_{t,z}}{3}$$

When a load is applied to a body internal resistance or stresses ' $\sigma$ ' are developed in the body that oppose the applied load. If the stresses in the body are uniformly distributed over a planar area that is perpendicular to the applied load then an equilibrium equation ( $\sum F = 0$ ) may be written [119]

$$P = \sigma dA \quad \dots(2.6)$$

$$P = \sigma A \quad \text{where : } \sigma = \text{average stress}$$

or  $P = \frac{P}{A}$   $P = \text{applied load}$   
 $A = \text{area perpendicular to the load.}$

The total stress 'S' acting on a plane may not be perpendicular to the plane usually for convenience the total stress is broken into a component perpendicular to the plane ' $\sigma$ ' (a tensile or compressive stress) and a component in the plane ' $\tau$ ' (a shear stress) as shown in Fig. 2.1. These components of the stress are broken-down further into components that are parallel to an orthogonal system of loading may be represented by the normal and shear components of the stress shown in Fig. 2. Figure 2 shows that there are 3 normal stresses ( $\sigma_x, \sigma_y, \sigma_z$ ) and 6 shear stress ( $\tau_{xy}, \tau_{yx}, \tau_{xz}, \tau_{zx}, \tau_{yz}$  and  $\tau_{zy}$ ). However, for isotropic polycrystalline cubic materials

$$\tau_{xy} = \tau_{yx}$$

$$\tau_{xz} = \tau_{zx}$$

$$\tau_{yz} = \tau_{zy}$$

Therefore, only 6 independent stresses have to be defined to describe completely the stress system ( $\sigma_x, \sigma_y, \sigma_z, \tau_{xy}, \tau_{xz}$  and  $\tau_{yz}$ ). These quantities can be expressed as stress tensor 'S' shown below [120]:

$$S = \begin{vmatrix} \sigma_x & \tau_{xy} & \tau_{xz} \\ \tau_{yx} & \sigma_y & \tau_{yz} \\ \tau_{zx} & \tau_{zy} & \sigma_z \end{vmatrix} \quad \dots(2.7)$$

Once again it is possible to orient x, y and z axes in such a way that all shear stresses are zero. The remaining normal stresses are called the 'Principal Stresses' and are assigned subscripts of 1, 2 and 3 rather than x, y and z. Thus, the stress tensor for the principal stress is given by

$$S = \begin{vmatrix} \sigma_1 & 0 & 0 \\ 0 & \sigma_2 & 0 \\ 0 & 0 & \sigma_3 \end{vmatrix} \quad \dots(2.8)$$

where  $\sigma_1 > \sigma_2 > \sigma_3$

Now, the total stress S may be separated into two parts :

$$S = S' + S'' \quad \dots(2.9)$$

where  $S'$  = deviator stress

$S''$  = spherical part (hydrostatic or pressure part)

The spherical (pressure) stress tensor is given by :

$$S'' = \begin{vmatrix} \sigma_m & 0 & 0 \\ 0 & \sigma_m & 0 \\ 0 & 0 & \sigma_m \end{vmatrix} \quad \dots(2.10)$$

where :  $\sigma_m = \frac{\sigma_x + \sigma_y + \sigma_z}{3} = \text{mean stress}$

This part of the stress causes volume changes and contributes to the deformation. The effect of this stress on ductility at fracture is shown for several materials in Fig. 2.3. It is clear from this figure that more negative the mean stress the greater the apparent ductility.

The sum of the three normal stresses ( $\sigma_x + \sigma_y + \sigma_z$ ) or ( $\sigma_1 + \sigma_2 + \sigma_3$ ) is one of the invariants of stress and will therefore have a constant value regardless of the orientation of the axes x, y and z axes. There are two other important stress invariants that are relatively simple expressions in terms of the principal stresses. The three invariants are given below :

$$I_1 = \sigma_1 + \sigma_2 + \sigma_3 = \sigma_x + \sigma_y + \sigma_z \quad \dots(2.11)$$

$$\begin{aligned} I_2 &= \sigma_1\sigma_2 + \sigma_2\sigma_3 + \sigma_3\sigma_1 \\ &= \sigma_x\sigma_y + \sigma_y\sigma_z + \sigma_z\sigma_x \\ &\quad - \tau_{xy}^2 - \tau_{yz}^2 - \tau_{zx}^2 \end{aligned} \quad \dots(2.12)$$

$$\begin{aligned} I_3 &= \sigma_1\sigma_2\sigma_3 = \sigma_x\sigma_y\sigma_z + 2\tau_{xy}\tau_{yz}\tau_{zx} \\ &\quad - \sigma_x\tau_{yz} - \sigma_y\tau_{zx} - \sigma_z\tau_{xy} \end{aligned} \quad \dots(2.13)$$

These invariants are the coefficients of the cubic equation for stress :

$$\sigma^3 - I_1\sigma^2 + I_2\sigma - I_3 = 0 \quad \dots(2.14)$$

Solving the cubic equation for  $\sigma$  gives the three principal stresses. Other important aspects of the invariants will be discussed while discussing flow theoreis for both fully dense and porous powder preforms.

Thus the deviator stress  $S'$  is obtained by subtracting the mean stress each of the normal components of the total stress

$$S' = S - S'' = \begin{vmatrix} (\sigma_x - \sigma_m) & \tau_{xy} & \tau_{xz} \\ \tau_{yx} & (\sigma_y - \sigma_m) & \tau_{yz} \\ \tau_{zn} & \tau_{xy} & \sigma_z - \sigma_m \end{vmatrix} \quad \dots(2.15)$$

therefore, the deviator stress,  $S'$ , is responsible for flow and plastic deformation of conventionally fully dense material.

The elastic relationship between the stress and strain tensors are given by :

$$S' = 2GE' \quad \dots(2.16)$$

$$S'' = 2KE'' \quad \dots(2.17)$$

where:  $G$  = shear modulus

$K$  = bulk modules

Since the hydrostatic part of the strain is associated with the volume changes whereas deviator part of the strain is associated with the deformation of conventionally dense materials, therefore, hydrostatic part of the strain is effective while deforming porous materials, but, for fully dense materials deviator part of the strain is applicable. While explaining the plastic deformation of fully dense materials particularly in the case of P/M preforms volume changes during deformation (density increases) and the hydrostatic components of stress ( $S''$ ) and strain ( $E''$ ) become responsible for the flow of porous P/M preforms.

## 2.7.1 Elastic Deformation

### 2.7.1.1 Fully Dense Material

For general three dimensional loading the stress-strain relations for the principal directions are given as below :

$$e_1 = \frac{1}{E} [ \sigma_1 - \nu (\sigma_2 + \sigma_3) ] \quad \dots(2.18)$$

$$e_2 = \frac{1}{E} [ \sigma_2 - \nu (\sigma_1 + \sigma_3) ] \quad \dots(2.19)$$

$$e_3 = \frac{1}{E} [ \sigma_3 - \nu (\sigma_1 + \sigma_2) ] \quad \dots(2.20)$$

where:  $E$  = Young's modulus of elasticity

$\nu$  = Poisson's ratio.



For the simple case of uniaxial loading (i.e. tension test or compression test) Hooke's Law reduced to :

$$e_1 = \frac{\sigma_1}{E} \quad \text{or} \quad \sigma_1 = E e_1 \quad \dots(2.21)$$

### 2.7.1.2 Porous Material

The application of Hooke's laws to porous materials requires some modification since the presence of pores reduces the effective cross-sectional area for carrying load. The affect of porosity is reflected in an apparent modulus of elasticity ( $E_p$ ) and an apparent Poisson's Ratio ( $\nu_p$ ) that is less than the values for fully dense material. The values of  $E_p$  and  $\nu_p$  are not simple linear functions of the fraction of voids indicating that the shape and distribution of porosity also has an affect.

If a simple 'equivalent strain criteria' to a porous material in order to determine the modulus of elasticity results in the following equation :

$$E_p = E (1-f_v) \quad \dots(2.22)$$

However, experimental results yield the following empiricil relationship for a variety of ferrous materials [121]

$$E_p = E(1-f_v)^{3.4} \quad \dots(2.23)$$

Similarly an empirical relationship for Poisson's Ratio of porous iron preforms has been presented as shown below [122] :

$$\nu_p = 0.5 (1-f_v)^{1.92} \quad \dots(2.24)$$

where:  $E_p$  = apparent modulus of elasticity

$f_v$  = volume of fraction of pores

$E$  = modulus of elasticity for the solid material

$\nu_p$  = Poisson's Ratio for a porous preform.

Therefore, it is now possible to write the elastic relations for porous materials using the appropriate elastic constants as shown below :

For general loading,

$$e_1 = \frac{1}{E_p} [ \sigma_1 - \nu_p(\sigma_2 + \sigma_3) ] \quad \dots(2.25)$$

For uniaxial loading,

$$\sigma_1 = E_p e_1 \quad \dots(2.26)$$

Hence, owing to the stress concentration affect, that the voids create, localized plastic deformation may occur at low loads or small strains. Furthermore during deformation the volume will change and the volume fraction of voids will change and therefore  $E_p$  and  $\nu_p$  will change.

## 2.7.2 Yielding

Since metalworking is concerned with plastic deformation or yielding, then a 'yield criterion' is required as the first step to the development of a theory. Yield criteria for fully dense materials were developed many years ago by (Tresca (1865) and Von Mises (1913) as quoted [123]. Yield theories for porous material have also been presented but these have been more recent [124-125].

### 2.7.2.1 Fully Dense Material

The principal mechanism of flow in metals is by slip, which is a shearing mechanism, it is logical that flow occurs when the maximum shearing stress reaches a critical value. This is Tresca's Maximum-Shear-Stress criterion. Yielding occurs when :

$$\sigma_0 \leq \sigma_1 - \sigma_3 \quad \dots(2.27)$$

$$\sigma_1 - \sigma_3 = \tau_{\max} \quad \dots(2.28)$$

where:

$\sigma_0$  = yield strength in tension

$\sigma_1$  = maximum principal stress

$\sigma_3$  = minimum principal stress

$\tau_{\max.}$  = maximum shear stress.

This yield criterion completely ignores any contribution that the intermediate principal stress ( $\sigma_2$ ) has on yielding. The Von Mises Distortion Energy

criterion includes the intermediate principal stress. This theory states that only the deviator part of the stress ( $S'$ ) is responsible for yielding and therefore yielding will occur when the deviator strain energy per unit volume reaches a critical value. Yielding occurs when :

$$\sigma_0 \leq \frac{1}{\sqrt{2}} [(\sigma_1 - \sigma_2)^2 + (\sigma_2 - \sigma_3)^2 + (\sigma_3 - \sigma_1)^2]^{1/2} \quad \dots(2.29)$$

where:

$\sigma_0$  = yield strength in tension or compression

$\sigma_1, \sigma_2$  and  $\sigma_3$  = principal stress.

It has been reported [120] that the Von Mises distortion energy theory fits experimental results better than the Tresca maximum - shear theory. Figure 2.4 shows the plot in support of the above.

### 2.7.2.2 Porous Materials

The Von Mises Criterion for yielding is really a function of the second invariant of the stress deviator [120],  $I_2'$

$$I_2' = -\frac{1}{6}[(\sigma_1 - \sigma_2)^2 + (\sigma_2 - \sigma_3)^2 + (\sigma_3 - \sigma_1)^2] \quad \dots(2.30)$$

Therefore, the Von Mises yield condition may be written as :

$$\sigma_0 = (-3 I_2')^{1/2} \quad \dots(2.31)$$

As stated earlier the hydrostatic part of the stress does not affect yielding in completely dense materials, but it does affect yielding in P/M preforms. Therefore, any yield condition for P/M preforms must include some function of the hydrostatic component of stress which will be some function of :

$$\sigma_1 + \sigma_2 + \sigma_3 = I_1 : \text{ the first invariant of stress}$$

and also in addition must contain some function of  $K \cdot I_2'$ , the second invariant of the deviator stress.

The Mohr-Coulomb yield criterion as mentioned by Suh [124] and Kuhn and Downey [125] involve both the required invariants,  $I_1$  and  $I_2$ .

Thus for P/M preforms yielding, is stated as a function of  $I_1$  and  $I_2$  or mathematically as :

$$\text{Yielding} = f(I_1, I_2') \quad \dots(2.32)$$

But:

$$I_1 = [3(I_2 - I_2')]^{1/2} \quad \text{and}$$

therefore :

$$\text{Yielding} = f_2(I_2, I_2') \quad \dots(2.33)$$

It was proposed by Kuhn and Downey that yielding for P/M preforms may be expressed as :

$$\text{Yield function} = [-3I_2' + (1 - 2 \nu_p)I_2]^{1/2} \quad \dots(2.34)$$

where:

$$\nu_p = \text{Poisson's Ratio for porous material.}$$

Poisson's ratio for fully dense materials is equal to 0.5 for plastic deformation. This is a requirement if volume is to remain constant. In all the cases of porous P/M preforms Poisson's ratio is less than 0.5 but increases to a limiting value of 0.5 as the density approaches to nearly 100 per cent [122]. It can be clearly seen that as the density increases ( $\nu_p \rightarrow 0.5$ ) the hydrostatic component part of yielding, i.e.,  $(1-2\nu_p) I_2$  contributes less and less to yielding. When full density is reached ( $\nu_p = 0.5$ ) the hydrostatic part of yielding vanishes and yielding depends only on  $I_2'$ , Von Mises yielding criterion applies to full density materials.

### 2.7.3 Plastic Deformation

#### 2.7.3.1 Fully Dense Material

Under the condition of uniaxial loading the plastic deformation for simple tensile type of loading of polycrystalline material can be expressed by a mathematical expression :

$$\sigma = K e_t^n \quad \dots(2.35)$$

where:

$\sigma$  = true stress

$K$  = strength coefficient

$e_t$  = true strain

$n$  = strain hardening exponent.

A log-log plot of  $\sigma$  versus  $e_t$  (flow curve) will give a straight line if the material behaves in accordance with the above equation. The value of 'n' is equal to the slope of the straight line, while K is equal to the value of  $\sigma$  when  $e_t = 1$ . Values of 'n' and K are given in Table 2.1 for conventional wrought materials. The values reported in Table 2.1 for 'n' and 'K' are for room temperature deformation. Increasing the deformation temperature usually decreases both 'n' and 'K' provided that a phase transformation, precipitation or some other hardening process does not occur. Ultimately the material approaches a perfectly plastic condition (no strain hardening) as the temperature is increased.

Table 2.1 : Values of n and K for Metals at Room Temperature

Metal	Condition	n	K, ksi
0.05 % C Steel	Annealed	0.26	77
SAE 4340 Steel	Annealed	0.15	93
0.6 % C Steel	Quenched and tempered 100°F	0.10	228
0.6 % C Steel	Quenched and tempered 1300°F	0.19	178
Copper	Annealed	0.54	46
70/30 Brass	Annealed	0.49	130

### 2.7.3.2 Porous Material (Uniaxial Loading)

Uniaxial compression and plane strain compression tests were made on a variety of iron-carbon alloys and several low alloy steels [18]. Log-log plots of the  $\sigma$  vs  $e_t$  data approximated straight line behaviour. The values of  $n_p$  (hardening exponent for porous material) and  $K_p$  (strength coefficient for porous material) are given for the iron-carbon alloy preforms in Table 2.2 and for the low alloy steel preforms in Table 2.3. It can be seen from these data that ' $n_p$ ' increases and ' $K_p$ ' decreases as porosity is increased as porosity is increased. Thus the flow characteristics of porous preforms can be represented by :

$$\sigma = K_p e_t^{n_p} \quad \dots(2.36)$$

It is interesting to note that in the case of fully dense materials  $n \rightarrow 0$  as temperature is increased (perfectly plastic material, no work hardening). In contrast for porous material  $n_p$  does not approach to zero as temperature is increased since  $n_p$  is result of two factors:

- (1) Porous preforms harden during deformation because the metallic matrix strain hardens, and
- (2) Porous preforms harden during deformation because the density is increasing (pore volume decreases) and effective load carrying cross-section increases.



Table 2.2  
 Work Hardening Exponents ( $n_p$ ) and ' $K_p$ ' Values From Log-Log Plots  
 of  $\sigma$  vs.  $\epsilon$  For Iron-Carbon Alloys.

Material	Uniaxial Compression For Preform Densities of				Plane Strain For Preform Densities of				
	5.3 g/cm <sup>3</sup> $n_p$	6.2 g/cm <sup>3</sup> $n_p$	7.2 g/cm <sup>3</sup> $n_p$	7.2 g/cm <sup>3</sup> $K_p$ (ksi)	5.3 g/cm <sup>3</sup> $n_p$	6.2 g/cm <sup>3</sup> $n_p$	6.2 g/cm <sup>3</sup> $K_p$ (ksi)	7.2 g/cm <sup>3</sup> $n_p$	7.2 g/cm <sup>3</sup> $K_p$ (ksi)
Sponge Iron	0.66	0.54	0.37	115	0.66	0.49	125	0.33	125
Atomized Iron	0.74	0.58	0.39	115	0.74	0.52	115	0.33	125
1006	0.70	0.62	0.41	120	0.70	0.57	130	0.36	130
1009	0.67	0.54	0.39	120	0.66	0.52	127	0.32	130
1014	0.69	0.67	0.39	130	0.70	0.50	138	0.29	135
1018	0.69	0.52	0.38	130	0.65	0.50	132	0.33	140
1020	0.62	0.54	0.37	140	0.69	0.53	142	0.30	145
1024	0.73	0.57	0.35	137	0.67	0.51	143	0.33	152
1032	0.67	0.53	0.30	132	0.66	0.52	160	0.33	163
1041	0.66	0.48	0.32	150	0.74	0.50	168	0.30	170

Table 2.3  
Work Hardening Exponents ( $n_p$ ) and ' $K_p$ ' Values For Low Alloy Steels

Material	Uniaxial Compression For Preform Densities of				Plane Strain For Preform Densities of						
	5.3 g/cm <sup>3</sup> $n_p$ $K_p$ (ksi)	6.2 g/cm <sup>3</sup> $n_p$ $K_p$ (ksi)	7.2 g/cm <sup>3</sup> $n_p$ $K_p$ (ksi)	7.2 g/cm <sup>3</sup> $n_p$ $K_p$ (ksi)	5.3 g/cm <sup>3</sup> $n_p$ $K_p$ (ksi)	6.2 g/cm <sup>3</sup> $n_p$ $K_p$ (ksi)	7.2 g/cm <sup>3</sup> $n_p$ $K_p$ (ksi)	7.2 g/cm <sup>3</sup> $n_p$ $K_p$ (ksi)			
Sponge Iron	0.66	0.54	110	0.37	115	0.66	115	0.49	125	0.33	125
Atomized Iron	0.74	0.58	105	0.39	115	0.74	100	0.52	115	0.33	125
AS-1020	0.62	0.54	130	0.37	140	0.69	122	0.53	142	0.30	145
AS-4620	0.57	0.42	160	0.38	170	0.59	160	0.38	175	0.25	185
AS-1330	0.67	0.53	135	0.30	132	0.66	135	0.52	160	0.33	163
AS-4630	0.60	0.38	165	0.28	185	0.59	180	0.36	185	0.20	195
AS-8620	0.62	0.59	175	0.34	174	0.62	155	0.49	175	0.29	180

The first factor is sensitive to temperature but the second factor is not sensitive to temperature. Therefore, there is an effective deformation hardening of porous preforms at elevated temperatures. It has been reported [126] that when porous iron preforms are deformed at 2100°F the material behaves in accordance with an exponential function ( $\sigma - \sigma_y = K_p e_t^{n_p}$ ). It was found in this work that 'n<sub>p</sub>' was a constant for true strains upto  $e_t = 0.5$ . Above  $e_t = 0.5$ , n<sub>p</sub> increased with increasing strain.

#### 2.7.4. Complex Loading

##### 2.7.4.1 Fully Dense Material

There are no simple relationships between stress and strain for a general or complex type of loading during plastic deformation. The two basic approaches to the problem for fully dense materials are that since the deviator part of the stress is responsible for deformation then :

$$S' = f(\dot{E}') \quad [\text{flow theories}] \quad \dots(2.37)$$

or

$$S' = f(E') \quad [\text{deformation theories}] \quad \dots(2.38)$$

where:

$S'$  = deviatoral stress

$E'$  = deviatoral strain

$\dot{E}'$  = deviatoral strain rate.

Development of a flow theory leads to the following equations [119-120].

$$\frac{2\sigma_1 - \sigma_2 - \sigma_3}{2\sigma_2 - \sigma_1 - \sigma_3} = \frac{d e_{t,1}}{d e_{t,2}} \quad \dots(2.39)$$

$$\frac{2\sigma_1 - \sigma_2 - \sigma_3}{2\sigma_3 - \sigma_1 - \sigma_2} = \frac{d e_{t,1}}{d e_{t,2}} \quad \dots(2.40)$$

Using the two above equations with the constancy of volume equation of full density materials ( $d e_{t,1} + d e_{t,2} + d e_{t,3} = 0$ ) provides a system of differential equations. These equations must be integrated along a given stress path or a given strain path to obtain in any specific case, a finite stress-strain relationships during plastic deformation. The above equations neglect the elastic range and does consider that work-hardening is not there.

If plastic deformation is small then elastic deformations must be considered and then other theories must be used [120]

#### 2.7.4.2 Porous Materials

The basic requirements for deriving the relationship between stress and strain for plastic deformation involve:

- (1) establishing a yield criterion.
- (2) establishing a flow rule.

The above factors apply to both conventional full density materials and porous preforms. The principal differences of the problem in deforming porous materials are :

- (1) The hydrostatic or pressure component of stress does affect yielding, and
- (2) Volume changes during plastic deformation.

The yield function of Kuhn and Dowrie as presented previously combined with the normality flow rule of St. Venant [125] was used to develop the following equations for deforming porous preforms :

- (1) For repressing powder preforms

$$\sigma_{re} = [(1-\nu_p)/(1-\nu_p^2)^2]^{1/2} \sigma_{uc}$$

- (2) For plane strain compression where  $e_{t,z} = 0$

$$\sigma_x = \frac{\sigma_{uc}}{(1-\nu_p^2)^{1/2}}$$

where :

$\sigma_{re}$  = stress required for repressing

$\sigma_{uc}$  = yield stress in uniaxial  
compression

$\nu_p$  = Poisson's Ratio

$\sigma_x$  = axial compressive stress for  
plane strain compression.

These equations are analogous to those developed by using slip-line field theory for fully dense materials. The equations may be used to predict flow curves for more complex type loadings (i.e. repressing

and plane strain compression) from simple uniaxial compression flow curves, provided that Poisson's ratio as a function of density is known.

### 2.7.5 Deformation and Densification

The application of a compressive type of load to a porous P/M preform causes a decrease in volume and thus an increase in density. The amount of density increase depends on type of loading, magnitude of load, preform density and the type of material. The type of loading is important if maximum efficiency of densification is to be achieved.

#### 2.7.5.1 Pores and Inclusions

One unique difference in deforming P/M preforms is that a large volume of pores are present (upto 30 or 40 %). Therefore, it is necessary to consider the manner in which pores deform during loading. In Fig.2.5(a) the shaded area represents a pore in an unloaded body. Applying a hydrostatic type load ( $S''$ ) will cause the volume to decrease; however, as shown by Bockstiegel the pressure for any practical process and even may be infinite, depending on the model that is chosen [127].

Although hydrostatic loading(Fig.2.5b)contributes to yielding and densification, a practical deformation

process for completely eliminating pores must be one where conventional shear or flow type deformation ( $E'$ ) occurs. Deforming with shear and hydrostatic loading could produce pore closure as illustrated in Figs. 2.5(c) and 2.5(d). The dramatic effect that the application of shear type loading has been demonstrated by Koerner [128]. At this stage it is also necessary to consider the effect of applied load over the inclusions during deformation. An inclusion (shaded area) in an unloaded material is shown in Fig. 2.6(a). If the relative strength of the inclusion to the matrix is high, the inclusion may not deform and cracks or pores may open at the matrix/inclusion interface, as illustrated by the black regions in Fig. 2.6(b), or the inclusion itself may crack without appreciable deformation. A high hydrostatic stress ( $S''$ ) helps to minimize these types of cracks. If the inclusion is not significantly stronger than the matrix, then the inclusion may be deformed and elongated in the direction of maximum straining. There is a tendency for pores to form at the ends of deformed inclusions too (Fig. 2.6(c)). Increasing the deformation beyond the point shown in 'C' may cause the inclusion to fracture and leave pores between the fragments (Fig. 2.6(d)). These phenomena have been observed in formed preforms [129].

It has been reported [126,130,131] that strain densification seems to be relatively insensitive to

alloy composition 'stress-densification' is sensitive to both alloy composition and mode of deformation. Strain densification and stress-densification data have been presented by other investigators [126, 130, 131].

### 2.7.6 Strain-Change in Volume Calculations

It has been reported earlier that densification is independent of alloy composition and therefore it is possible to predict densification from strain measurements.

The final density of the forged component can be calculated from the measurements of three normal strains [117].

$$\rho_f = \frac{M}{V_f} = \frac{M}{V_o e^{(e_{t,n} + e_{t,y} + e_{t,z})}} \quad \dots(2.41)$$

where :

$\rho_f$  = final or deformed density

M = mass

$V_o$  = original volume

exp = 2.718

or 
$$\rho_f = \rho_{pre} e^{-\Delta p} \quad \dots(2.42)$$

where:

$\Delta p = (e_{t,x} + e_{t,y} + e_{t,z})$

$\rho_{pre} = \frac{M}{V_o} = \text{Preform Density}$



The above equation is valid for porous materials or any material that can experience a volume change when deformed.

### 2.7.7 Effects of Flow and Residual Porosity on Properties

The recent studies [132-133] on the effects of preform density on impact properties of atomized iron preforms indicate the importance of deformation or flow during forming process. Some of the results of the above work on plane strain deformed and densified material indicate that when the formed density reached to a level of  $7.4 \text{ gm/cm}^3$  and  $7.6 \text{ gm/cm}^3$  (or approximately 5 % and 3.5 % porosity) the impact properties are not much affected. However, when the formed density reached  $7.7 \text{ gm/cm}^3$  (approximately 2 % porosity) there is slight improvement in impact strength with a  $6.7 \text{ gm/cm}^3$  preform density. In case of components deformed to a density level of  $7.8 \text{ gm/cm}^3$  i.e. less than 1 % porosity maximum properties were obtained with a  $6.2 \text{ gm/cm}^3$  preform. Similar trends have been reported for hot formed atomized iron preforms. It has been further reported that 'V' notch impact test is most sensitive test for assessing the integrity of P/M formed material. However, tensile strength and yield strength are much less sensitive than the tensile ductility (% elongation and reduction in area. But, tensile ductility could be

misleading also. If a P/M formed component is not processed properly, it may be possible to achieve all tensile properties and yet fall far short in impact strength in comparison to conventional wrought material. Therefore, in the development of P/M forming material and processing techniques, it is important to measure impact properties.

The mechanical properties of P/M formed material are basically affected by :

- (1) Residual porosity
- (2) Inclusions, and
- (3) Flow

Impact properties are extremely sensitive to small amounts of residual porosity. The effect of porosity on the impact strength can be seen from the values of 25 ft-lbs. for a porosity level of  $\sim 2\%$  whereas over 180 ft-lbs for porosity level below 1%.

Literature reports [134] that the iron-carbon alloys exhibited an increase in tensile strengths but a marked decrease in impact resistance. The iron samples showed the structures of uniform fine grains of ferrite with varying amounts of oxides. The iron-carbon samples consisted of ferrite grains with both pearlite and coarser iron carbides at the grain boundaries.

The influence of residual porosity on mechanical properties which are severely affected are fatigue and impact strength [135-138] and therefore forging to full density is the ultimate condition if dynamic applications are required.

The importance of inclusions have been realised by number of investigators [139-144] when they observed that the properties of the powder forgings have been drastically affected. In general, inclusions in any form show extremely detrimental effects on impact properties. It has been well understood that inclusions matrix interfaces are the weak spots of any component under impact loadings, cracks readily follow these weak directions and this is why the presence of inclusions in a matrix show poor impact properties as far as conventional forging in the transverse direction is concerned. However, in the longitudinal loading the weak spots may cause the diversion and branching of cracks and thus increased impact strength. Powder forgings have rather an isometric inclusion distribution [145-148] and therefore weak directions are practically absent. Thus, dynamic properties lie some where in between those measured in the transverse and longitudinal direction of conventional forgings [149-151]. The implication of this difference between conventional and powder forging is that an actual component which will have to function under complex stress conditions

may well give better performance in the powder forged condition, in spite of lower longitudinal values of test bars. Several investigators seem to support this [152-153].

Many investigators have reported that powder forging of iron and low alloy steels can yield properties which are comparable with those of conventionally forged materials [154-165]. It can be seen that controlling the residual porosity one can alter the mechanical properties of the powder forged products, but eliminating the last traces of porosity the process becomes uneconomical. Similarly, elimination of inclusions becomes further uneconomical and therefore a compromise is to be made in between mechanical properties and the level of inclusions and porosity of the forged products.

## 2.8 PRODUCTS PRODUCED THROUGH POWDER METALLURGY ROUTE

Since it has become possible to achieve forged density close to theoretical density, a large number of components have been produced through powder metallurgy route and these components succeeded in trial runs. Therefore, with the march of time, a great deal of research work has been put in for the development of components. Impact, fatigue and tensile properties of high density carbon and low alloy steels have shown

to compare with wrought steels of the same composition. Thus, available property combinations place several iron base alloys in direct competition with wrought products in the automotive industry. Forged plain carbon steels and the 4000, 4400, 4600 and 8600 series steels have been found suitable for transmission gears, drive shaft flanks, connecting rods, side gear and pinions, alternator poles and ring gears etc.

Other components such as bearings [166] brackets [167], bushings [168], cams [169], chain saws [170], clutch parts [171], combustion chambers drive trains [172], end plates [173], fasteners [174], gears [175], guns [176], hubs [177], knobs [178] magnetic parts [179], powder hammers [180], pulleys [181], races [182], ratchet [183], refrigerators [184], rotors [185], stockets, spark plug, straps, sprockets, torque converter transmission parts [186] and turbine parts.

The overall analysis of the parts produced through powder metallurgy had a variety of applications used under static condition of loading or used to bear marginal loads on subjected for static and dynamic conditions of loading. These conditions require the product to be metallurgically sound i.e. free from porosity, inclusions etc. This implies that the theoretical density achieved must reach as close as to theoretical density. Therefore, the soundness of the product is to be evaluated on the basis of its density.

It has been also shown earlier that densification can be obtained either repressing, upsetting, or upset-repress forgings. During repressing complete densification can not be achieved but upsetting too does not lead to complete densification whereas upset-repress condition brings down the density as close to theoretical density as possible. Literature provides enough information on the mode of densification such as through upsetting, repressing or upset-repressing process, to attain theoretical density is a remote possibility, but, however through upset-repressing very close to theoretical density can be achieved.[186-190].

Seeing, the wider aspects of the applications of powder products - the fundamentals of densification mechanism, effect of alloying elements on densification and various parameters affecting densification have been discussed in detail. Since the theoretical principles involved in densification during deformation are discussed earlier in this chapter therefore, densification mechanism has not been described in detail later in subsequent chapters. However, mode of densification, effect die constraints, temperature of forging and effect of alloying elements are detailed.



177777

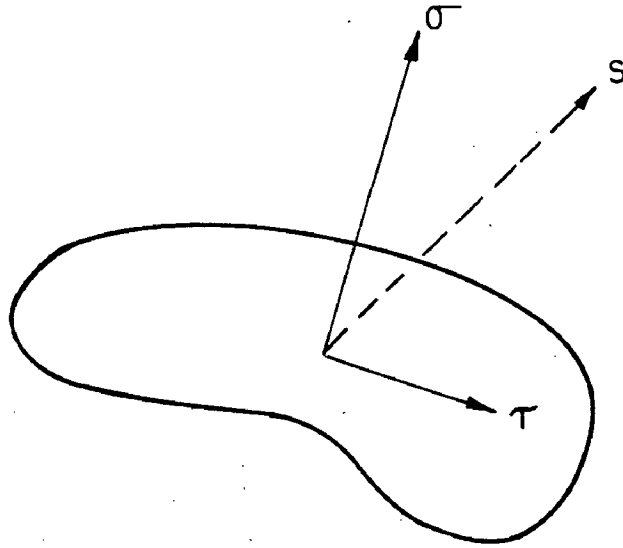


Fig.2.1—Total stress  $S$ , its normal component  $\sigma$  and its shear component  $\tau$  [119]

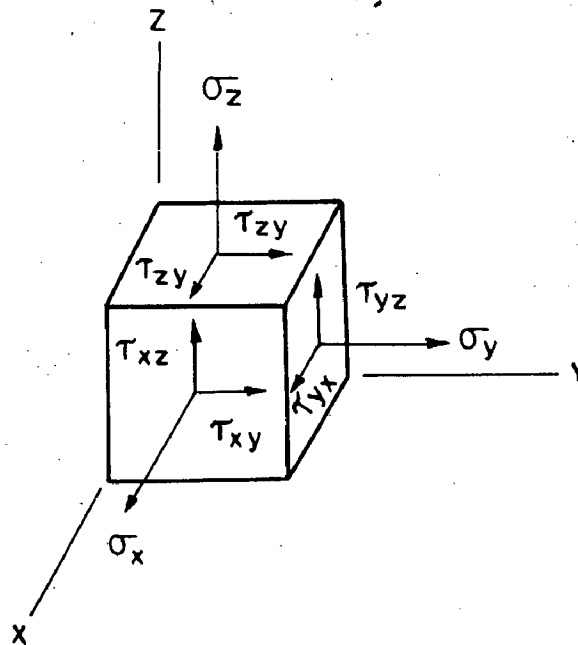


Fig.2.2—Components of total stress at a point relative to an  $x, y, z$  orthogonal system (equal stresses must act on opposite faces of the unit cube for equilibrium) [119]

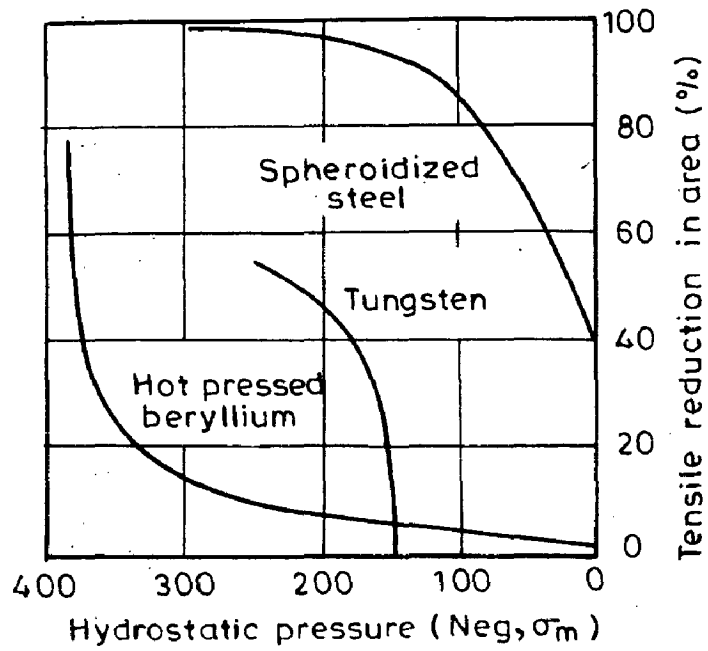


Fig.2.3—Effect of hydrostatic pressure (mean stress  $\sigma_m$ ) on tensile ductility [119]

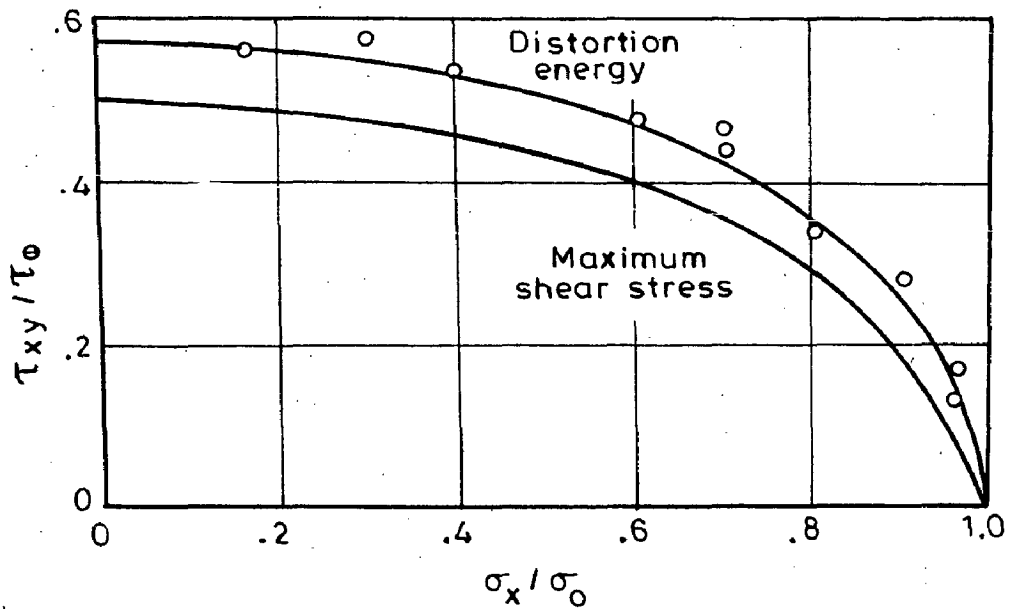


Fig.2.4—Comparison between maximum shear stress theory and von mises distortion energy theory Actual data points shown by the dots [119].



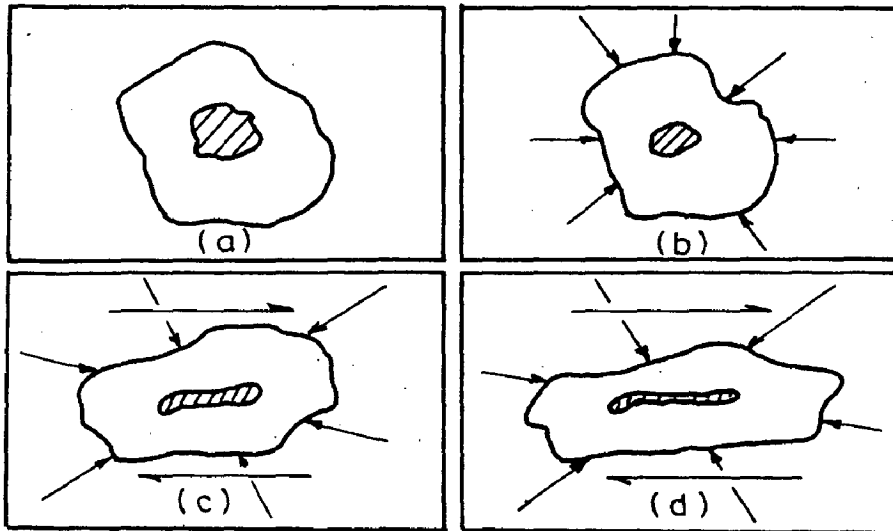


Fig.2.5 —Deformation of pores [1,127]

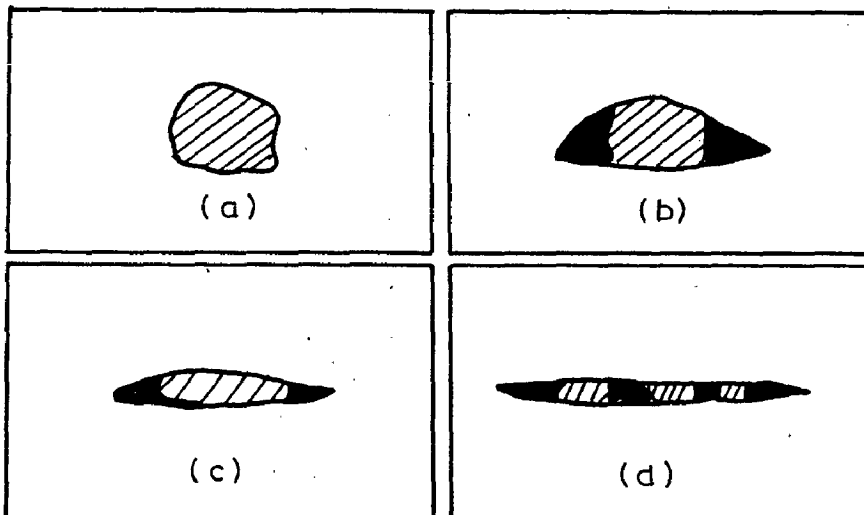


Fig.2.6 —Deformation of inclusions [127,129]

## CHAPTER - 3

### FORMULATION OF THE PROBLEM

A critical scrutiny of the literature reveals that in powder preform forging two routes are followed, to densify the sintered preform either by cold forging or by hot forging in different shaped dies. The basic purpose of forging sintered preforms - following either of the routes mentioned above, is to enhance mechanical properties of the products. Several [1,191] investigations indicate that to achieve mechanical properties comparable to wrought products, it is essential to achieve the final forged density close to theoretical density. Kahlow's proposal was that the effect of deformation in enhancing mechanical properties is two-fold :

- (1) the deformation flow pattern can alter void geometry and lower the critical pressure [192] necessary to initiate void closure, and ,
- (2) the shear induced during deformation causes sliding of the internal void surfaces of a pore which may become welded in intimate contact.

With the above in view Moyer [ 193 ] concluded in his investigation that less strain is required to achieve full density for preforms having high densities and additional work is required to produce flow necessary to promote strong bonding at interfaces caused by pore closure. In the case of low density preforms, most of the work is spent initially on closing pores and again additional work is required to attain optimum properties.

### 3.1 STATEMENT OF THE PROBLEM

" Densification Behaviour of Iron and Iron based Alloy Powder Preforms during Hot Forging. "

As the deformation in any metal forming operation is never strictly homogeneous, pore closure should also be never homogeneous. The pores situated along the surfaces of the component will never be able to close down either on account of predominance of tensile forces (at free surfaces) or of hydrostatic forces (at the die confinement) present in the dead metal zones. So it is expected that particulate structure will be prevalent at the component surfaces irrespective of the preform and die designs set for any forging operation. In the interior of the component and just below the surfaces of the component, pore closure kinetics is expected to drastically

differ and is dependent upon the preform and the die designs. The present investigation is aimed at studying in detail these aspects of pore structures and their influence on over all properties attained. It is needless to point out that while cent percent densification is never possible, our endeavour for any successful forging process should be to destroy the earlier particulate structure and build upon new refined structure at maximum possible areas inside the component. In other words interparticle pores should be effectively closed down. In addition to die and preform design, such kind of pore closure is also expected to be dependent upon :

- (1) Initial pore geometry
- (2) Composition of the metal/alloy system, and
- (3) Temperature of forging.

The choice of material and other forging parameters have been made keeping these factors in mind. The literature does not give elaborate account of these parameters with respect to pore closure.

### 3.2 SELECTION AND ALLOY COMPOSITIONS

Selection of metal/alloy composition for studying densification behaviour was not random rather it was on the basis of their industrial applications. The basic study was planned for iron, iron-carbon and

iron-phosphorus systems. The criterion of selection was on the basis of the fact that graphite admixed iron powder sintered preforms will have irregular shaped porosities after sintering. Very few of them might acquire partially round surfaces, whereas, iron-phosphorus alloy powder sintered preforms will have more stabilized rounded pores just after the sintering operation.

Following three plain carbon steels were planned for the study of densification behaviour :

- (a) 0.35 % carbon steel
- (b) 0.8 % carbon steel and
- (c) 1.3 % carbon steel.

The other steel which was also planned to be studied at a forging temperature of  $960^{\circ}\text{C}$  had the composition of 0.45 % phosphorus and balance being iron.

### 3.3 Applications of Carbon and Phosphorus Steel

#### 3.3.1 0.35 % Carbon Steel

Properties of steels containing 0.35 % carbon are likely to be improved by heat treating and, therefore, are best adapted for machine parts.

### 3.3.2 0.8 % Carbon Steel

0.8 percent carbon steels are most suitable for springs and some wood-working tools.

The above two steels come in the category of medium carbon steels. Steels containing carbon in the range of 0.35 to 0.83 percent are the most widely used steels for the construction of equipments etc. In general, steels containing less than 0.35 percent carbon do not harden appreciably by quenching [ 194 ], and, therefore, carbon composition below 0.35 % were not selected.

### 3.3.3 1.3 % Carbon Steel

Steels containing carbon in the range of 1.2 % to 1.5 % are basically useful for producing saws, files, razors, jewelers' files, balls and races for ball bearings. Therefore, a steel of carbon content of 1.3 % was also planned to be studied.

### 3.3.4 0.45 % Phosphorus Steel

Phosphorus as alloying element in steels has deleterious effect such as decreasing ductility and dynamic properties whereas amounts greater than 0.05 %P increase strength phosphorus in small amounts dissolves

in the ferrite and increases strength and hardness.

In cast irons phosphorus upto 0.30 % is added to improve fluidity. However, some cast irons contain as much as 0.90 % of phosphorus which forms, a hard, brittle compound, iron phosphide ( $\text{Fe}_3\text{P}$ ). But through the powder metallurgical route even higher amounts of phosphorus than 0.90 % could be successfully used with beneficial effects in steels [194(a),(b)]. Figure 3.1 shows the phase diagram of Fe-P system. In the present investigation Fe - 0.45 %P steel was used to study the forgeability ductility and strength.

### 3.4 POISSON RATIO

Studies conducted by Kuhn et al on cold and hot upsetting for various sintered powder preforms showed that the variation of Poisson ratio with per cent theoretical density on a log-log plot was a straight line. For values of actual density to theoretical density Poisson ratio has been reported as 0.5 which is the case for purely dense material. However, it has been also reported by them that the behaviour of Poisson ratio with respect to per cent theoretical density for Al 601 AB alloy forged at  $700^\circ\text{F}$  ( $373^\circ\text{C}$ ) is a straight line though the actual points do not approximate to a straight line (Fig. 3.2). Since Poisson ratio is one of the fundamental tools

in powder preform design and basically representing the ratio of the two true strains namely diameter strain and height strain, it needs thorough investigation. According to Kahlow and other investigators shear strains are necessary for completely closing the pores by sliding the pore surfaces and ultimately bringing them to intimate contacts. Therefore, in the light of this argument,  $\nu$  needs thorough investigation.

It is true that vast literature on sintered powder preform forging is available but they lack in evaluating  $\nu$  values in depth. In the opinion of the author the material variables such as composition and forging parameters such as level of deformation, preform geometry and initial preform density must play a role while evaluating Poisson ratio and subsequently die design for close die forgings and extrusion forging dies.

### 3.5 PORE STRUCTURES

Literature reveals [130] that the forged component when examined for metallography exhibits that pore size varies within the same component right from the centre to the periphery in the increasing order of coarseness whereas in the opinion of the author there is always a possibility of larger size pores being present anywhere in the component. This could possibly be because of the fact that, two or more



than two pores may coalesce to form larger sized pores under the condition of upsetting. During shearing action as the metal flows in the diametrical direction, kinetics of pore movement are likely to be differential in this direction. Hence, conditions are likely to be set for pore coalescence.

It is therefore proposed to investigate the problem of densification under upsetting through the careful evaluation of Poisson ratio and thorough metallographic investigations.

### 3.6 EXTRUSION FORGING

Scanty reports [195] are available in extrusion forging of powder preforms (sintered). The mode of densification through extrusion forging involves the studies of shape, size and orientation of pores in the forged product. This type of study through metallographic examination is likely to give the extent of pore deformation i.e. pore flattening under shear strains and structure might reveal the possibility of grain flow or grain deformation. With the above in view two types of extrusion forging (partially open step down cylindrical and partially open hemi-spherical) dies were designed. Effect of composition on mode of densification and pore closure kinetics were planned to be studied.

### 3.7 CLOSED DIES

Literature is in plenty [2,195] on closed die forgings of sintered ferrous alloy powder preforms. In general cent per cent density is not reported possibly due to the fact that repressing develops hydrostatic condition where final elimination of pores become difficult. Therefore, it was aimed at producing products with minimum possible residual porosities so as to obtain products having properties comparable to wrought products.

In the present investigation with the closed die forgings repressing action was planned to be introduced at various stages of deformation to find out if theoretical density of the product could be achieved. The effect of composition on the level of densification and the effect of height strain at which repressing was to be introduced with respect to densification were planned. Through the study of densification and metallurgical structure, the soundness of the product produced through these dies was planned to be examined.

### 3.8 EXPERIMENTAL APPROACH

In the light of the above it was approached to investigate the following :-

- (1) Forging through flat dies in the temperature range of 800 - 1120°C for iron, iron-carbon and iron-phosphorus sintered preforms.
- (2) Extrusion forging through partially open step-down cylindrical die for iron and iron-carbon alloys at 1120°C and iron-phosphorus alloy at 960°C.
- (3) Extrusion forging through partially open hemi-spherical die for iron and iron carbon alloys at 1120°C and iron-phosphorus alloy at 960°C.
- (4) Closed die forgings for iron and iron-carbon alloys at 1120°C at varying levels of repressing (by changing the final diameter of the product).
- (5) Closed die forgings for iron-phosphorus alloy at 960°C at varying levels of repressing (by changing the final diameter of the product).
- (6) Square cross-section bar production for mechanical testing through upsetting.
- (7) To evaluate cracking behaviour with respect to forging temperature for iron, iron-carbon and iron-phosphorus systems under upset forgings through visual observations and then quantifying them.

- (8) To evaluate the densification behaviour with respect to height strain with process parameters such as material variable as composition and forging parameter as deformation. Thus, density measurements for each sintered and forged specimen were planned.
- (9) To investigate in detail the microstructural changes and change in pore geometry during hot upsetting, extrusion forgings and closed die forgings for each metal/alloy systems.
- (10) To investigate the kinetics of pore movement in sintered preforms of iron upset forged at  $900^{\circ}\text{C}$  for  $H/D = 0.97$ .
- (11) To study the pore shape changes and the possible material movement in closing down the porosity under shear in partially open dies and then to establish the mode of densification through these type of die forgings.
- (12) To study the effect of additional stroke of the press even though the preform acquired the shape of the partially open die cavities and attained close to the theoretical density. This effect was likely to be reflected by hardness

measurements and therefore, hardness values were planned, to be taken for each forged component under partially open dies (extrusion forging dies).

- (13) Hardness measurements were planned to be taken for each deformed preform under any of the forging techniques adopted.
- (14) For upset forging, per cent height reduction, per cent diameter increase, true diameter strain, true height strain, Poisson ratio, forged aspect ratio, density, fractional density and hardness evaluation were planned to be executed.
- (15) In extrusion forging  $h_c$ ,  $h_{ct}$ ,  $v_c$ ,  $v_{ct}$ ,  $f_{hc}$ ,  $f_{vc}$  and parameters with fractional density and hardness were planned to be taken.

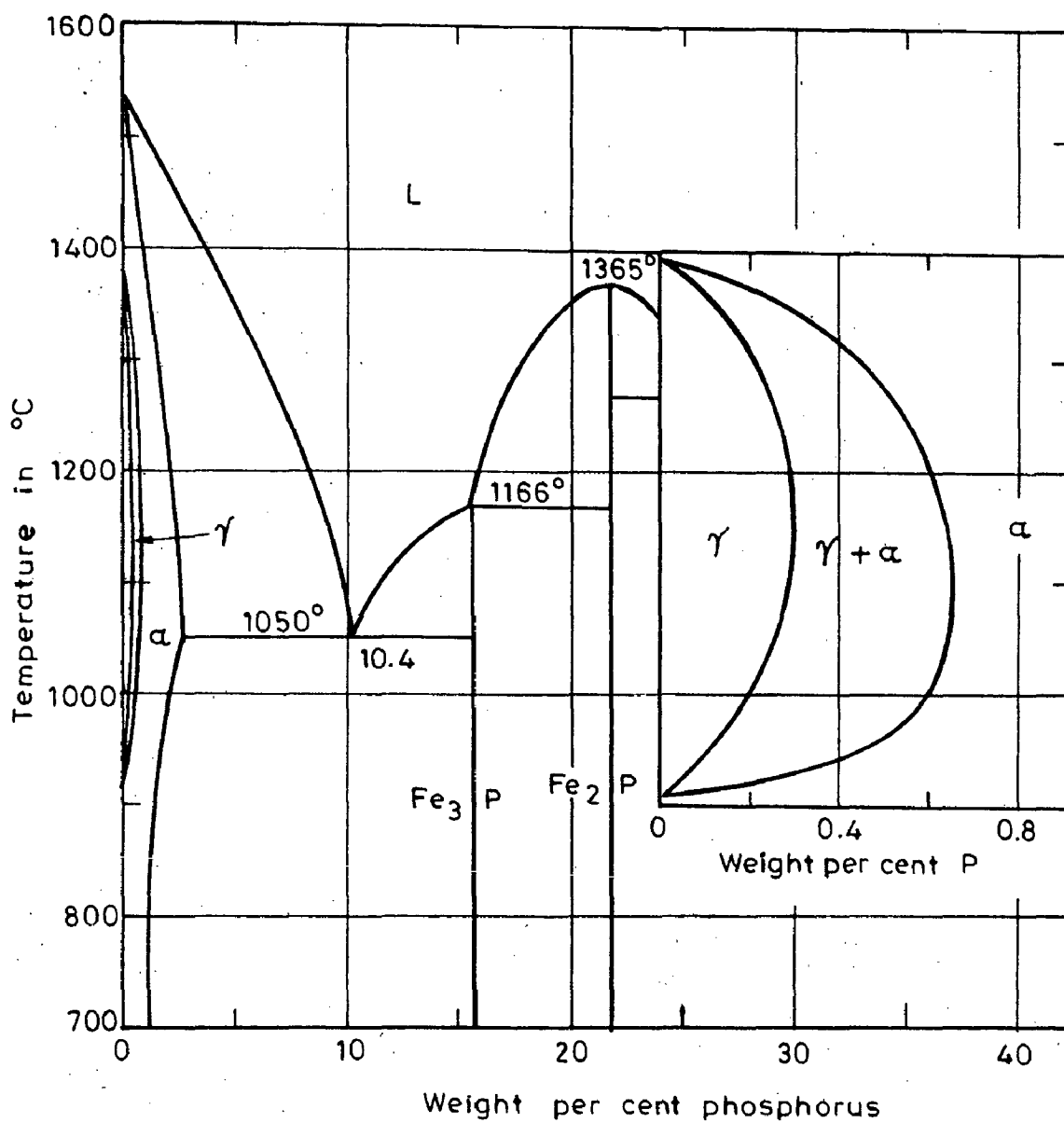


Fig.3.1- Phase diagram of iron-phosphorus system according to metals handbook eight edition, 1973 vol. 8 [17]

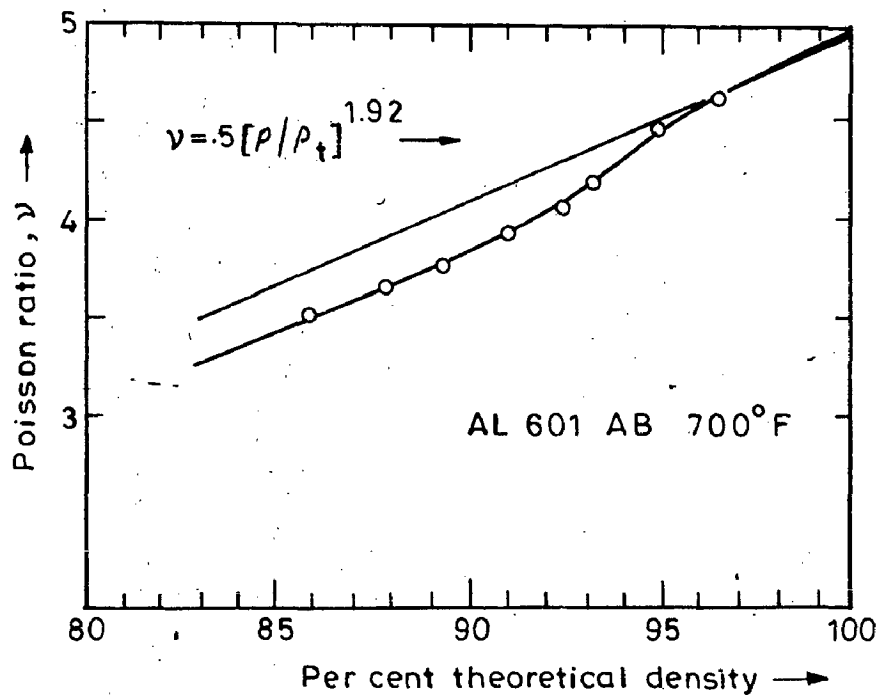


Fig.3.2-Relation between poisson ratio and density of forging of 601 AB preforms (Preform density 83%) [130]

## C H A P T E R - 4

### DESIGN CONSIDERATION IN POWDER PREFORM FORGING

Execution of any type of forging, involves basically a forging press and the most suitable set of die and punch. To design a suitable die and punch, the press details were studied and consequently the dimensions of die and punch were decided. Thus for 100 tons capacity Friction Screw Press, a set of upsetting die and punch with a working area of  $75 \times 240 \text{ mm}^2$  was designed.

Results reported by Yoshio et al [196] on hot upsetting of 0.45 % graphite admixed and those of the present investigation, under the similar conditions on forging of iron and iron based alloy powder preforms on appearance of cracks and their further enhancement in size with propagation as a function of forging temperature and percent height deformation, were utilized as basic guidelines for introducing varying modes of constraints during partially open and closed die forgings. This approach was undertaken to achieve complete densification at varying degree of constraints.

#### 4.1 PRESS CONSIDERATION

Literature [ 10 ] cites various type of presses presently in use for powder preform forgings. Since



in powder preform forging nearly 98 percent theoretical density is achieved in a single stroke involving fast pore closures and thus the mechanics of metal flow is governed by the role played by inherent porosities present in the preform. The quality of metallurgical bond depends on time of contact between preform surfaces with that of die and punch, temperature and pressure. Therefore, it is essential that the working stroke be carried out as fast as possible to avoid excessive cooling of the surface particles due to die chilling, causing thereby poor bond strengths and consequently producing a metallurgically unsound product. Hence, minimum time of contact between the workpiece and die-punch surfaces be permitted. Therefore mechanical presses, which are generally fast compared to hydraulic forging presses, must be used for hot forging [ 10 ]. Literature reports [ 10 ] that nearly 6.5 to 12.0 Tons/cm<sup>2</sup> pressure is required to achieve full density. Therefore, on the basis of available data Friction Screw Press of 100 Tons capacity was selected for the entire set of hot forging operations. Figure 4.1 shows the schematic representation of the forging press.

#### 4.2 UPSETTING DIES

Based on the above Friction Screw Press, a set of die and punch of suitable working area was designed. Holding devices for the die and punch respectively were designed as per provisions available with the press. Schematic representation of upsetting dies are shown in Fig. 4.2.

#### 4.3 PARTIALLY OPEN DIES

Partially open dies were designed with the concept that with a gradual increase in constraint, the forged density is likely to approach theoretical density at a much faster rate than what is achieved in upsetting. Keeping this in view, varying conditions of flow and constraints were introduced by step down cylindrical die. Set of experiments are proposed to be carried out with this die to evaluate dead metal zone, flow of pores and subsequent elimination of pores to enhance densification. Hemi-spherical partially open die was designed to create hydrostatic condition in the hemi-spherical portion of the die, whereas in the upper part of the die, a late application of diametrical constraint was introduced to study if at all theoretical density could be achieved under such type of constraints.

#### 4.3.1 Step-Down Cylindrical Die

Step-down cylindrical die was designed to study the rate of densification with respect to increasing amount of constraint. Criterion for design of such a die was that the hot metal (sintered preform at suitable temperature) should be allowed to flow diametrically at the upper part of the die freely while remaining confined along the lower part of the die but, however, free to flow downward along the vertical axis of the die. In order to meet these requirements, a step-down cylindrical die was designed having steps along the height of the die leading to overall decrease in diameter from 29.8 to 17 mm. Figure 4.3 shows the actual die. However, the punch used was that of the flat die.

#### 4.3.2 Partially Open Hemi-Spherical Die

Basic fundamental concept introduced by Stassi and quoted by Kuhn et al [ 197 ] if there exists only hydrostatic conditions during powder preform forging, the pore geometry, if spherical in shape, can not be closed under the application of the finite amount of force. In many cases it is expected that nearly spherical pores may not be closed as they require infinitely large amount of force.

Following equation represents relationship between pressure and pore/void geometry based on physical model [ 197 ] :

$$p = 2 \sigma_0 \left( \ln(r_0/r_i) \right) \quad \dots(4.1)$$

where,

$p$  = applied pressure

$\sigma_0$  = flow stress of the material

$r_0$  = outside radius equivalent to mean space between pores, and

$r_i$  = pore radius.

As  $r_i$  tends to zero,  $p$  required for densification becomes unbounded. With this in view hydrostatic condition, through this die, was expected to develop and thus the study of confinement on pore closure was planned. Figure 4.4 represents the Hemi-spherical die cavity.

In a hemi-spherical die gradual increase in constraint is offered in a continuous manner and when the material completely fills the die cavity it has no chance to flow further. At this stage and additional pressure applied must result in reduction in pore size leading to better densification any a sound metallurgical product. But, however, few of the pores acquire spherical shape due to prevalent hydrostatic condition in which stresses generated

across the pore (spherical shaped) are equal in all directions and thereby restricting further densification.

#### 4.4 CLOSED DIE

Literature reveals [130 ] that forgings under flat dies involve crack initiation and its propagation inside the bulged region of the specimen as the degree of deformation is enhanced. This is due to developed circumferential tensile stresses. This phenomenon is a function of such forging parameters as forging temperature, strain rate of deformation, die lubricants and the material. In general, the observations of others [196 ] and of the present investigation showed circumferential cracking after a height reduction of 50 to 60 percent and there onwards pronounced cracks developed at the bulged regions of the deformed samples. Therefore, it was decided to introduce circumferential confinement at various height reductions, varying from 30 to 55 percent. The constraint at lower height reduction was aimed to produce fast densification whereas delayed constraint was introduced to reweld the already generated cracks within the bulged regions while preform experienced upsetting practically upto this level. Figure 4.5(a) represents the closed die cavity and Fig. 4.5(b) shows the design of the rings used during closed die forgings.

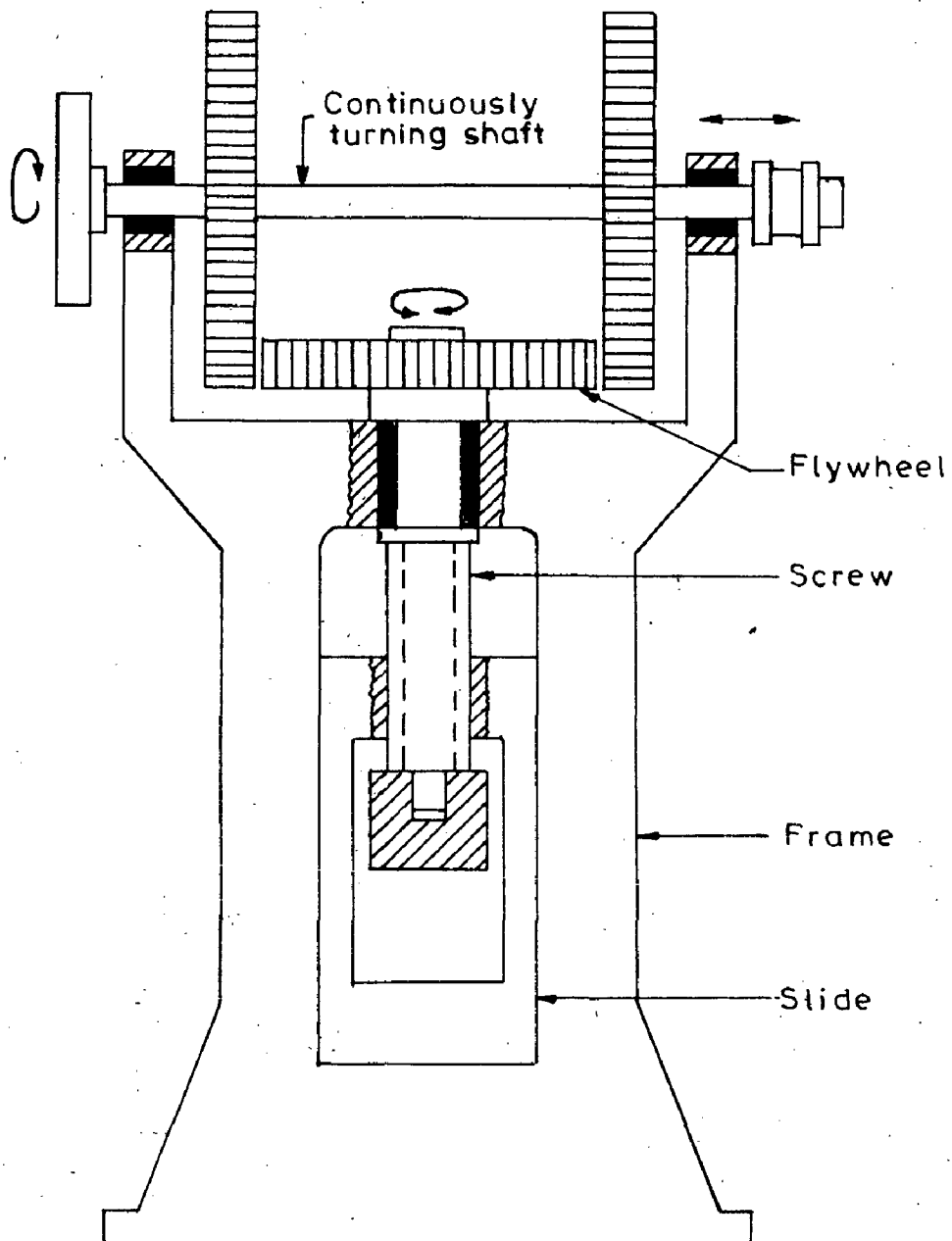


Fig.4.1-Friction screw press

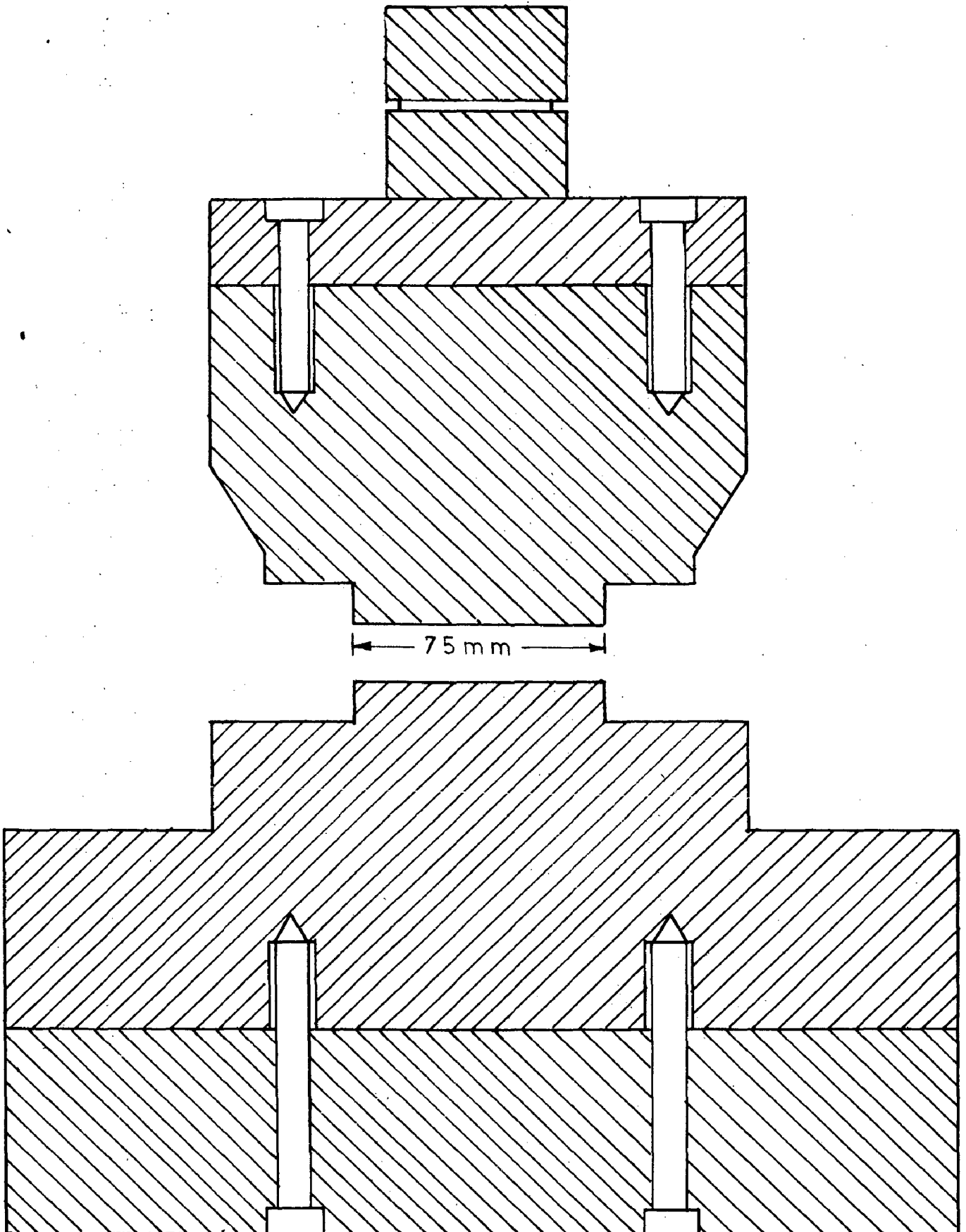
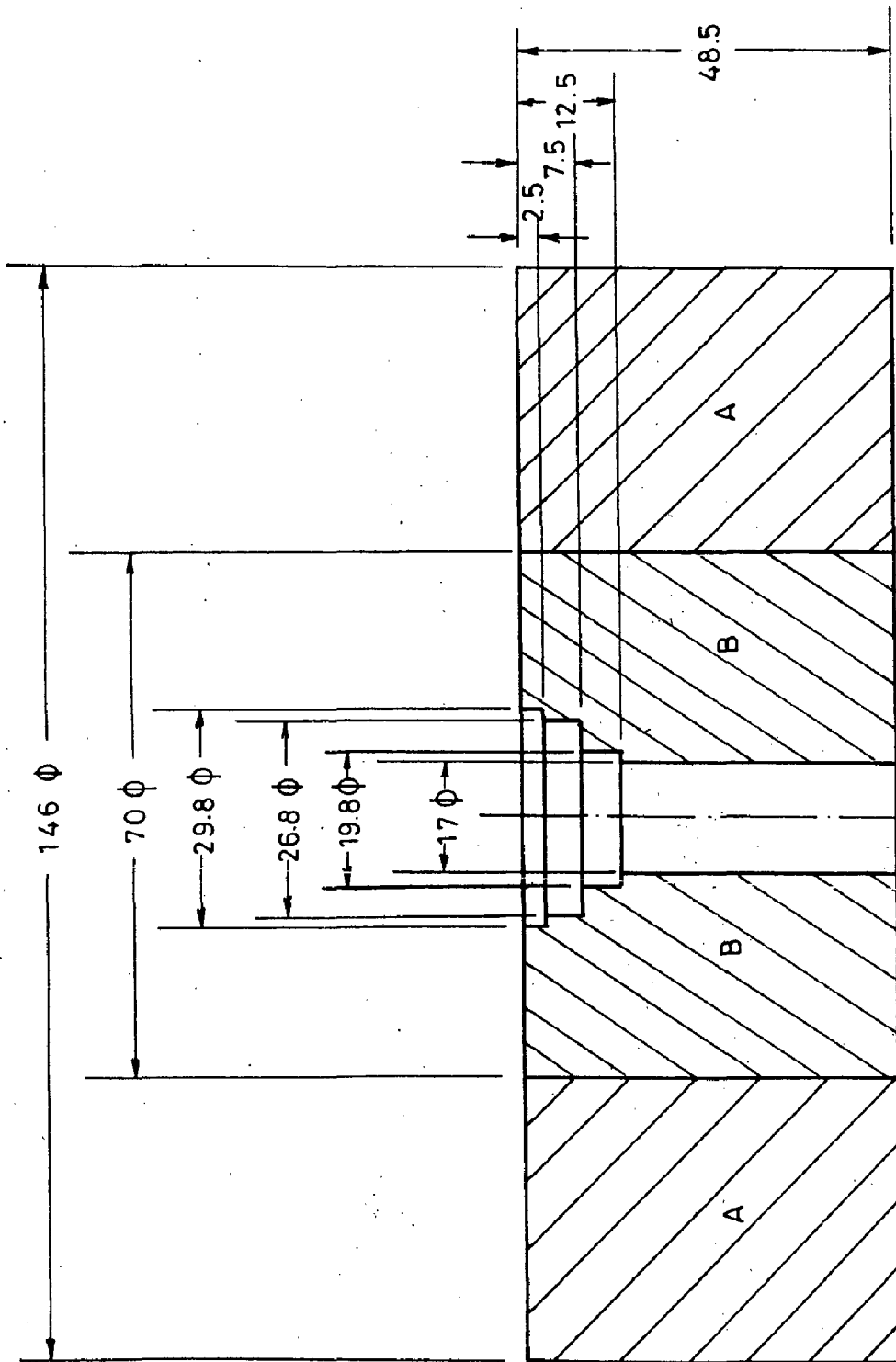


Fig.4.2-Upsetting dies



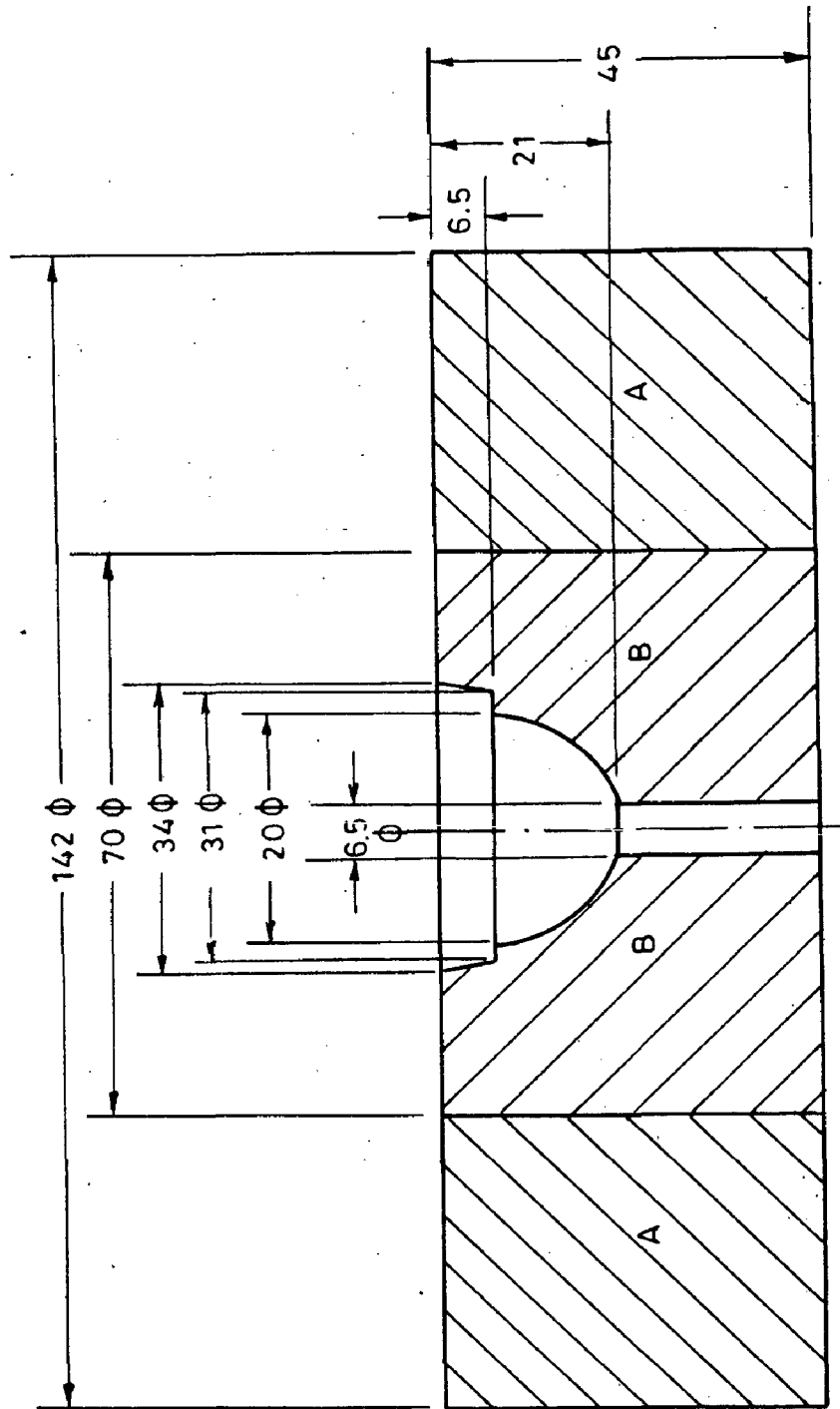
All dimensions in mm

A-A: M/S

B-B: Hot die steel heat treated to RC-42  
and shrunk fitted in A-A

Fig.4.3-Partially open step-down cylindrical die cavity





All dimensions in mm

A-A Material: M/S

B-B Material: hot die steel heat treated to

RC 42 and shrunk fitted in A-A

Fig. 4. 4--Partially open hemi-spherical die cavity

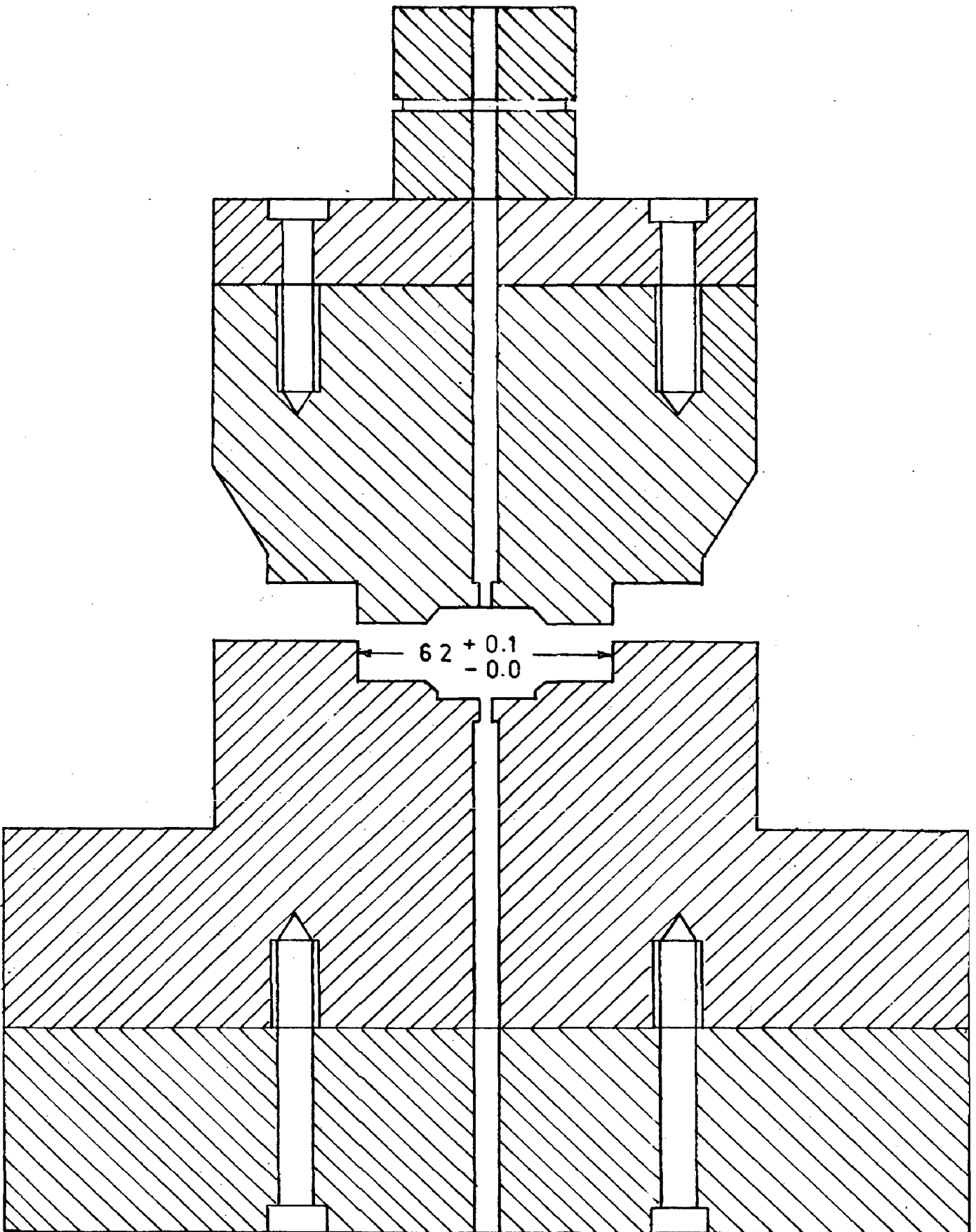


Fig. 4. 5 (a) Closed die

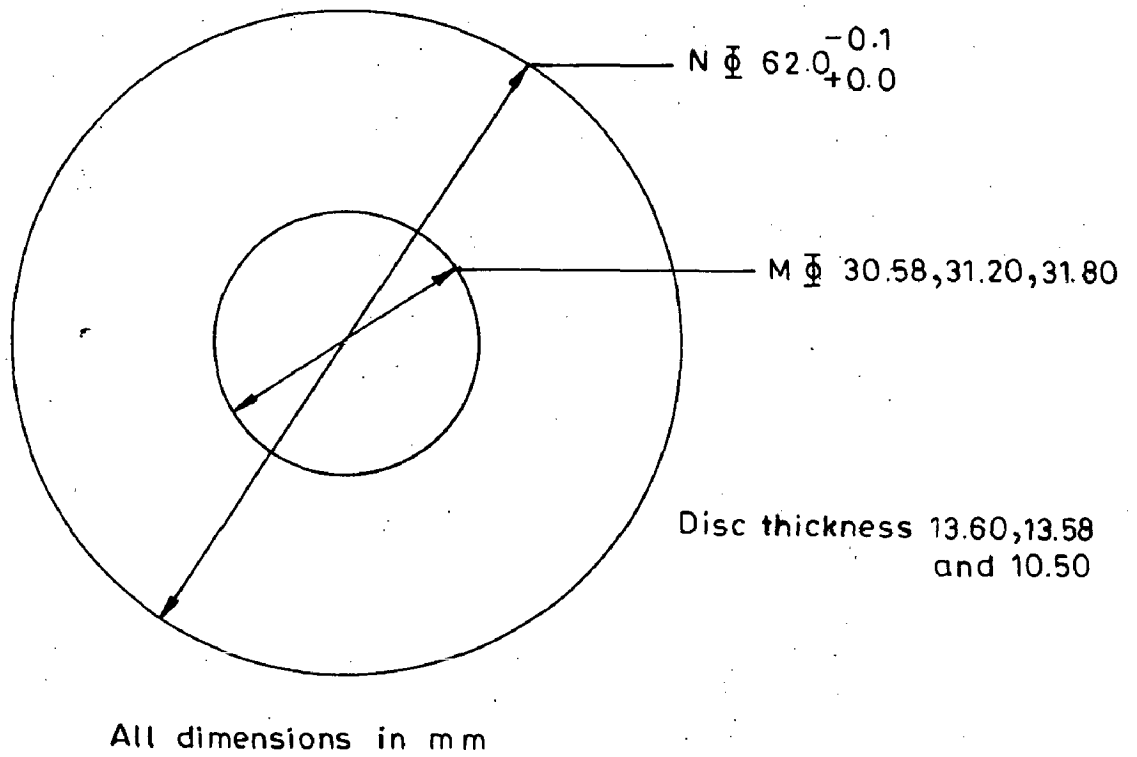


Fig.4.5(b)–Die rings of the closed die cavity

## C H A P T E R - 5

### EXPERIMENTAL PROCEDURE

This chapter deals with powder characterization, cold compaction, application of ceramic coating, sintering and subsequently hot forging of sintered preforms at different temperatures in different shaped dies.

Upsetting experiments were conducted on iron, iron-graphite admixed and iron-phosphorus alloy powder preforms of different H/D ratios. Optimum forging temperature and H/D ratio were selected on the basis of upsetting results for subsequent forgings. Kinetics of pore closure were studied in the case of iron powder preforms (H/D = 0.97) forged at 900°C. Effect of graphite addition to iron powder on densification during hot upsetting was also evaluated. Similar studies were conducted for an iron-phosphorus alloy powder.

#### 5.1 MATERIALS AND THEIR CHARACTERIZATION

Iron powder, iron powder-graphite admixed and iron-phosphorus alloy powder were characterized for flow rate, apparent density, compressibility and sieve analysis wherever it was feasible.

### 5.1.1 Iron Powder

Electrolytic iron powder, 99.7 % pure supplied by M/s Shudhakar Products, Bombay, India was used. Characteristics of this powder evaluated by standard procedures [ 198 ] are given in Table 5.1.

Table 5.1

Characterization of Iron Powder

Flow Rate Secs/ 50 gms	Apparent Density	(Sieve Analysis % )								
		+180	+150	+125	+106	+90	+63	+53	+37	-37
24	3.37	0.00	0.00	2.12	26.94	0.00	25.84	21.66	16.77	6.51

Compressibility data determined as per specification [198 ] are given in Appendix A.1 and shown in Fig. 5.1 which reveals that the powder is highly compressible.

### 5.1.2 Iron-Graphite Mixes

Three different iron-graphite mixes having 0.43, 1.14 and 1.86 percent graphite respectively were prepared using crystalline graphite powder of -300 mesh size. Mixing was carried out for a period of 10 hours using pot-mill. Samples were taken at one hour interval and after subjecting them to standard drying treatments [198 ], they were used to evaluate apparent density [198 ] and flow rate [198 ]. After having conducted the above

tests, powder samples were returned to their respective pots so as to maintain charge to ball ratio. Observations are reported in Appendix A.2 and plotted in Figs. 5.2 and 5.3. Results show that mixing for a period of 6 to 7 hours was appropriate as after this period no appreciable change was recorded in flow rate and apparent density.

Since the flow rates were observed to be poor, flow data were therefore, obtained using larger orifice [ 198 ].

Compressibility data are given in Appendices A.3, A.4 and A.5 and are plotted in Fig. 5.1 which reveals that compressibility is not appreciably affected by mixing increasing amounts of graphite with iron powder. However, compressibility becomes superior to that of iron powder.

### 5.1.3 Iron-Phosphorus Alloy Powder

The phosphorus content of the alloy was analysed, following standard procedure [199 ], to be 0.45 percent.

Flow rate and apparent density of this powder along with sieve analysis, are given in Table 5.2

Table 5.2

## Characterization of Iron - 0.45 % P Alloy Powder

Flow Rate Secs/ 50 gm	Apparent Density gms/CC	Sieve Analysis % wt.								
		+180	+150	+125	+106	+90	+63	+53	+37	-37
		0.00	0.00	6.47	34.28	0.30	25.85	16.79	11.43	3.99

Compressibility data are reported in Appendix A.6 and are plotted in Fig. 5.4 which shows that it is appreciably inferior to iron powder.

## 5.2 MICRO-STRUCTURES OF IRON AND IRON-PHOSPHOROUS ALLOY POWDER

Surface nature of the powder particle and internal porosities of iron and 0.45 % P-iron alloy were studied prior to their use in the present investigation.

### 5.2.1 Iron Powder

Scanning Electron Microscopic examination shows the iron powder particle exhibiting plane facets associated with small amount of surface porosities, Fig.5(a). This is possibly due to the fact that the pulverisation treatment after annealing electrolytic iron powder has been carried out. When seen at lower magnification particles appear longitudinal in shape with rough surfaces.

The powder particles were mounted using lucite granules for microstructural examination shows procedure described elsewhere [ 17 ] Fig.5.5(b) as per the micro-photograph of few particles. Majority of the powder particles were small but fairly rounded. Few of the particles were large and flaky. Finely dispersed porosities were observed within the powder particles. Figure 5.5(c) is the etched structure of a single big particle revealing in it the presence of few grains. However, majority of the powder particles did not show the presence of grains indicating that the powder size was smaller than the grain size in general.

### 5.2.2 Iron-Phosphorus Alloy Powder

Scanning electron microscopic examination shows the 0.45 % P-Fe alloy powder particles having surface roughness of higher order compared to iron powder particles. It appears that at the surface of the particles there is a formation of localized dendritic structure possibly because of the diffusion alloying of phosphorus with iron at the surface (Fig.5.6(a)). Figure 5.6(b) shows the magnified view of the above powder particles.

As described in Section 5.2.1 the sample was prepared and examined. Polished and unetched section shows reduced amount of internal particle porosities.



Figure 5.6(c) shows no. of particles taken together. Surfaces of these particles are fairly rough. Internal particle porosities are of lower order than that of iron powder particles. Figure 5.6(d) shows few etched particles showing no. of grains within themselves indicating that the few powder particles are large enough to have two or more than two grains whereas majority of the powder particles were smaller in size than the size of the grains. Porosities within the particles are explicitly seen.

### 5.3 GOLD COMPACTION

The powders were cold compacted in the pressure range of 4.5 to 7.5 tons/cm<sup>2</sup>. Compact diameters were kept constant, 26.8 mm. Height was varied from 15.0 to 33.0 mm to obtain different H/D ratios. To maintain the density well within  $\pm 0.01$  gm/CC range, pre-weighed powders were compacted at a given pressure for a given system. Zinc stearate was applied over the die walls for lubrication during compaction.

### 5.4 CERAMIC COATING

Stalhgaurd PM-2 ceramic coating [ 99 ] was applied to all the compacts as per procedure described in Appendix D to protect the samples from oxidation during

sintering and forging operations. The coating was first tested for high temperature protection upto  $1300^{\circ}\text{C}$  by micro-examination of the sintered specimens and it was observed that the interface of metal/coating did not contain any oxidized layer in case of iron powder compacts and decarburization to a depth 0.0 to 2.5 mm in the case of sintered iron-carbon was observed.

### 5.5 SINTERING

Ceramic coated compacts were sintered at  $1120^{\circ}\text{C}$  for one hour in Kanthal-A<sub>1</sub> wound muffle furnace.

In the case of sintering of iron-graphite compacts frequent explosions were observed when they were subjected to sintering without preheating. In such cases, therefore, an additional step involving slow heating upto a temperature of  $500^{\circ}\text{C}$  for a period of fifteen minutes was introduced prior to sintering at  $1120^{\circ}\text{C}$ . This modification completely eliminated the chances of explosion in these compacts.

### 5.6 SOAKING TREATMENT

Soaking treatment was carried out in another muffle furnace. The temperature was controlled to  $\pm 10^{\circ}\text{C}$ . All those samples which were forged at temperatures lower than  $1120^{\circ}\text{C}$  were transferred after

sintering to this furnace. The sintered samples were allowed to remain in this furnace till they attained uniform temperature prior to forging. The soaking temperatures were selected in the range of 800-1000°C. Soaking was done for half an hour after attaining the given temperature.

### 5.7 FORGING

Sintered preforms were forged at pre-selected temperatures to various deformation levels on a Friction Screw Press of 100 ton capacity. Each forged compact was immediately transferred to oil bath at room temperature to retain the forged structure and to avoid any further oxidation. The time taken in the whole process of transferring the compact from furnace to the forging platform and after forging, to oil quenching bath was well within 3-5 seconds.

In the case of iron-phosphorus alloy, forging was carried out only at 960°C using all sets of dies of different shapes.

Following types of forging experiments were carried out :

### 5.7.1 Upset Forging

Hot upsetting was carried out for three different H/D ratios namely 0.57, 0.98 and 1.17 for sintered iron preforms in the temperature range of 800° to 1120°C to evaluate densification during forging. Similar experiments were carried out for graphite admixed iron powder (H/D ratios being 0.57 and 0.98) and for iron-phosphorus alloy powder (H/D ratio being 0.59). Working faces of die were lubricated with graphite powder.

### 5.7.2 Partially Open Die Forging

Sintered preforms (H/D ratio, 1.16 to 1.18), in case of iron and iron-carbon alloys, were forged only at 1120°C in partially open dies (details are given in Chapter-4). Iron-phosphorus preforms were sintered at 1120°C for one hour but forged only at 960°C.

### 5.7.3 Closed Die Forging

Closed dies as described in Chapter-4 were chosen to forge various iron, iron-carbon sintered alloy at 1120°C and 0.45 % phosphorus-iron sintered preforms at 960°C. The aim of the closed dies was to obtain complete densification. The H/D ratio for these dies were chosen in the range of 1.16 to 1.18.

#### 5.7.4 Upset Forging For Square Section

Cylindrical specimens (H/D ratio 1.16) were upset forged from two sides to produce bars of square section (14 x 14 x 75) mm<sup>3</sup> for making specimens for tensile and impact tests. The temperature during this forging dropped from 1120° to 800°C whereas for iron phosphorus alloy the higher temperature range was restricted to 960°C.

#### 5.8 REMOVAL OF CERAMIC COATING

Residual ceramic coating was removed by grinding. The ground specimens were further smoothed using emery paper for density and dimensional measurements. This procedure of removing ceramic coats was made common to all specimens to keep uniformity.

#### 5.9 DIMENSIONAL MEASUREMENTS

For all upset forged samples cleaned in the manner specified in Section 5.9 measurements of heights and diameters were made. Minimum of three readings were taken for each dimension and were averaged. Dimensional measurements were also done prior to removal of residual coating. No substantial difference was noticed in the dimension in both the cases. The difference in the measurements of height

and diameter in both the cases, i.e., with and without coating were of the order of 0.3 to 0.5 mm and 0.15 to 0.20 mm respectively. Thus, dimensions were measured on the cleaned specimens for calculating degree of deformation diametrical flow,  $\lambda_n$  (height strain) and forged aspect ratio.

Similarly, dimensional measurements were carried out on the specimens of partially open dies and closed dies so as to reproduce the geometry of the forged specimen in such a way that all the deformation parameters could be calculated.

#### 5.10 DENSITY MEASUREMENTS

Density measurements as per I.S. 4841-1968 [200] of the forged component at various deformation levels were conducted for all the cleaned specimens. During the course of experimentation the room temperature varied quite widely, hence temperature corrections were incorporated [ 201 ].

Key Roy balance having sensitivity of  $10^{-3}$  gm was used. Porous specimens were dipped in liquid paraffin wax to prevent the water from entering into the pores. Before weighing the specimens, the excess wax was removed from the outer surface of the forged specimens. However, this treatment could not be given to samples which were heavily deformed.

### 5.11 HARDNESS MEASUREMENTS

Hardness measurements were carried out using Vickers Hardness Testing Machine on suitably prepared surfaces.

10-12 indentations were taken over each sintered/forged specimens and averaged.

### 5.12 TENSILE TEST

Basically tensile test specimens were prepared from the double sided forged samples as described in Section 5.8.4. Minimum of three test samples were used to evaluate the tensile properties. It was conducted on motorized Monsanto Tensometer, Type 'W' at a strain rate of 1.6 mm/minute at room temperature. Specimen details are described elsewhere [ 202 ]

### 5.13 IMPACT TESTS

Standard Charpy impact specimens [ 203 ] were prepared and they were annealed at 850<sup>o</sup>C for two hours before conducting the actual tests. These tests were conducted on Impact Testing Machine using Charpy impact attachments.

#### 5.14 CHEMICAL ANALYSIS

Chemical analysis was performed on sintered alloys and their compositions are given in Table 5.3 Carbon analysis was made on 'Leco' equipment.

Table 5.3

Chemical Analysis For Carbon.

Per cent Graphite Admixed	Analysis of Sintered Alloy	Analysis of Forged Component
0.00	0.00	0.00
0.43	0.35	0.35
1.14	0.83	0.83
1.86	1.36	1.36

#### 5.15 METALLOGRAPHIC STUDIES

Metallographic studies were carried out to study the kinetics of pore closure in iron powder preforms upset forged at 900°C. Deformed surface layer developed during grinding was removed by deep etching using 5 % nital for a period of 2-3 minutes and then samples were repolished gradually and gently to avoid any further formation of deformed layer. Finally wheel polishing was done on a sylvet cloth using 3-5  $\mu$  alumina dispersed



in water. Polished surface was cleaned by acetone and dried. Polished and etched structures were recorded using Metavert Incident Light Microscope Model No. 2 GA.

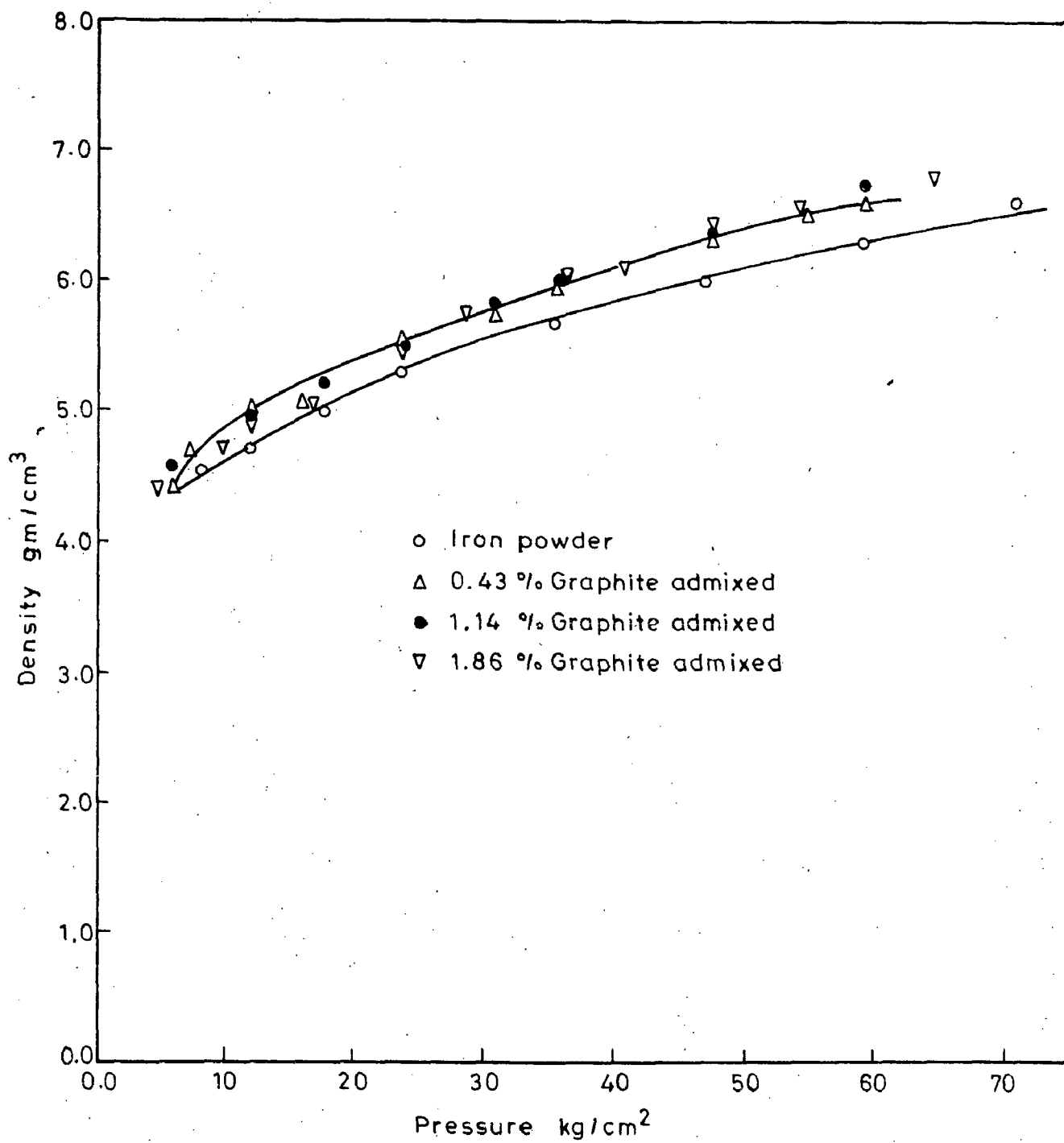


Fig.5.1- Compressibility plots of iron and graphite admixed iron powder

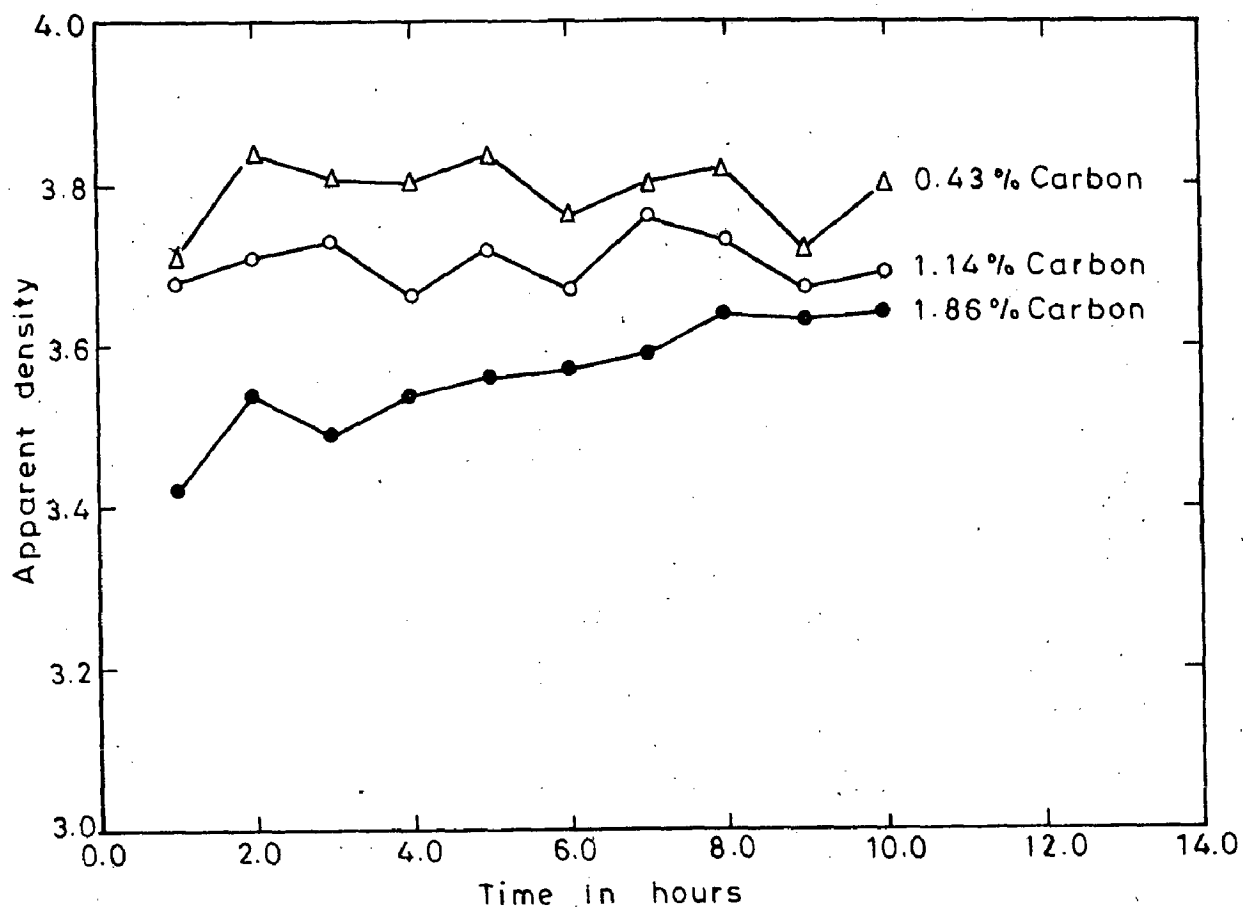


Fig 5.2- Apparent density v/s time of mixing of graphite powder in iron powder

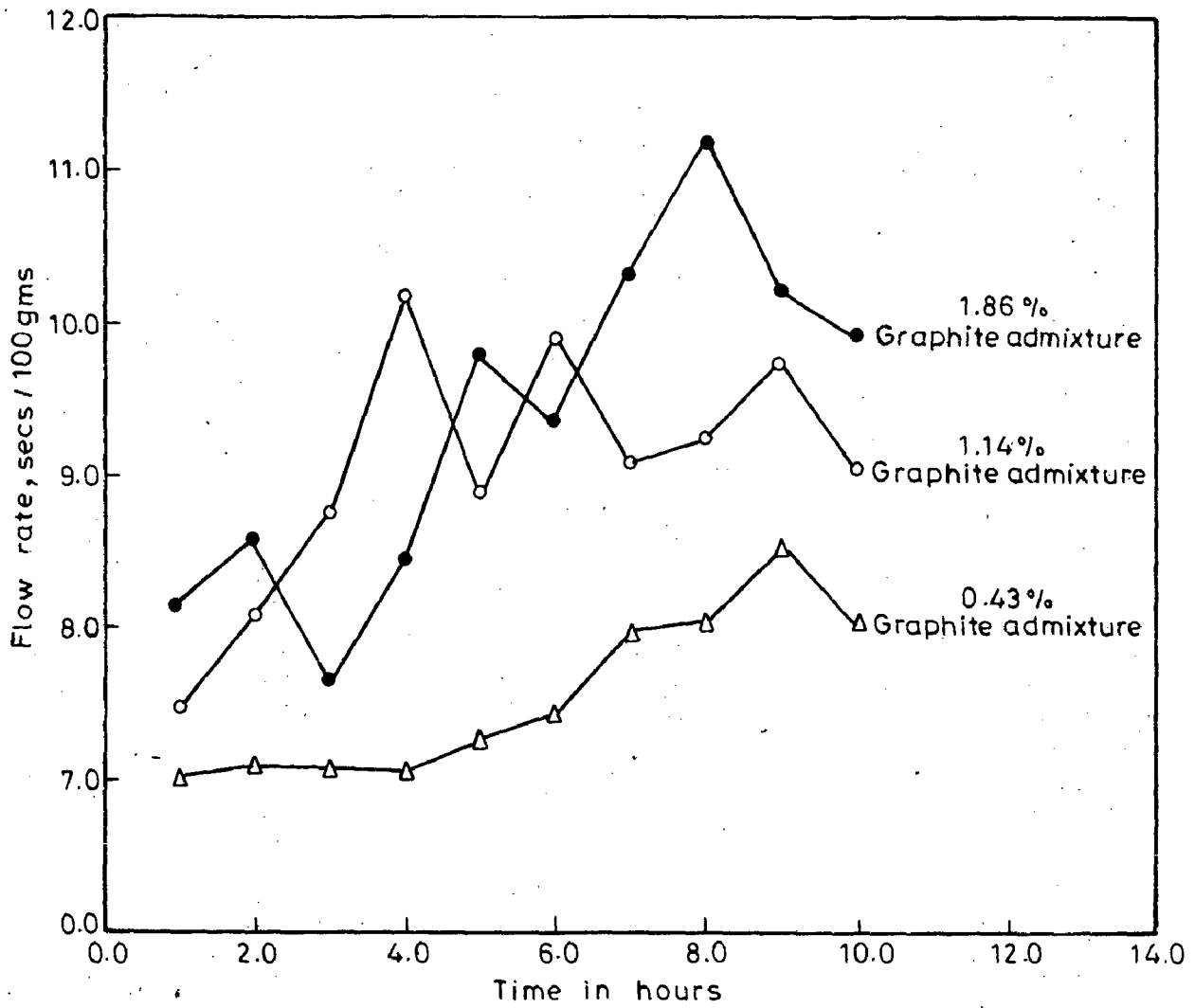


Fig.5.3-Plot of flow rate v/s mixing time of graphite powder in iron powder

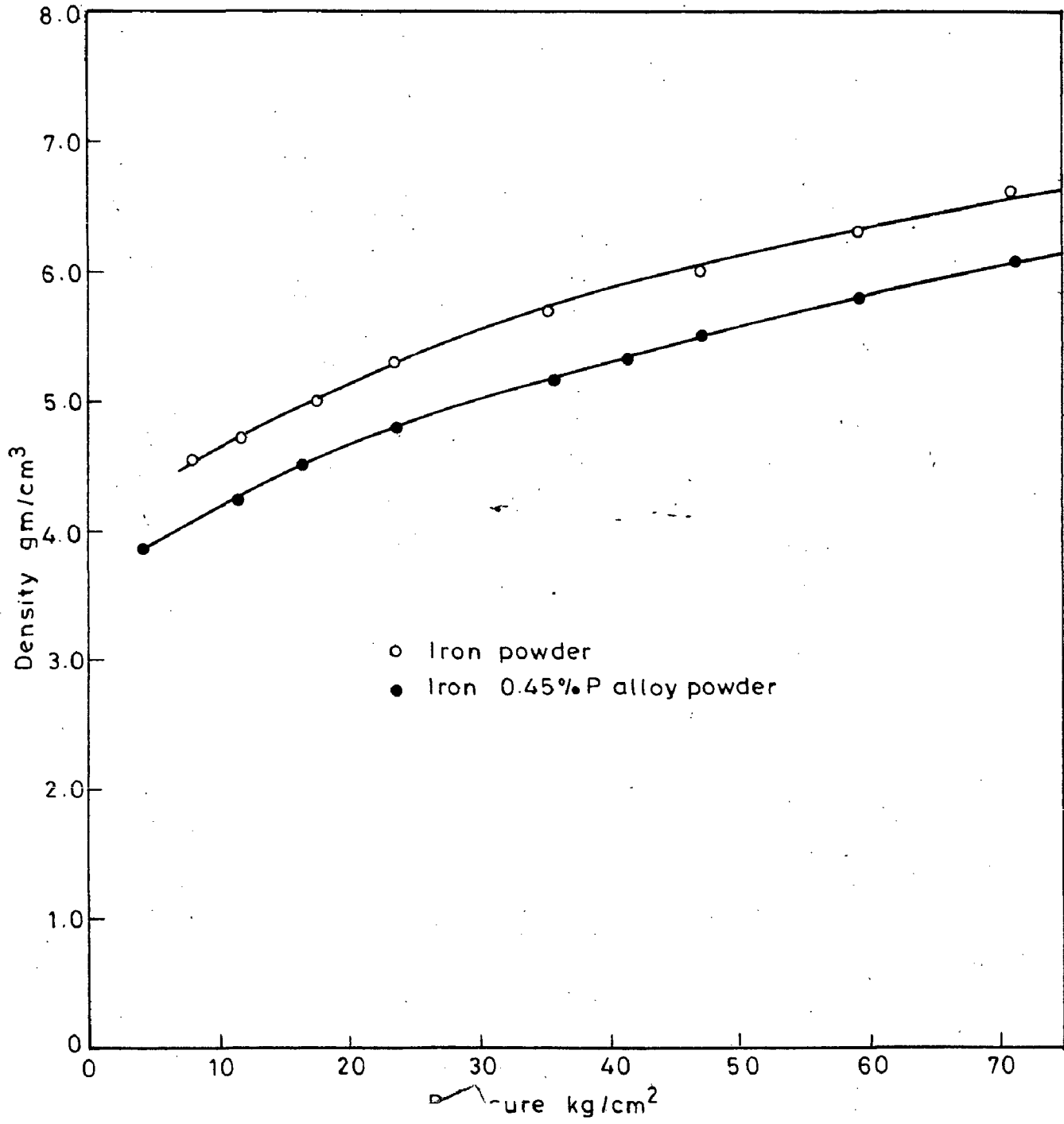
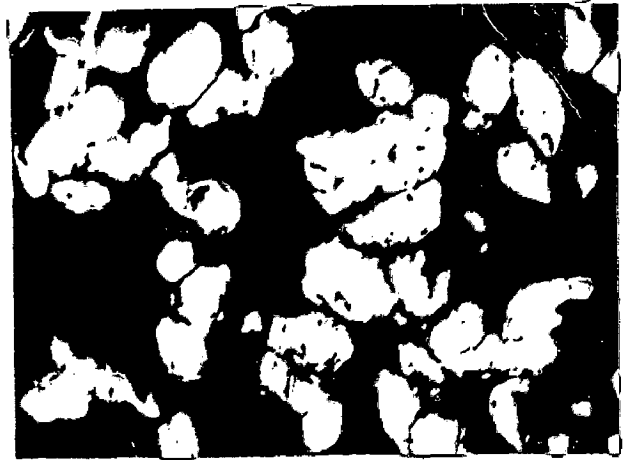


Fig 5.4

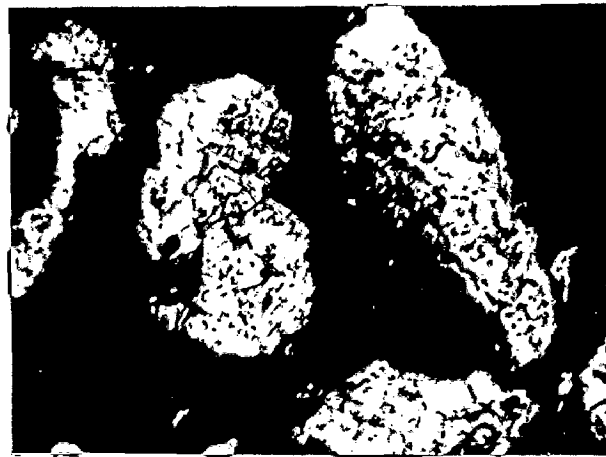
and iron-phosphorus alloy powder



(a)

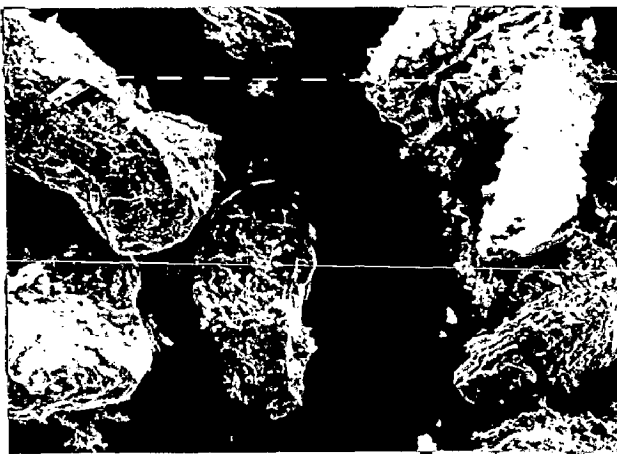


(b)

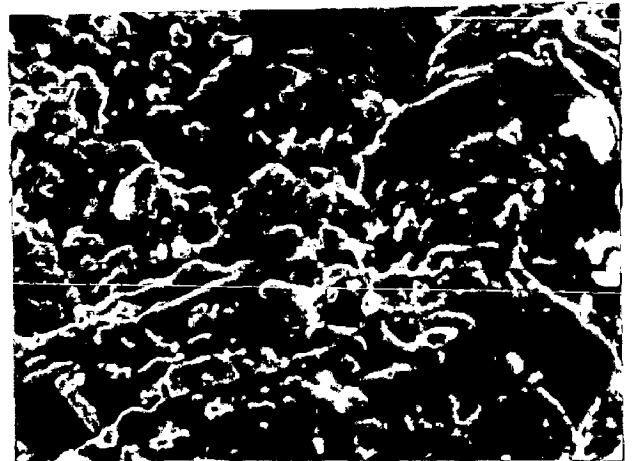


(c)

FIG. 5.5



(a)



(b)



(c)



(d)

FIG. 5.6

## CHAPTER - 6

### RESULTS AND DISCUSSION

Present chapter deals with the results obtained from upset forging, partially open die (step-down cylindrical and hemi-spherical) forging and closed die forgings of iron, iron-carbon and iron-phosphorus powder preforms. These results are basically analysed and discussed for densification behaviour with respect to suitable parameters.

Upsetting experiments were carried out for sintered preforms of iron and iron-carbon alloys for varying H/D ratio in the temperature range of 800-1120°C. However, iron-phosphorus alloy powder preforms (sintered), H/D = 0.59 were upset forged at 960°C. Densification behaviour was evaluated w.r.t. forging parameters, preform geometry and alloy composition etc. Cracking behaviour w.r.t. temperature of forging is also discussed for each type of sintered powder preforms.

Results of partially open dies are discussed in the light of new parameters such as  $h_c$ ,  $h_{ct}$ ,  $v_c$ ,  $f_{hc}$ ,  $f_{vc}$  and  $\bar{Q}$  defined later in this chapter. Mode of densification w.r.t. above parameters and their geometrical relationships among themselves are highlighted.

Detailed pore morphology has been conducted. On the basis of the above findings pore shape changes leading to densification is discussed.

Closed die forgings were carried out for obtaining components in the theoretical density levels. Sintered preforms of H/D ratio 1.18 and temperature of forging as  $1120^{\circ}\text{C}$  were maintained for each type of powder preforms except iron phosphorous alloy powder. Sintered preforms of phosphorous-iron alloy were forged at  $960^{\circ}\text{C}$ . Results of these forgings are discussed in the light of metallurgical structures.

Hardness of each forged component under each type of forgings were taken and are discussed w.r.t. percent theoretical density.

Wherever possible, empirical relationships were developed and compared with the existing relations.

Mechanical properties such as tensile strength and impact strengths were carried out. Results are discussed and compared with the results of the other workers.

#### 6.1 UPSETTING OF IRON, IRON-CARBON AND IRON PHOSPHORUS POWDER PREFORMS

During upset forging of iron, iron carbon and iron-phosphorus powder preforms it was noticed that



densification is never complete and the pore distribution inside the hot forged product always remains heterogeneous. Larger pores segregate just near the free surfaces of the product and finally give rise to crack formation at higher deformations whereas smaller pores remain distributed throughout the component and their shape, size and size distribution is dependent upon forging parameters, alloy composition etc. The tendency of crack formation through larger pores situated near the free surface is also dependent upon the alloy composition. Sintered preforms of iron were subjected to detailed study as it forms the base of other alloy compositions and thereafter the behaviour of other alloys was investigated. In the following sections, effect of preform geometry, deformation parameters, forging temperature and composition on densification has been described. Also described are cracking behaviour, density variations inside the forged products, hardness, micro-structural changes, kinds of pores, their movement and closure during forging. Wherever possible, empirical relationships have been developed and compared with those developed earlier [ 130 ].

#### 6.1.1 Height Strain Versus Percent Theoretical Density

Figures 6.1(a) and 6.1(b) show the effect of height strain on percent theoretical density for

sintered iron powder preforms under hot deformation. The increasing strain shows increase in density and for the same strain value increasing temperature of forging (in the temperature range of 800-1120°C) favours densification. The curves shown in Figs.6.1(a) and 6.1(b) corresponding to different forging temperatures and different H/D ratios exhibit similar trend and can be expressed mathematically as a polynomial of second order.

Increasing H/D ratio of the powder preform delays densification by shifting these curves to higher height strain values and at the same time depressing these curves to lower percent theoretical densities. However, the nature of these curves do remain the same. Figure 6.2 shows the effect of H/D ratio on densification for sintered iron preforms forged at 800° and 1120°C. It can be observed that increasing H/D ratio leads to poorer densification at a given temperature and height strain. To compare these quantitatively, 99.4 % theoretical density is attained at 1120°C at 0.55 height strain value for H/D = 0.57 whereas to attain the same level of densification for H/D ratios of 0.99 and 1.17 at 1120°C, it is required to incorporate a strain of the order of 0.75 and 1.15 respectively.

Figures 6.3 and 6.4 show the densification plots with respect to height strain for 0.35 % C-Fe

whereas Figs. 6.5 and 6.6 represent for 0.83 % C-Fe while Fig. 6.7 is for 1.36 % C-Fe. Observations of these plots reveal that their nature is parabolic. Figures 6.3, 6.5 and Figs. 6.4, 6.6 are for H/D ratios of 0.57 and 0.99 respectively whereas Fig. 6.7 shows both H/D ratios taken together.

Increasing level of carbon in sintered iron based preforms also affects densification. However, upto 0.83 % carbon the effect is not much predominant, but, corresponding to 1.36 % carbon the density values are much lower as well as their attainment is at fairly high values of strains. Figure 6.8 shows the effect of carbon on these curves drawn for fixed H/D ratio (0.57) and temperature ( $1120^{\circ}$ ). The family of curves drawn for various carbon contents, H/D ratios and temperatures do not exhibit any noticeable change from what has been stated above. Another important general observation about carbon steel forgings is that although densification is poorer compared to that of sintered iron preforms - the level of deformation to which these could be deformed without cracking increases with increasing carbon content upto 0.83 %. This indicates that the forgeability improves by carbon addition upto 0.83 % within the temperature range of  $800-1120^{\circ}\text{C}$ .

Figure 6.9 shows the plot between percent theoretical density attained and percent carbon in steels for different H/D ratios, namely 0.57 and 0.98 for a forging temperature of  $1120^{\circ}\text{C}$  at a height strain of 0.5. The effect of H/D ratio at higher carbon levels on these plots appear to enlarge.

Figure 6.10 shows the relationship between height strain and percentage theoretical density for iron - 0.45 % P alloy powder sintered preform (H/D=0.59) upset forged at  $960^{\circ}\text{C}$ . The rate of densification in this alloy is of the same order as that of pure iron or iron - 0.35 % carbon steel. However, the alloy exhibits comparatively better deformability during forging as height strain of the order of 1.1 could be incorporated in this alloy without resulting any cracking in the forged component. It is therefore, most ideal alloy to forge amongst the compositions studied in the present investigation.

During upset forging it has been reported [130] that densification is never complete. The reasons for incomplete densification are presence of the dead metal zones inside the component and predominance of tensile forces along the free surface of the component. As a result, density varies to considerable extent inside the forged component. Since similar results were obtained in the present investigation also, it was decided to quantitatively assess this variation

with different levels of hot deformation. The components were first sectioned along the forging direction and square shaped prisms were cut from the different locations across the diameter of the component. The density of these prisms were plotted against the ratio of distances of the centre of these prisms with respect to the centre of the component and the radius of the component ( $r/r_{\max}$ ). Figure 6.11 shows the density variation of these prisms for sintered iron components forged at  $900^{\circ}\text{C}$  ( having H/D ratio = 0.57 and 0.98 ). Assuming density variation with the prisms as negligible (being very small in size compared to that of the component), the density was observed to be highest near the centre of the component and lowest towards the periphery. It was also observed that the difference in density levels inside the component decreases with increasing deformation levels. However, the peripheral region always remains porous irrespective of amount of deformation imparted to the component. It is also clear from these results that presence of dead metal zones confined near the centre of top and bottom surfaces of the component do not affect the density values as effectively as the porosity situated along the periphery of the component. At higher deformation levels the peripheral porosity leads to initiation of cracks.

It was further observed that the deformation required to initiate such cracks is a function of forging temperature and preform geometry (H/D ratio). From Fig. 6.12, it is clear that higher H/D ratio shows delayed cracking with respect to percent height deformation when compared to lower H/D ratio. However, density achieved in case of higher H/D ratio is lower. Increasing temperature also delays cracking but its dependency on cracking behaviour is not as strong as preform geometry. It is therefore imperative to employ higher forging temperatures and introduce die constraints at suitable level of upsetting to avoid these cracks. The data on cracking as illustrated above has been employed to design closed forging dies used in the present investigation with a view to obtain optimum densification and deformation without resulting in cracking.

On comparing the cracking behaviour of carbon steels it was noticed that 0.83 percent carbon steel specimens resisted cracking to the best possible extent. Figure 6.13 shows the comparative pattern of cracking of 0.35, 0.83 and 1.36 percent carbon steels samples (H/D ratio being 0.57-0.58 and 0.98-0.99). It may also be observed that the forging temperature retards cracking, however, at higher temperature the curves representing cracking behaviour tend to flatten i.e. cracks are bound to occur at certain strain value

- Preform density range lies 84-87 % of the theoretical value
- Preform geometry is in the range of  $H/D = 0.57 - 1.17$
- Height strains (  $\ln(H_0/H_t)$  ) lie in the range of 0 - 1.18
- Forged samples do not crack.

Table 6.1 gives the values for  $a_0$ ,  $a_1$  and  $a_2$  corresponding to different forging temperatures and H/D ratios. Here  $a_0$  is a constant corresponding to initial preform density.  $a_1$  and  $a_2$  are temperature and preform dependent factors. From the table it is clear that  $a_1$  always remains positive, and, therefore it contributes toward densification, however  $a_2$  is negative and its influence leads to consistent values of density at high strain values. The values of these constants suggest that increasing forging temperature favours densification while effect of H/D ratio is not well defined through these constants. Tables 6.2, 6.3 and 6.4 give the values of these constants corresponding to different carbon steels. While Table 6.5 shows the constants involved in the evaluation of the characteristic nature of the density vs height strain for 0.45 % P-Fe alloy powder sintered preform ( $H/D = 0.59$ ) upset forged at  $960^\circ\text{C}$ . Here too, the above argument holds good.

Table 6.1

Coefficients of Parabolic Curves of the Form :  $y = a_0 + a_1x + a_2x^2$  for Iron Powder Preforms during Hot Upsetting.

Temperature °C	H/D = 0.57			H/D = 0.97			H/D = 1.17		
	a <sub>0</sub>	a <sub>1</sub>	a <sub>2</sub>	a <sub>0</sub>	a <sub>1</sub>	a <sub>2</sub>	a <sub>0</sub>	a <sub>1</sub>	a <sub>2</sub>
800	0.864	0.310	-0.194	0.847	0.251	-0.112	0.825	0.305	-0.159
900	0.868	0.303	-0.168	0.849	0.282	-0.143	0.832	0.307	-0.164
950	0.874	0.271	-0.120	0.852	0.281	-0.144	0.834	0.308	-0.165
1000	0.868	0.338	-0.218	0.857	0.276	-0.136	0.844	0.311	-0.179
1120	0.868	0.413	-0.339	0.864	0.284	-0.146	0.849	0.311	-0.180

$$y = \left( \frac{\rho_f}{\rho_{Th}} \right) ; x = \left( \frac{h_0}{h_f} \right)$$



Table 6.2

Coefficients of Parabolic Curves of the Form  
 $y = a_0 + a_1x + a_2x^2$  for 0.35 % C-steel Sintered  
 Preforms during Hot Upsetting.

Temperature °C	H/D = 0.57			H/D = 0.99		
	$a_0$	$a_1$	$a_2$	$a_0$	$a_1$	$a_2$
800	0.866	0.321	-0.210	0.851	0.264	-0.132
850	0.866	0.356	-0.257	0.854	0.276	-0.144
900	0.871	0.357	-0.261	0.856	0.286	-0.156
950	0.870	0.362	-0.263	0.859	0.293	-0.164
1000	0.872	0.363	-0.265	0.861	0.304	-0.178
1120	0.875	0.360	-0.265	0.866	0.308	-0.182

$$y = \left( \frac{\rho_f}{\rho_{Th}} \right) ; x = \left( n \left( \frac{H_o}{H_t} \right) \right)$$

Table 6.3

Coefficients of Parabolic Curves of the Form  
 $y = a_0 + a_1x + a_2x^2$  for 0.83 %C-steel Sintered  
 Preforms during Hot Upsetting.

Temperature °C	H/D = 0.57			H/D = 0.988		
	$a_0$	$a_1$	$a_2$	$a_0$	$a_1$	$a_2$
800	0.839	0.315	-0.193	0.823	0.277	-0.147
850	0.844	0.310	-0.190	0.825	0.274	-0.137
900	0.844	0.328	-0.209	0.825	0.284	-0.143
950	0.846	0.340	-0.223	0.824	0.307	-0.167
1000	0.848	0.345	-0.227	0.828	0.290	-0.143
1120	0.852	0.349	-0.231	0.826	0.312	-0.164

$$y = \left( \frac{\rho_f}{\rho_{Th}} \right) ; x = \ln \left( \frac{H_o}{H_t} \right)$$

Table 6.4

Coefficients of Parabolic Curves of the Form  
 $y = a_0 + a_1x + a_2x^2$  for 1.36 %C-steel Sintered  
 Preforms during Hot Upsetting.

Temperature °C	H/D = 0.57			H/D = 0.988		
	$a_0$	$a_1$	$a_2$	$a_0$	$a_1$	$a_2$
800	0.841	0.316	-0.214	0.831	0.209	-0.092
850	0.845	0.308	-0.204	0.830	0.226	-0.104
900	0.844	0.324	-0.221	0.830	0.244	-0.118
950	0.847	0.325	-0.218	0.835	0.243	-0.121
1000	0.848	0.338	-0.226	0.833	0.262	-0.131
1120	0.852	0.332	-0.220	0.834	0.273	-0.140

$$y = \left( \frac{\rho_f}{\rho_{Th}} \right) ; x = \ln \left( \frac{H}{H_t} \right)$$

Table 6.5

Coefficients of Parabolic Curve of the form :  $y = a_0 + a_1x + a_2x^2$  for 0.45 %P-Fe Alloy Powder Sintered Preform ( $H/D = 0.59$ ) during Hot Upsetting.

$a_0$	$a_1$	$a_2$
0.862	0.269	-0.140

$$y = \left( \frac{\rho_f}{\rho_{Th}} \right) \quad ; \quad x = \left( n \left( \frac{H_o}{H_t} \right) \right)$$

Table 6.6

Variation of  $a_1/a_2$  with Composition, Forging Temperature and H/D Ratio.

Temp. of Forging  °C	Alloy Composition  %C	H/D ratio	
		0.57 - 0.58 ( $a_1/a_2$ )	0.97 - 0.99 ( $a_1/a_2$ )
800	0.00	1.60	2.24
	0.35	1.53	2.00
	0.83	1.63	1.88
	1.36	1.48	2.27
900	0.00	1.79	1.97
	0.35	1.39	1.92
	0.83	1.63	2.00
	1.36	1.51	2.17
950	0.00	2.26	1.95
	0.35	1.39	1.79
	0.83	1.53	1.84
	1.36	1.49	2.00
1000	0.00	1.55	2.03
	0.35	1.37	1.71
	0.83	1.52	2.03
	1.36	1.50	2.00
1120	0.00	1.22	1.94
	0.35	1.36	1.69
	0.83	1.51	1.90
	1.36	1.51	1.95

Table 6.6 shows the variation of ratio  $a_1/a_2$  with composition, forging temperature and H/D ratio. Higher value of this ratio means better rate of densification and hence faster pore closure during the range of deformation stated earlier. However, this ratio is not the sole factor for predicting final density achieved after forging because the final density is a function of initial preform density as well. It may be pointed out that barring iron preforms all other carbon steels preforms exhibit characteristic values of this ratio for different forging temperatures but the value is higher in general for 0.83 % C steel meaning thereby that 0.83 %C steel exhibits better densification when compared with other compositions. At higher H/D ratio the value of  $a_1/a_2$  also increases for all compositions and forging temperature. This means that higher H/D ratio offers better rate of densification. However, the final density values corresponding to higher H/D ratio are poor (see Fig. 6.14). This appears to be so because the initial preform densities are lower corresponding to higher H/D ratios. Similar effect of H/D is observed for other carbon steels. Figures 6.15 to 6.17 show the effect of forging temperatures on densification for a fixed amount of height strains for different H/D ratios for 0.35, 0.83 and 1.36 % carbon steels respectively. The close observations of these plots show that higher H/D ratio for a given

amount of fixed deformation always shows lower order of densification for each composition. With the above in view it is disadvantageous to select higher H/D ratio for hot upsetting.

### 6.1.3 Poisson Ratio

It has been pointed out earlier [130] that Poisson ratio for porous powder preforms always remain lower than 0.5 (a value corresponding to that of 100 percent dense metal) during hot/cold deformation. This fact is verified in the present investigation also. However, till now Poisson ratio has so far been understood as material constant only but the present investigation provides additional information about Poisson ratio.

Figures 6.18 to 6.20 show the plots of diameter strain with respect to height strain for iron powder sintered preforms of varying H/D ratios (0.57, 0.97 and 1.17) deformed under hot upsetting in the temperature range of 800-1120°C. Figures 6.21 and 6.22 show the similar plots for 0.35 %C steel, Figs. 6.23 and 6.24 for 0.83 %C steel, Figs. 6.25 and 6.26 for 1.36 % steel, for H/D ratio of 0.58 and 0.99 respectively. Figure 6.27 shows the plot for 0.45 % P steel for H/D ratio of 0.59. These plots in general reveal that they fall below the theoretical line and become parallel to this line in the late stage of

deformation. This observation predicts that Poisson ratio will always remain less than 0.5.

Figure 6.28 shows the variation of diameter strain with height strain for various carbon steels and H/D ratio. While plotting this curve it was observed that temperature of forging (within 800-1120°C) has virtually no effect on it. Similarly carbon content of the steel also does not show significant effect on it but H/D ratio does alter the position of the curve. Higher H/D ratio depresses this curves towards lower diameter strains, meaning thereby, diametrical spread of preforms having larger H/D ratio is of lower order for any given height strain. In this figure there is a theoretical line corresponding to  $\nu = 0.5$ . It appears that the preforms of higher H/D ratio tend to deviate more from the theoretical behaviour (corresponding to dense metal) than those having lower H/D ratio. This observation implies that the behaviour of preform is dependent upon the number of pores and their mode of change during deformation.

Figure 6.29 shows the comparison of sintered iron preforms and Iron - 0.45 %P preforms in regard to these strain variations. It may be seen that 0.45 %P steel is relatively closer to the theoretical curve indicating thereby that the behaviour of this alloy is similar to that of 100 % dense metal as far as deformation is concerned. This may be attributed to



simultaneous flow of rounded pores and the material.

In Figs. 6.28 and 6.29 it is further observed that the experimental curves become parallel to theoretical curve at higher high strain values. This means that after attaining certain level of densification the poisson ratio rises towards theoretical value of 0.5 corresponding to that of 100 % dense metal.

Figures 6.30 to 6.32, 6.33 to 6.34, 6.35 to 6.36 and 6.37 to 6.38 are the plots of poisson ratio with percent theoretical density of the forged components having different compositions with varying H/D ratios. These plots show that temperature has no effect on these curves, however to see the effect of H/D ratios on  $\nu$  values Figs. 6.39 to 6.43 were drawn (without showing actual data points). It was observed that H/D ratio does affect the position of these curves. The general pattern of these curves indicate that there are three stages of variation of  $\nu$  with respect to density. In the first stage there is rapid rise of  $\nu$ , the second corresponds to steady state rise and the third stage again shows rapid rise of values. These stages remain consistent with respect to density irrespective of composition, temperature and H/D ratio. For instance, Stage-II starts from 90-92 percent of theoretical density and Stage-III starts from 98 percent theoretical density. When the components approach to theoretical density the Poisson ratio tends to attain 0.5 (a value corresponding to

100 percent dense metal as per theoretical deductions [130] . Fluctuations of experimental data in Stages-I and II are of fairly high order whereas in Stage-III the data points are confined close to the curves drawn.

The three different stages in these curves are well defined in case of iron at lower H/D ratios (see Fig. 6.39) while the first stage in other carbon steel compositions is not well defined. Steep rise in Poisson ratio in Stages- I and III suggests that material movement and pore movement are simultaneously of high order leading to large geometrical variations in the component. The first stage, however, is due to the fact that pore movement and pore shape change predominates the pore closure. Whereas, the third stage corresponds to the fact that pores, whatever, left do not close down and their movement is again of the same order as that of remaining material. In other words the pores have been stabilized in the structure just like a second phase and thus, become part and parcel of the structure. In this stage, therefore, although the Poisson ratio rises fast but it never approaches theoretical value and the density of the material also remains lower than theoretical density. Stage-II is an actual stage of densification where Poisson ratio remains somewhat consistent and density changes are quite fast. In this stage pores close down at a faster rate while there is gradual change in the geometry of the component during forging. Summing up

the three stages - Stage-I could be described as the one where pore maintain their separate identity as regards material movement. Stage-II where pore collapse is faster leading to better adjustment between material and pores. Stage-III corresponds to a stage where pore closure is practically not operative and it becomes part of the structure itself

Effect of H/D ratio and composition of steel on Poisson ratio curve is not very significant. Both these parameters do not affect the nature of the curve as described above, however, these parameters do shift the position of curve. Higher H/D ratio in general shifts this curve to higher  $\nu$  values. Composition of steel upto 0.83 %C does not show any significant shift but 1.3 %C steel shows fairly significant upward shifting of the curve (compare Figs. 6.39, 6.40, 6.41 and 6.42). Phosphorous in steel again appears to shift this curve very significantly (compare Fig. 6.39 and 6.43).

A mathematical relationship has been worked out to relate  $\nu$  with percent theoretical density in Stages I and II of these curves. It was possible to predict the position of this curve from this relationship within  $\pm 5\%$  accuracy.

Figure 6.32 shows the variation of  $\nu$  with percent theoretical density for H/D = 1.17 for iron powder sintered preform during hot upsetting in the temperature range of 800 - 1120°C. The effect of

forging temperature is again negligible. The curve converges to  $\rho = 0.5$  corresponding to 100 percent dense metals/alloys. However at lower values of density the fluctuations in  $\rho$  values is fairly substantial. The increasing porosity lowers down  $\rho$  value to very appreciable extent. An empirical relationship has been worked out to relate  $\rho$  with percent theoretical density (in the range of 84-100 %) which predicts the experimentally obtained values within  $\pm 5\%$  accuracy. The relationship is as follows :

$$\rho = 11.78 \left( \frac{\rho_f}{\rho_{Th}} \right)^2 - 19.84 \left( \frac{\rho_f}{\rho_{Th}} \right) + 8.54$$

This relationship differs from the one proposed by Kuhn et al

$$\rho = 0.5 \left( \frac{\rho_f}{\rho_{Th}} \right)^2$$

for hot upsetting of aluminium powder preforms.

The reason for difference in relationships lies with the fact that it is strongly dependent upon H/D ratio. In fact H/D ratio in the present case is 1.17 whereas in the case of Kuhn's investigation it was varied in between 0.37 to 0.94. Higher H/D ratio shows faster rate of densification in the beginning and the later stages show practically steady state densification and ultimately the final stages do not incorporate much densification but show steep rise in  $\rho$  values.

#### 6.1.4 Hardness Versus Per Cent Theoretical Density

Figures 6.44 to 6.46 represents hardness vs per cent theoretical density for sintered iron powder preform during hot upsetting in the temperature range of 800-1120°C for three different H/D ratios namely 0.57, 0.99 and 1.17 respectively. These hardness data with respect to per cent theoretical density at different temperatures do not show any regular behaviour. However, maximum data points can be bound within a band of the lower and upper lines. Data points falling far away from this region are ignored. However, the last two H/D ratios namely 0.99 and 1.17 show the divergence of the band. A mean line for hardness vs percent theoretical could, however, be drawn passing through the mid region of all the hardness bands. This implied that H/D ratio merely contribute towards hardness fluctuations in case of iron.

Figures 6.47 and 6.48 show the plots of hardness vs per cent theoretical density for 0.35 % carbon steel for two H/D ratios (0.58 and 0.99). Figure 6.47 exhibits linear behaviour at different forging, temperatures. All the lines appear to be parallel and spacing may be due different quenching conditions after forging. However Fig. 6.48 approximates to a single straight line corresponding from these curves that quenching response of these products is dependent on the pore structure because pores are poor conductor of heat.

Figure 6.53 shows the plot of hardness versus per cent theoretical density of 0.45 %P steel for H/D ratio equal to 0.59. This is a straight line behaviour indicating that hardness is a linear function of per cent theoretical density. At maximum theoretical density its hardness is nearly equal to 177 VPN which is far superior than iron and slightly inferior to 0.35 per cent carbon steel.

For carbon steels containing carbon in the range of 0.35 to 1.36 per cent, a general conclusion would be drawn such as higher H/D ratios are favourable for uniform hardness as well as higher values of hardness.

#### 6.1.5 Metallographic Studies

Structural details of iron, iron-carbon alloys and iron-phosphorus alloy are discussed in this section. Iron, 0.35 per cent carbon and 0.45 per cent phosphorus steel are discussed in detail whereas 0.83 and 1.36 per cent carbon steels too are discussed in detail but only selective micro-photographs are reproduced. Wherever, necessary inferences are drawn from direct micro-structural observations under the microscope.

### 6.1.5.1 Iron Powder Sintered Preform Upset Forged at 900°C

Figure 6.54 represents the pore morphology of sintered and sintered deformed products. Deformation level was varied from 0.0 to 53 per cent. Polished unetched pore morphology is qualitatively assessed. These structures were taken directly at the centres of the specimens. Figure 6.54(a) shows the pore morphology of sintered iron-powder preforms. The observations shows that the structure retains particulate structure. At places large sized coalesced pores (dark region) are seen. Figures 6.54(b) and (c) both show the pore structures more or less in the same deformation level (39.6 and 42 %). It is noticed that pore shape, size and its distribution is practically uniform. However, Fig. 6.54(d) shows finer pore morphology associated with few coarser pores at places. Thus, pore size varies in the decreasing order from 0.0 to 53 % deformation. Evidence of pore flattening in the direction of diametrical flow of metal during deformation is also exhibited.

While scanning each of the sintered and sintered deformed iron-powder preforms under the microscope, a regular pattern of coarser pores in the direction of diametrical flow has been noticed. Figure 6.55 shows the plot of per cent height reduction with relative position of the coarse pores. This plot

clearly demarcates the regions of fine pores, mixtures of fine and coarse pores, virtually pore free region and extremely coarse pores. These observations show that either the pores have moved differentially in the direction of the diametrical flow of the material or few of the smaller pores have come together and coalesced. This plot also depicts the clear cut movement of the pores as deformation level is raised. Visualizing the individual curves one can assess that coarse pores near to the centre of the preform move with the faster rate compared to other two locations of the coarse pores in the direction of diametrical flow of the material. After this practically a stage comes when pore movability inside the forged preform is practically nil with respect to degree of deformation. As the deformation is further enhanced pore movability is increased. All these observations lead to conclusion that there is a pore movability inside the deformed preform and their movability rate is a function of degree of deformation during hot upsetting. It is also established that four clear cut regions inside the forged preform exist and they are as follows :

- (i) a fine pore region from the centre upto the curve no.(1)
- (ii) a region between curves (1) and (2) - a mixture of fine and coarse pores



- (iii) virtually pore free region of extremely fine pores in between curves (2) and (3), and
- (iv) a region of coarse pores - away from curve (3) upto the bulged region.

One of the most significant observation was that size of the coarse pores in region (ii) and (iv) varied in the increasing order of size. Table 6.7 shows the deformation with respect to relative position of the coarse pores in a forged preform :

Table - 6.7

Per cent Deformation With Respect to the relative position of the coarse pores

Percent Deformation	Relative position of the coarse pores w.r.t deformation in a given deformation		
	$\left(\frac{r}{r_{\max}}\right)_1$	$\left(\frac{r}{r_{\max}}\right)_2$	$\left(\frac{r}{r_{\max}}\right)_3$
11.15	0.439	0.683	0.779
26.15	0.658	0.782	0.853
41.92	0.659	0.784	0.866
53.08	0.727	0.831	0.886

Figures 6.56(a), (b) and (c) show the polished and etched structure of sintered iron-powder preform at three different locations. Figure 6.56(a) shows the particle identity and pore distribution along the

particle boundaries. At places coarser pores are seen. Figure 6.56(b) shows very low order of porosity near free surface, whereas practically at the free surface very high order of porosity of larger size are seen. The identity of particulate structure is still retained. Figure 6.56(d) shows the grain structure associated with fairly high order of porosity (dark regions). Pore flattening in the direction of metal flow is not explicitly seen whereas Figs.6.55(e) and (f) show the grain structure at 40 and 53 per cent of deformation respectively. Directionality of pore flattening in the later two cases is lost. White region in all the micro-photographs represents the typical structure of ferrite, whereas black region shows porosity. At the low deformation ( per cent height reduction of 11 per cent ) material has undergone microstructural changes such as recrystallization with substantial decrease in pores (Fig.6.56(d)). The individual sintered particles have undergone recrystallization and the internal particle porosity is not affected. On further deformation (40 to 53 per cent height reduction), the grain size becomes finer and so the pore size. Internal porosities within the grains still persists (Figs. 6.56(e) and 6.56(f)). Pore shape appears to be rounded at higher deformation.

### 6.1.5.2 0.35% C-Steel Upset Forged at 900°C

Sintered and polished specimen of 0.35 % carbon steel shows irregular shaped but fairly interconnected pores all along the interparticle boundaries which is in conformity to the expected results. However, Fig.6.57(a) shows the etched structure at 250 X (magnified six times) having pearlite and ferrite structure associated with porosities. Figure 6.57(b) shows the same structure as shown in Fig.6.57(a) taken at 500 X (magnified six times). While observing the specimen deformed nearly 50 % it is seen that pores are more or less very fine in size and uniformly distributed. One of the edge shows rounded equal sized, randomly distributed pores indicating that the 'dead metal zone' is practically free of the material movement and hence densification.

Polished and etched specimen shows very fine grain structure at the centre (Fig.6.57(c)) and also in the vicinity of the centre very fine ferrite-pearlite structure, Fig.6.57(d), is noticed. This structure predominantly remains the same while scanning the specimen for a long distance in the direction of flow of material. Figure 6.57(e) shows coarse equiaxed grains with pearlitic structure associated with rounded porosity but finer than the sintered structure.

One of the bulged edges show coarse structure whereas the other edge shows fine structure relatively. Fairly good amount of pores are present at or near the surface. Coarser structures are present with coarser pores more in amount and finer structure with finer pores. This effect is possibly present, because of the fact that differential quenching might be responsible.

#### 6.1.5.3 0.83 % Carbon Steel

Figure 6.58(a) shows sintered 0.83 %C steel under polished condition at the centre of the specimen. It can be observed that good number of pores are generally rounded. At few places cock-tail appearance is also visible. The pore shape, size and its distribution is more or less uniform. Porosity in comparison to pure iron sintered preform is much less here. Particle identity is not noticeable. Pores are also finer in size compared to sintered pure iron preform.

Heavily deformed (50 % height reduced) polished unetched specimen shows very low order of porosity whereas some localized places show higher concentration of pores of larger sizes. However, the micro-photographs are not reproduced here. Very fine eutectoid structure is observed in etched samples. Few places (bright areas)

show the presence of cementite though in traces noticed under light etched condition. No cementite network is seen. Decarburisation appears to be practically nil as all across the specimen complete pearlitic structure is observed. One of the extreme edges of the bulged portion shows very little decarburisation where extremely fine structure is observed.

The entectrid structure observed above are 100 % pearlitic but at places cementite structure was also observed which indicates the presence of localized concentration in the form of iron carbides.

#### 6.1.5.4 1.36 % Carbon Steel

The sintered 1.36 % steel shows the thin network of iron-carbide as compared to the closed die forgings. No micro-photographs are reproduced here. The deformed specimen (55-58 % height reduced) shows porosity of extremely low order whereas polished and etched specimen observed under the phase contrast shows thick carbide network associated with finer network too. Evidence of recrystallization is seen.

Carbon additions show virtually no or very less order of porosity in the heavily deformed specimens whereas actual density measurement shows poorer densification in case of carbon steels.

#### 6.1.5.5 0.45 % P-Fe (Phosphorous- Steel)

Sintered specimen shows distributed porosity of not very high magnitude. Pores are more or less rounded (Fig. 6.60(a)). Pore concentration near the outer surface (Fig.6.60(b)) of the bulged region is of the higher order than at the centre.

Polished and lightly etched specimen reveals the structure at the centre showing few of developed grains which are rounded. No pitting is observed within the grains indicating that pores are practically eliminated from the grains during sintering. Whereas at the grain boundaries pitting of high magnitude is observed. Grain boundaries are explicitly visible. Porosities (black regions) too are observed but less in number (see Fig. 6.60(c)). Near the edge, Fig. 6.60(d) shows coarse porosity and finer grains with thick boundaries.

Specimen having gone a deformation ( % height reduction ) of the order of 50-55 per cent shows very clearly the pore flattening. Collapsibility of pores are explicitly visible. Width of the collapsed pores are reduced in the centre of the specimen compared to that of close to the free surface.

Polished and etched specimen shows the tendency of grain flow (Fig.6.60(f)) in the direction of the diametrical flow of the material. Some places show the development of recrystallized grains Micro-photographs

have been taken under the phase contrast. Edges show lower order of porosity compared to that of pure iron and other carbon steels investigated in the present study. This is possibly due to the fact that phosphorus helps to enhance densification of much faster rate.

## 6.2 PARTIALLY OPEN DIES

Before discussing the results obtained from partially open die cavities, the mode of deformation, geometry of die cavities, constraint parameters are highlighted. New parameters are defined.

During forging, sintered powder preforms show the tendency of assuming the shape of the die cavity. Depending upon the load applied during forging or in other words depending upon the forged density, the preform flows into the die cavity to the extent of applied load which is distributed in performing the following :

1. Spent in pore closure
2. Spent in overcoming the frictional forces of the die walls
3. Spent in plastically deforming the preform.

All above mentioned factors ultimately result in enhancing the density of the product.

In case of the hemi-spherical die cavity there is a continuous change in shape of forged component and therefore, it is anticipated that the pores present in the preform will assume the flow pattern as the geometry of the die cavity. On the basis of the change of the shape, size and orientation of the pore with respect to the densification pattern, it is possible to predict the mode of flow of metal.

Once the preform assumes the shape of the die cavity and it attains nearly theoretical density it may still not ensure sound metallurgical structure resulting in mechanical properties comparable to the wrought product/s. Therefore, even though preform acquired the shape of the die cavity, extra forging force (full capacity of the press) has been used and a very drastic change in hardness values have been obtained. This shows that extra forging force must be used for the following two reasons :

1. To ensure sound metallurgical bands/sound metallurgical structure
2. To ensure comparable mechanical properties with that of wrought products.

In case of partially open step-down cylindrical die cavity, sudden discontinuities are introduced in the design of the die cavity. Once



the sintered preforms are subjected to deformation conditions through this die they experience sudden discontinuities after having attained certain density levels. Therefore, the mode of densification pattern gets affected at each stage of the discontinuity and the mode of flow of material and mode of closure and flow of pores also change. Such type of study is essential once intricate parts are to be produced through powder metallurgical routes.

Parameters used here to express the fractional theoretical density were evaluated on the basis of the geometry of the die cavity and ultimately the shape, the preform acquires at given forged density level. Basically two parameters were evaluated on the ground that the total surface area in contact with the die cavity after forging preform has two components - namely horizontal surface area ( $h_c, \text{cm}^2$ ) and vertical surface area ( $v_c, \text{cm}^2$ ) respectively. Then the total surface area of the preform which comes in contact with the die cavity at the maximum forging load for a given alloy was resolved into horizontal ( $h_{cm}, \text{cm}^2$ ) and vertical ( $v_{cm}, \text{cm}^2$ ) components. The other relevant parameters were mathematically defined as follows :

$$f_{hc} = \frac{(hc)_s}{(hc)_m} = \frac{\text{Spontaneous horizontal component of the surface area}}{\text{Maximum horizontal component of the surface area at full load}}$$

...(6.4)

Therefore,  $f_{hc}$  is defined as 'the ratio of the spontaneous horizontal component of the surface area of the forged product in intimate contact with the part of the die to the maximum horizontal component of the surface area of the preform in intimate contact with the die cavity at full load.

$$f_{vc} = \frac{(v_c)_s}{(v_c)_m} = \frac{\text{Spontaneous vertical component of the surface area in intimate contact with the part of the die cavity}}{\text{Maximum vertical component of the surface area of preform in contact with the die cavity at full load}} \quad \dots(6.5)$$

Therefore,  $f_{vc}$  is defined as 'the ratio of the spontaneous vertical component of the surface area of the forged product in intimate contact with the part of the die to the maximum vertical component of the surface area of the preform in intimate contact with the die cavity of full load.

$$O = \frac{f_{hc}}{f_{vc}} = \frac{(h_c)_s}{(h_c)_m} \times \frac{(v_c)_m}{(v_c)_s} \quad \dots(6.6)$$

Therefore,  $O$  is defined as the fraction of the ratio of the horizontal constraint to that of the ratio of the vertical constraint.

### 6.2.1 Partially Open Step-Down Cylindrical Die Cavity

In the light of the parameters defined in Section 6.2, the results of forging through partially open step-down cylindrical die cavity are discussed. Forging results of plain carbon steels (containing carbon from 0.00 to 1.36 %) at 1120°C and 0.45 % phosphorus steel at 960°C are tabulated in appendix 'C' from C.1 to C.5. Effect of horizontal and vertical constraints on densification behaviour are shown in Figs. 6.61 to 6.65. Observations of these plots, in general, show that for achieving the same level of densification, it is required to introduce more amount of fractional vertical constraint ( $f_{vc}$ ) as compared to fractional horizontal component of the constraint ( $f_{hc}$ ). As densification level approaches near to theoretical density, both horizontal and vertical fractional constraints converge to the same value indicating that single component is not predominant, but, both the components are equally responsible for densification. However, at this stage the residual pores get stabilized and do not get affected by any further deformation. Ultimately these pores act as sources of stress raiser and become finally responsible for poor mechanical properties as compared to that of wrought products [192]. .

### Effect of alloy addition on densification.

through the above components of constraints could be quantitatively and qualitatively assessed. For instance, to achieve density levels of 95, 97, 98 and 99 per cent of the theoretical, it is required to provide a compromise between  $f_{hc}$  and  $f_{vc}$ , which is discussed later in this chapter. However, Table 6.8 shows the effect of alloy addition on density levels and  $f_{hc}$  and  $f_{vc}$ . Observation of this table reveals that for all levels of densification, as the carbon content is raised from 0.00 to 1.36 % carbon,  $f_{hc}$  always increases. However, the similar trend is not observed in the values of  $f_{vc}$ . For 95 per cent of theoretical density it is observed that  $f_{vc}$  is in the increasing order as carbon content is varied from 0.00 to 1.36 %. At other higher density levels fluctuations in  $f_{vc}$  are recorded. In case of pure iron  $f_{vc}$  is towards the much higher side compared to 0.35 per cent carbon at density levels of 97 and 98 per cent, indicating that in these density levels pores start showing resistance against closure. Whereas, other two compositions i.e. 0.83 and 1.36 % carbon show still higher degree of resistance against pore closure. The alloy 0.35 per cent carbon steel shows lesser resistance in these density levels. Still higher order of densification requires higher values of vertical constraints associated with higher values of horizontal constraints. Therefore, in general, it

Table 6.8

Values of  $f_{hc}$ ,  $f_{vc}$  at Different Density Levels for Iron, Iron-Carbon Steels and a Phosphorus Steel for Partially Open Step-Down Cylindrical Die Cavity Forgings.

Level of Densifi- cation	Alloy Composition									
	Pure Iron		0.35 % C-Steel		0.83 % C-Steel		1.36 % C-Steel		0.45 % P-Steel	
	$f_{hc}$	$f_{vc}$	$f_{hc}$	$f_{vc}$	$f_{hc}$	$f_{vc}$	$f_{hc}$	$f_{vc}$	$f_{hc}$	$f_{vc}$
95	0.12	0.41	0.24	0.42	0.25	0.49	0.33	0.58	0.23	0.48
97	0.22	0.50	0.29	0.45	0.39	0.64	0.44	0.66	0.36	0.62
98	0.30	0.58	0.32	0.48	0.50	0.73	0.53	0.73	0.53	0.74
99	0.50	0.71	0.60	0.85	0.65	0.86	0.66	0.82	0.90	1.00

can be conclusively said that as carbon content was raised the values of  $f_{hc}$  shot up, indicating that higher horizontal constraint is to be introduced to impart same level of densification. Hence, alloy addition adversely affects densification as far as the results of above die cavity are concerned with respect to  $f_{hc}$ .

Behaviour of  $f_{hc}$  and  $f_{vc}$  are in the increasing order for 0.45 per cent phosphorus in iron (phosphorus-steel) compared to pure iron. All these observations show that the addition of alloying element such as carbon and phosphorus in the above type of die forgings leave behind the residual porosity, which is generally not closed but is of lower order of magnitude compared to flat Die Forgings.

To explain the densification behaviour and to show the combined effect of  $f_{hc}$  and  $f_{vc}$  on densification, a new parameter,  $O$ , has been defined such that the ratio of  $f_{hc}$  to  $f_{vc}$  does not exceed unity. Figure 6.66 shows the plot of fractional theoretical density with respect to the new parameter  $O$  for the case of step-down cylindrical but partially open die cavity. It is obvious from the plot that as the value of  $O$  is increased, the rate of densification rapidly goes up in the case of pure iron and 0.83 %C steel whereas, 0.35 % and 1.36 %C steels show very rapid increase in densification with little variation in the value

of  $\Phi$  though it is towards much higher side compared to pure iron and 0.83 %C steel. This explains that the initial pore closure in case of pure iron and 0.83 % carbon steel is achieved at much lower values of  $\Phi$ , whereas the same phenomenon in the case of 0.35 and 1.36 % carbon steels is exhibited at higher values of  $\Phi$ , indicating thereby that higher order of resistance is shown by the pores against closure. This leads to show that good amount of energy is absorbed by the pores before showing any evidence of their closure. This is clearly revealed by the fact that to achieve the same level of densification, for instance, say 93 % of the theoretical one, it is required to introduce a constraint of the order of 0.22 for pure iron and 0.83 % carbon steel, while it is 0.47 in case of 0.35 %C and 1.36 %C steels. Ultimately increasing the value of  $\Phi$  close to unity, no substantial upward trend of the curve is observed, in case of 0.35 and 1.36 % steels, in showing better densification. Whereas, substantial upward trend is noticed for pure iron, 0.83 % and 1.36 % carbon steels while still in the range of theoretical density levels.

Forging of 0.45 % phosphorus steel at 960°C in the above die does show the upward trend but even after exerting full load of the press full theoretical density could not be achieved indicating

that phosphorus, as an alloying element in such type of die forging, acts as pore stabilizer rather than to assist pore closure. Simple reason could be phosphorous, which during sintering, has the tendency to create rounded pores which are energetically more stable and hence even in the final stage of the deformation do not close down following Stassi's relation of a critical pressure [197 ].

The log-log plot (Fig. 6.67) of per cent theoretical density with respect to percent  $\Phi$  has yielded a single straight line for all alloys studied with the slope of 0.052. The generalized relation has been obtained for step-down cylindrical partially open die as follows :

$$\left( \frac{\rho_f}{\rho_{Th}} \right) = 1.009 \Phi^{0.052} \quad \dots(6.7)$$

where,

$$\frac{\rho_f}{\rho_{Th}} = \text{fractional theoretical density,}$$

$$\text{and, } \Phi = \frac{f_{hc}}{f_{vc}} = \text{ratio of fractional horizontal constraint to the fractional vertical constraint.}$$

The above relationship suggests that  $\Phi$  could be a function of applied force which causes the metal to flow into the die cavity. Temperature of forging does not affect  $\Phi$  appreciably and therefore, it can be conclusively established that



$\Phi$  is a geometrical parameter which could be mildly affected by the mode of lubrication of the die. In the present investigation die was preheated to a temperature of 300 - 350°C and lubricant used was graphite powder sprayed over the internal surfaces of the die cavity.

### 6.2.2 Forging Through Partially Open Hemi-Spherical Die Cavity

Results of forging through partially open hemi-spherical die cavity are reported in appendix 'C' (Tables C.6 to C.10) for plain carbon (0.00 to 1.36 % carbon) steels and 0.45 % phosphorus steel. Plain carbon steels sintered preforms were forged at 1120°C whereas 0.45 % phosphorus steel (sintered preforms were forged at 960°C.

Fractional theoretical density as a function of  $f_{hc}$  and  $f_{vc}$  are plotted in Figs. 6.68 to 6.72. The general observations of these plots reveal that the fractional vertical constraint ( $f_{vc}$ ) is of higher magnitude than fractional horizontal constraint ( $f_{hc}$ ) except at the final stages of densification where individual effects of  $f_{hc}$  and  $f_{vc}$  merge to the final density level for all the alloy systems studied.

From Figs. 6.68 to 6.72, Table 6.9 has been derived for a fixed amount of densification against  $f_{hc}$  and  $f_{vc}$ . A close observation of this table shows

that 95 % of theoretical density level with the increase in carbon content of the steels, values of  $f_{hc}$  is raised. However, the value of  $f_{hc}$  for 0.45 % phosphorus remains same as that of pure iron. At higher density levels, value of  $f_{hc}$  rises with the increase in carbon content, however, exception being 0.83 %C steel, where the magnitude of  $f_{hc}$  shows a decreasing trend. In case of 0.83 % carbon steel, however the value of  $f_{hc}$  remains greater than that of pure iron at 96 and 97 % theoretical density levels, becomes equal to 98 % density while it falls below the  $f_{hc}$  value of pure iron at 98.5 % theoretical density level. In general,  $f_{hc}$  values increase with the increasing density levels. However, in contrast to plain carbon steels, 0.45 % phosphorus steel practically shows the same magnitude of  $f_{hc}$  upto 98 % theoretical density level as those obtained for pure iron, while at 98.5 % density level a value with decreased magnitude of  $f_{hc}$  is obtained in comparison to pure iron.

All the steels studied in the present investigation reveal that magnitude of  $f_{vc}$  increases with the increase in the density levels from 96 to 98.5 % theoretical density. Practically, all the alloys studied show a constant level of  $f_{vc}$  values, whereas in the case of 0.83 % carbon steel the  $f_{vc}$  values of lower magnitude are obtained at all the density levels reported in Table (6.9).

Table 6.9

Values of  $f_{hc}$ ,  $f_{vc}$  at Different Density Levels for Iron, Iron-Carbon Steels and a Phosphorus-Steel for Partially Open Hemi-Spherical Die Cavity Forgings.

Level of Densifi- cation	Alloy Composition									
	Pure Iron		0.35 % C-Steel		0.83 % C-Steel		1.36 % C-Steel		0.45 % P-Steel	
	$f_{hc}$	$f_{vc}$	$f_{hc}$	$f_{vc}$	$f_{hc}$	$f_{vc}$	$f_{hc}$	$f_{vc}$	$f_{hc}$	$f_{vc}$
95	0.32	0.73	0.35	0.76	0.35	0.48	0.42	0.75	0.32	0.67
96	0.38	0.78	0.46	0.81	0.40	0.54	0.48	0.78	0.38	0.73
97	0.45	0.82	0.59	0.87	0.47	0.62	0.54	0.82	0.48	0.78
98	0.55	0.87	0.75	0.94	0.55	0.65	0.60	0.85	0.62	0.81
98.5	0.76	0.97	0.90	1.00	0.65	0.75	0.65	0.86	0.58	0.89

Though the independent effect of  $f_{hc}$  and  $f_{vc}$  over densification has been observed but there is a strong need to assess the combined effect of  $f_{hc}$  and  $f_{vc}$  over mode of densification. Hence, the plot of  $\left(\frac{\rho_f}{\rho_{Th}}\right)$  versus  $\bar{\Phi}$  are drawn in Fig. 6.73 for all alloy systems. The close scrutiny of Fig. 6.73 reveals the fact that 0.83 % and 1.36 % carbon steels move more or less parallel and ultimately converge to a point. Pore closure in these two cases show fairly high order of resistance before deformation leads to a substantial rise in density as compared to iron and 0.35 % carbon steel. It seems that in these two systems, pores do not show much resistance before initiation of pore closure. This is possibly due to the fact that pore surfaces were energetically not much stable and more rounded pore surfaces were absent. However, still higher  $\bar{\Phi}$  values are required for 0.35 % carbon steel. Further, it is observed that 0.35 % carbon, pure iron and 0.45 %P steels do not approach to the theoretical density level inspite of the fact that full load of the press has been applied. Even though, higher values of  $\bar{\Phi}$  has been incorporated but final density level shows flattening behaviour at much lower values than the fractional theoretical density in the case of 0.45 % phosphorus alloy during final stage of deformation. This effect can be argued on the basis of the fact that phosphorus has the tendency of rounding off the pores during sintering stage itself

and the pores are energetically more stable. During final stage of deformation still energetically stable pores do exist and ultimately do not close down under the highest feasible shear strain provided through this die cavity and consequently, shearing surfaces of a pore do not come in intimate contact to give rise to a strong metallurgical bond and forged density achieved falls far below the theoretical density.

The log-log plot of percent theoretical density versus percent values of  $\Phi$  shows a single straight line (Fig. 6.74) indicating that alloy composition and forging temperature do not play predominant role and thus a relationship has been established as below for partially open hemi-spherical die cavity forgings :

$$\left( \frac{\rho_f}{\rho_{Th}} \right) = 0.719 \Phi^{0.071} \quad \dots(6.8)$$

### 6.2.3 Geometrical Parameters and Their Relationships

Keeping all other parameters common to both dies used above, the comparison of equations 6.7 and 6.8 shows that they have different values of constants which are tabulated below in Table 6.10.

Table - 6.10Coefficients and Exponents of  $\bar{\Phi}$ 

Type of Die Cavity	Coefficient of $\bar{\Phi}$ $C_1$	Exponent of $\bar{\Phi}$ n
Partially Open Ste-Down Cylindrical Die Cavity	1.009	0.052
Partially Open Hemi-Spherical Die Cavity	0.719	0.071

Therefore, on the basis of equations 6.7 and 6.8, the relationship between fractional theoretical density and  $\bar{\Phi}$  can be expressed, in a general form, as follows :

$$\left( \frac{\rho_f}{\rho_{Th}} \right) = C_1 \bar{\Phi}^n \quad \dots(6.9)$$

Now replacing the values of  $\bar{\Phi}$ , one obtains the following relation from equation (6.9) :

$$\left( \frac{\rho_f}{\rho_{Th}} \right) = C_1 \left( \frac{f_{hc}}{f_{vc}} \right)^n \quad \dots(6.10)$$

where,

$$f_{hc} = \frac{(h_c)_s}{(h_{ct})_m} \quad \text{and}$$

$$f_{vc} = \frac{(v_c)_s}{(v_{ct})_m}$$

Therefore,

$$\Phi = \left[ \frac{(h_c)_s \cdot (v_{ct})_m}{(h_{ct})_m (v_c)_s} \right] \quad \dots(6.11)$$

The right hand side of the expression (6.11) enclosed in square bracket is a dimensionless quantity indicating that  $\Phi$ , too, is a dimensionless quantity. Each quantity in the square bracket, individually represents a geometrical quantity, therefore,  $\Phi$  is also influenced by the geometry of the die cavity. Further, Figs. 6.67 and 6.74 support the statement that  $\Phi$  is a geometrical parameter as composition and temperature variation do not play any significant role.

Equation (6.11) involves the spontaneous values of horizontal constraint and vertical constraint as well as maximum values of horizontal and vertical constraints obtained for each alloy composition by subjecting atleast one or two preforms to the maximum possible deformation to obtain the shape of the die cavity at the full capacity of the press load (100 tons).  $(v_{ct})_m$  and  $(h_{ct})_m$  are obtained from the above deformation. Hence, this goes to show that the preform design is governed by the final geometry of the component. However, geometrical relationships have been developed from the data obtained out of the results of partially open step-down cylindrical and partially open hemi-spherical die cavities. These

plots are subsequently shown in Figs. 6.75(a) and 6.75(b) for  $v_c$  versus  $h_c$  for both dies mentioned above. The log-log plot for both the dies between  $v_c$  and  $h_c$  are shown in Fig. 6.76 and empirical relationships have been established which are shown in Table 6.11.

Table-6.11

Empirical Relations For Different Geometries of the Partially Open Dies.

Type of the Die Cavity	Relation Between $v_c$ and $h_c$	Relation Between $f_{vc}$ and $f_{hc}$
Partially Open Step-Down Cylindrical Die Cavity	$v_c = 3.78(h_c)^{0.85}$	$f_{vc} = 1.02(f_{hc})^{0.47}$
Partially Open Hemi-Spherical Die Cavity	(i) $v_c = 0.35(h_c)^{2.24}$ for $3.7 < h_c < 5.2\text{cm}^2$ (ii) $v_c = 9.47(h_c)^{0.244}$ for $5.2 < h_c < 16.0\text{cm}^2$	(i) $f_{vc} = 3.67(f_{hc})^{1.48}$ $0.1 < f_{hc} < 0.36$ (ii) $f_{vc} = 1.01(f_{hc})^{0.27}$ $0.36 < f_{hc} < 1.00$

Similar relationships have been obtained in between  $f_{hc}$  and  $f_{vc}$  from Fig. 6.77 for both dies. These relations between  $v_c$  and  $h_c$  and  $f_{vc}$  and  $f_{hc}$  deduced from Figs. 6.76 and 6.77 for both dies can be safely used even in different shaped dies to produce intricate shapes of the final products. Thus, relations in between  $f_{hc}$  and  $f_{vc}$  for both dies are also reported in Table 6.11.



#### 6.2.4 Hardness Versus Per Cent Theoretical Density In Partially Open Die Forgings

Figure 6.78 shows the plots of hardness versus per cent theoretical density for pure iron, iron carbon alloys and a iron phosphorus alloy powder preforms (sintered) during hot forging through partially open dies. The careful examinations of the curves in this plot show the following :

- (1) there is a gradual but linear rise in hardness upto a density level of 98.5 per cent of theoretical, while
- (2) a sharp linear variation in hardness from 98.5 per cent theoretical density onwards, almost upto 100 per cent density level, for all the compositions of study under present investigation.

The rise in hardness and its linearity with respect to per cent theoretical density and composition is more or less as obtained in the case of upsetting. But, sharp rise in hardness values in the later stage of densification may be either or all of the following reasons :

- (a) Residual stresses, developed during the process of forging and subsequently quenching,

- (b) Work-hardening, as the temperature of forging drops just at the time of the second blow of the punch over the already deformed component [second blow does not result in substantial rise in densification and ultimately may result in work-hardening].
- (c) Establishment of sound metallurgical bond across the shearing surfaces of a pore.

Thus, abrupt rise in hardness could be possibly attributed to the existence of residual stresses or to work-hardening at high temperatures of forgings but their effect may not be so predominant as to have a wide variation of hardness at the same density level (near to theoretical density) in the range of 195 to 330 VPN. However, this effect might have taken place possibly due to the development of strong metallurgical bond across the shearing surfaces of a pore. Thus, attaining a product of having properties comparable to wrought products.

It has been observed that density measurement and the geometrical measurements of the component do not show significant changes in the final stages of densification. Therefore sharp rise in hardness values in the later stage of porosity elimination (1.5 to 1.0 %) does play a predominant role where shearing surfaces of a pore come in intimate contact giving rise to a strong metallurgical bond/s. The above conclusion,

logically derived from the Fig. 6.78 falls in confirmity with Kahlow's assumption [ 192 ] and Moyer's experimental results [ 193 ]. Now, therefore, in the light of the above it can be conclusively established that the sharp rise in hardness values; a direct reflection of tensile strength which is a function of porosity [ 162 ], could be only due to strong metallurgical bond. Thus, for a powder product of the same density level, wide difference in tensile strength (hardness values) must be associated only with the strength of the bond. Hence, higher the hardness values higher is the bond strength and structurally a sound product.

### 6.3 METALLOGRAPHIC STUDIES ON FORGED PRODUCTS OBTAINED THROUGH THE PARTIALLY OPEN DIES

Metallographic observations were carried out on polished and polished and etched surfaces of forged products obtained through partially open die forgings. These observations were analysed with the aim of determining the mode of pore deformation and its flow indicating the characteristic of the metal flow. Polished and etched surfaces were examined with the idea of determining the mode of grain flow, if any, and also recrystallization which may lead to better densification. Structures are also discussed in the light of alloy composition and their effects on densification. With the above in mind, the results of both dies are discussed

in subsequent sub-sections.

### 6.3.1 Partially Open Hemi-Spherical Die Forgings

#### 6.3.1.1 Pure Iron

While examining the pore shape changes along the vertical axis of the forged component of pure iron, it has been observed that in the region well within the field of upsetting (region of the rim) where predominantly the metal flow was in the horizontal direction, the pore flattens in the horizontal direction whereas it bends in the vertical direction showing the vertex in the direction of the applied load. While scanning more or less the centre region of the vertical cross-section it has been observed that the pores show more or less the tendency of aligning in the direction of the force and close to the exit point of the metal flow these pores appear like fine vertical streaks, Fig. 6.79 (a to h).

Examining the pore structure along the other vertical line parallel to the central axis but 12 mm away from it exhibits that

Well within the rim - the magnitude of porosity is exceptionally low having flattening in the horizontal direction showing a little bend in the vertical direction. As one moves further downwards, exceptionally high order of directionality is acquired by the shearing pore.

The bend in these pores is directed towards the central vertical axis of the component. Pore elongates or in other words flows as the geometry of the confinement beneath it. Once again close to the exit point of the metal flow, the pore elongates in the vertical direction. These microphotographs are shown in Fig.6.79(i) to (l).

Figure 6.79 [(m) and (n)] shows the polished and etched structure on the cross-section at the centre location which reveals no pitting within the grains while at the grain boundaries moderate to heavy pitting is observed. Fairly equiaxed grains are visible.

### 6.3.1.2 0.35 % Carbon Steel

While scanning the vertical cross-section of 0.35 % carbon steel under forging conditions of hemispherical partially open die cavity, no orientation in porosity was observed. Since, the porosity observed was of very low order and extremely small in size the orientation of porosity could not be identified. Dead metal zone shows high order of porosity indicating poor order of densification in this region. Micro-structure at other places (different than dead metal zones) is of pearlite-ferrite type, while, the dead metal zone and the region of the rim show the absence of pearlite. At the point of the exit of the metal, extensive directionality and flattening of the pores are noticed, indicating that

pore flattening due to shearing action must have been present but the added graphite during blending stage must have alloyed with iron at sintering temperature and enhanced the rate of densification. Therefore, it can be possibly said that alloyed graphite aids to densification. Figure 6.80 shows clearly the flow of ferrite and pearlite.

#### 6.3.1.3 0.83 % Carbon Steel

Scanning the vertical cross-section of the component forged through the partially open hemi-spherical die cavity, shows porosity of fairly low order. Pores are elongated a little with no defined directionality and non-uniform distribution, Fig. 6.81.

#### 6.3.1.4 1.36 % Carbon Steel

Pore size observed was very very even at 100X. Directionality is not observed possibly due to the extremely fine of the pore size. Graphite aids to the densification. Edges show the porosity whereas centre shows virtually no porosity, Fig. 6.82.

While comparing effect of carbon on these forgings it can be conclusively established that densification is enhanced by the addition of the carbon on the basis of already evaluated pore structures.

### 6.3.1.5 0.45 % Phosphorus Steel

Figures 6.83(a) and (b) show the polished structure at the edge as well as at the centre of the vertical cross-section of the component. Edges show thin layer of porosity but the nature of the pores are different than pure iron. Pores elongate along the curvature of the die (Fig. 6.83(a)). Centre of the specimen shows pin point porosity, rounded in nature but uniformly distributed, Fig. 6.83(b).

Figures 6.83(c) and (d) show the etched structure where fine grain boundaries are seen and the grains appear to be deformed. However porosities, in fairly good amount are also seen. At few places big size porosities are observed. This is possible due to the fact that etchant reacts much faster at the open porosities.

Thus, it can be seen that the mode of the shape changes of pores depends on composition of steel and also the type of alloying element. Phosphorus as an alloying element shows the tendency of creating rounded (smooth) surfaces whereas carbon as an additive does not leave behind any rounded pores even near to theoretical density. Therefore, obviously final stage of densification obtained using carbon as alloying element is better than using phosphorus as an alloying element. Following Stassi [ 197 ] concept of pore closure it is difficult to obtain 100 % dense product with phosphorus as alloying

element because of the fact that closure of nearly rounded pores require large amount of press load which is a major constraint on the presently available forging equipments. This effect is in confirmation with others [ 10 ].

### 6.3.2 Partially Open Step-Down Cylindrical Die Cavity

#### 6.3.2.1 Pure Iron

Vertical cross-section of the component produced through partially open step-down cylindrical die cavity has been examined under polished and polished and etched conditions. The overall examination of the section shows that pores tend to elongate assuming the shape of the die geometry. As one reaches to the point of the exit of the metal, the pore appears like a vertical streak. Once the central vertical axis is examined, pores bend downward (concave upward) and at other locations they elongate showing directionality towards the central axis of the component. Wherever the constraint is met to the advancing metal, the reduction shows the clear cut dead metal zones in which practically, the densification is either not there or is of very low magnitude (Evidently seen in the structure of the dead metal zone). However, at transition point, a clear cut demarcation pattern is seen between the metal which has moved and the metal which has not moved.



The metal which has moved shows within itself finer streaks of pores, whereas, the pore in larger size is seen in the dead metal zone. However, the possibility of little movement of metal within the localized region of dead metal zone is observed which goes in confirmation with the findings of other investigators [ 204 ]. Since the material movement is evident in dead metal zone it is more appropriate to call it hydrostatic zone. Therefore, it is better to identify these regions as regions of hydrostatic pressure where overall material movement is low.

Note : Pore morphology is not being presented here as it was quite similar to the pore morphology obtained for pure iron in the case of partially open hemi-spherical die cavity forgings (see Fig. 6.79).

Figure 6.84(a) shows the micro-photograph taken from the dead metal zone. Dark region shows substantial amount of undeformed pores during hot forging in a cylindrical step-down die cavity. No grain flow is seen confirming to the concept that in dead metal zone practically no flow of material is there and shape of pores also do not change substantially indicating that dead metal zone virtually remains free of densification or at the most very little densification occurs.

Metallograph (Fig.6.84(b)) is taken off from the transition boundary of dead metal zone and the deformed region. Here, the recrystallization appears to have occurred.

Moving further across the second confinement in the horizontal direction pores appear in the form of streaks with coarser grains which goes on refining as centre is approached. At the centre virtually porosity free micro-structure with recrystallized grains are seen. Figures 6.84(c), (d) and (e) show the above observations in a sequence. Recrystallized equiaxed grains with rounded porosities are also observed close to third confinement level slightly away from the dead metal zone (Fig.6.84(f)). At the top of the first confinement pore flattening is larger towards the constraint and assumes curvature according to the geometry of the die. With the same field pore flattening is extensive.

#### 6.3.3.2 0.35 % Carbon Steel

While scanning the vertical cross-section of the component under polished and etched condition across the second stage of confinement following observations were recorded :

Figure 6.85(a) was taken slightly away from the dead metal zone i.e. a region where dead metal zone diminishes, a clear cut evidence of pore flow is noticed. Fine grain size, effect of recrystallization appears. Figure 6.85(b) shows the microstructure revealing in it heavy pore flattening with directionality which has been acquired due to the mode of deformation and

constraints against metal flow. Here, too, the grain elongates and acquires directionality. Therefore, it can be concluded that not only pores flow but prevalent conditions through the die walls and temperature of forging with sprayed graphite as lubricant helps the flow of grains. Structure shows large size wider streaks as well as small size fine streaks of pores. As expected, metallograph (Fig. 6.85(c)) shows half region consisting of extensive pore and grain flattening while the other half shows no evidence of pore flattening. However, grain flattening is present. Therefore, it can be assumed that during the process of pore flattening there existed shear stresses of high magnitude which stretched the pores to a level where they have completely collapsed giving rise, either to a localized elongated or fragmented pores of a very low order thus resulting in enhanced densification. Evidence of recrystallization though localized appears. Scanning the specimen still further across the second confinement but in the horizontal direction, fine recrystallized grains associated with occasionally low porosities otherwise for all practical purposes no porosity is observed (Fig.6.85(d)). Figure 6.85(e) shows uniform grains which appear to be recrystallized ones. Whereas Fig. 6.85(f) shows grain coarsening with lower order of porosities. All grains appear to be equiaxed showing no evidence of recrystallization.

General observation is that wherever recrystallization has taken place, the porosity is reduced to the minimum giving direct evidence to support that recrystallization aids to densification.

Structures observed across the central axis of the component of the above cross-section reveal the following observations while travelling from top to the bottom :

Figure 6.85(g) shows coarse grained equiaxed with low porosity while slightly below shows fine grained structure with a trace of recrystallization showing porosity level approaching to zero indicating that shearing stresses prevalent during forging aid to densification by means of closing the pores. Predominantly, shear forces act to establish a mechanical bond. On further shearing action the collapsing surfaces of a pore may lead to a strong metallurgical bond. [192] by movement of material across the shearing surfaces.

Across the centre line, further down to earlier position of Fig. 6.85(g) shows finer structures than earlier one not recorded. This structure is completely recrystallized. Further, down to the earlier structure, extremely fine recrystallized structure is seen which shows the effect of high order of deformation (metallograph not taken). Figure 6.85(h) shows absence of grain identity. Pearlite structure is observed only when deep etched. While examining the specimen at the **last** confinement (Fig.6.85(i)), structure shows

elongated pores having well defined directionality. This region is confined to a smaller area compared to earlier confinements.

Now scanning the specimen horizontally at the first confinement, Fig. 6.85(j) shows at one side low porosity whereas the other side reveals high order of porosity. A well defined demarcation between dead metal zone and the deformed metal zone could be seen. Figure 6.85(k) shows grain flow quite explicitly whereas Fig. 6.85(l) reveals coarse structure with no sign of recrystallization though the grains are equiaxed.

#### 6.3.2.3 0.83 % Carbon Steel

This steel specimen was also examined very thoroughly as 0.35 % carbon steel, but, only representative micro-photographs are taken. The behaviour of pores during deformation is more or less similar as that in the case of 0.35 % carbon steel.

Figure 6.86(a) shows the structure taken as the central axis of the component, but only in the dead metal zone fine grain structure with low porosity level was observed. Figure 6.86(b) shows still finer structure than Fig. 6.86(a). Throughout the cross-section nearly 100 % pearlitic structure was observed and they were fine. Excess carbon has

come out as cementite network which are also seen in the structure.

#### 6.3.2.4 1.36 % Carbon Steel

Vertical cross-section of the component (forged through the partially open step-down cylindrical die cavity) was suitably prepared for metallographic examination. The polished and etched section was examined under the microscope thoroughly. Behaviour of porosity was almost similar as seen in the case of 0.35 % carbon steel.

Examination of the structures across the horizontal direction of the second stage of confinement, reveals the following :

- (1) Figure 6.87(a) shows decarburized grains of ferrite and pearlite. This has happened possibly because of the fact that just before forging ceramic coating might have been removed whereas in the other specimens this was not observed.
- (2) Figure 6.87(b) shows ferritic network. Porosity level approaches to zero.
- (3) Figure 6.87(c) shows fragmented fine ferrite in amounts ranging from 10 to 20 %, whereas rest all is pearlitic in character.

- (4) Figure 6.87(d) reveals nearly 100 % pearlitic structure.

Combined observations from (1) to (4) shows that heavy decarburization has occurred due to possibly spalling off the ceramic coating during sintering.

- (5) Figure 6.87(e) shows coarse cementite network with a very fine grain size. This is present in half the region whereas the other half shows pearlitic structure.
- (6) Figure 6.87(f) shows relatively coarse grains of cementite with coarse network. The grain flow is not visible.
- (7) Figure 6.87(g) reveals coarse grained structure. Cementite plates grow into the pearlite colonies showing the effect of heavy deformation.
- (8) Figure 6.87(h) represents thin cementite network. Absence of cementite plates entering into the grains could be observed.
- (9) Figure 6.87(i) shows the increase in the number of cementite plates indicating the mode of heavy deformation.

It has been observed in general, that the addition of carbon has reduced the level of porosities in the final product. As the addition of carbon was raised, per cent theoretical density obtained was better

than the case of a pure iron. Therefore, it can be said that addition of carbon enhances the densification level. Also, the increase in number of cementite plates reflects the level of deformation which ultimately results in enhancing the final density of the product.

#### 6.3.2.5 0.45 % Phosphorus Steel

While examining the polished vertical cross-section of the component forged through the partially open step-down cylindrical die cavity the following observations are derived from the micro-photographs taken :

- (1) Figure 6.88(a) shows the shape and size of the pores in the dead metal zone. It can be clearly seen that pore collapsibility is very fast.
- (2) Figure 6.88(b) shows explicitly that the pores are thicker and larger in volume (appears) towards dead metal zone whereas in the deformed zone pores are elongated in finer streaks (low in volume) showing very high order of collapsibility.
- (3) Figure 6.88(c) shows length of the pores in general shortened whereas width has slightly increased.



- (4) Figure 6.88(d) shows that the length of the pores, in general, are further reduced and width still increased as compared to the case in (3).
- (5) Figure 6.88(e) reveals that the pores lack the sense of directionality.

Observing the polished and etched structure through the Fig.6.88 from (f) to (j) it can be clearly seen that away from the dead metal zone but well within the deformed metal region, the grains flow acquiring the shape of the die confinement. Wherever the metal experiences high order of deformation the grains are reduced in size, but, not much substantial difference has been recorded. Grain boundaries are very thin. Pores show rounded surfaces than the other carbon steels. As micro-structure shows porosity and density measurement, too, shows the same order of porosity.

### 6.3.3 Qualitative Approach to Metal Flow Through Partially Open Dies

Qualitative study of pore morphology of Figs. 6.79 to 6.88 reveals that there is a possibility of incorporating the pore shape changes in both the partially open dies (cylindrical step down and hemispherical). The general observations show that the

pores elongate (flow) more close to the die confinement leaving aside the region of dead metal zones. Further movement inside the component, away from the dead metal zone results in reduction of pore size which finally diminishes to zero around the centre. Pore diminishes to zero under shearing action associated with metal flow downward. At the exit of the metal it has been observed, in general, that pore shape acquires directionality which is parallel to the axis of the component. The phenomenon is schematically exhibited in Fig. 6.89(a). From this figure the mode of metal flow has been derived keeping in view that the velocity vectors of metal flow differ at various points of the component during impact forging or extrusion forging, e.g. metal flow downward vertically in the centre with much faster velocity in comparison to the metal close to the confinement. Therefore, Fig. 6.89(b) has been drawn to depict the velocity vectors of metal flow through partially open hemi-spherical die cavity. Similarly, the schematic representations of pore shape changes and velocity vector, in case of cylindrical step down partially open die, are given in Figs. 6.90(a) and (b).

Microstructural examinations of Fig. 6.79 to 6.88 also reveal that there exists a zone where metal movement is either absent or is to a limited extent. Whatever, may be the case, the presence of localized metal movement within the dead metal zone must not be

ignored and it should be explained only by presuming this dead metal zone as a hydrostatic zone. Therefore, the localized movement of metal within the hydrostatic zone falls in confirmity with the earlier work [ 204 ] on extrusion of aluminium preforms through square shaped and wedge shaped dies at different temperatures. In the present case, the cross-section of extrusion forged product experiences gradual, but, a continuous change (hemi-spherical die cavity) whereas step down partially open die products experience sudden drastic reduction in cross-sectional area leading to extensive plastic deformation of material in which strain induced recrystallization at hot forging temperatures occurs resulting in enhanced densification.

#### 6.3.4 Soundness of Products Produced Through Partially Open Dies

Figure 6.91 shows the photographs of components produced through partially open step down cylindrical die cavity at  $1120^{\circ}\text{C}$  of iron and iron carbon sintered alloys. The general observation is that as the amount of carbon is increased from 0.00 to 1.36 per cent the surface cracks go on increasing, but, however, their growth can be checked by providing repressing constraints at the free surfaces before they acquire dangerous proportions. The forgings of different carbon compositions showing fairly good amount of surface

cracks (at the free surfaces) show no sign of internal cracks. Therefore, if machining allowances are provided before hand the forged products could be safely used.

The tensile strength of the forgings assessed through hardness measurements show its superiority over the wrought products and even the interior of the component showed metallurgically sound structure.

Figure 6.92 shows the components produced through partially open hemi-spherical die cavity at  $1120^{\circ}\text{C}$  for iron and iron carbon (0.35 to 1.36 %) sintered alloys. None of the products of the above compositions show substantial cracks at the free surfaces revealing the fact that the die geometry, the mode of shear strains and compressive strains generated at the free surfaces are responsible for the initiation of cracks [ 196 ]. Therefore, in the light of this open die forgings/extrusion forging can be recommended for producing industrially applicable components provided suitable preform design and corresponding die design has been incorporated.

Figure 6.93 represents the powder products in various shapes produced from 0.45 % phosphorus steel through upsetting, partially open dies and closed dies. By altering die design while maintaining H/D ratio of the preform, it has been observed that no circumferential cracks at the free surfaces are present, indicating thereby that 0.45 % phosphorus steel is most suitable

for forging in different shaped dies.

#### 6.4. CLOSED DIE FORGINGS

The degree of non-uniformity of densification during upsetting has been used in designing closed dies and subsequently the forging of the preforms in these dies. In general closed die forging processes involve upsetting deformations to some extent (so as to permit flow of material) followed by repressing after the workpiece comes in contact with the die walls. The upsetting is very much non uniform and the expanding surfaces bulgeout. The bulged surfaces will cool very fast when it comes in contact with the die walls. Since the bulged surface contains large pores compared to any other portion of the compact, it will be difficult to eliminate them by the forging pressure, because cooling of this region will increase the local flow stresses. Therefore, in this region, it is common [ 130 ] to find some residual porosity at the surface of the hot forged powder preforms. It is then clear, that most of the densification should be achieved during the upsetting mode of deformation prior to the repressing mode preferably, with well lubricated dies [ 137 ]. With the above in view, the closed dies were designed such that the level of upsetting mode of deformation prior to repressing mode could be altered in the increasing order.

#### 6.4.1 Properties of Closed Die Forged Products

Table 6.12 shows the level of diametrical confinement during hot forgings in closed dies with respect to material composition, amount of densification obtained and hardness compared to various levels of upsetting before encountering repressing mode. It shows that per cent theoretical density obtained in each case of repressing mode, increases. Hardness, too, increases, but however at the last stage of repressing the overall density drops, whereas hardness has increased. This shows that some sort of work hardening might have been introduced which is basically called as 'geometrical work hardening [ 195 ], plays a predominant role during extended upsetting. Thus, it can be seen that, in general, addition of carbon shows better densification at the same level of repressing, while phosphorus steel shows poorer densification in the same range of repressing level. The behaviour of 0.45 % phosphorus steel and iron are similar. From Table 6.12, it is also seen that hardness variation is quite substantial in the range of density variation (99.3 to 99.8 %). The higher values of hardness possibly reflect the establishment of metallurgically sound bond all across the surfaces of the shearing pore which have come in intimate contact. This is in confirmation with the findings of other investigations [ 193 ].

Table 6.12

Data on Closed Die Forgings.

S.N.	Composition	Level of diametrical confinement during hot forging in closed dies							
		30.58 mm		31.15 mm		31.80 mm		35.5 mm	
		(P <sub>f</sub> /P <sub>Th</sub> )	Hardness VPN	(P <sub>f</sub> /P <sub>Th</sub> )	Hardness VPN	(P <sub>f</sub> /P <sub>Th</sub> )	Hardness VPN	(P <sub>f</sub> /P <sub>Th</sub> )	Hardness VPN
1	Fe	0.989	139-143	0.990	144-150	0.992	142-151	0.990	153-157
2	Fe-0.35 C	0.990	163-169	0.988	166-173	0.994	172-179	0.993	173-188
3	Fe-0.83 C	0.994	226-228	0.993	225-231	0.996	234-237	0.996	249-257
4	Fe-1.36 C	0.995	283-294	0.995	277-286	0.995	280-289	0.995	284-297
5	Fe-0.45 P	0.979	193-	0.983	189.0	0.985	186	0.987	199-203

#### 6.4.2 Metallographic Studies

Metallographic studies of closed die forgings of various alloys have been carried out. Figure 6.94 shows the grain structure of iron sintered preform forged where partial recrystallization is revealed indicating better densification in the central region. This is in confirmation with others' results [130].

Figure 6.95 represents the microstructures of 0.35 % carbon steel sintered preform ( $H/D = 1.18$ ) forged at  $1120^{\circ}\text{C}$  through closed dies. It shows 50 % ferrite which more or less confirms the composition of this alloy. Porosity is rarely seen in the centre of the component indicating that the centre has acquired density of the order of 100 %. However, at the periphery, diametrically flattened pores with higher width are present, which could not be closed down during repressing. Therefore, overall density of the product corresponds to the microstructural details.

Figure 6.96, however, represents similar forging of 0.83 % carbon steel showing completely eutectoid structure with no cementite network.

Figure 6.97 shows microstructure of the closed die forging of 1.36 % carbon steel revealing in it cementite network with fine cementite plates entering into the network. Scanning the entire cross-section it has been observed that no decarburization has occurred



but, however, extremely fine but scanty rounded pores are seen. This structure corresponds to  $\sim 1.36\%$  carbon steel and also shows the density of the product of the order of 100% dense.

Figure 6.98 shows the microstructural details of the closed die forging of 0.45% phosphorus steel forged at  $960^{\circ}\text{C}$ . Figure 6.98(a) represents the level of porosity with well defined directionality revealing the flattening in the direction of diametrical flow of the metal whereas, Fig. 6.98(b) shows the etched structure, at the centre, revealing fine grain boundaries along with the position of porosity and its nature as above. Figure 6.98(c), however, represents etched microstructure near the repressing surface. It shows porosities interconnected with the grain boundaries. The high order of porosity with fairly large amount of fragmented but rounded pores and good amount of open pores indicates the typical behaviour of 0.45% phosphorous forged steel. It shows that phosphorus is such an alloying element which creates more stabilized pores and these pores flow as the metal flows, ultimately contributing to lower theoretical density attainment. This goes to show that repressing introduced was at a late stage of deformation under upsetting mode where cracks have started opening out at the repressing surfaces.

General observation of microstructural details of all alloys studied in the present investigation in closed die forgings show that fairly good number of open porosities do exist close to the repressing surface which indicates that repressing confinement must be introduced much earlier to the deforming preform before it enters into the cracked region.

#### 6.5 MECHANICAL PROPERTIES OF UPSET FORGED SAMPLES FOR SQUARE SECTION BARS

Mechanical properties of iron and iron based alloys powder products (forged), such as tensile strength, yield strength, hardness, per cent elongation, per cent area reduction and impact strengths are tabulated in Table 6.13. It is seen from the above table that tensile strength increases as the carbon content is raised and so is the hardness, whereas per cent elongation and per cent area reduction decreases. Impact strength of forged and subsequently annealed at 800°C for a period of 2 hours, without notch are reported in the same Table 6.13. It shows, as the carbon content is raised, the impact goes up upto carbon limit of 0.83 % whereas it drops a little for 1.36 % carbon steel in comparison to 0.83 % carbon steel. Phosphorous steel shows fairly low impact value. After annealing one of the sample containing 1.36 % carbon bends like U and still does not fracture and no sign

°  
Table 6.13

Mechanical Properties of Iron and Iron Based Powder  
Forged Products.

Composition	T.S. Kg/mm <sup>2</sup>	Y.S.		Hardness VPN	%Elongation	% Area Reduction	Impact Strength Kg-m
		UYS	LYS				
Pure Iron	47.73	-	-	136.0	24.37	53.26	15.90
Fe-0.35 % C	73.01	69.11	67.56	184.5	16.87	41.07	16.70
Fe-0.83 % C	85.31	74.10	71.55	222.0	8.42	25.18	18.10 <sup>*</sup>
Fe-1.36 % C	98.68	83.3	80.1	29.70	7.94	16.39	16.20 and 8.70 <sup>*</sup>
Fe-0.45 % P	76.93	71.1	71.1	201.0	9.32	27.71	12.31

\* Specimens did not fracture Forged Density obtained of the order of 99.6 to 99.9 per cent.

of crack is seen. However, macrophotographs of some of the unbroken specimen are shown in Fig. 105.

Figures 6.99(a) to (e) show the stress versus per cent elongation curves (only relative magnitude is shown, not the actual units). All the forged alloys under tension reach to the limit of their elastic strain, show yield point clearly and then begin to flow just similar to annealed carbon steels. In the present investigation the behaviour of 0.35 % carbon steel is quite similar to that reported in literature for 0.40 % carbon steel [ 196 ]. Figure 6.99(f) shows the plot of hardness vs tensile strength for all steels studied and compared with the plot of the above parameters existing in literature. These points are well within the neighbourhood of the theoretical line [ 134 ]. Figure 6.99(g) depicts Harnness, T.S. vs composition.

Figure 6.100 shows the scanning electron micrograph of the tensile preform forged to 99.6 % theoretical density. Dimple fracture with large pores is visible indicating the characteristic of a ductile fracture. High order of porosity is observed in the micrograph than what it should have been by actual density measurements. This is apparent because the fracture occurs in the weakest part of the sintered forged product. The fracture seems to take place in the weakest part of the matrix along the pore before a plastic deformation of the matrix develops. 'Dimple

'Pattern' is normally a manifestation of a ductile fracture [ 205 ].

Figure 6.101(a) shows the scanning electron micrograph of the tensile fracture surface of 0.35 % carbon sintered steel preform forged to a density level of 99.9 % theoretical, revealing in it the presence of collapsed pores having directionality. Some of the pores appear as though their existence hails from residual porosity. Figure 6.101(b) represents another region of the fractured tensile surface revealing in it the 'dimple pattern' characteristic of ductile fracture along with the cleavage. Thus, 0.35 % carbon steel shows the fracture behaviour which is governed by the ductile as well the cleavage types of fractures.

Figure 102 represents the scanning electron micrograph of the tensile fracture surface of 0.83 % carbon sintered forged steel near to theoretical density. The observation of the microphotograph reveals 'dimple pattern', virtually free from pores associated with very fine and uniform grain structure. Occasional porosity is also visible. Thus, this structure corresponds to actual theoretical density of the component.

Figure 6.103 represents the scanning electron micrograph of the tensile fracture surface of 1.36 % carbon sinter forged steel to nearly 99.8 % theoretical

density. This figure shows 'dimple shaped fracture' as in Fig. 6.102 with much finer structure associated with fine porosity in considerable amount. The structure more or less corresponds to the theoretical density as reported through measurements following water immersion technique.

Figure 6.104 shows the scanning electron micrograph of the tensile fracture surface of 0.45 % phosphorus sintered steel forged to nearly 99.3 % theoretical density at 960°C. Mode of fracture appears to be mixed type involving 'intergranular brittle fracture', dimple structure at localized spots and cleavage type fracture associated with river line markings on some facets. Quantitative estimation of porosity, through the micrograph, is in accordance with the theoretical density measured by conventional method - Archimedian Principle.

## 6.6 KINETICS OF PORE CLOSURE

Average pore diameter were measured for the upset forged specimens having 0.00, 39.63, 42.00 and 53.08 % height reductions, which are tabulated in Table 6.15.

Table 6.14

Relative Pore Diameter with Respect to  
Per Cent Deformation.

Per cent deformation	Pore size - Average* diameter at 100X; enlarged 6 times (in mm)	Relative pore dia.
0.00	5.50	1.00
39.62	1.95	0.36
42.00	1.70	0.31
53.08	0.83	0.15

Figure 6.106 shows the plot of relative pore dia vs per cent deformation in case of upset forging of sintered iron powder preform ( $H/D = 0.99$ ) at  $900^{\circ}\text{C}$ . This plot shows that as the height reduction is enhanced, pore-size (diameter) reduces. The curve can be a guide in assessing the optimum deformation (height-reduction) level required to obtain a completely dense product i.e. when pore size is or near to zero. For iron powder preform upsetting, as is depicted by Fig. 6.54, no pore-flattening occurs even at the highest value of deformation (53.08 %).

\* Diameters of 150-175 pores (in 2-3 directions for each) were measured and averaged out for each deformation.

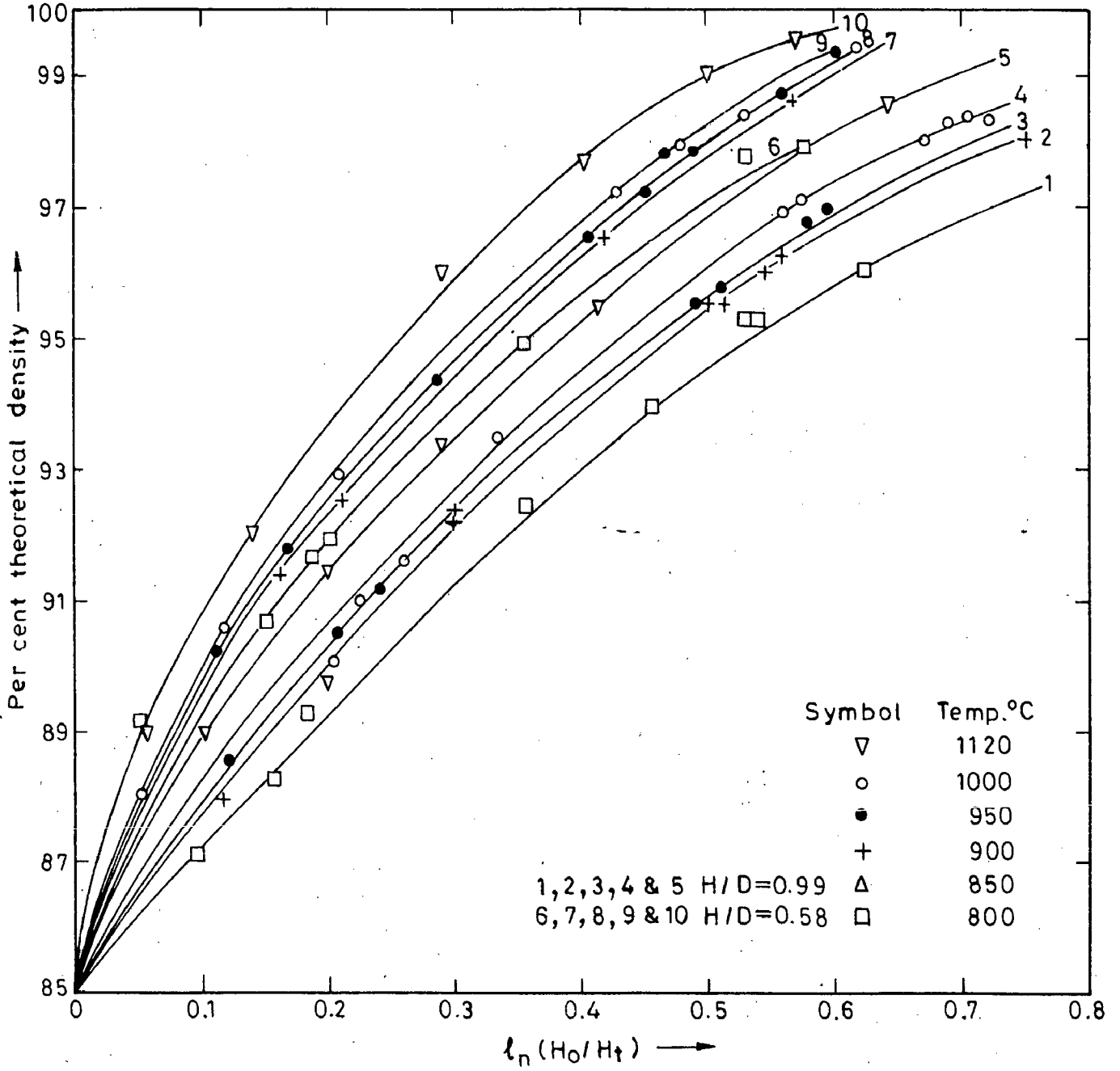


Fig.6.1(a)-Effect of height strain on percent theoretical density for sintered iron powder preform (H/D=0.57 and 0.99)



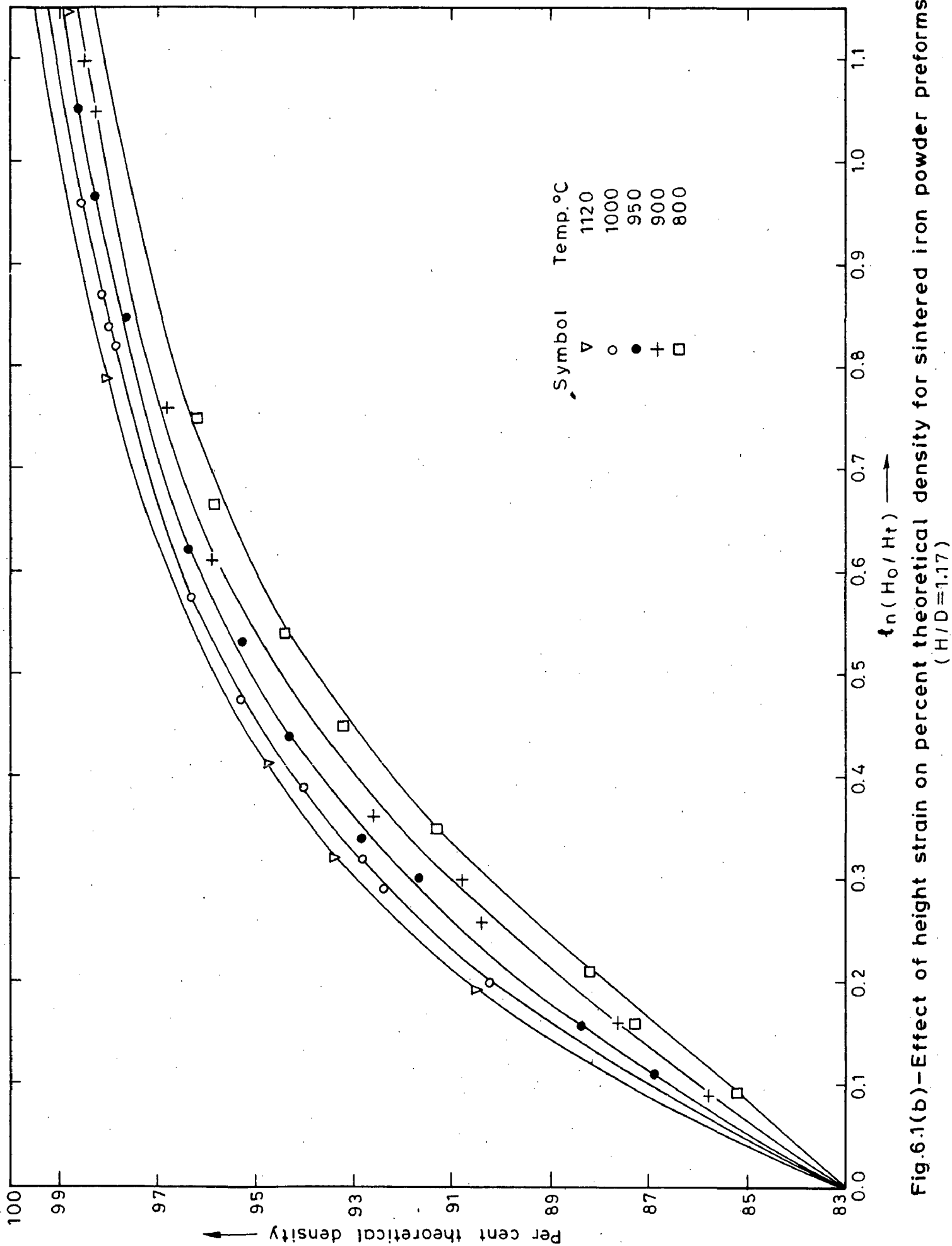


Fig.6.1(b)-Effect of height strain on percent theoretical density for sintered iron powder preforms (H/D=1.17)

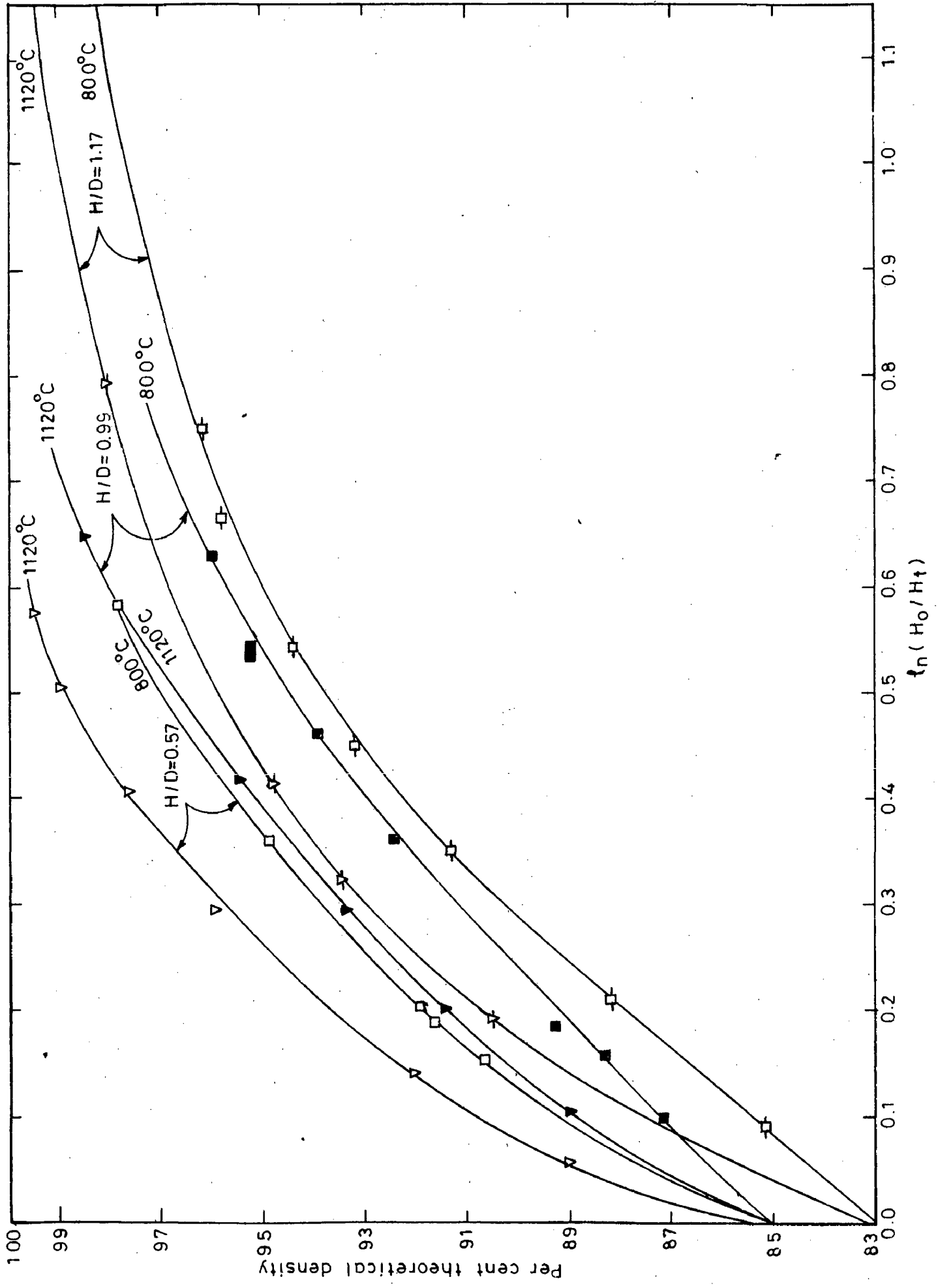


Fig.6.2-Effect of H/D ratio on percent theoretical density for sintered iron powder preforms

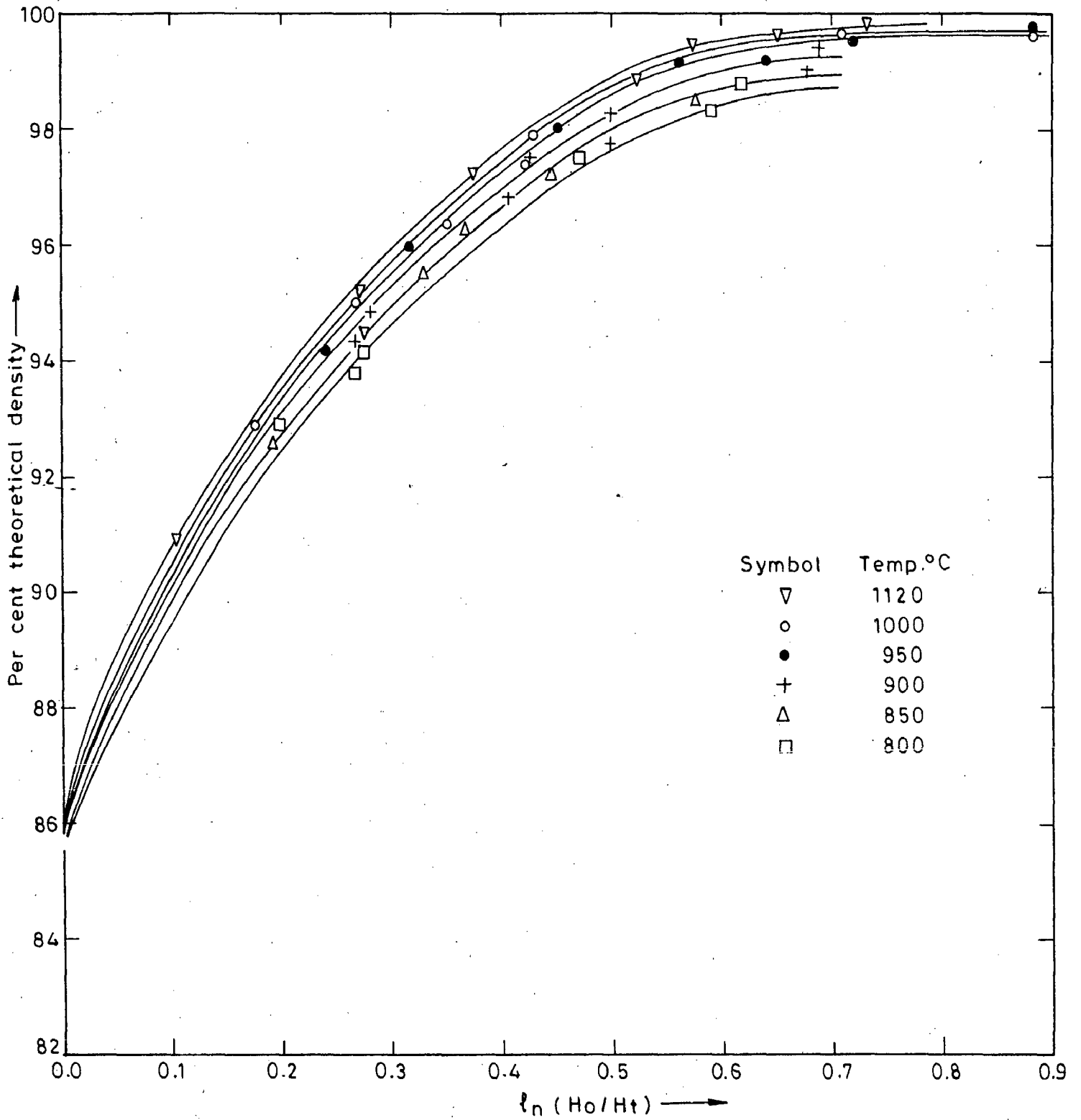


Fig.6.3—Effect of height strain on percent theoretical density for 0.43% graphite admixed iron powder sintered preform ( $\% C_a = 0.35$ ),  $H/D = 0.58$

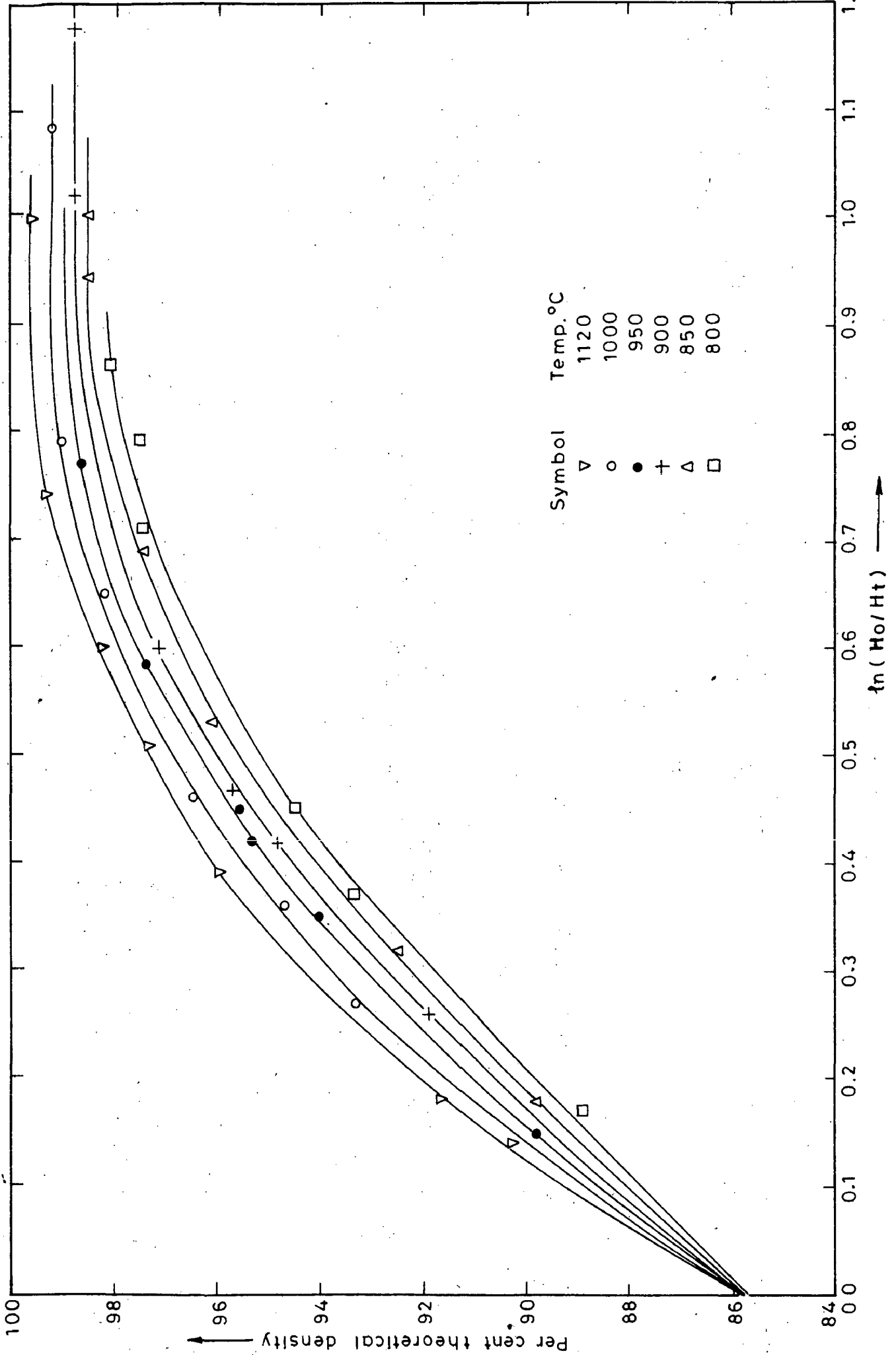


Fig.6.4-Effect of height strain on Percent theoretical density for 0.43% Graphite admixture iron powder sintered preform (%Ca=0.35), H/D=0.99

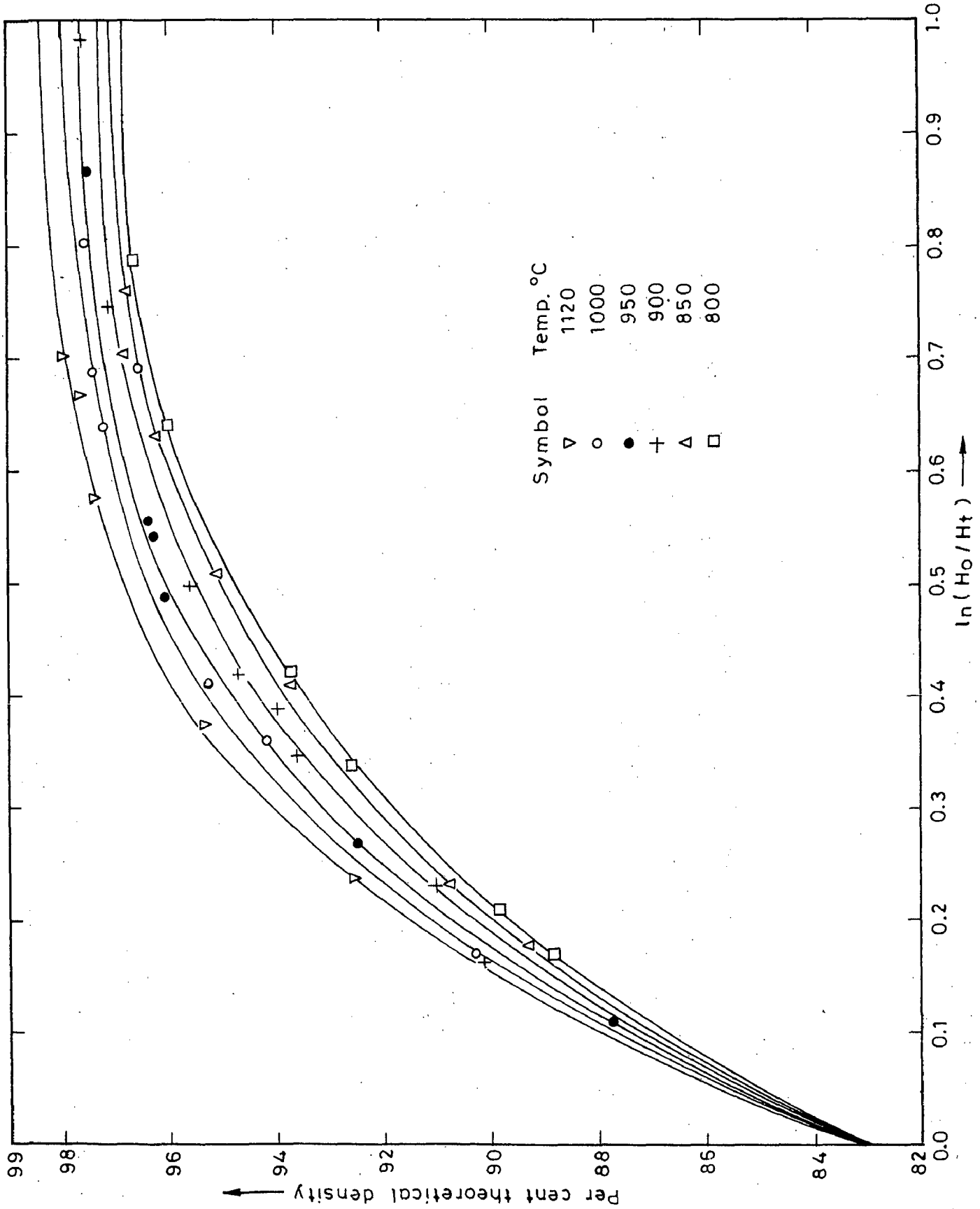


Fig.6.5-Effect of height strain on percent theoretical density for 1.14% graphite admixed iron powder sintered preform (%  $C_a = 0.83$ ),  $H/D = 0.58$

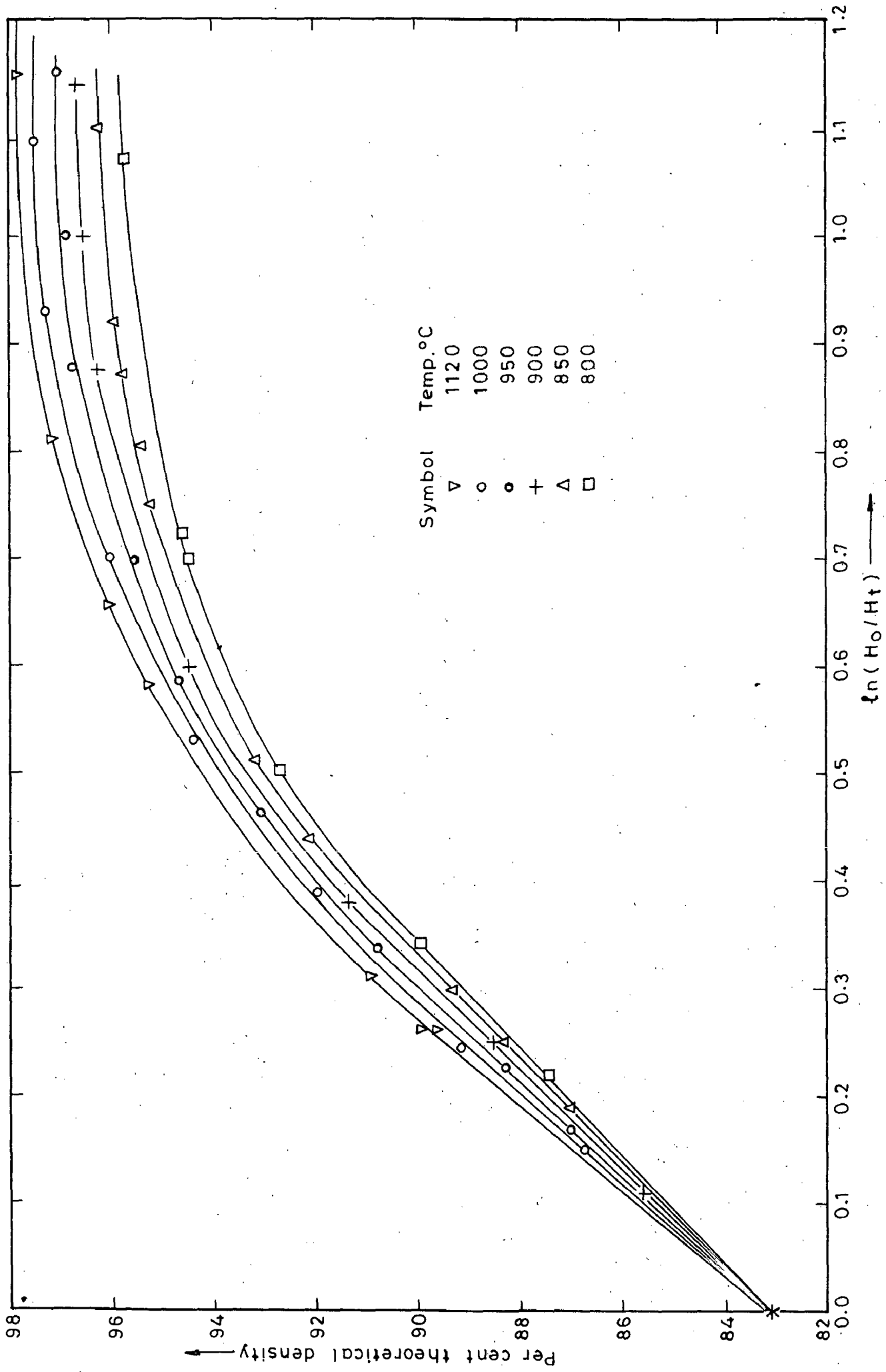


Fig.6.6-Effect of height strain on percent theoretical density for 1.14% Graphite admixed iron powder sintered preform (% Ca = 0.83) H/D = 0.99

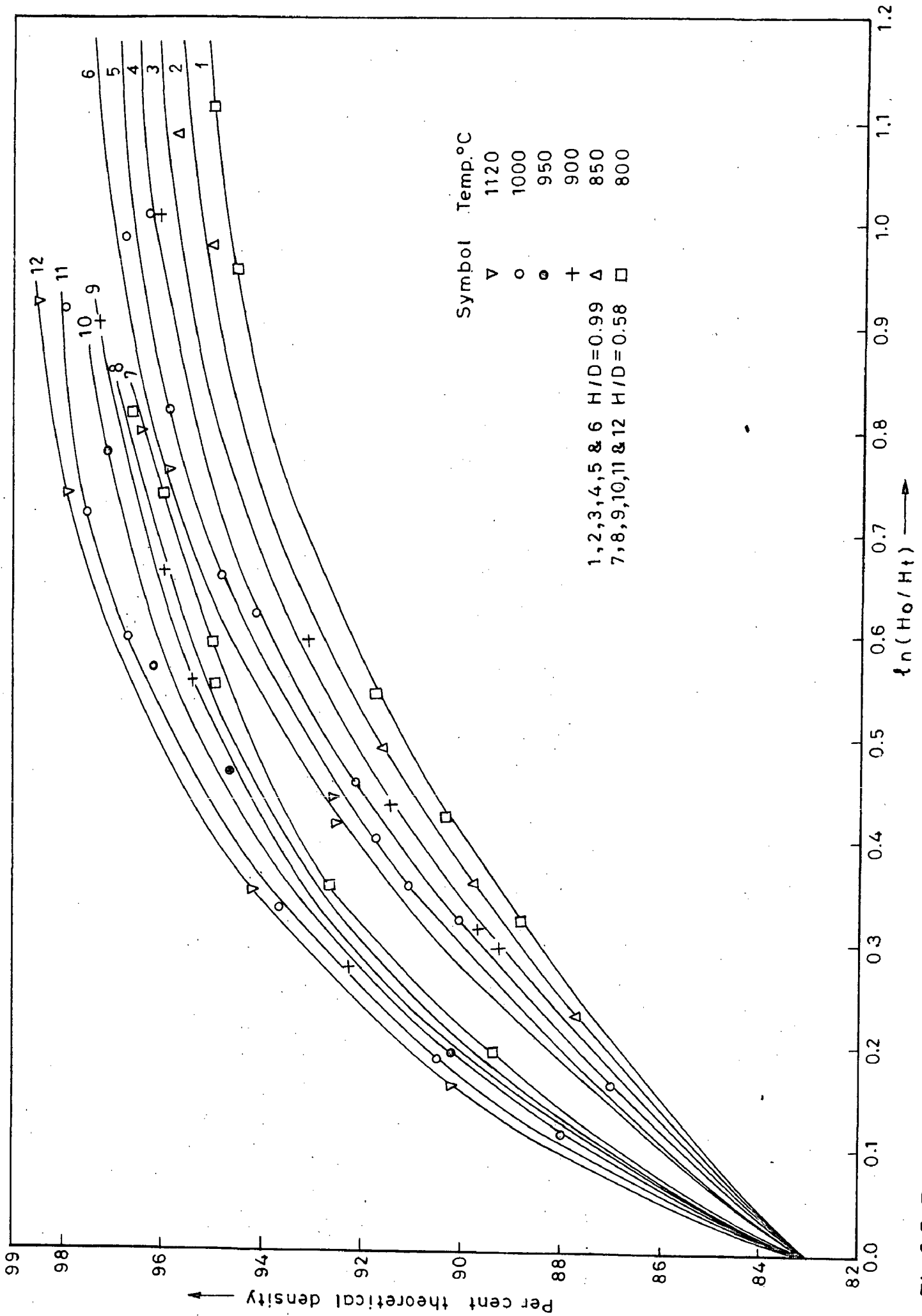


Fig.6.7-Effect of height strain on percent theoretical density for 1.86% graphite admixed iron powder sintered preform (% Ca = 1.34), H/D = 0.58 AND 0.99

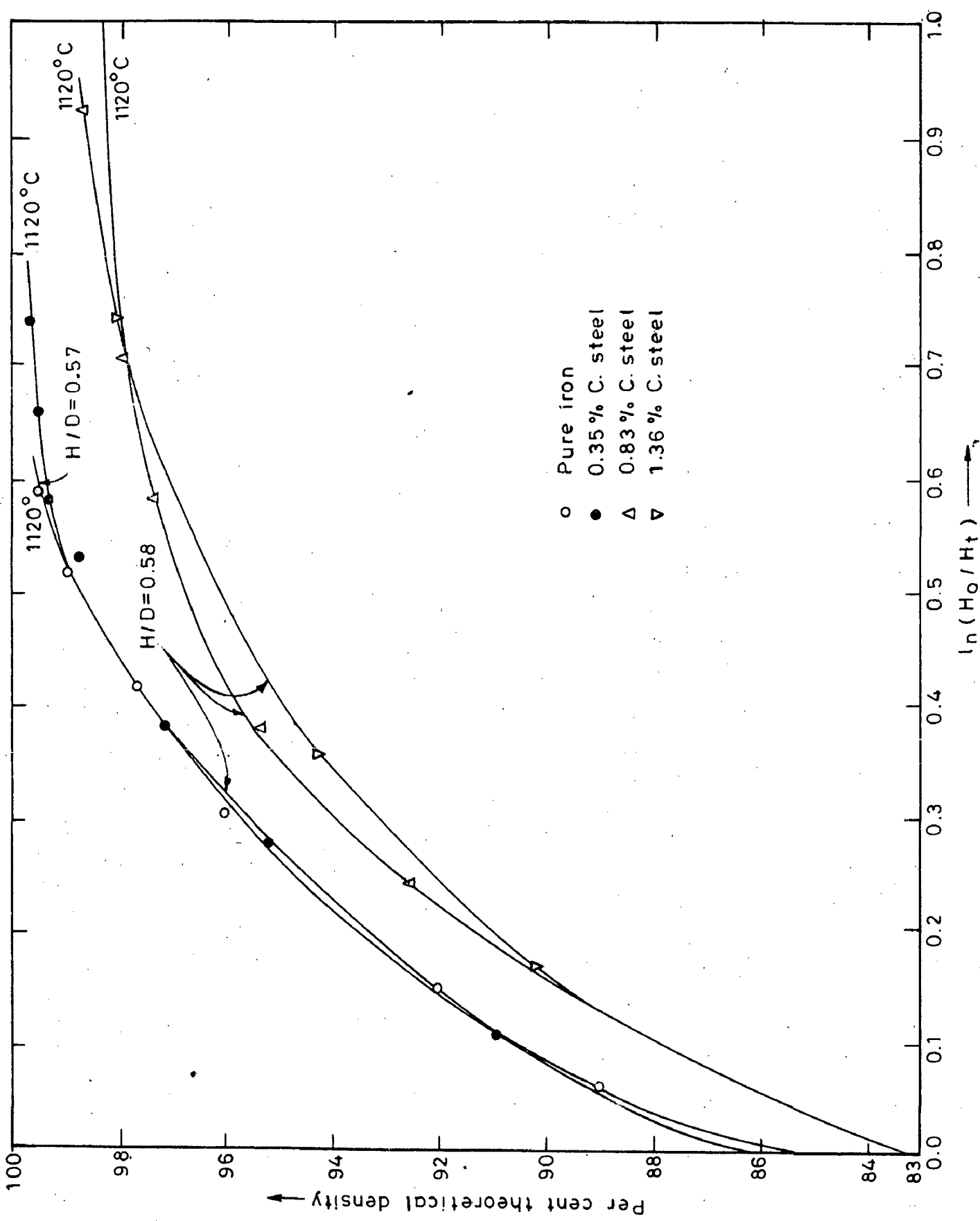


Fig.6.8-Effect of carbon on densification behaviour for  $H/D=0.57-0.58$  and temperature of forging  $1120^\circ\text{C}$



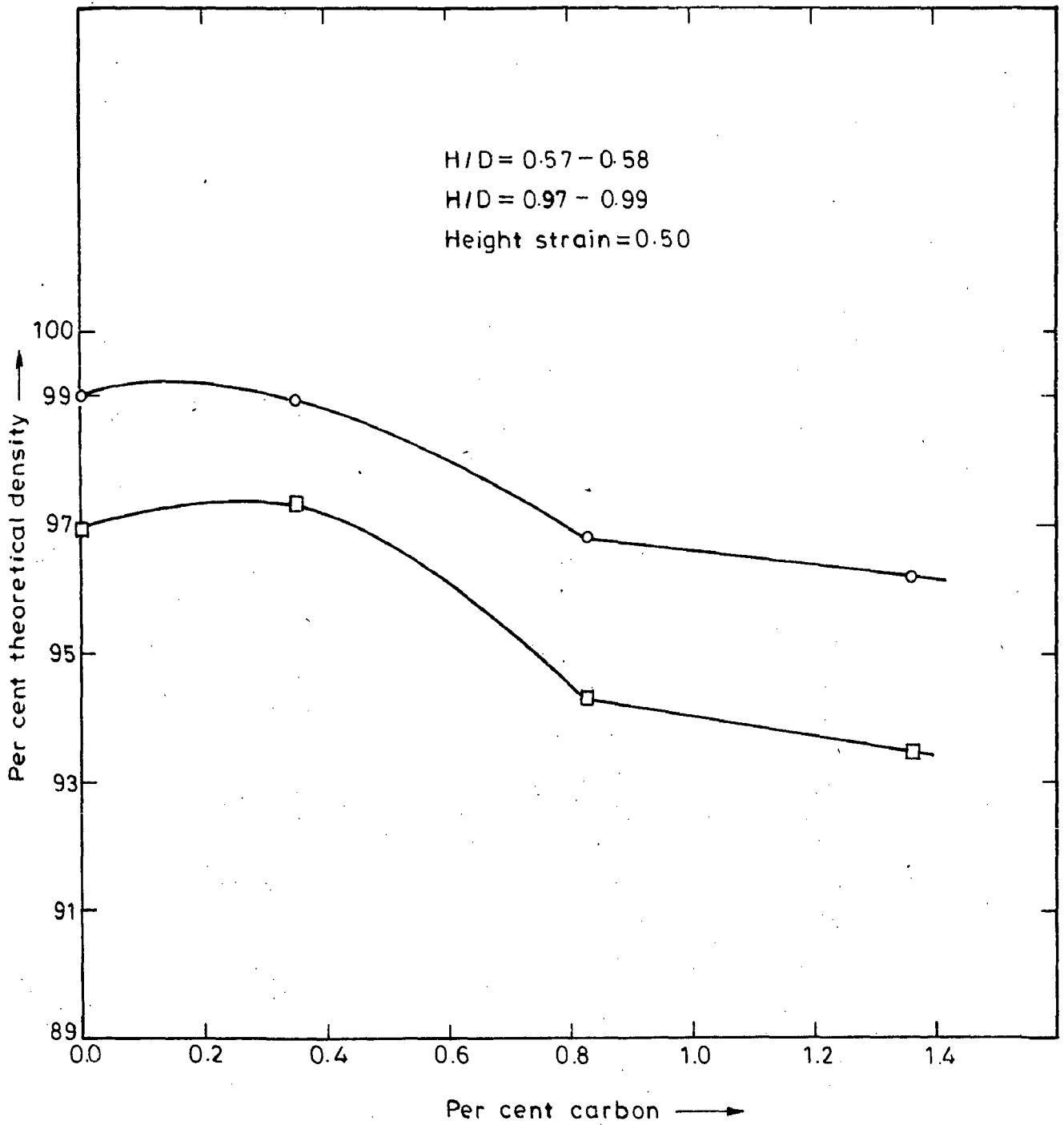


Fig.6.9-Plot of percent theoretical density with respect to per cent carbon in the alloy at the height strain of 0.50 at 1120°C

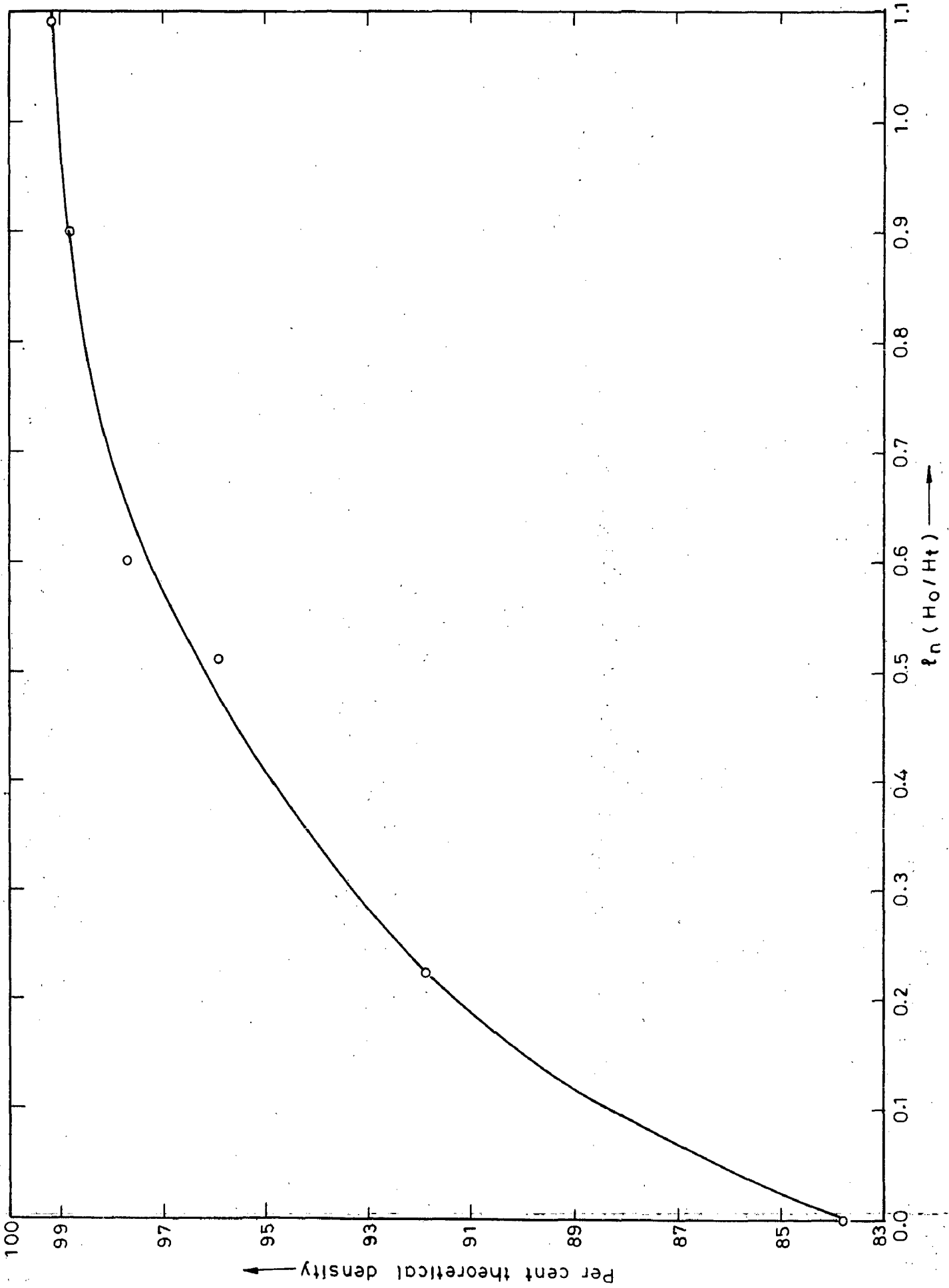


Fig.6.10-Densification behaviour of iron-0.45% phosphorus alloy powder sintered preform (H/D=0.59) upset forged at 960°

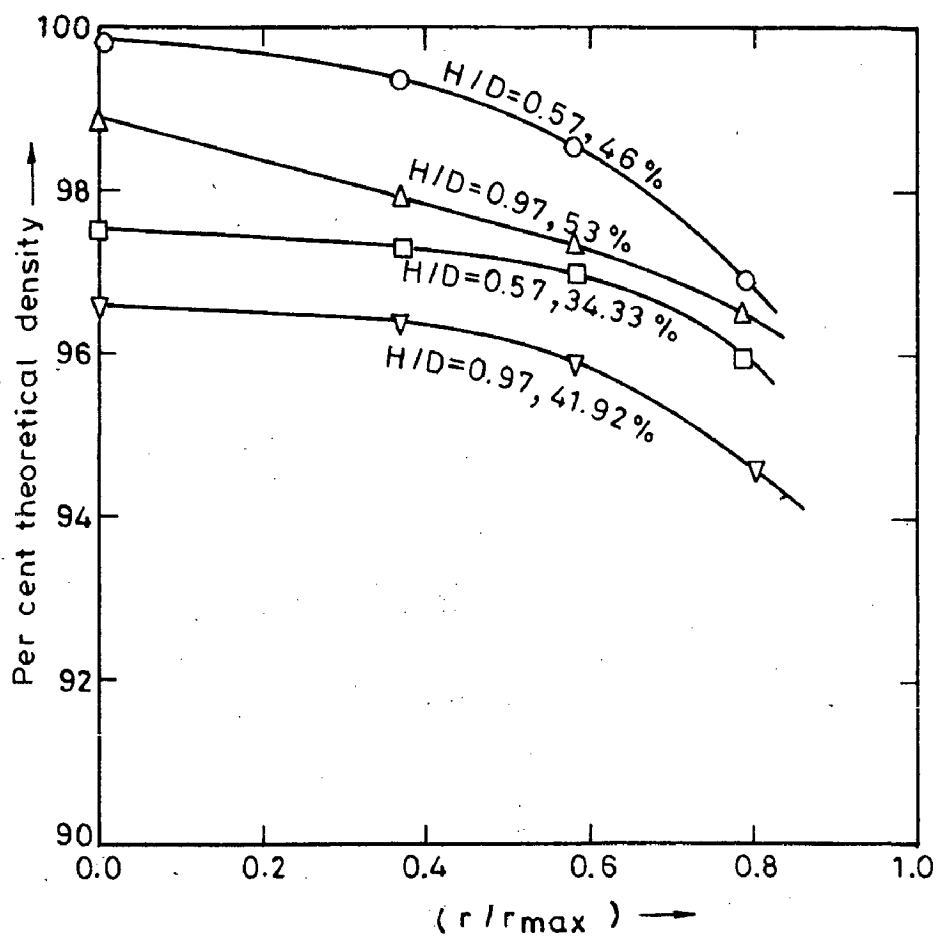


Fig.6.11-Density variation in forged components at 900°C for sintered iron powder preforms (H/D=0.57 & 0.97)

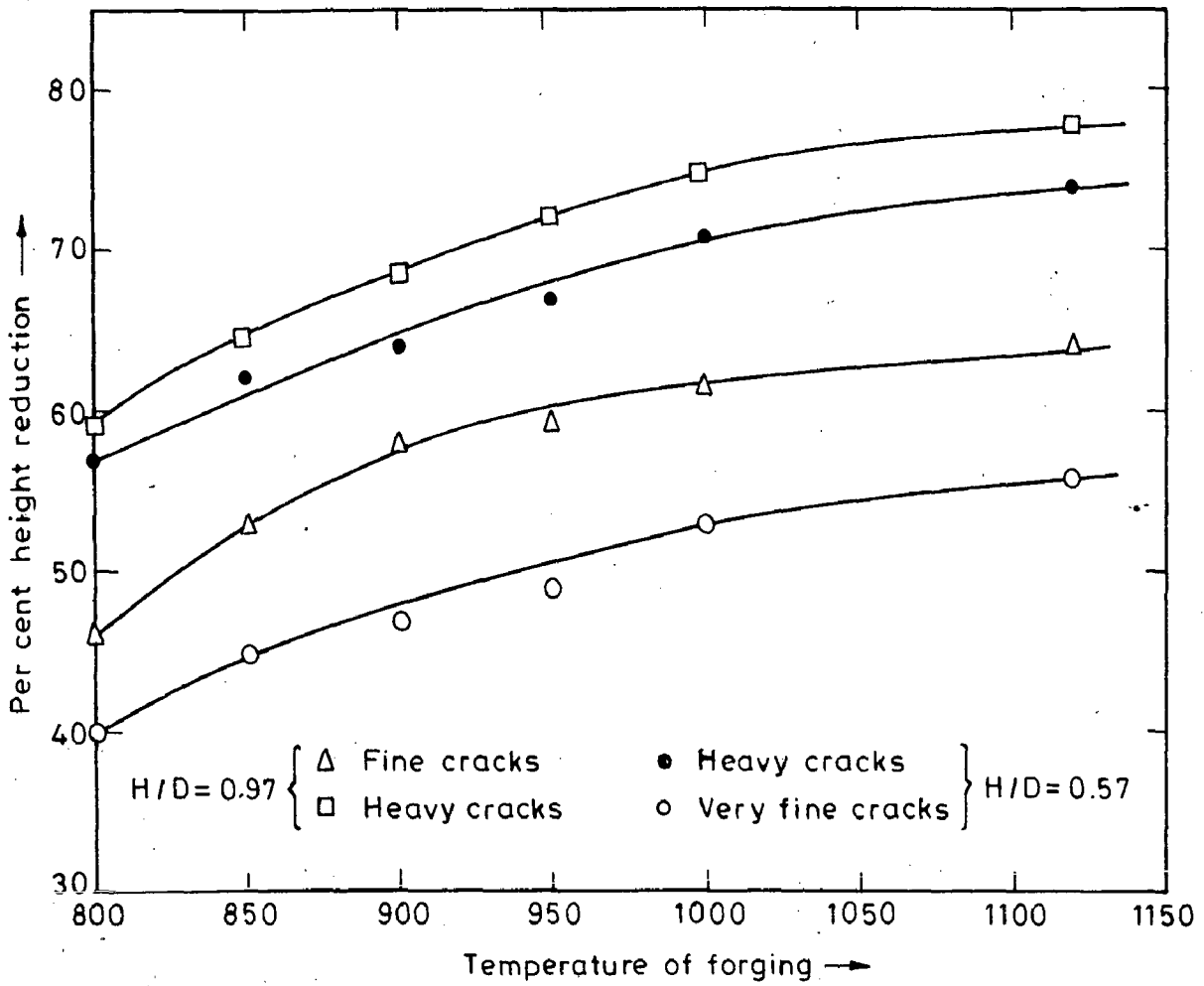


Fig.6.12-Relationship between reduction in height and forging temperature with respect to cracking for pure iron

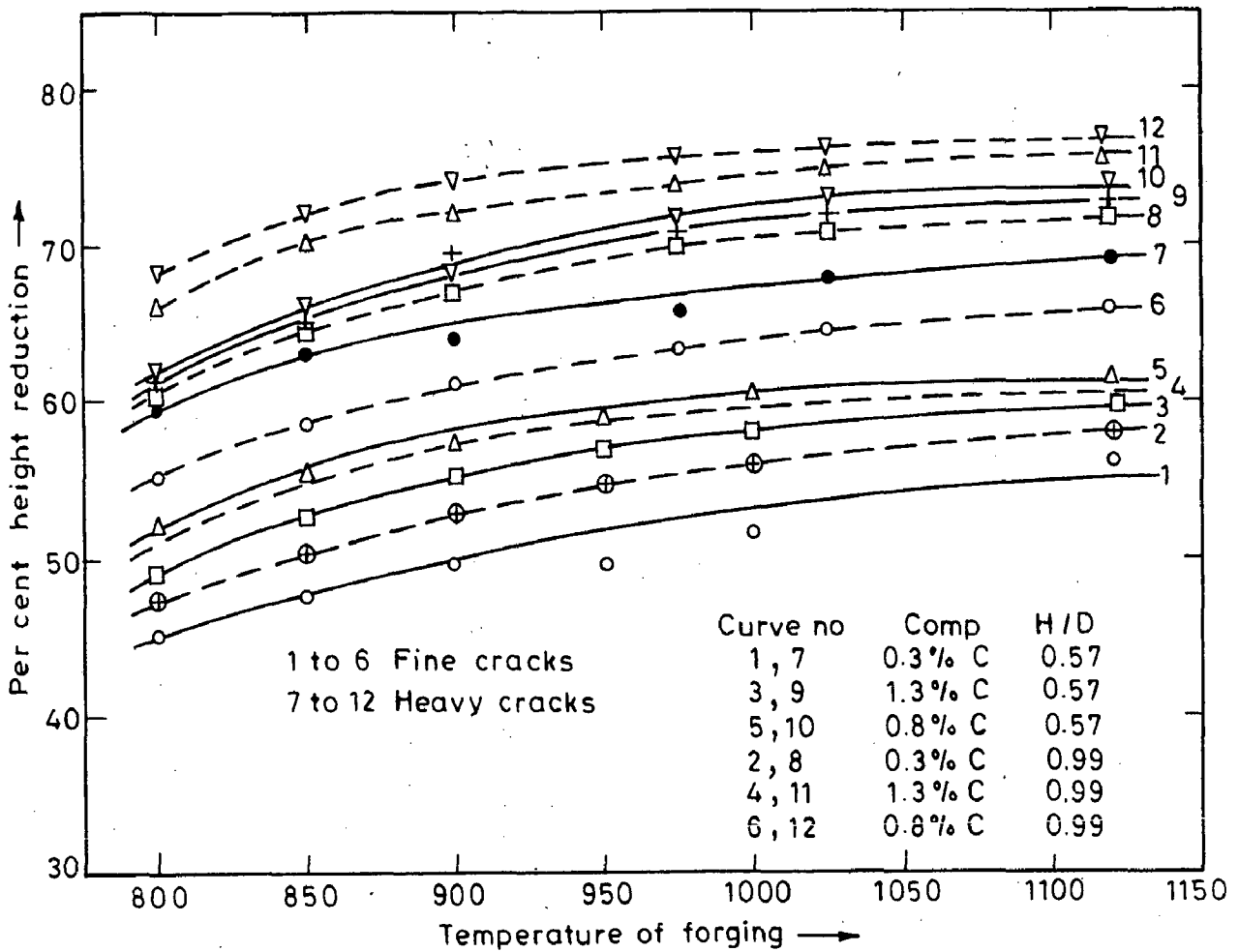


Fig.6.13-Relationship between reduction in height and forging temperature with respect to cracking during hot upset forging for different iron-carbon alloys

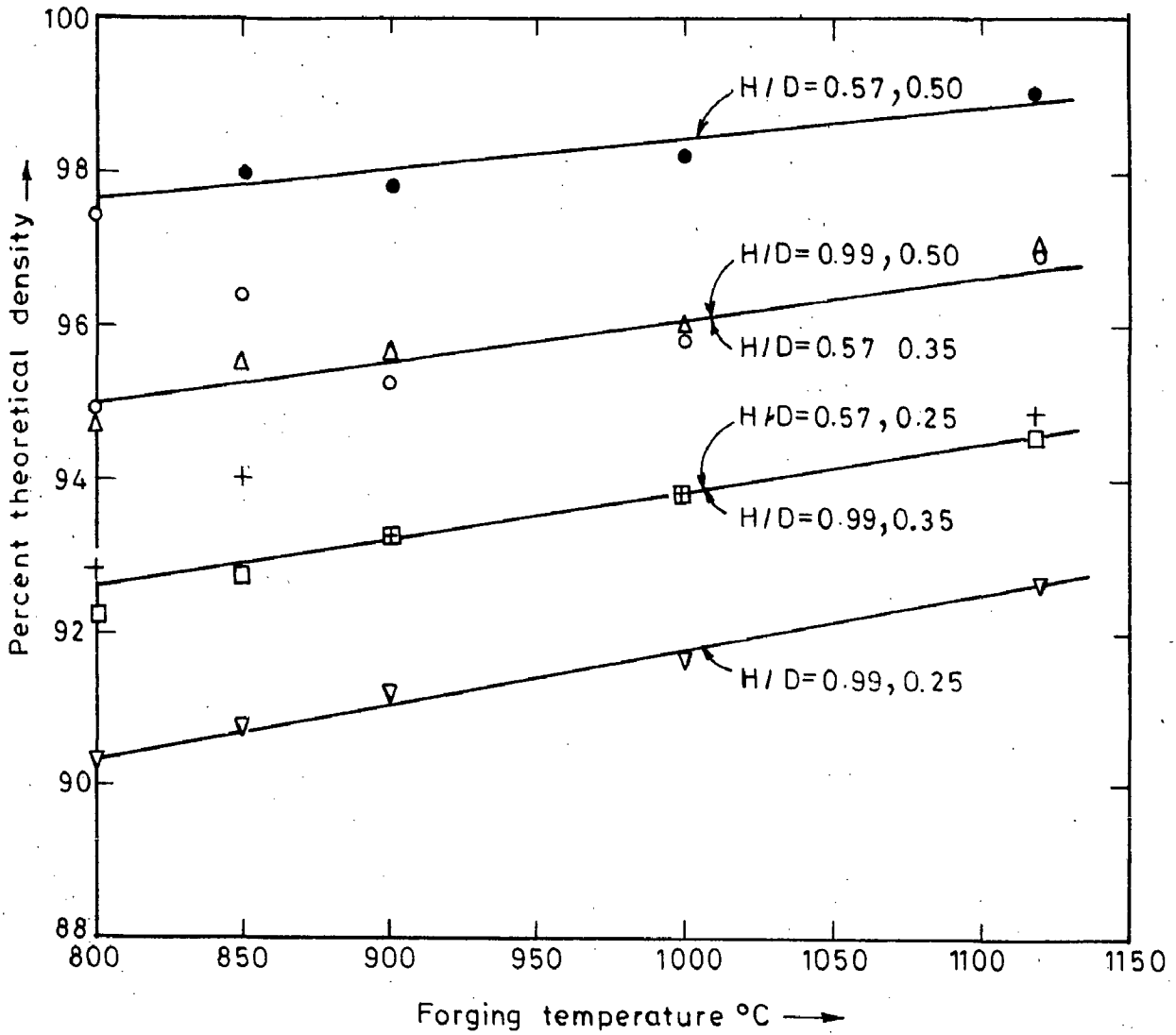


Fig.6.14-Effect of forging temperature upon densification for a fixed amount of deformation with different initial H/D ratio.

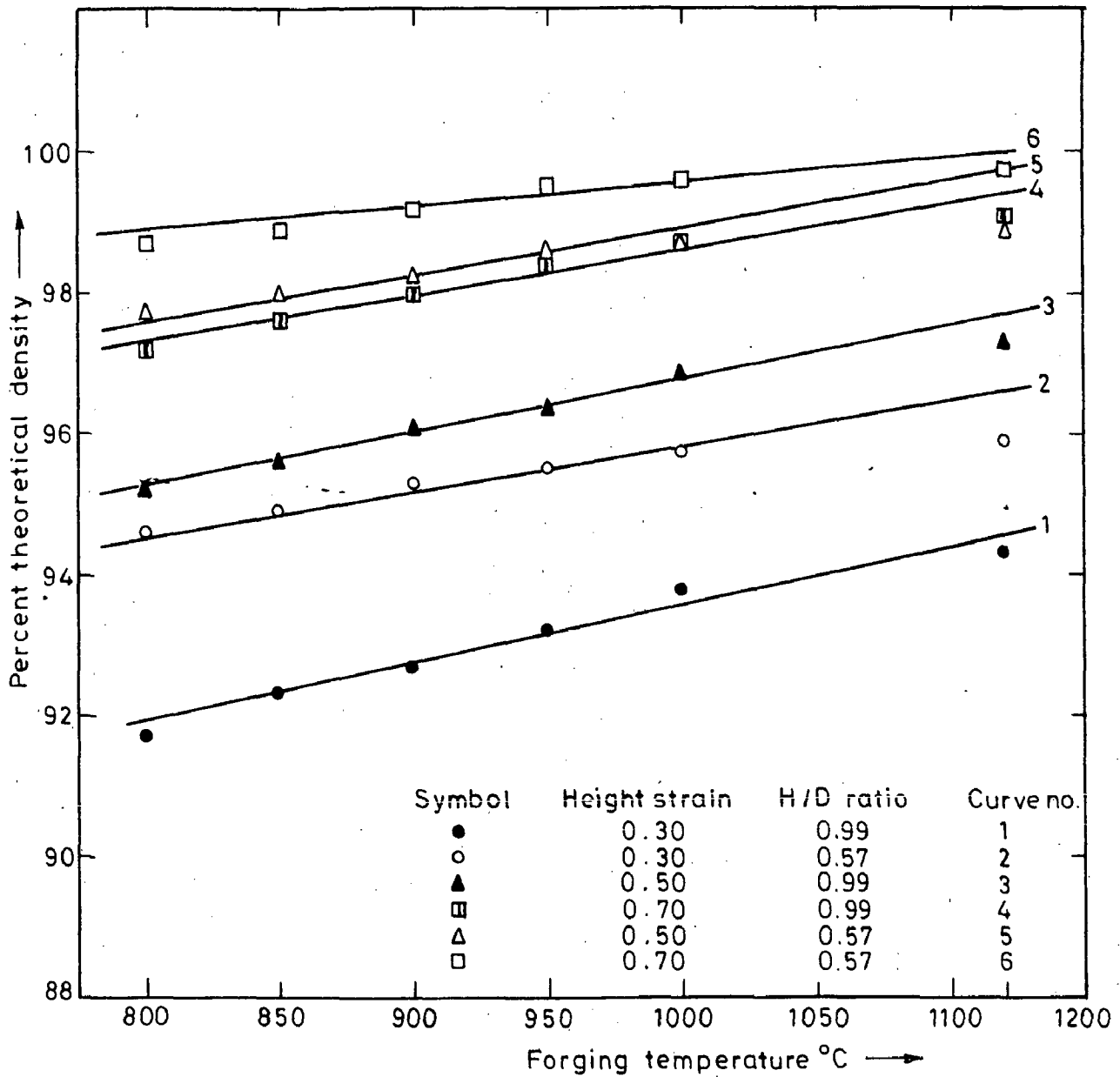


Fig.6.15-Effect of forging temperature on densification for a fixed amount of height strain for different H/D ratios for 0.35% carbon steel

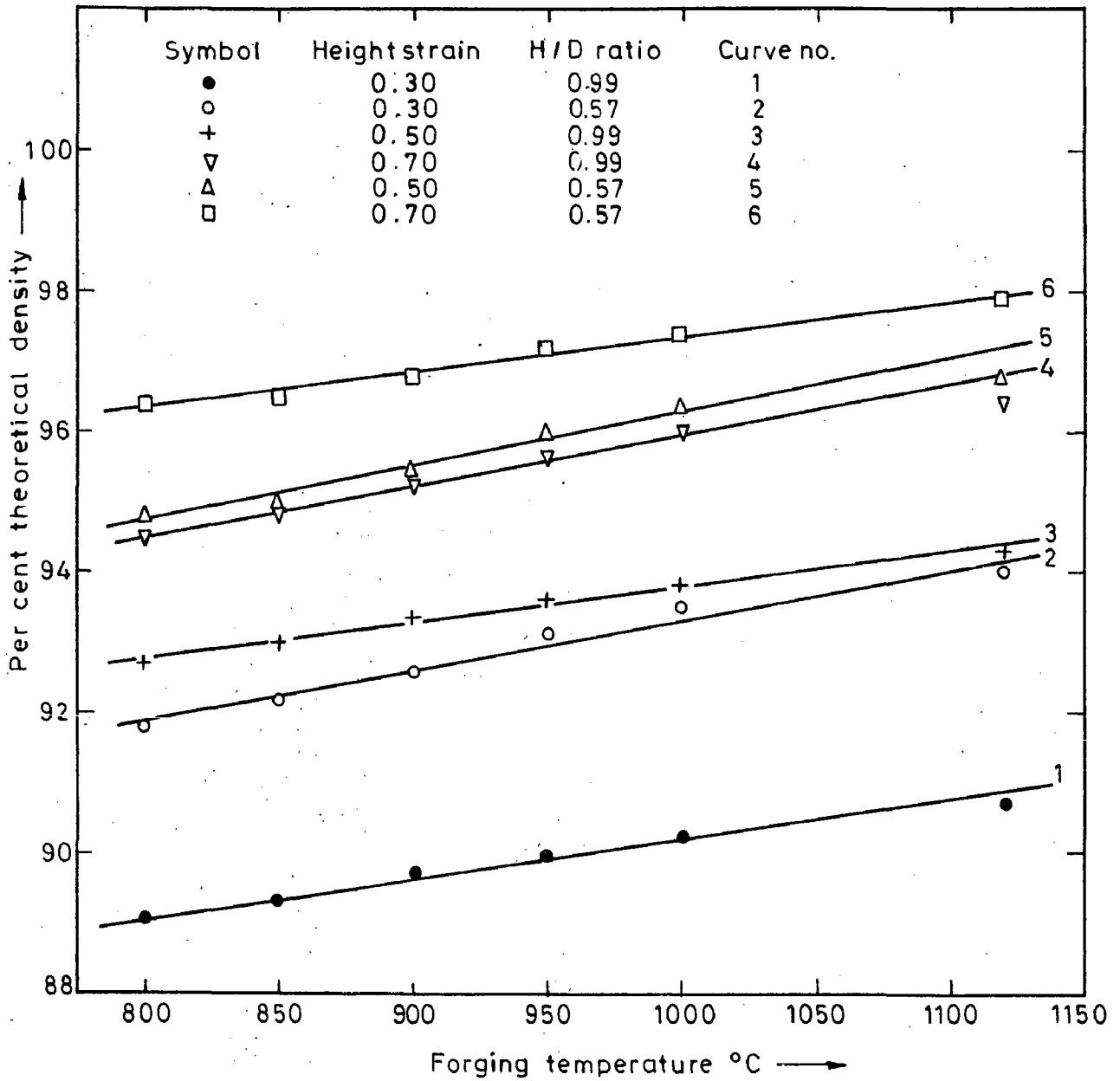


Fig.6.16-Effect of forging temperature on densification for a fixed amount of height strain for different H/D ratio for 0.83% carbon steel



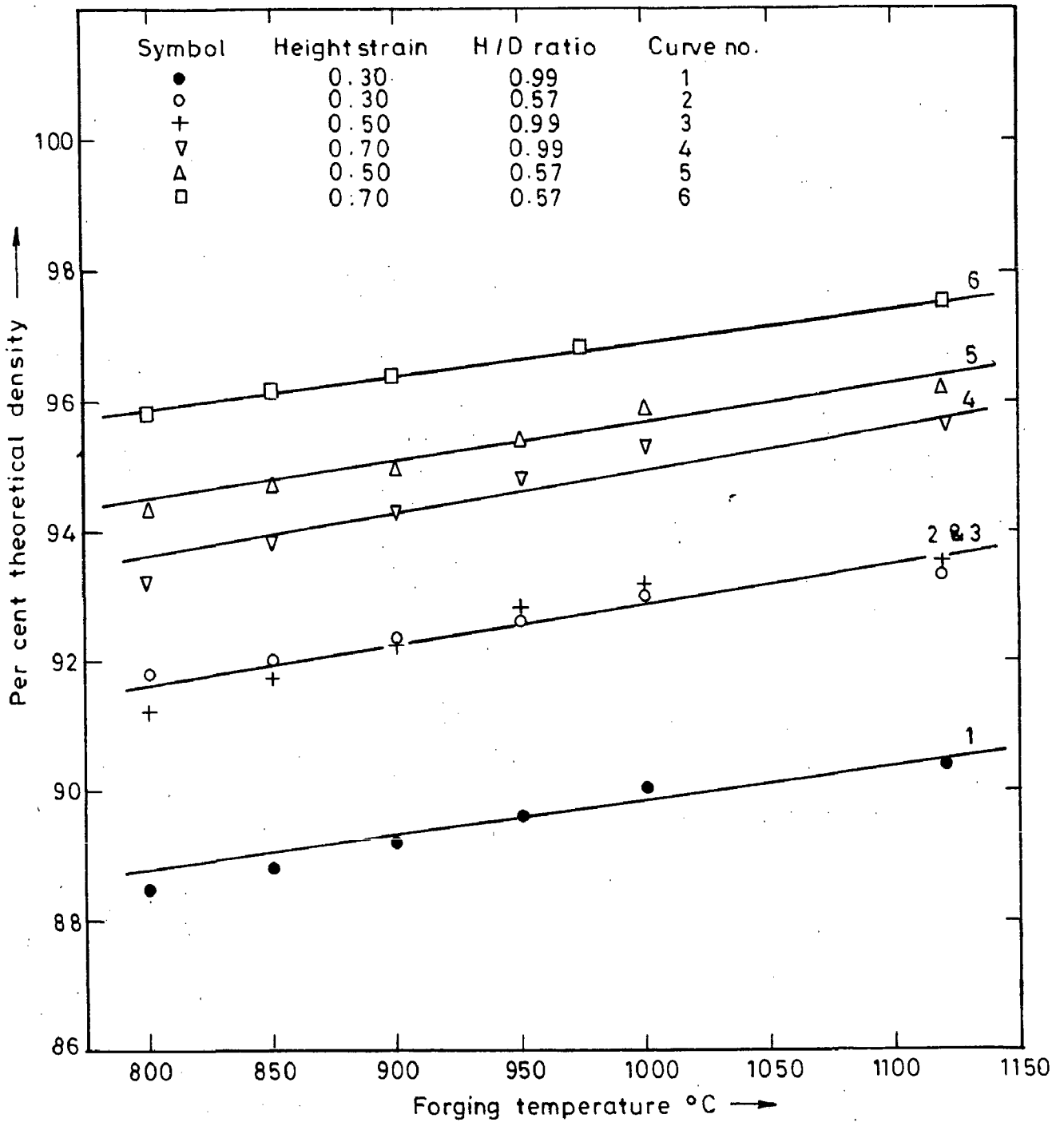


Fig.6.17-Effect of forging temperature on densification for a fixed amount of height strain for different H/D ratios for 1.36% carbon steel

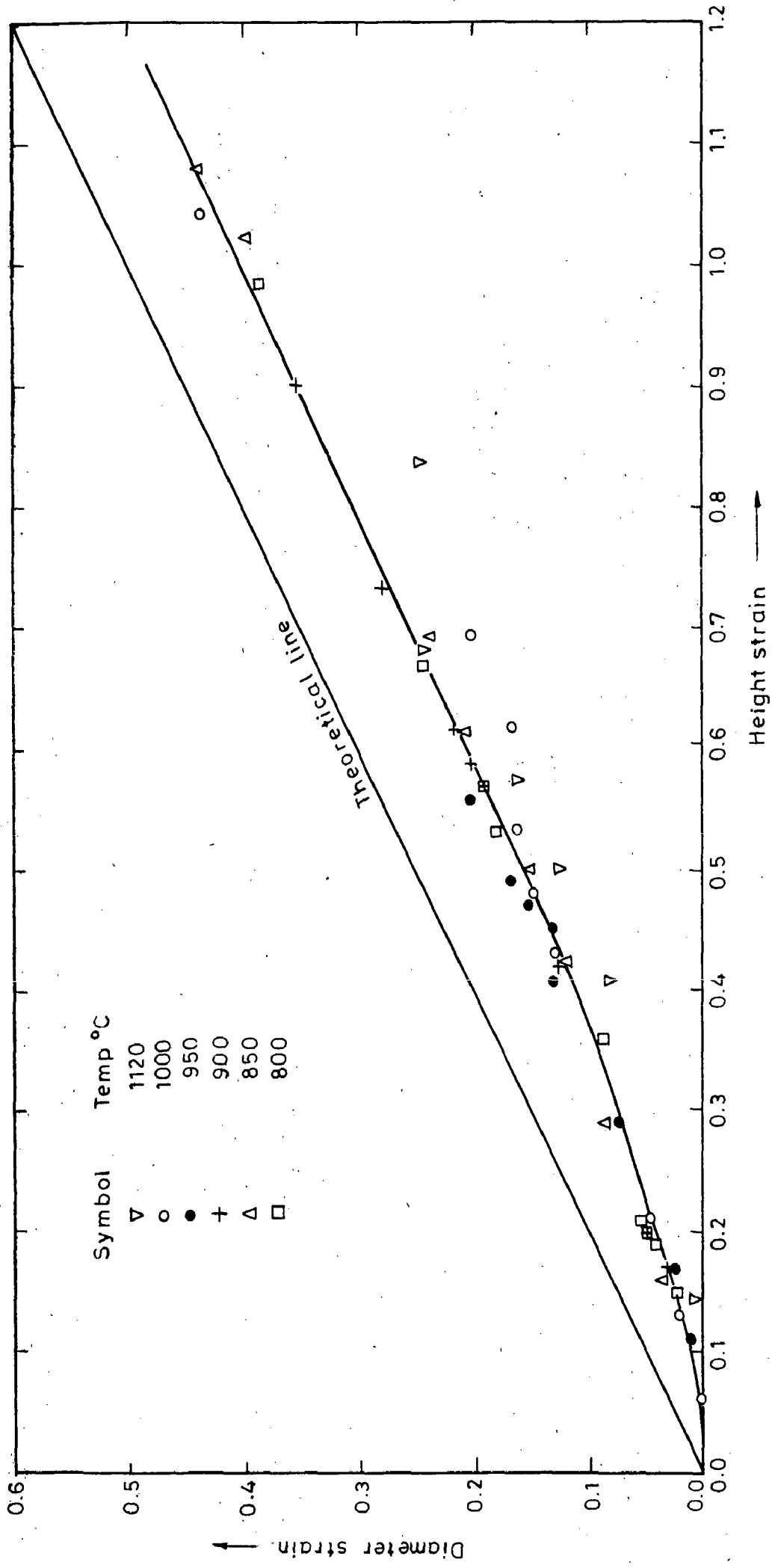


Fig.6.18- Relationship between diameter strain and height strain for iron powder sintered preform (H/D=0.57) during hot upsetting

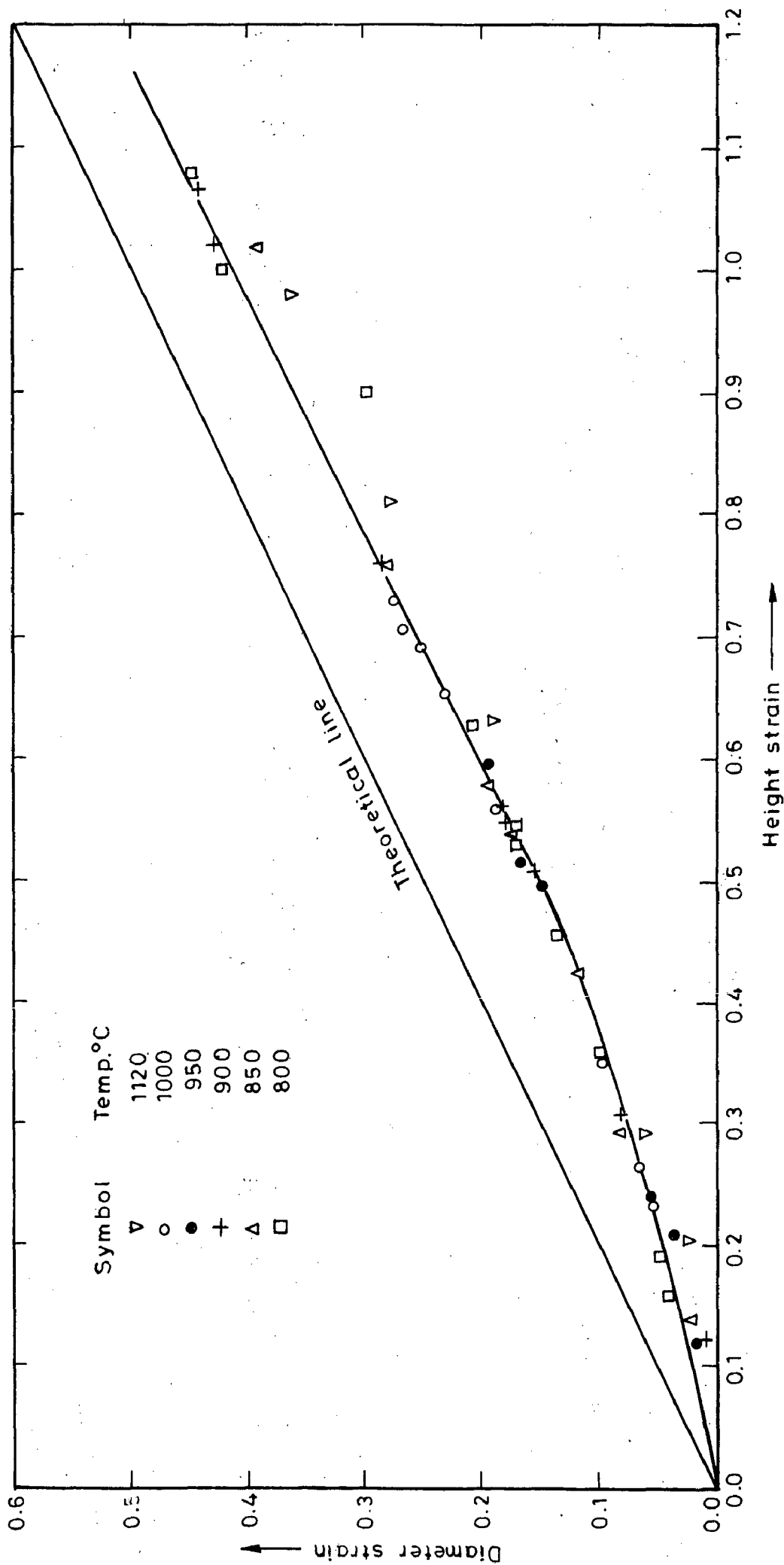


Fig.6.19-Relationship between diameter strain and height strain for iron powder sintered preform (H/D=0.99) during hot upsetting

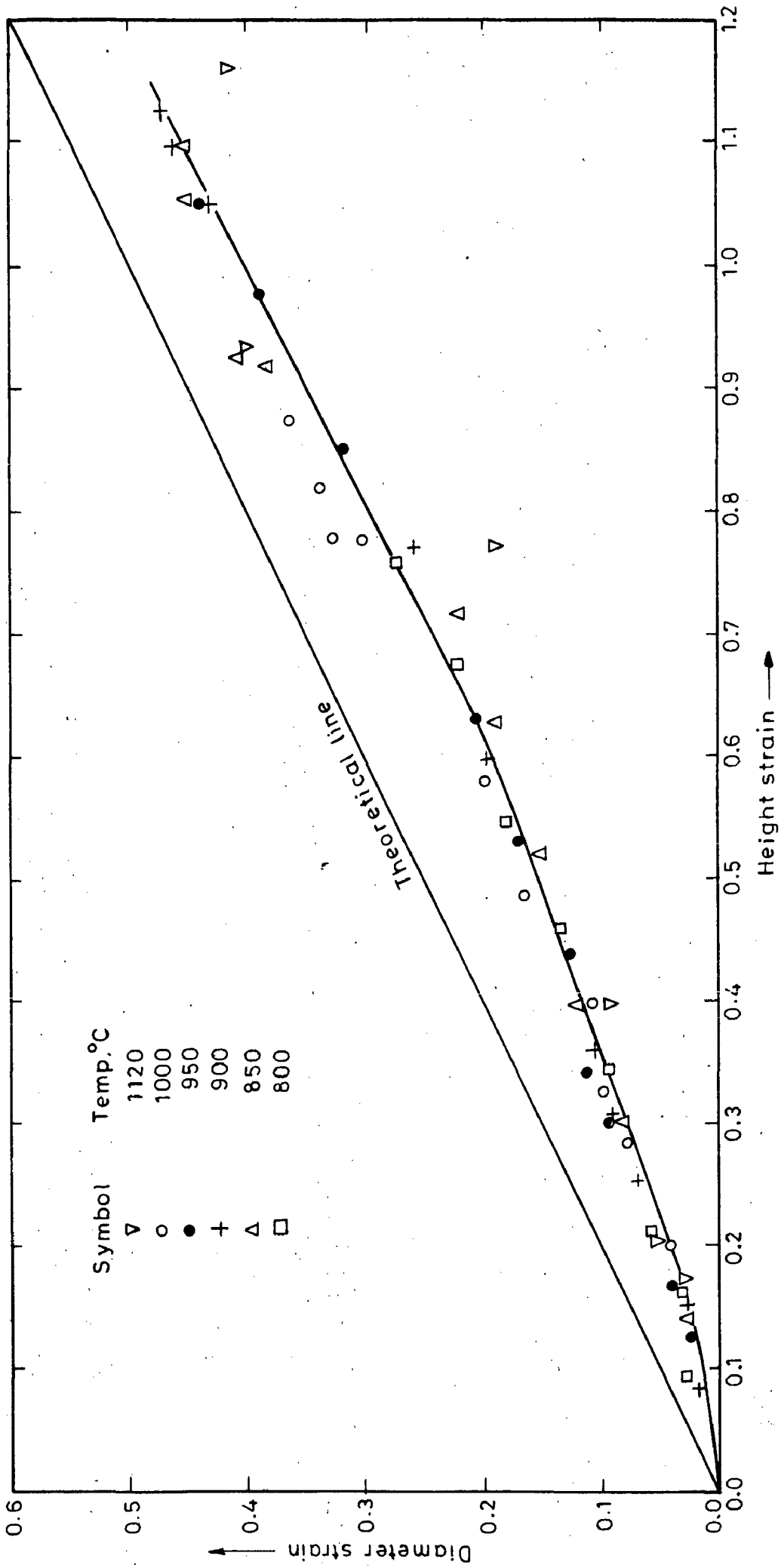


Fig.6.20— Relationship between diameter strain and height strain for iron powder sintered preform ( $H/D=1.17$ ) during hot upsetting

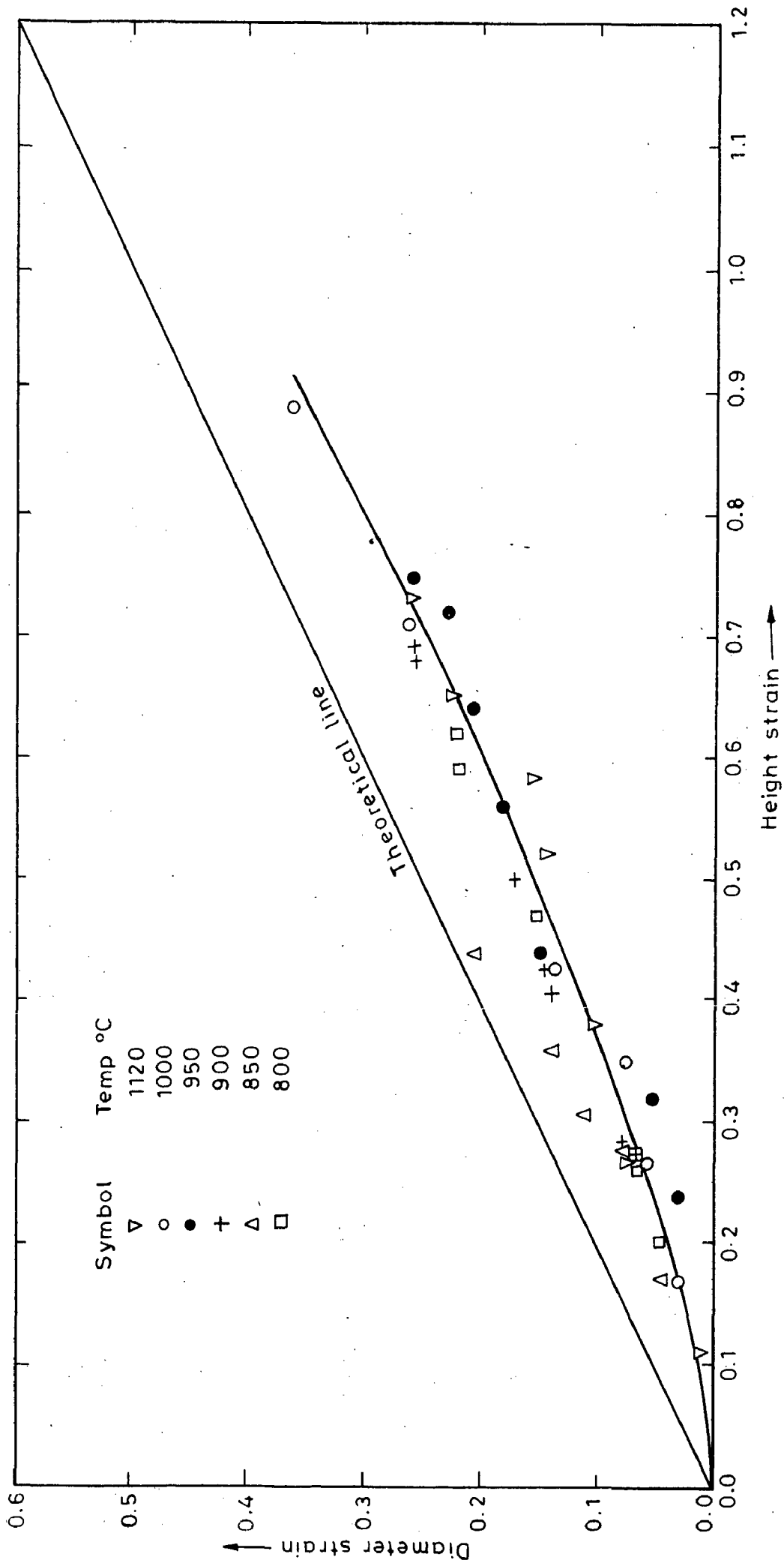


Fig.6.21-Relationship between diameter strain and height strain for 0.35 % C- Fe preform (H/D=0.98) during hot upsetting

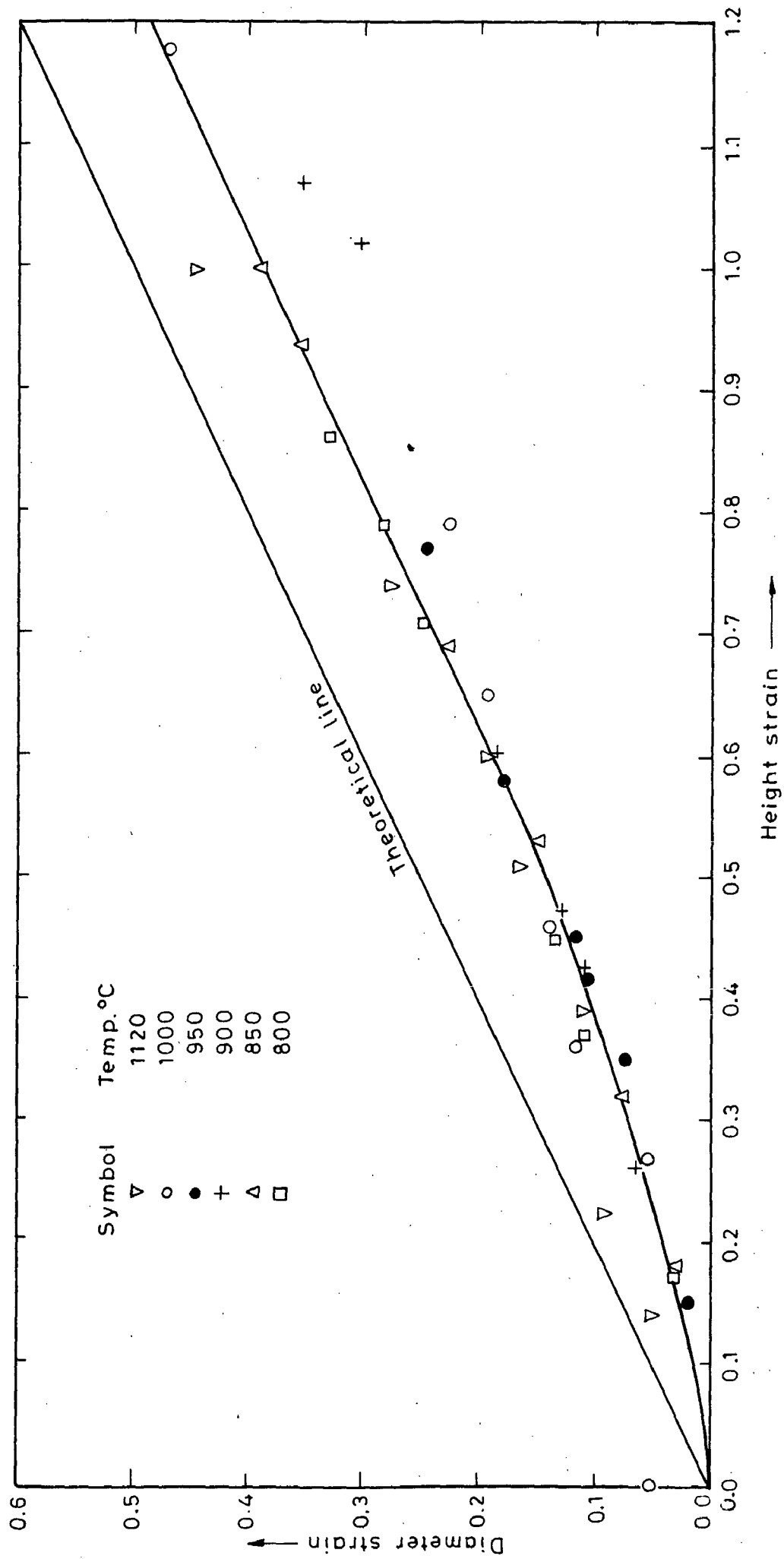


Fig.6.22-Relationship between diameter strain and height strain for 0.35% C-Fe preform (H/D=0.98) during hot upsetting

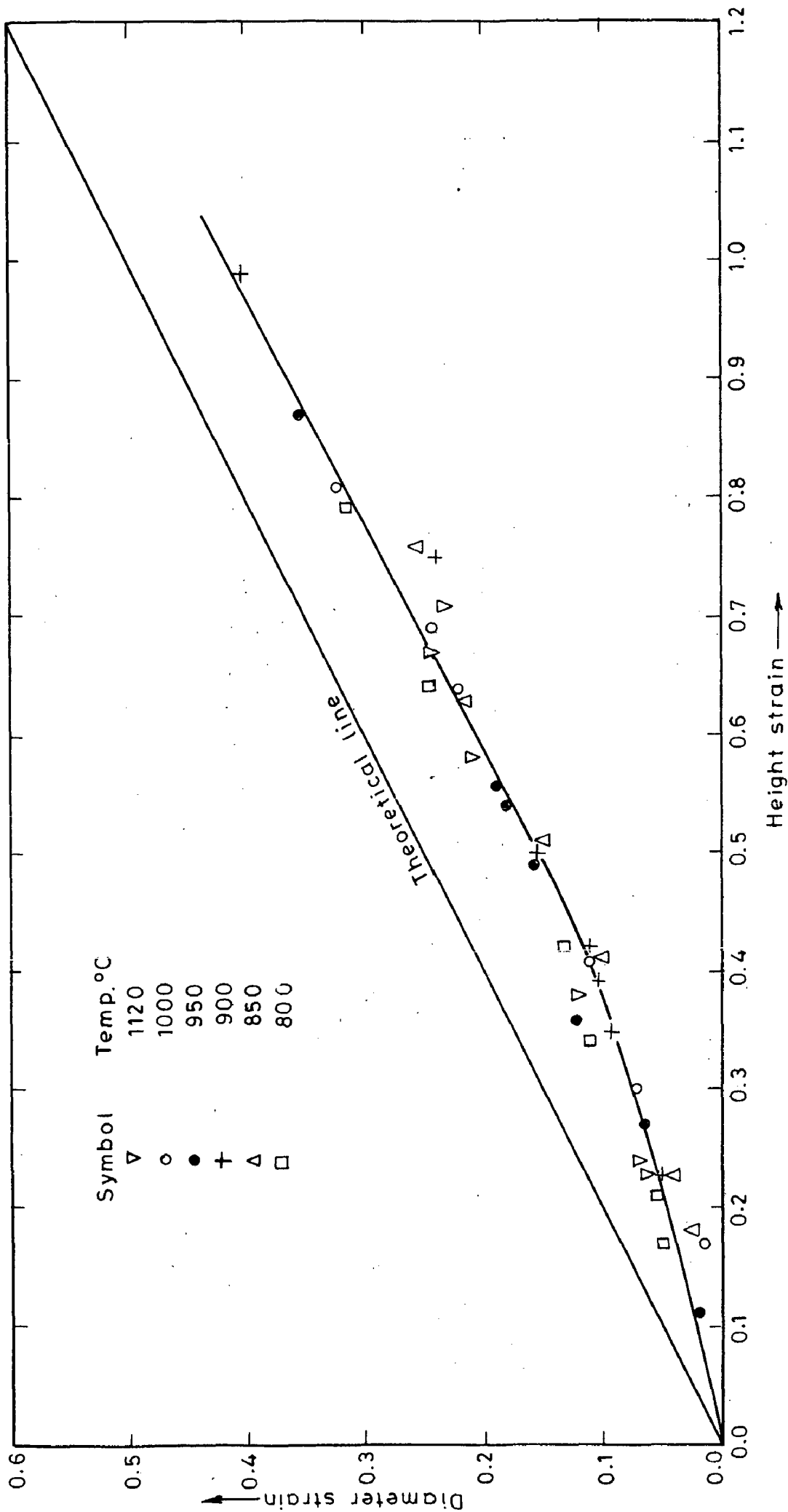


Fig.6.23-Relationship between diameter strain and height strain for 0.83% C-Fe preform (H/D=0.57) during hot upsetting

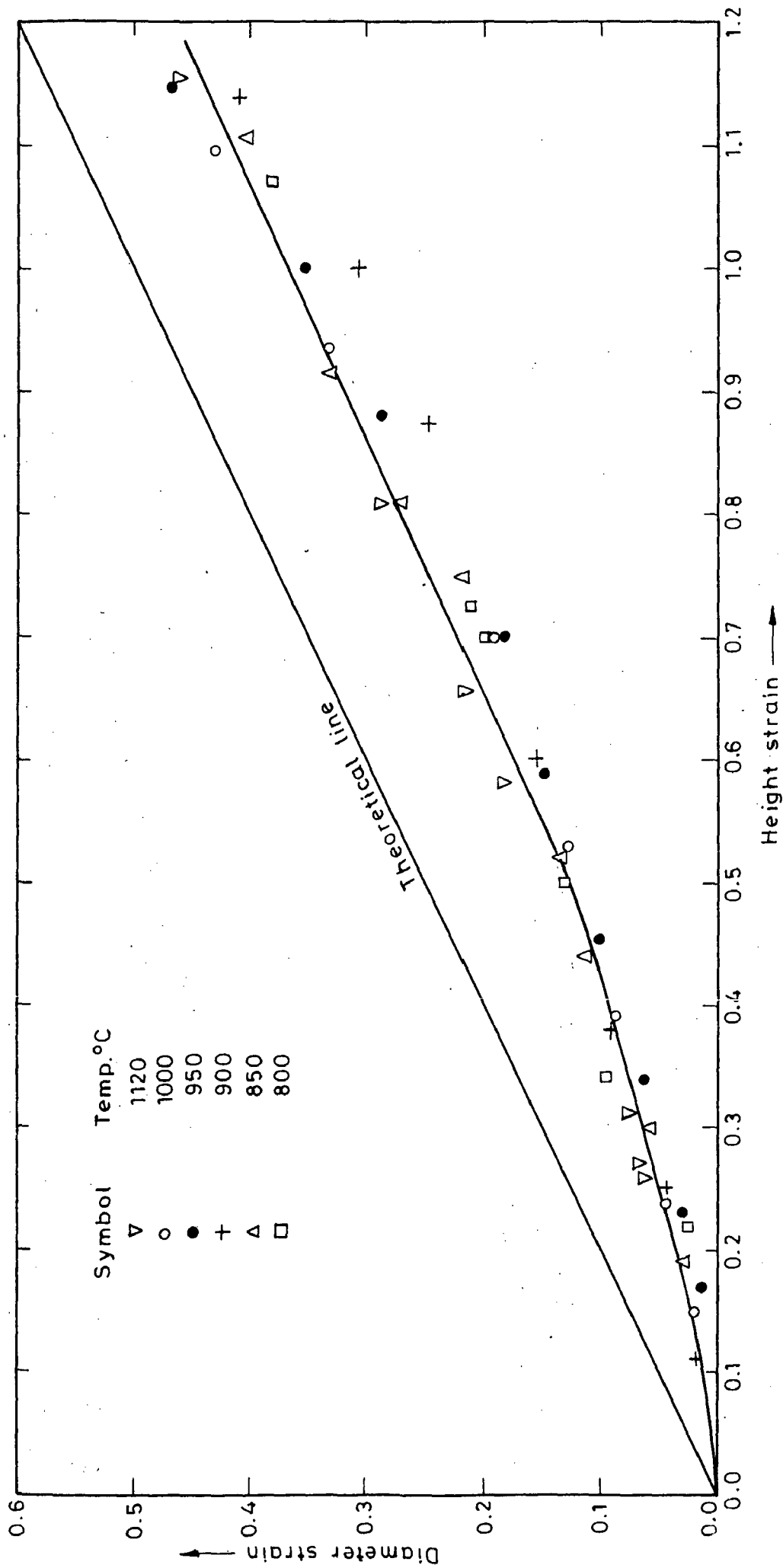


Fig.6.2.4-Relationship between diameter and height strain for 0.83% C-Fe preform (H/D=0.98) during hot upsetting.



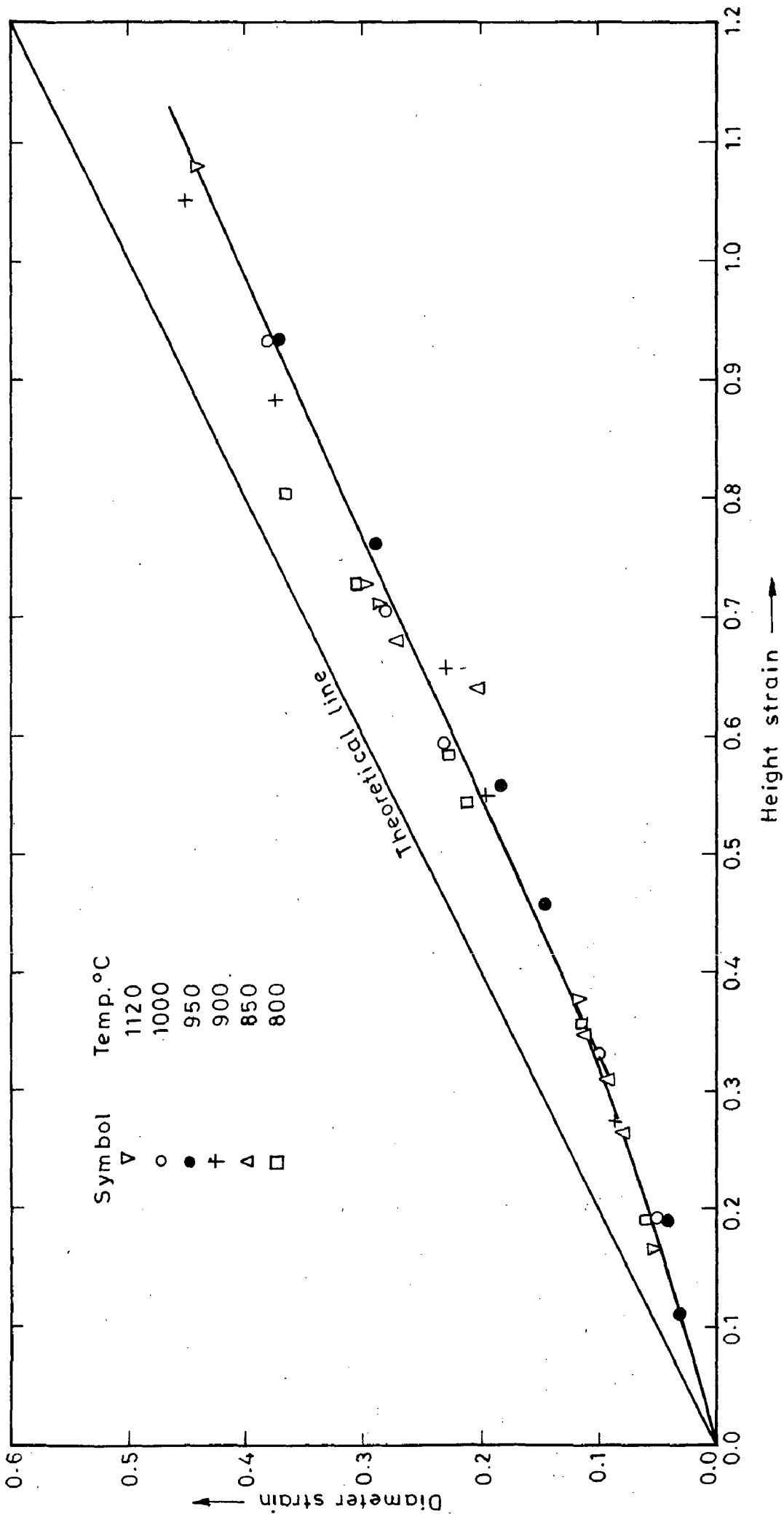


Fig.6.25- Relationship between diameter strain and height strain for 1.36% C-Fe preform ( $H/D=0.58$ ) during hot upsetting

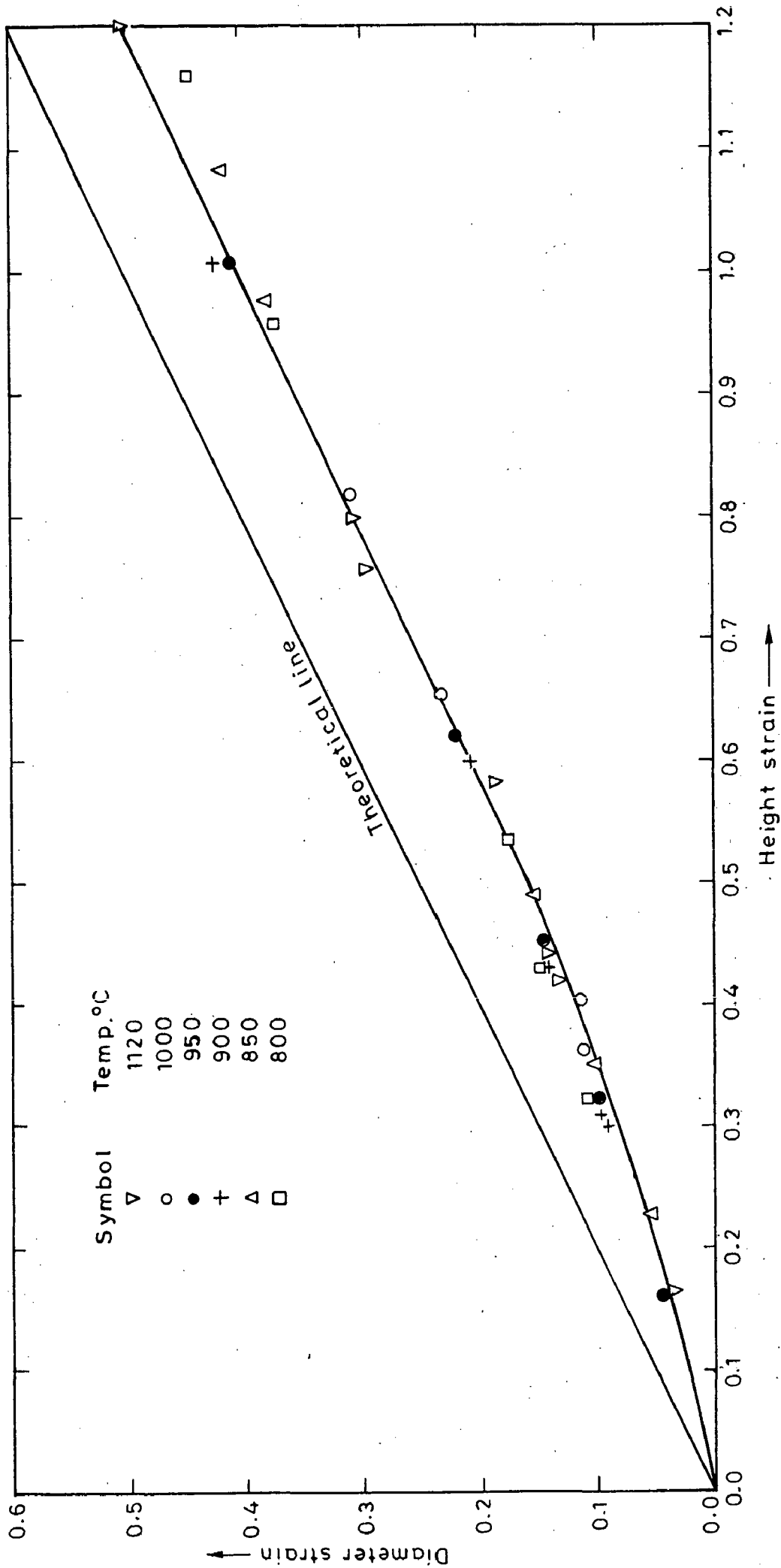


Fig.6.26-Relationship between diameter strain and height strain for 1.36% C-Fe preform (H/D=0.99) during hot upsetting

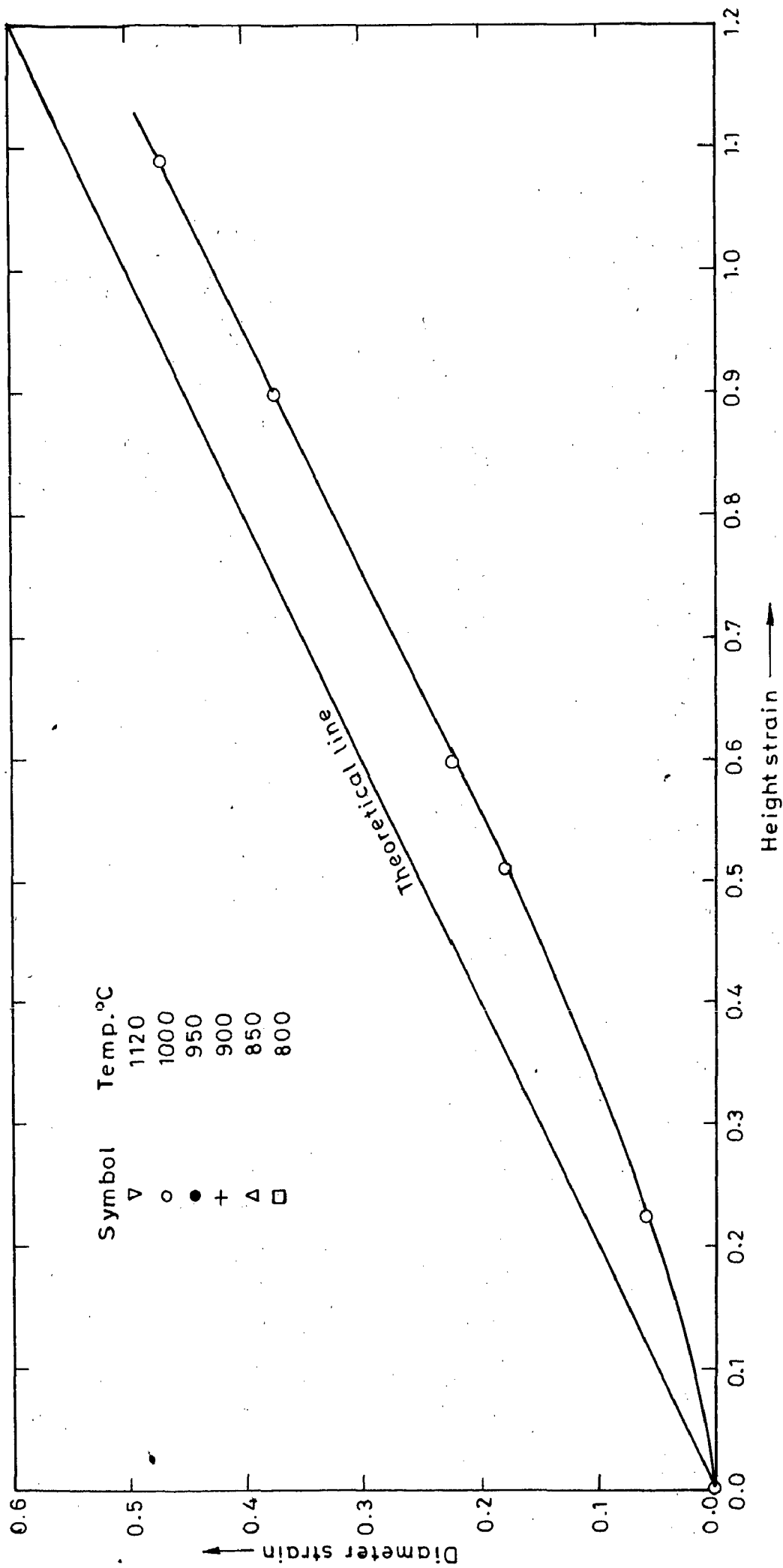


Fig.6.27-Relationship between diameter strain and height strain for 0.45% P-Fe preform ( $H/D=0.59$ ) during hot upsetting

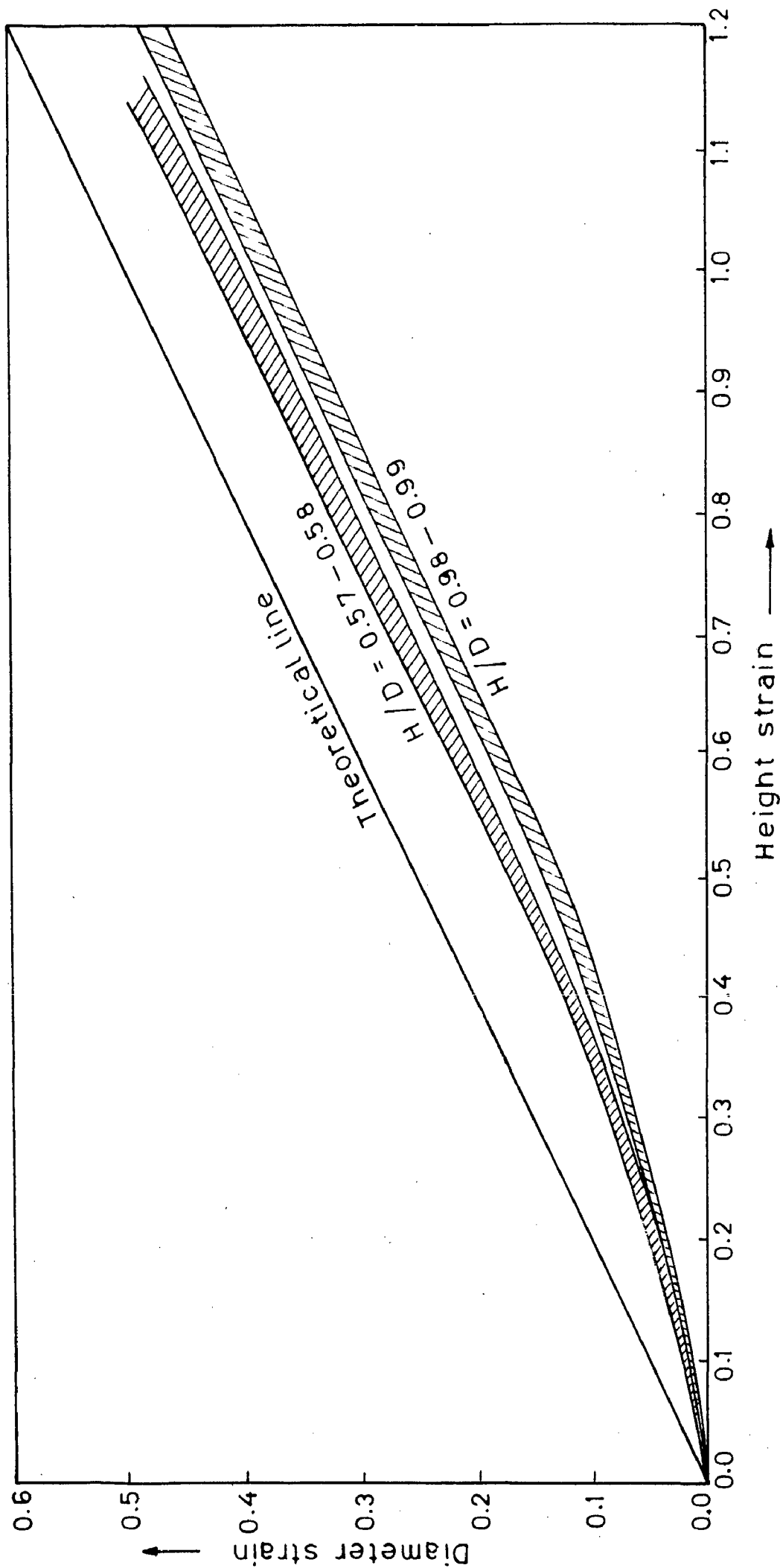


Fig.6.28 - Plot of diameter strain vs height strain for carbon steels (0.00 - 1.36 % C) with different H/D ratios

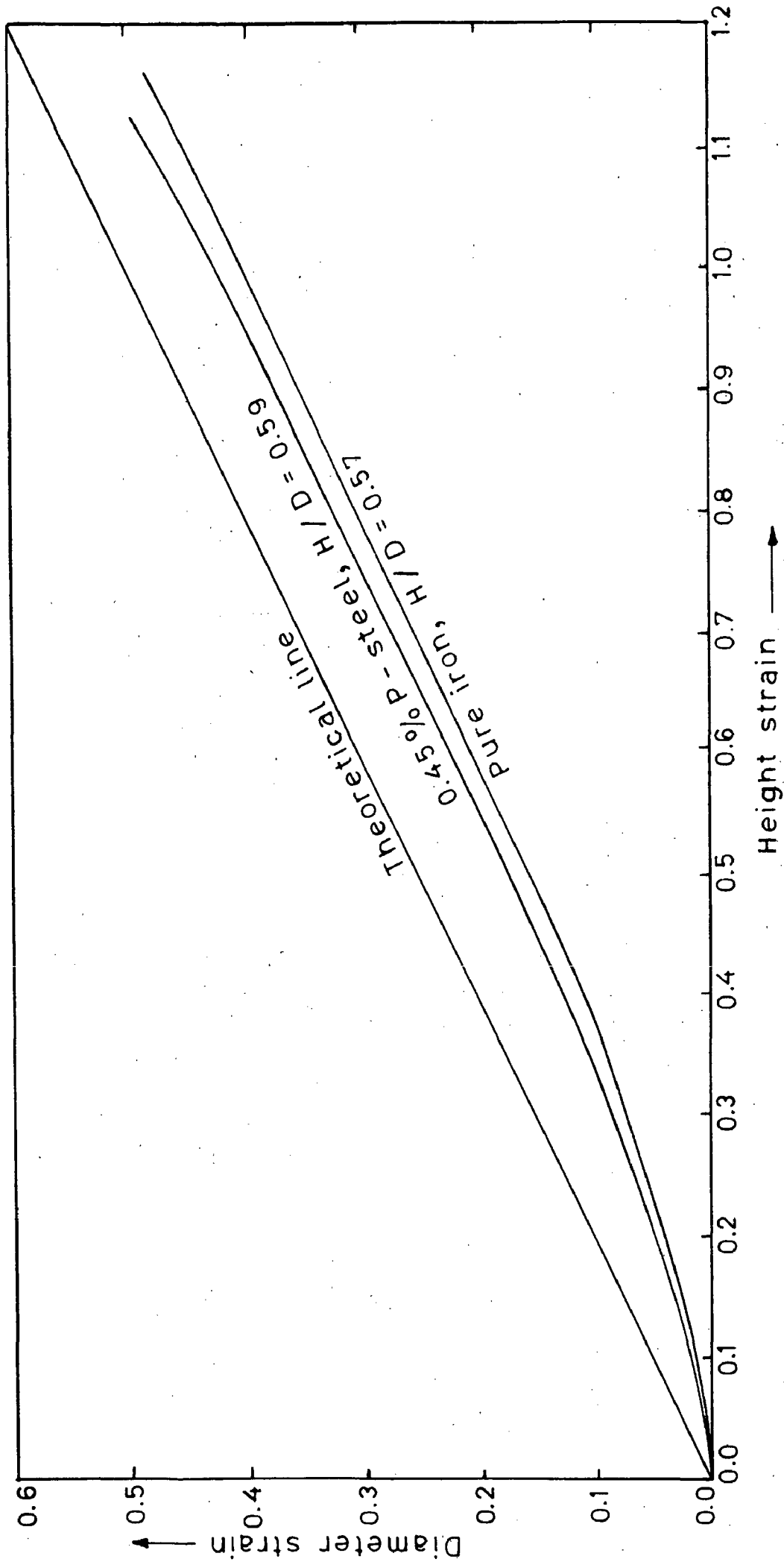


Fig.6.29 - Plot of diameter strain vs. height strain for iron and 0.45% P-steel sintered preforms during hot upsetting.

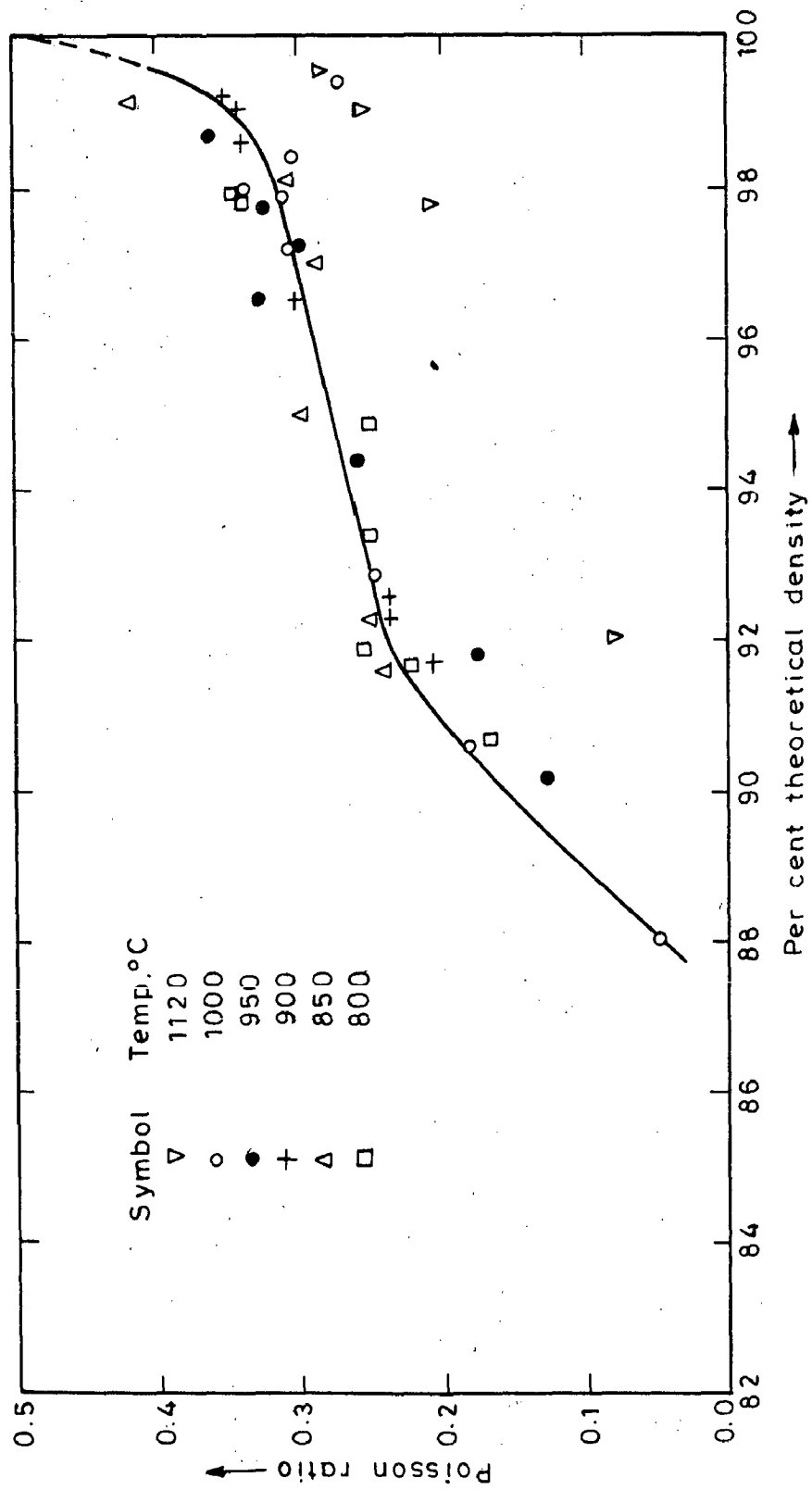


Fig. 6.30 - Variation of poisson ratio with increasing density in hot upsetting of sintered iron powder preforms (  $H/D=0.57$  )

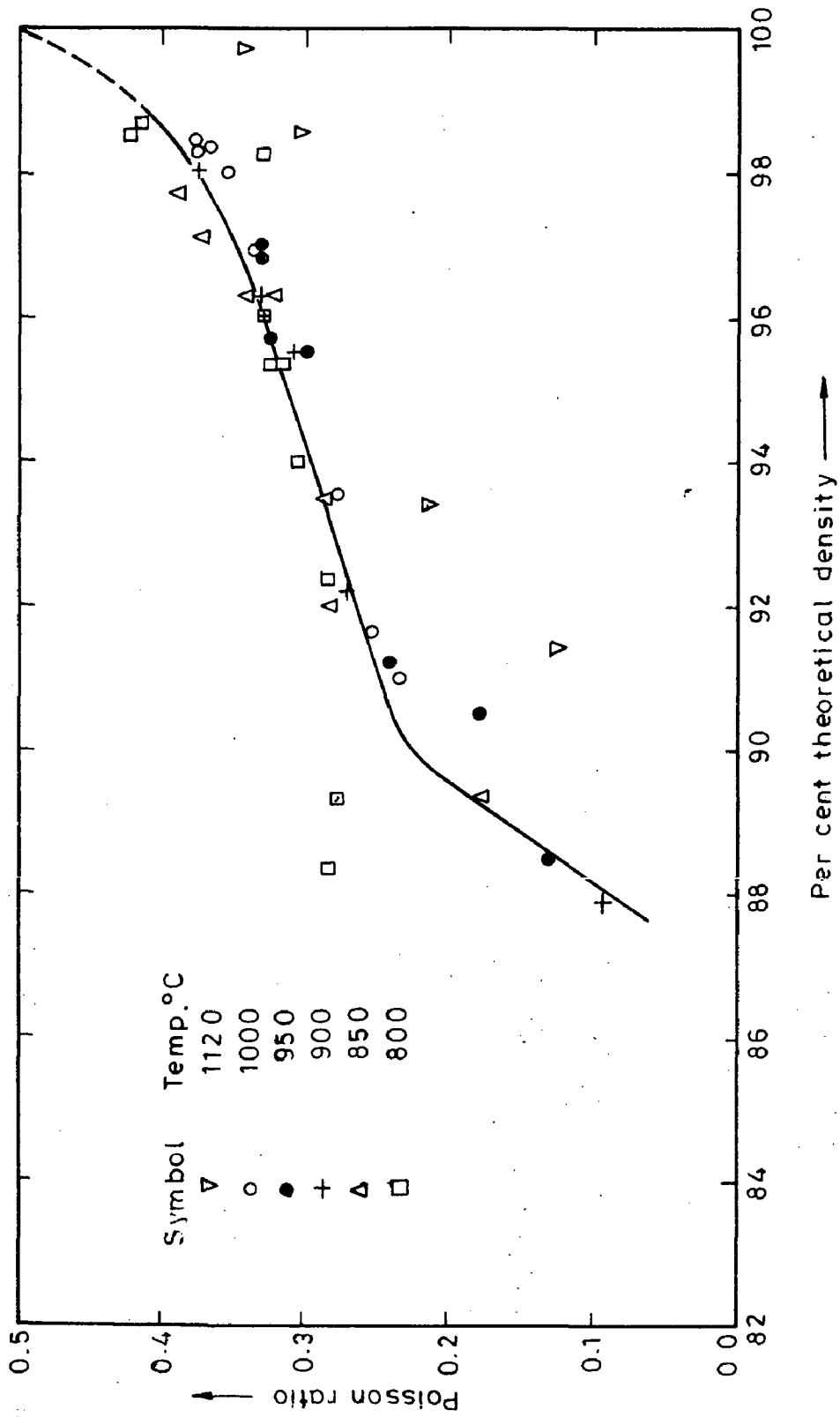


Fig.6.31-Variation of poisson ratio with increasing density in hot upsetting of sintered iron powder preforms (H/D=0.99)

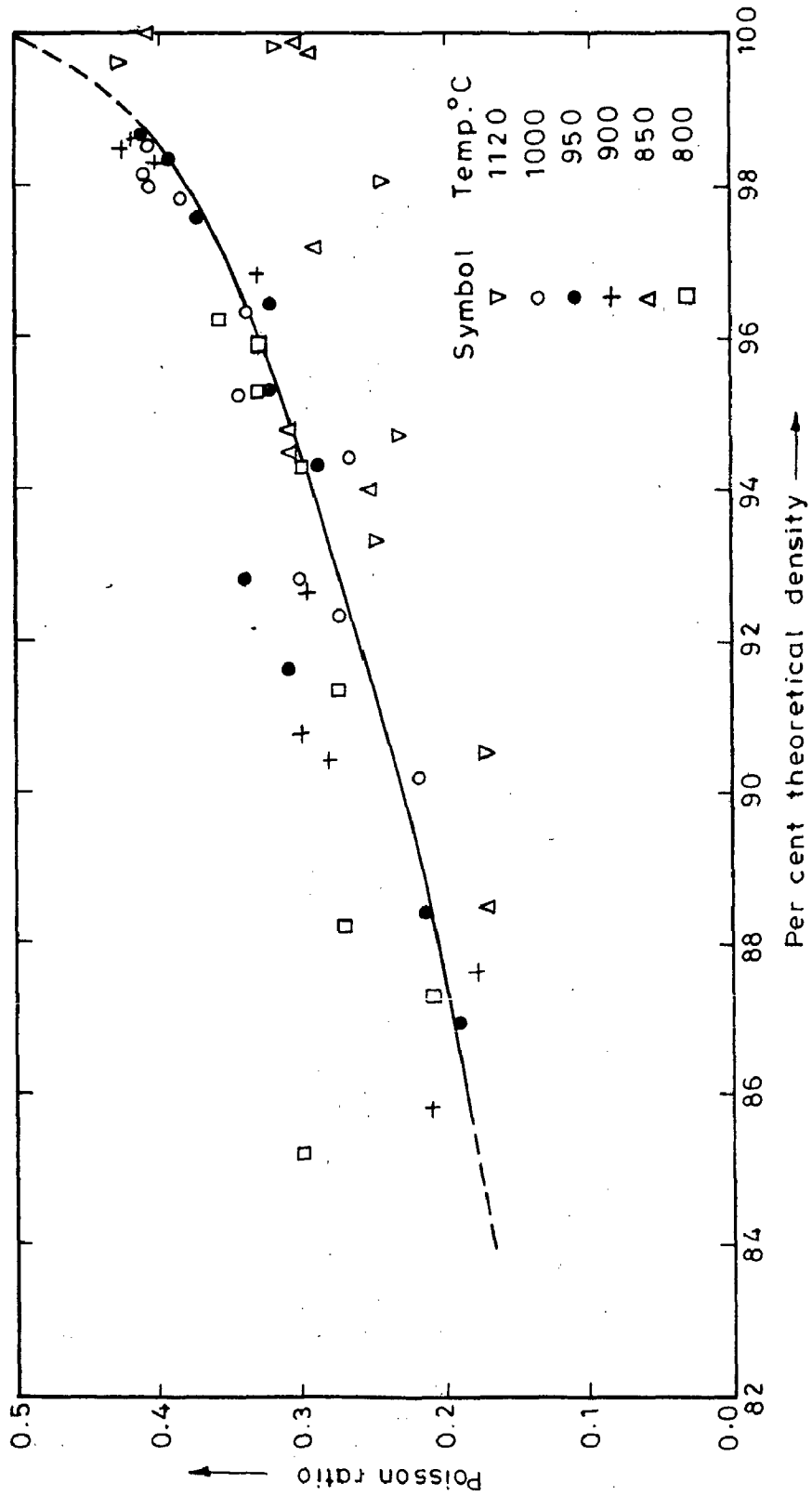


Fig.6.32 - Variation of poisson ratio with increasing density in hot upsetting of sintered iron powder preforms (H/D=1.17)



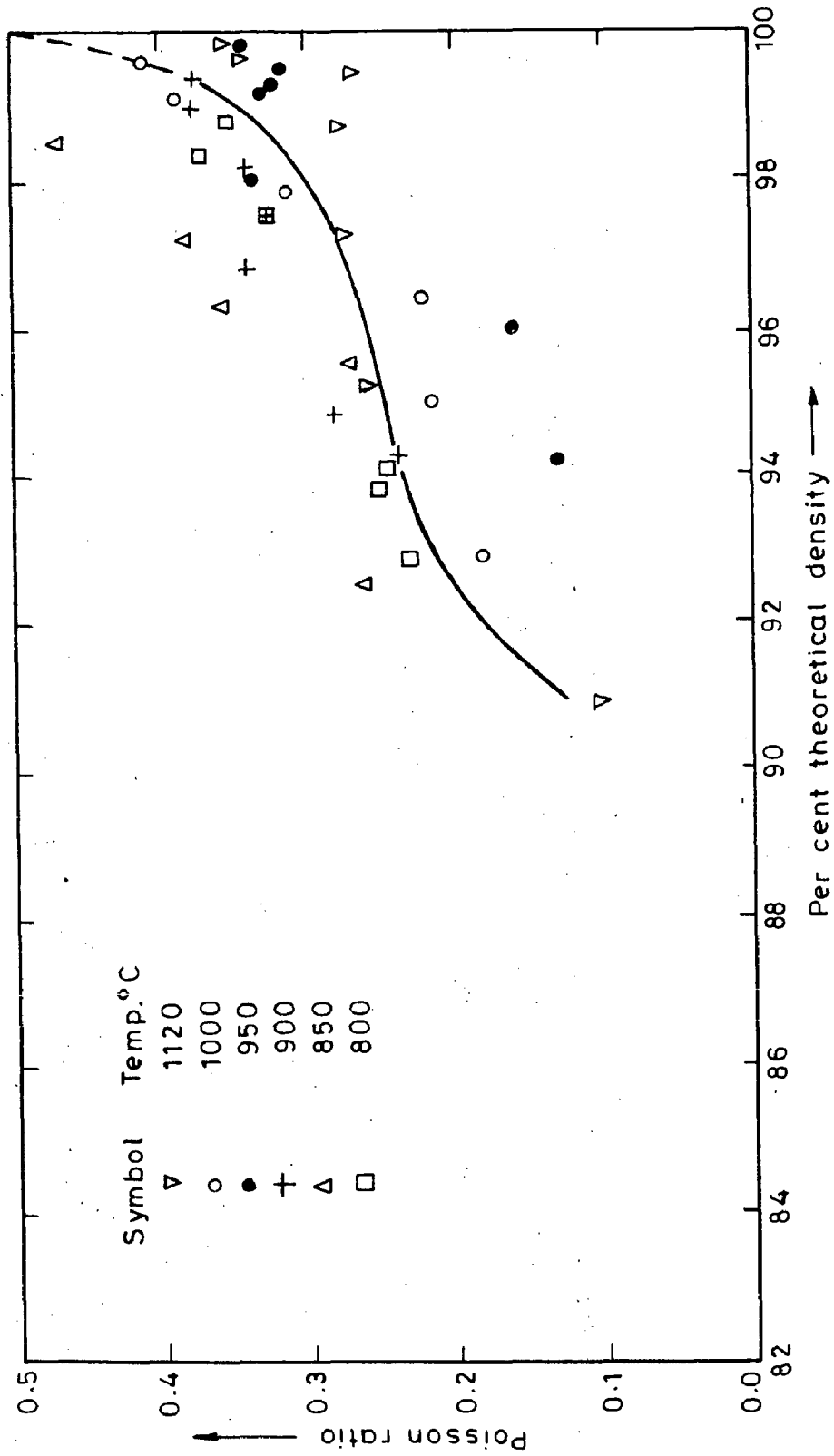


Fig.6.33—Variation of poisson ratio with increasing density in hot upsetting of 0.35% C steel sintered preform (H/D=0.57)

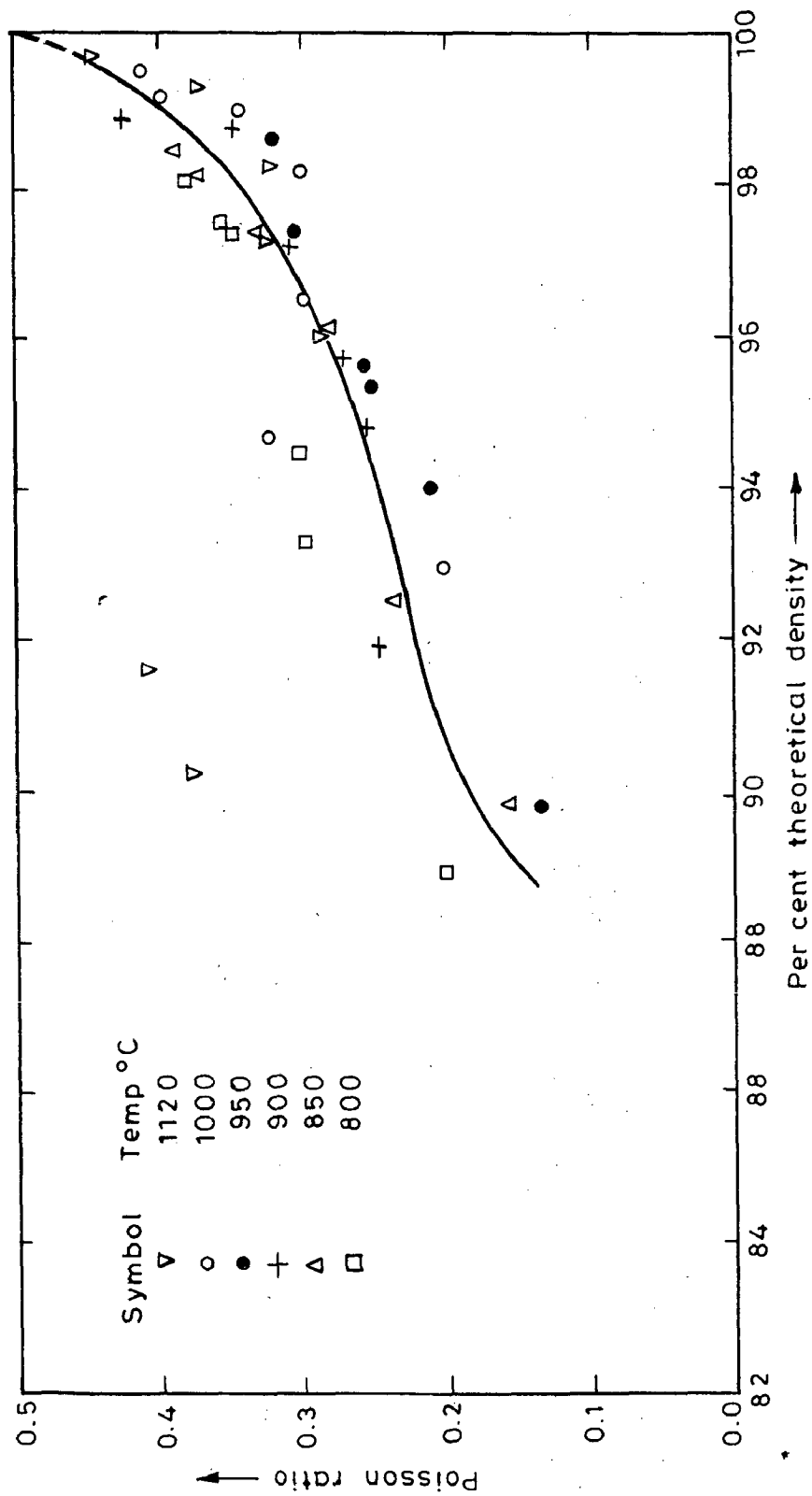


Fig.6.34--Variation of poisson ratio with increasing density in hot upsetting of 0.35% C steel sintered preforms (H/D=0.99)

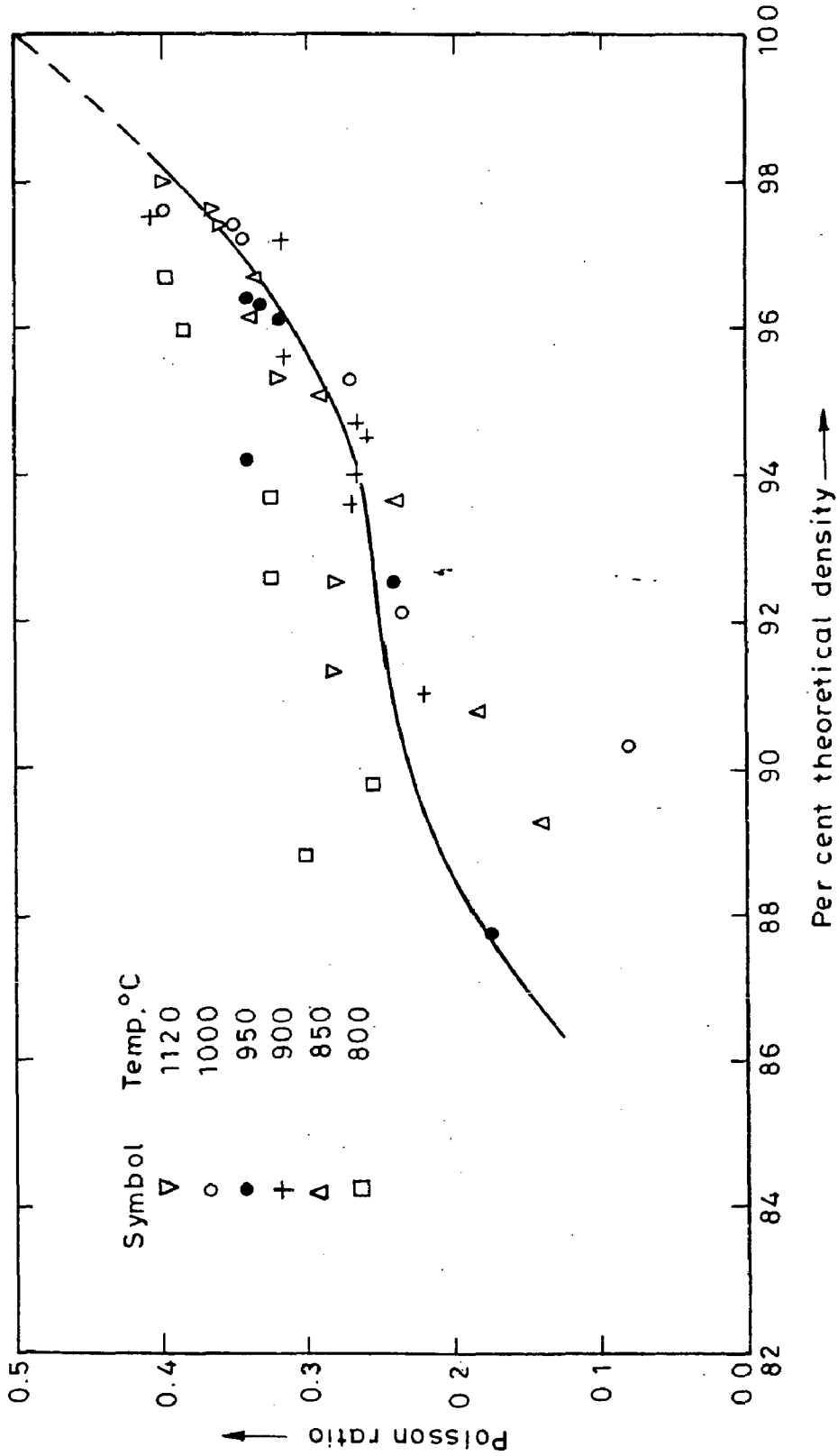


Fig.6.35 - Variation of poisson ratio with increasing density in hot upsetting of 0.83% C steel sintered preform ( H/D=0.57 )

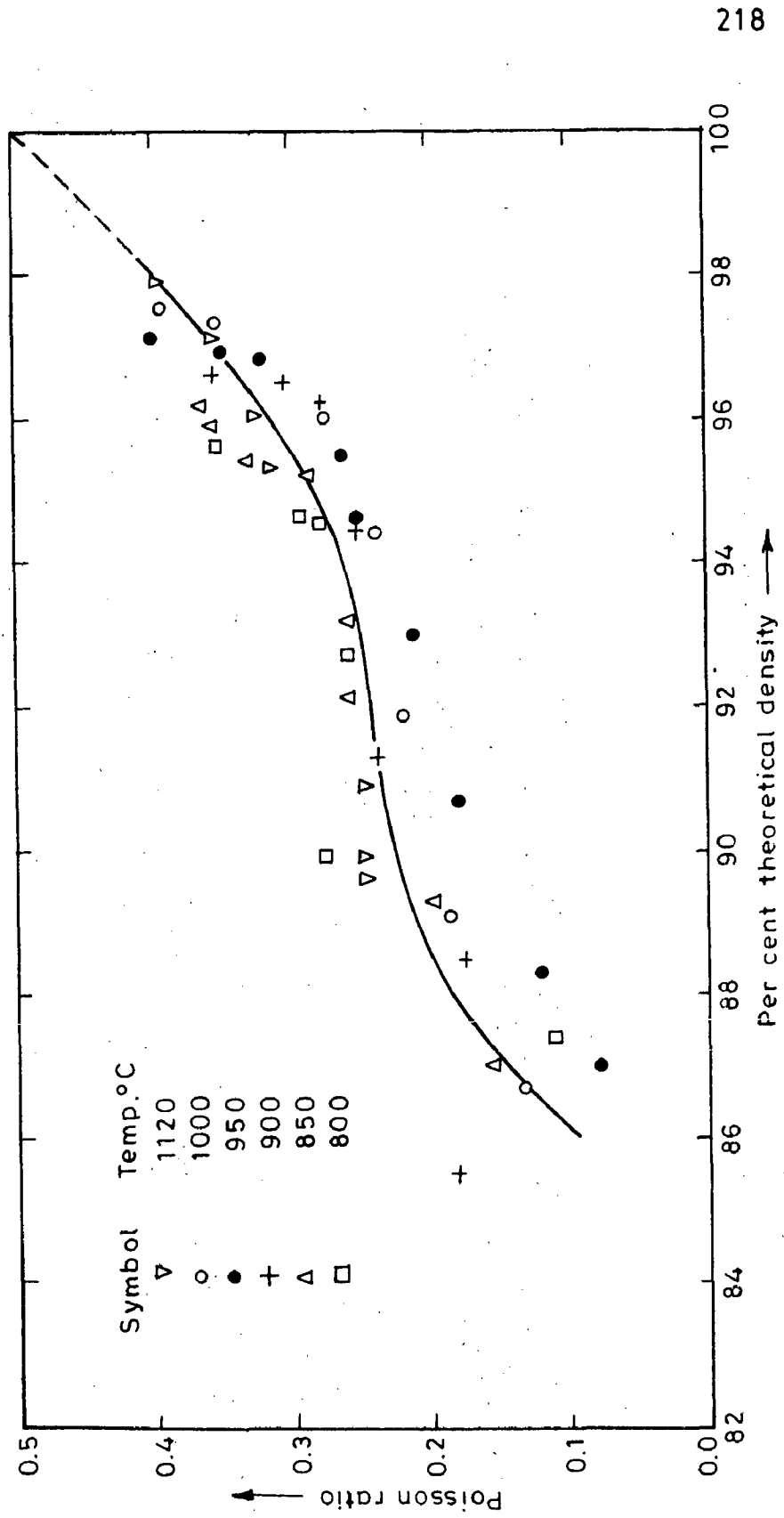


Fig.6.36-Variation of poisson ratio with increasing density in hot upsetting of 0.83% C steel sintered preforms ( H/D=0.99)

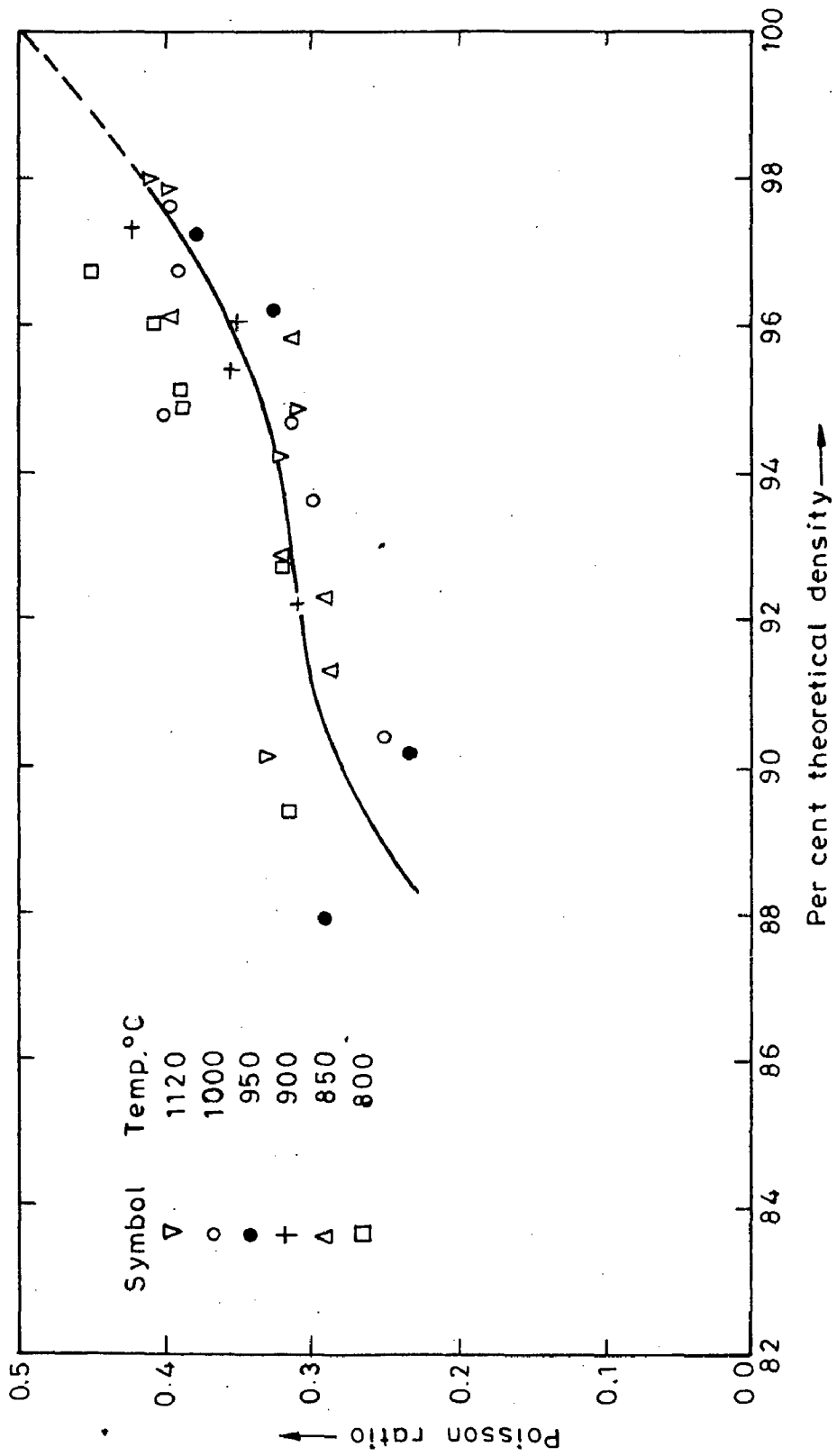


Fig.6.37(a) - Variation of poisson ratio with increasing density in hot upsetting of 1.36 %C steel sintered preforms (H/D=0.58)

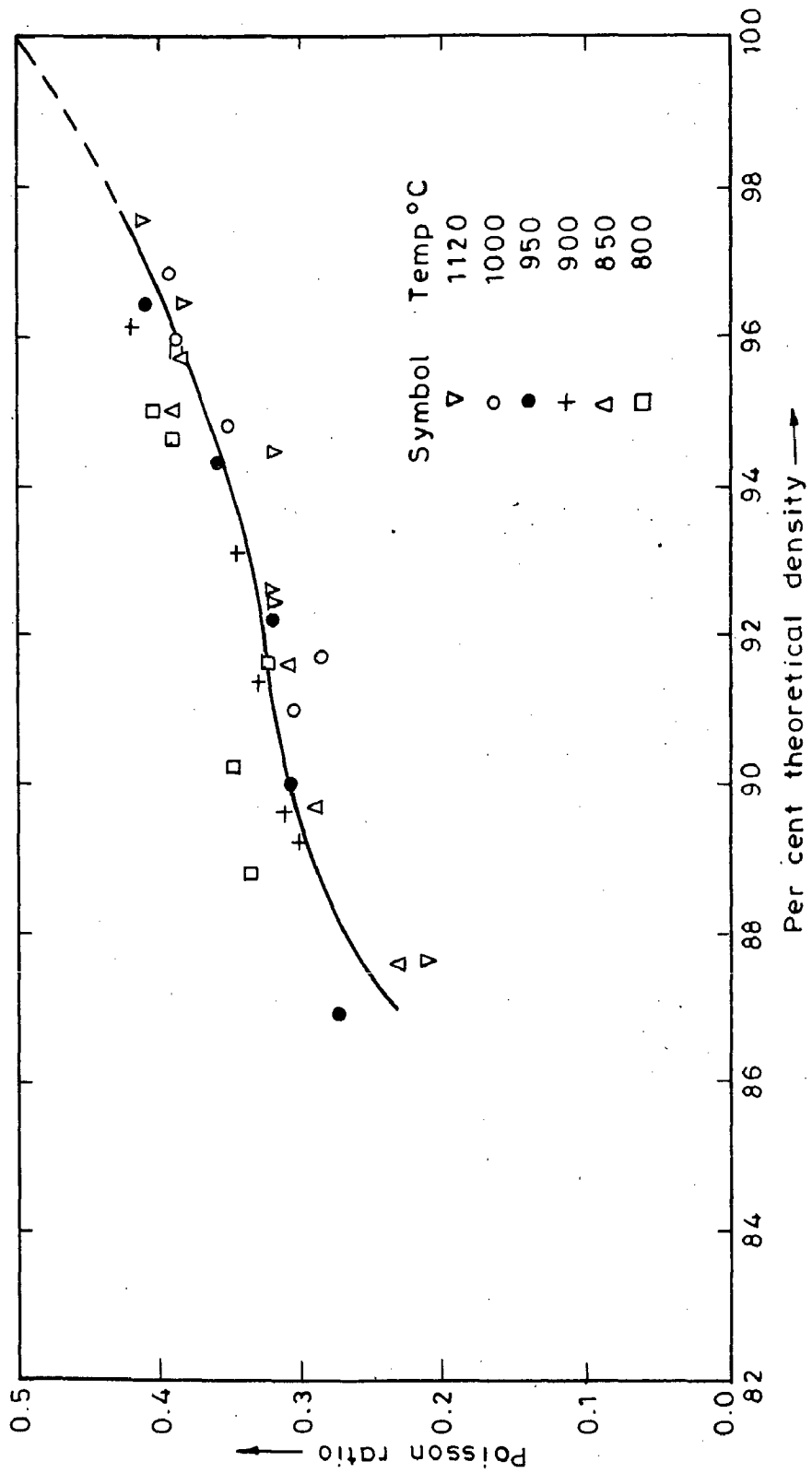


Fig.6 37(b)-Variation of poisson ratio with increasing density in hot upsetting of 1.36 % C. steel sintered preforms (H/D=0.99)

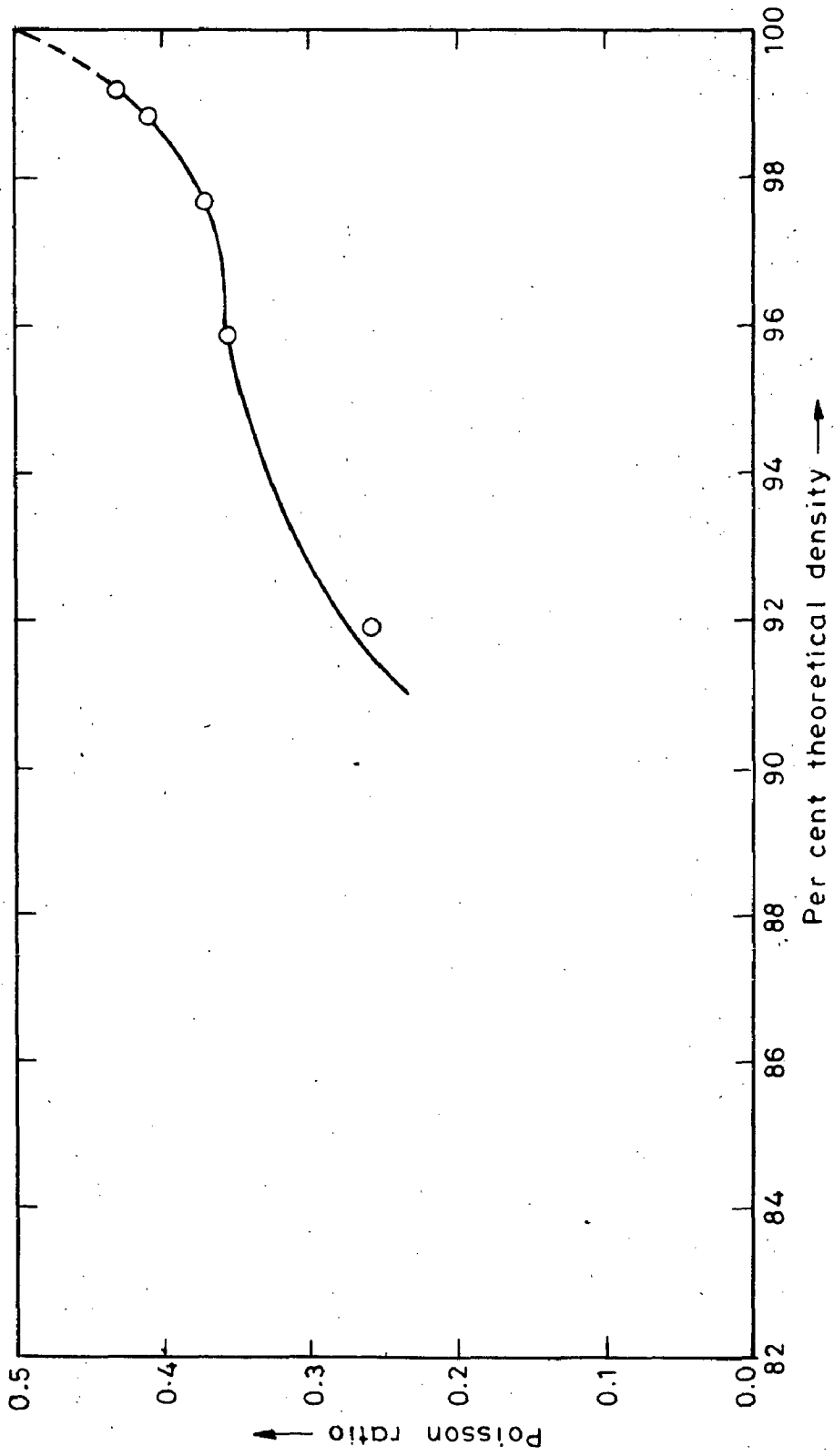


Fig.6.38—Variation of poisson ratio with increasing density in hot upsetting of 0.45% P steel sintered preforms ( H/D=0.59) at 960°C

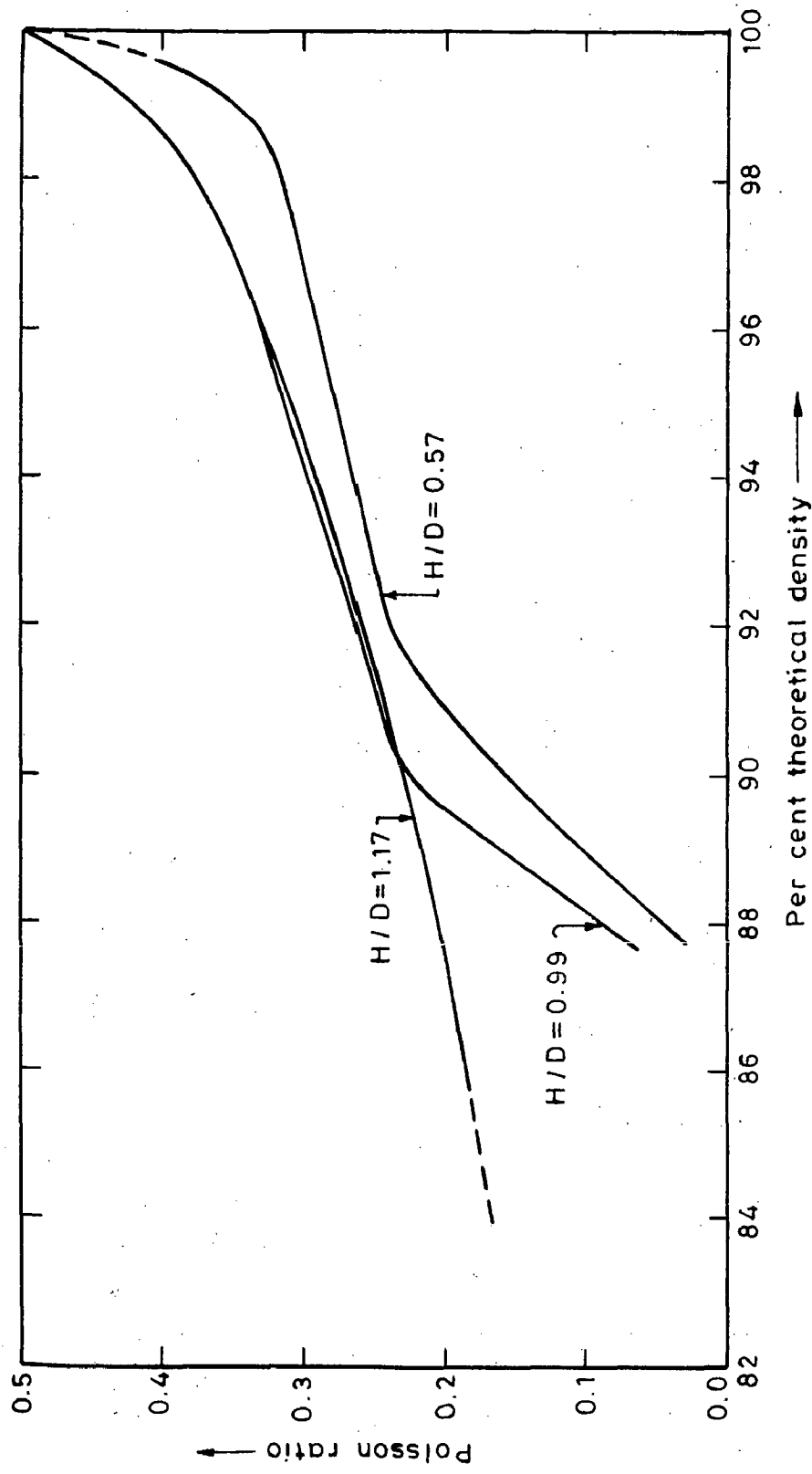


Fig.6.39-Effect of H/D on poisson ratio for hot upset forging of iron powder preforms (Sintered)



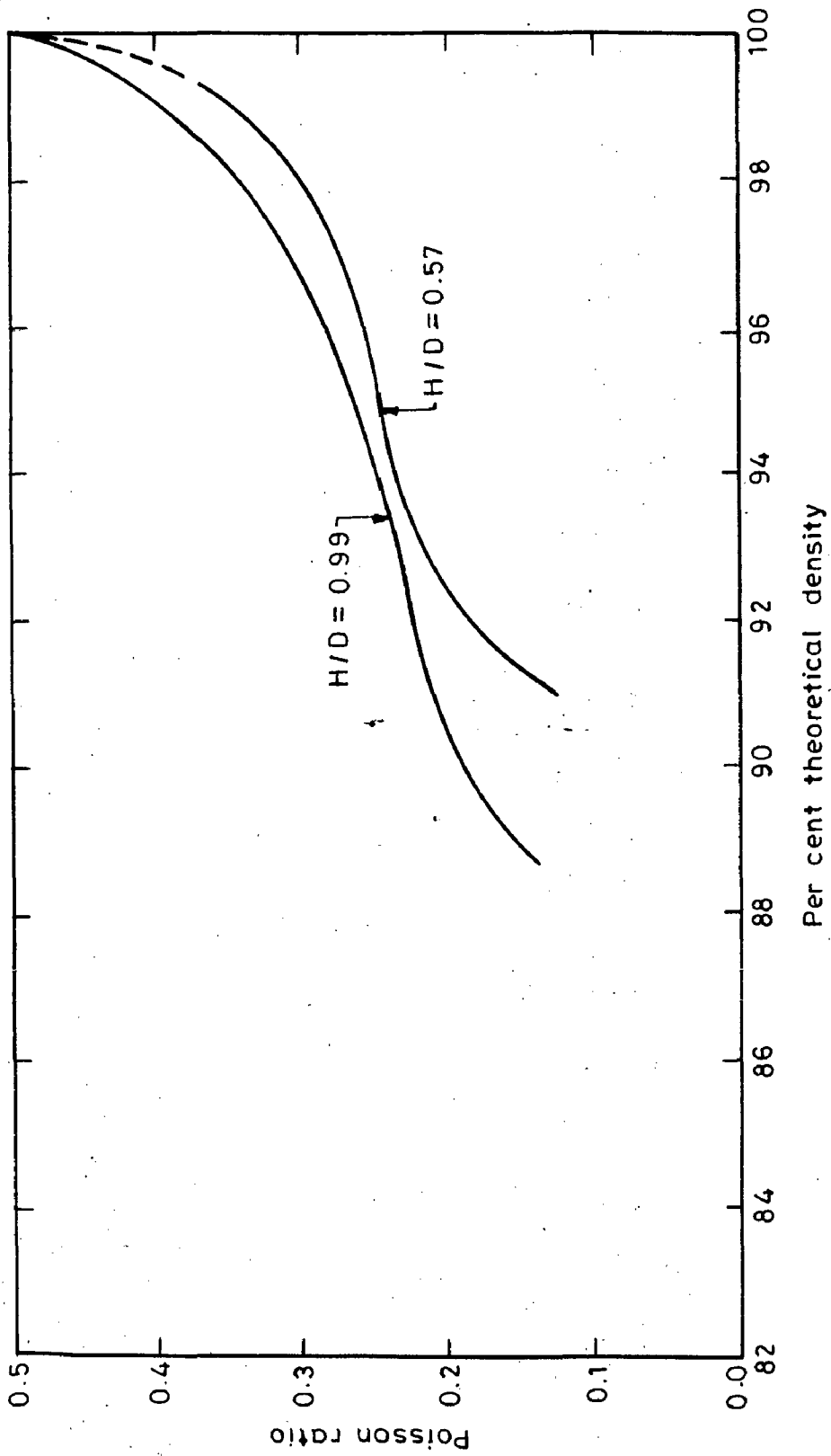


Fig.6.40-Effect of H/D on poisson ratio for hot upsetting of 0.35% C steel preforms (Sintered)

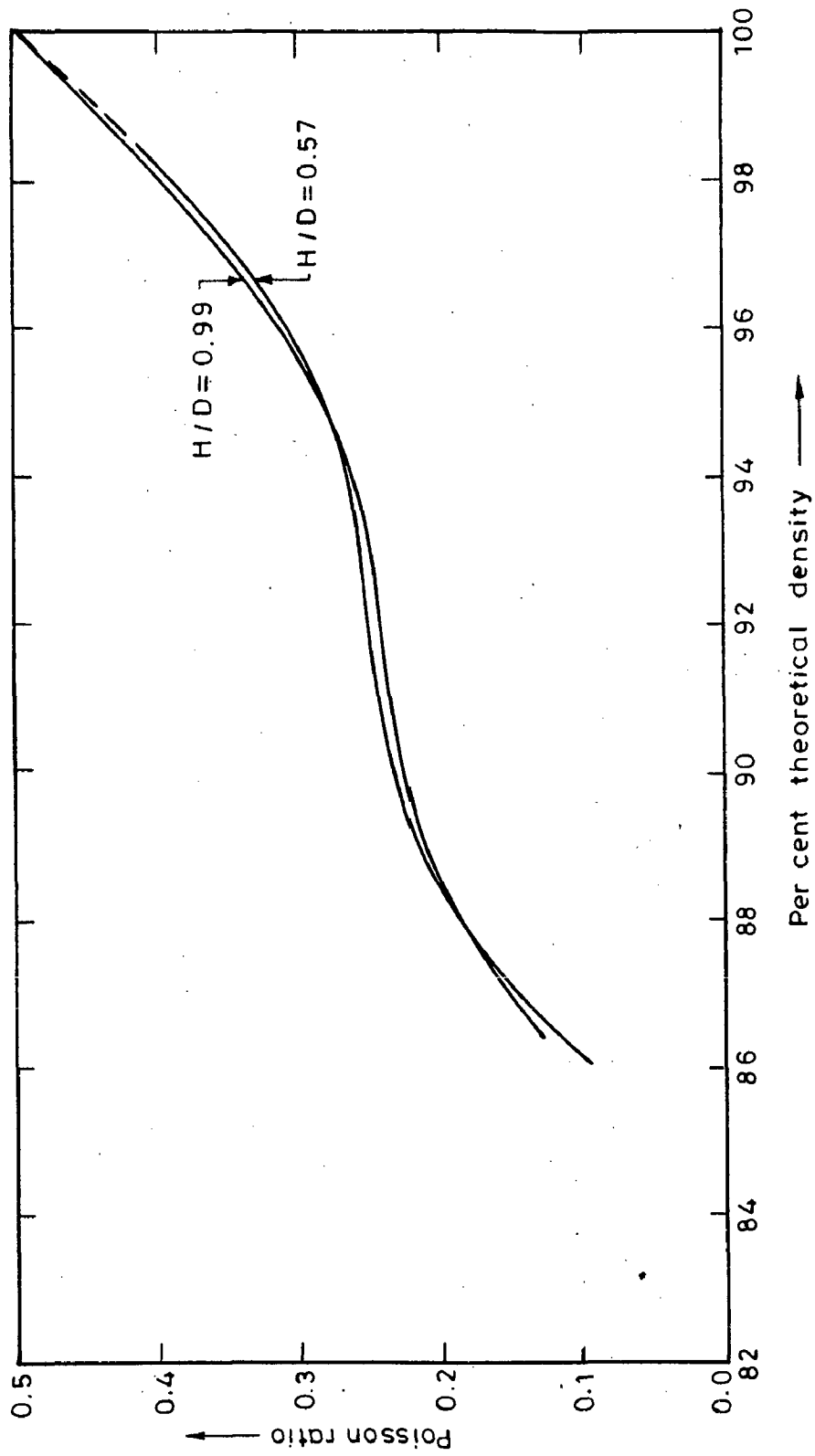


Fig.6.41-Effect of H/D on poisson ratio for hot upsetting of 0.83% C. steel preforms (Sintered)

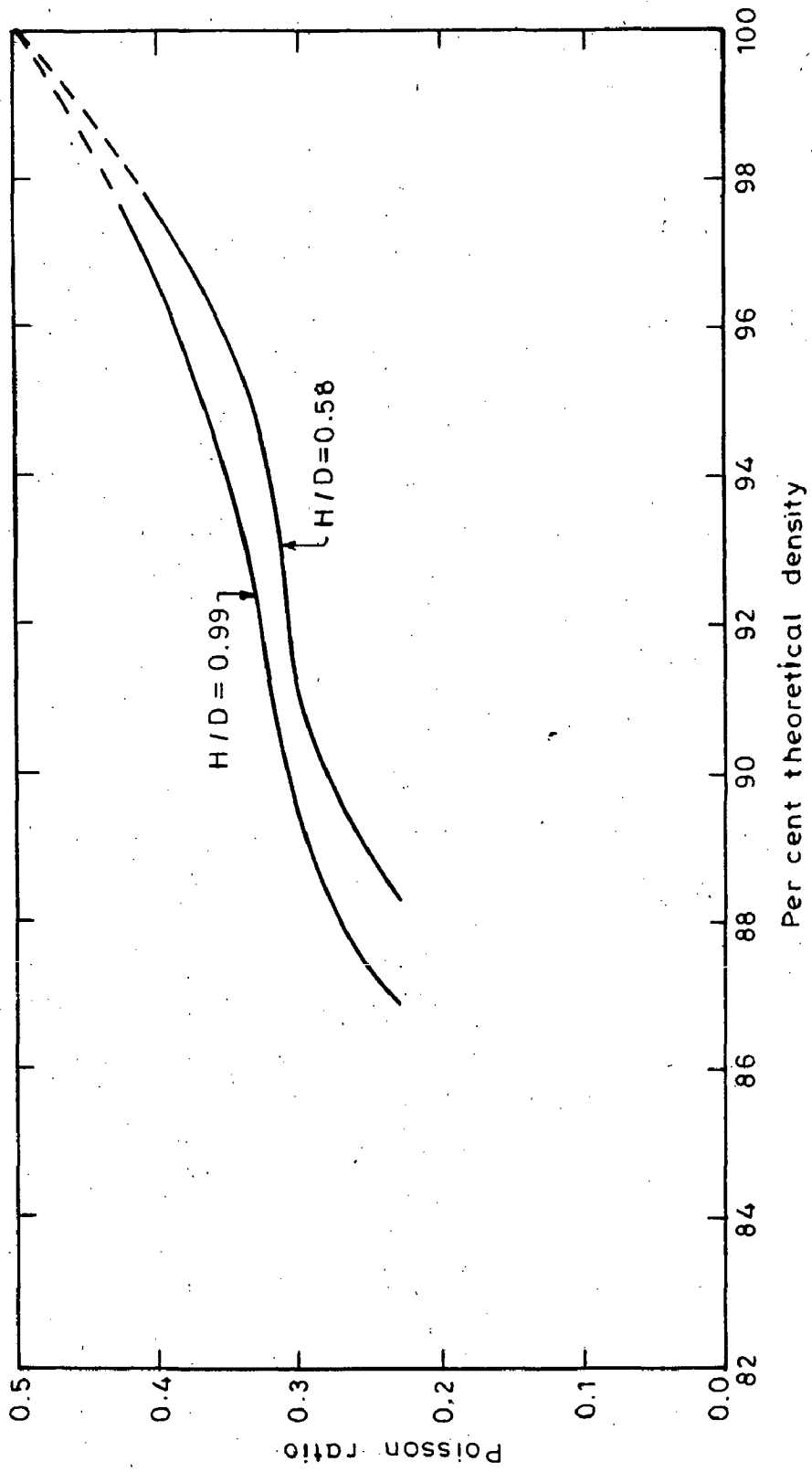


Fig.6.42-Effect of H/D on poisson ratio for hot upsetting of 1.36% C. steel preforms (Sintered)

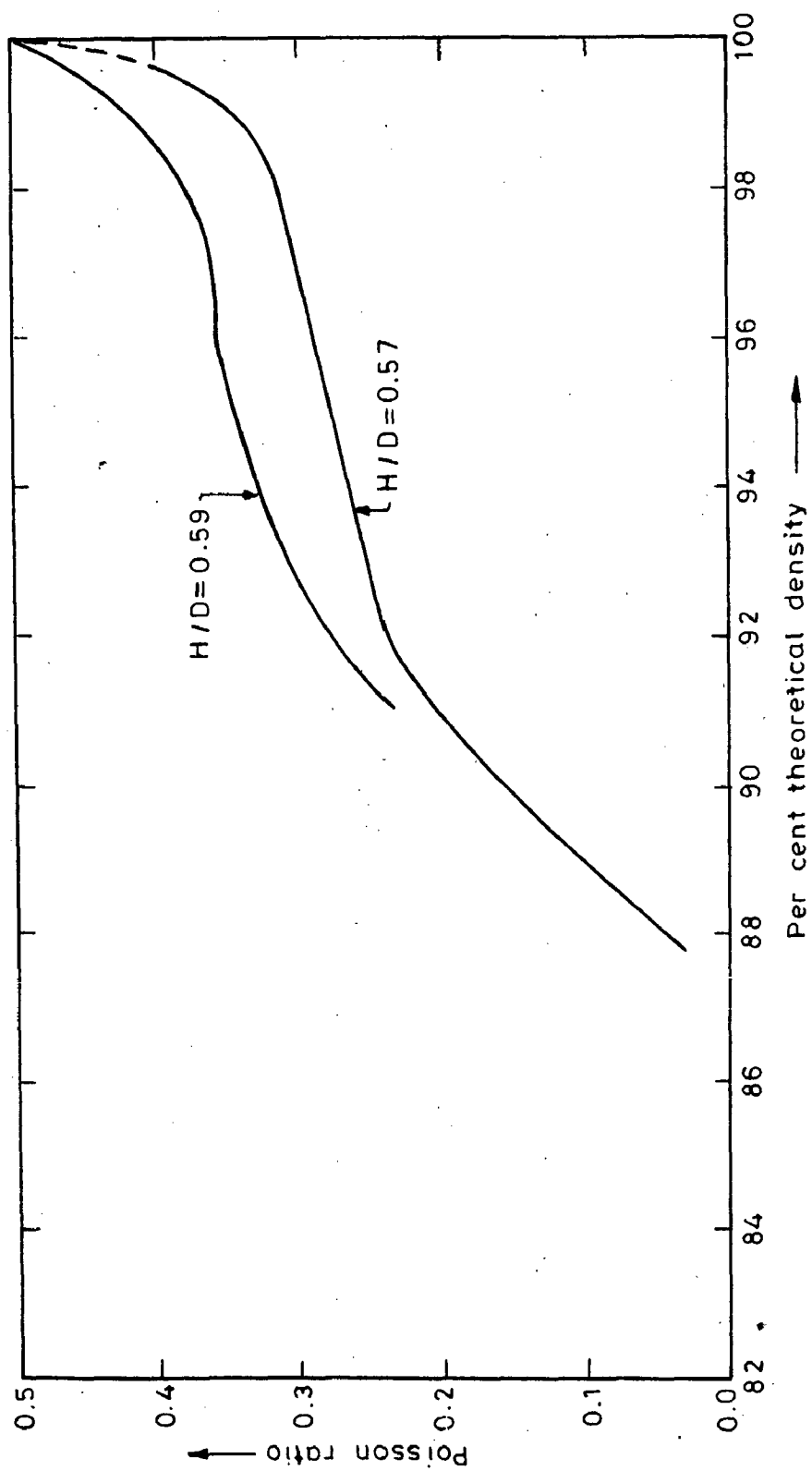


Fig.6.43 - Comparison of poisson ratio for hot upsetting of iron preforms 0.45 %P. steel preforms (H/D=0.57) (H/D=0.59) Sintered

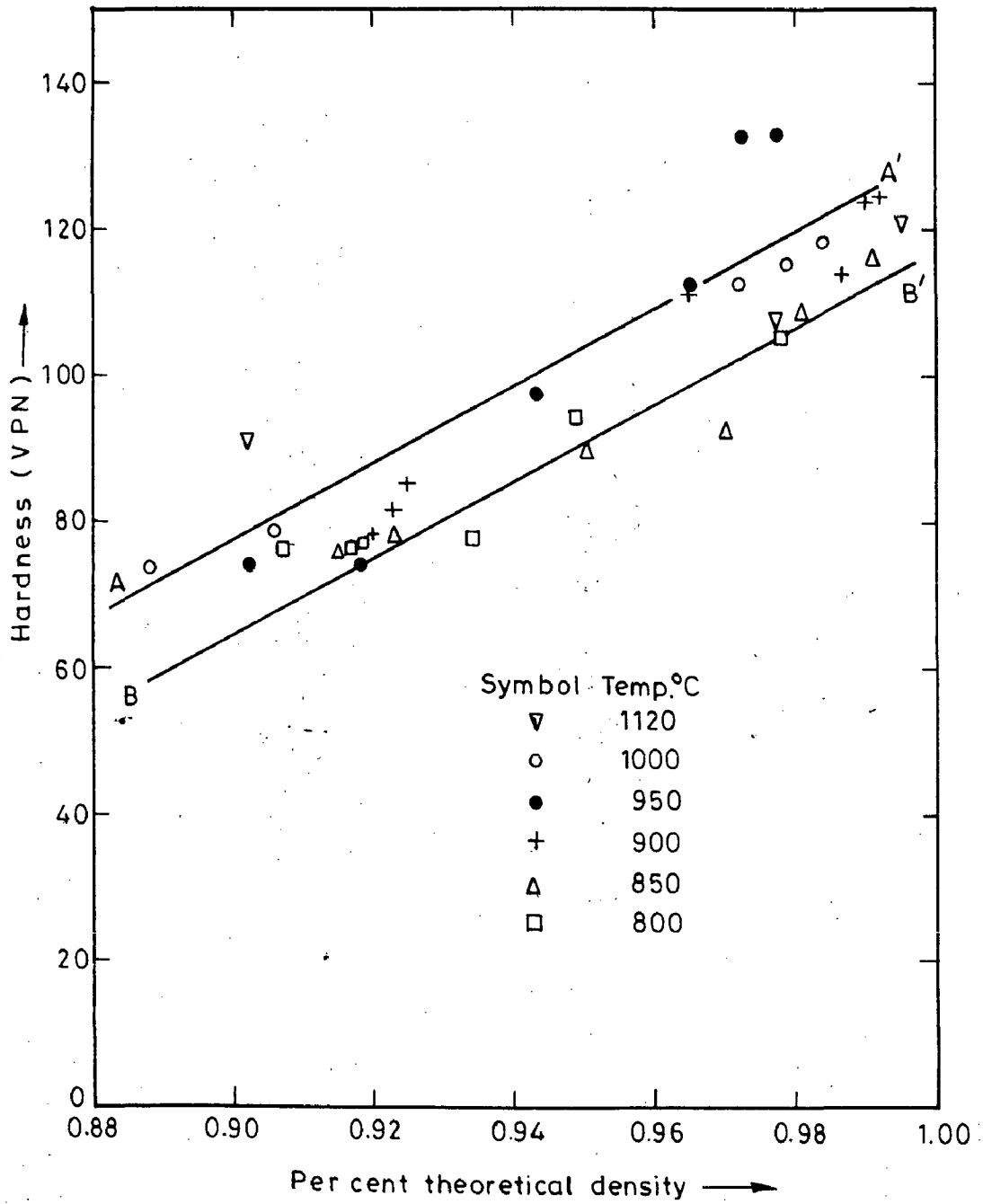


Fig.6.44- Plot of hardness v/s percent theoretical density for sintered iron powder performs of H/D=0.57

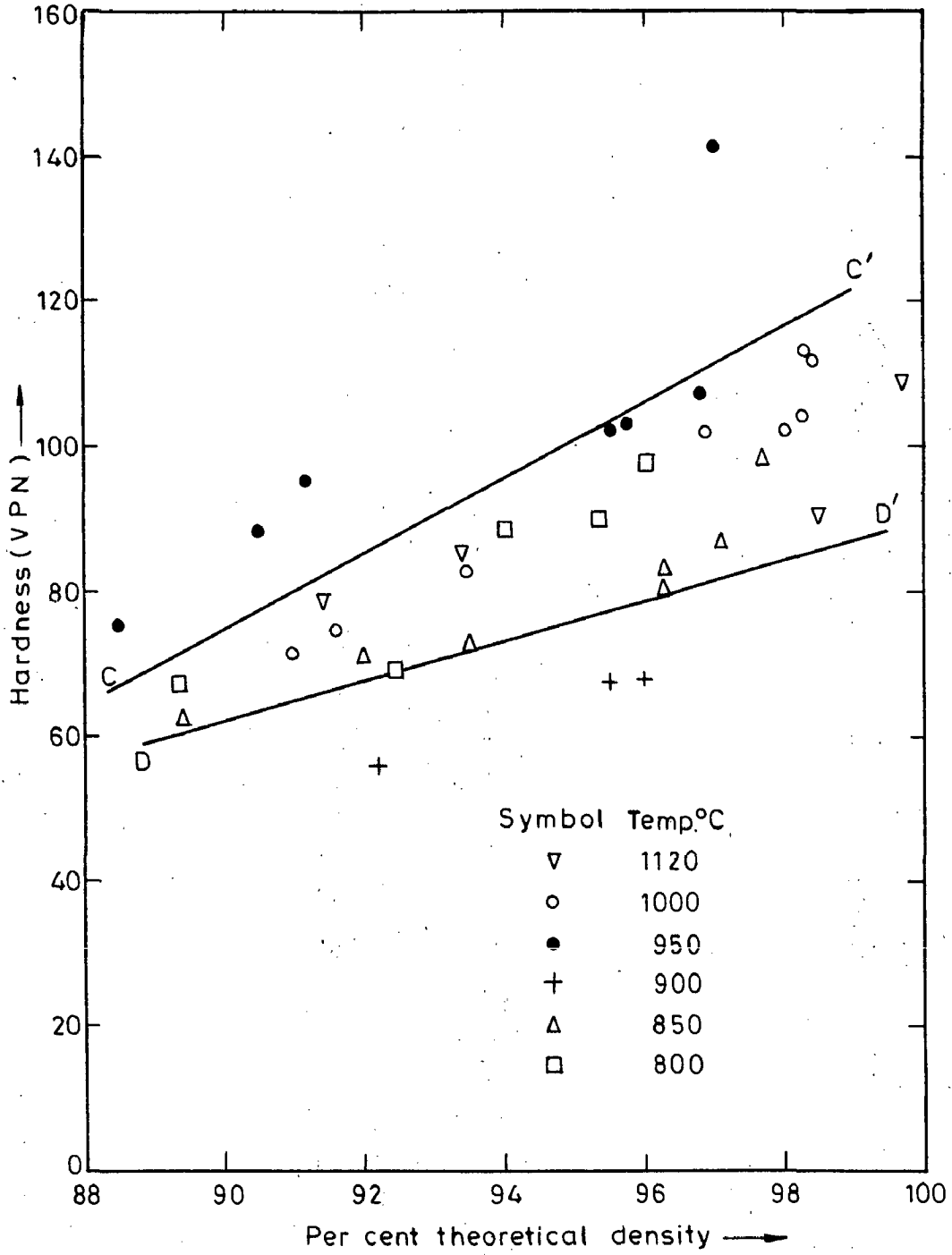


Fig.6.45-Plot of hardness v/s percent theoretical density of perform hot upset forging of H/D=0.99

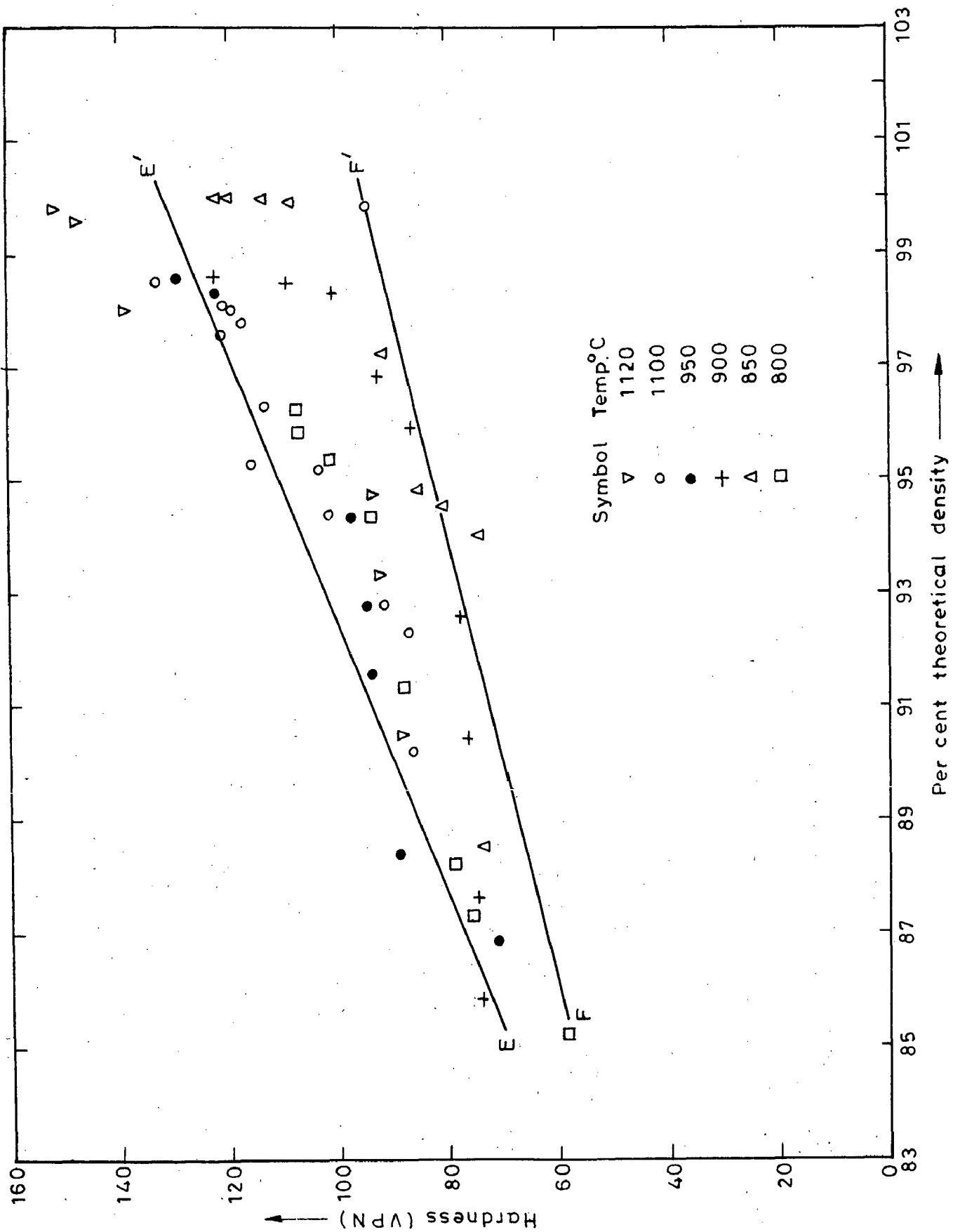


Fig.6.46-Hardness v/s percent theoretical density for sintered iron powder preforms upset-forged, H/D=1.17

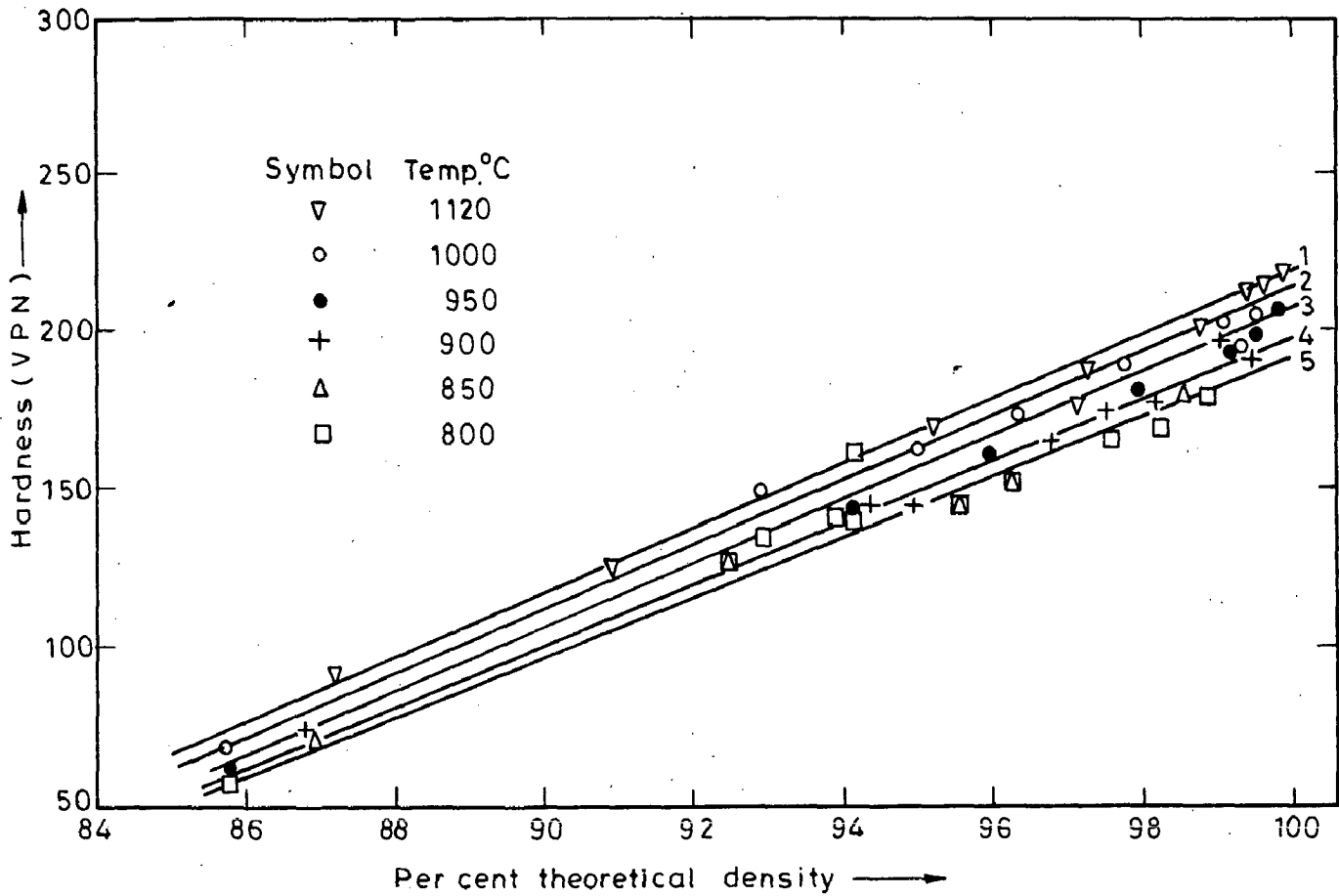


Fig.6.47-Variation of hardness with respect to percent theoretical density for 0.35 % carbon steel , H/D=0.58 during hot upset forging



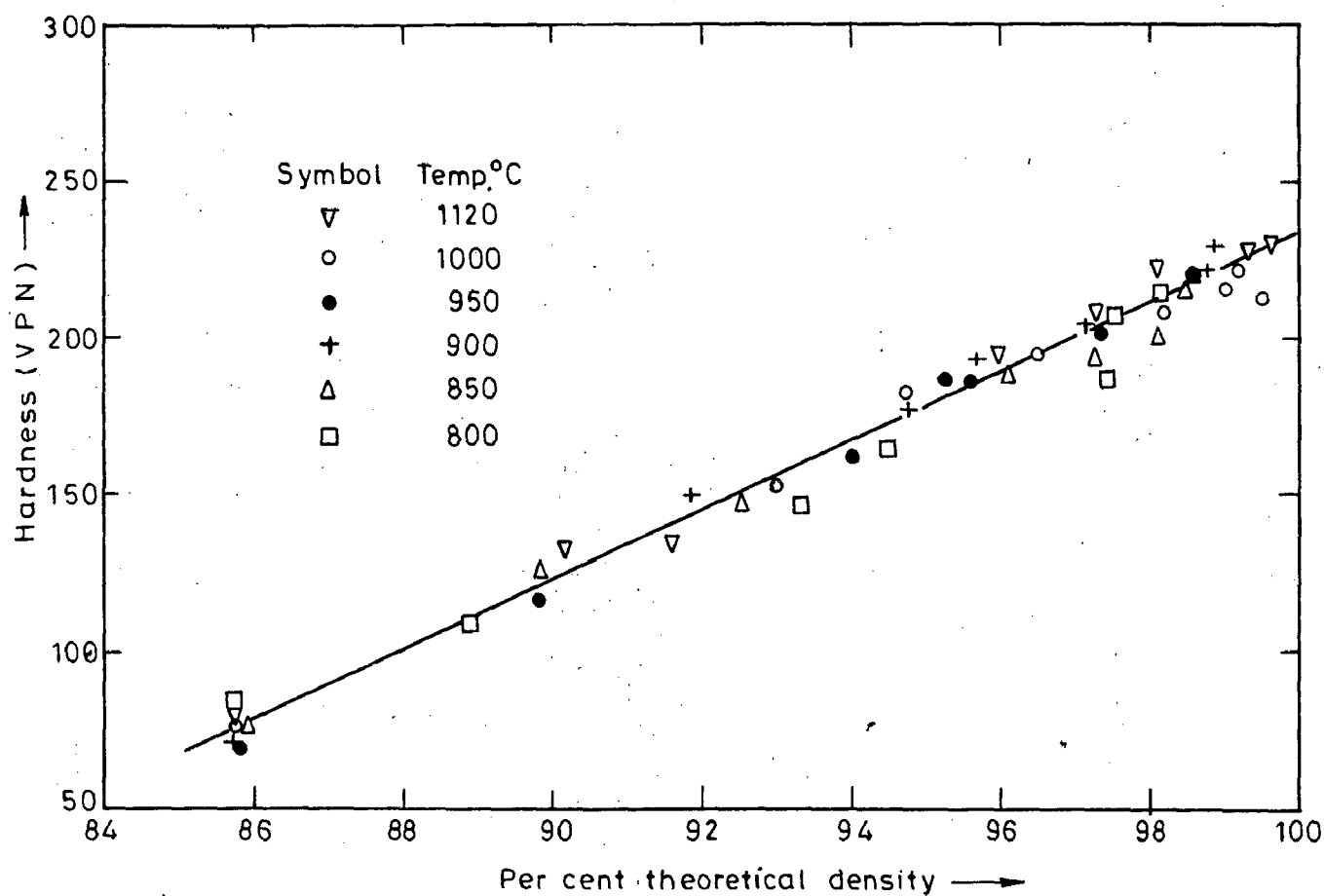


Fig.6.48-Relationship between hardness and percent theoretical density for 0.35% carbon steel,  $H/D=0.99$  during hot upset forging

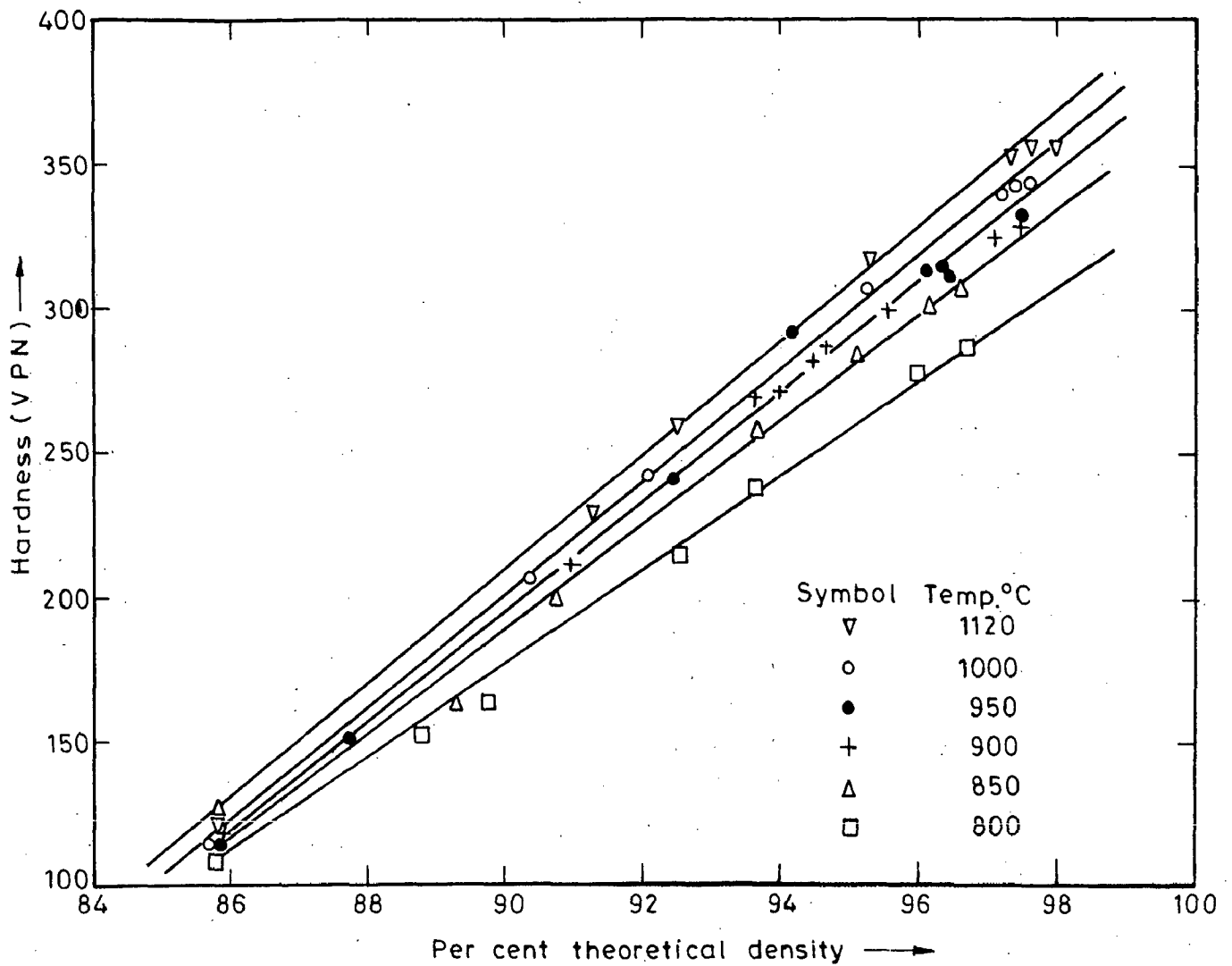


Fig.6.49-Relationship between hardness and percent theoretical density for 0.83% carbon steel,  $H/D=0.58$  during hot upset forging

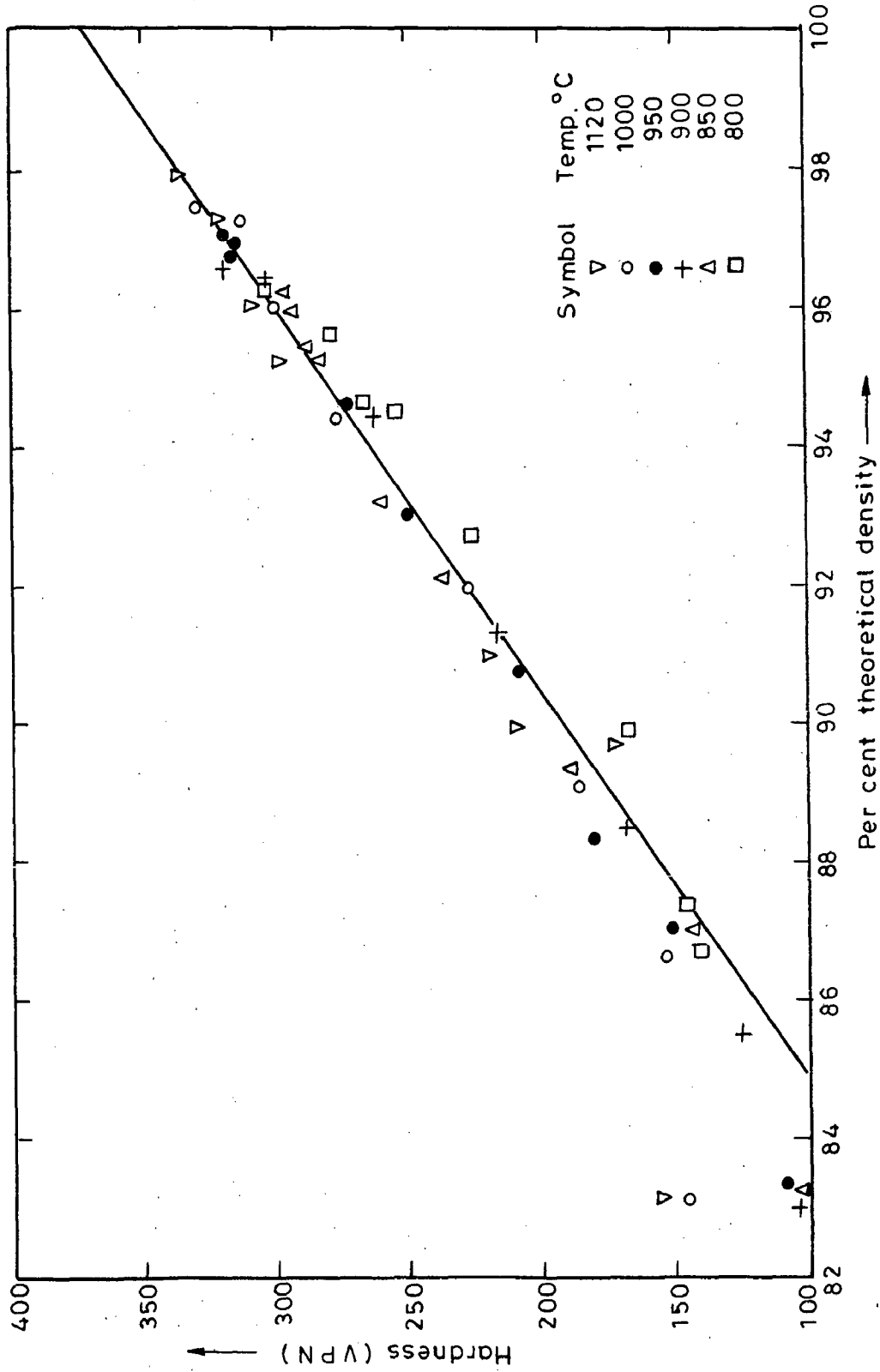


Fig. 6.50—Relationship between hardness and percent theoretical density for 0.83% carbon steel,  $H/D=0.99$  during hot upset forging

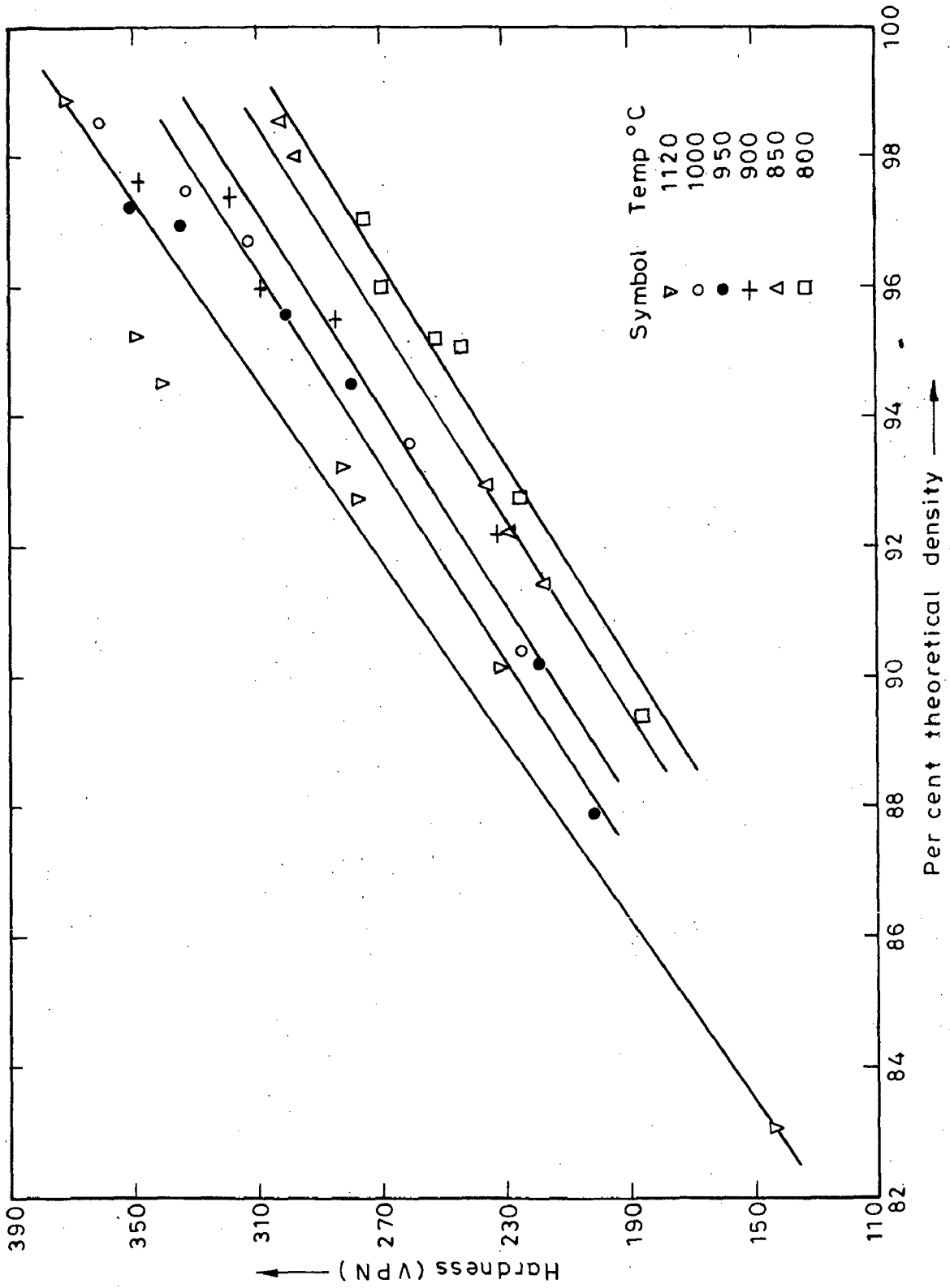


Fig.6.51-Relationship between hardness and percent theoretical density for 1.36% carbon steel, H/D = 0.58 during hot upset forging

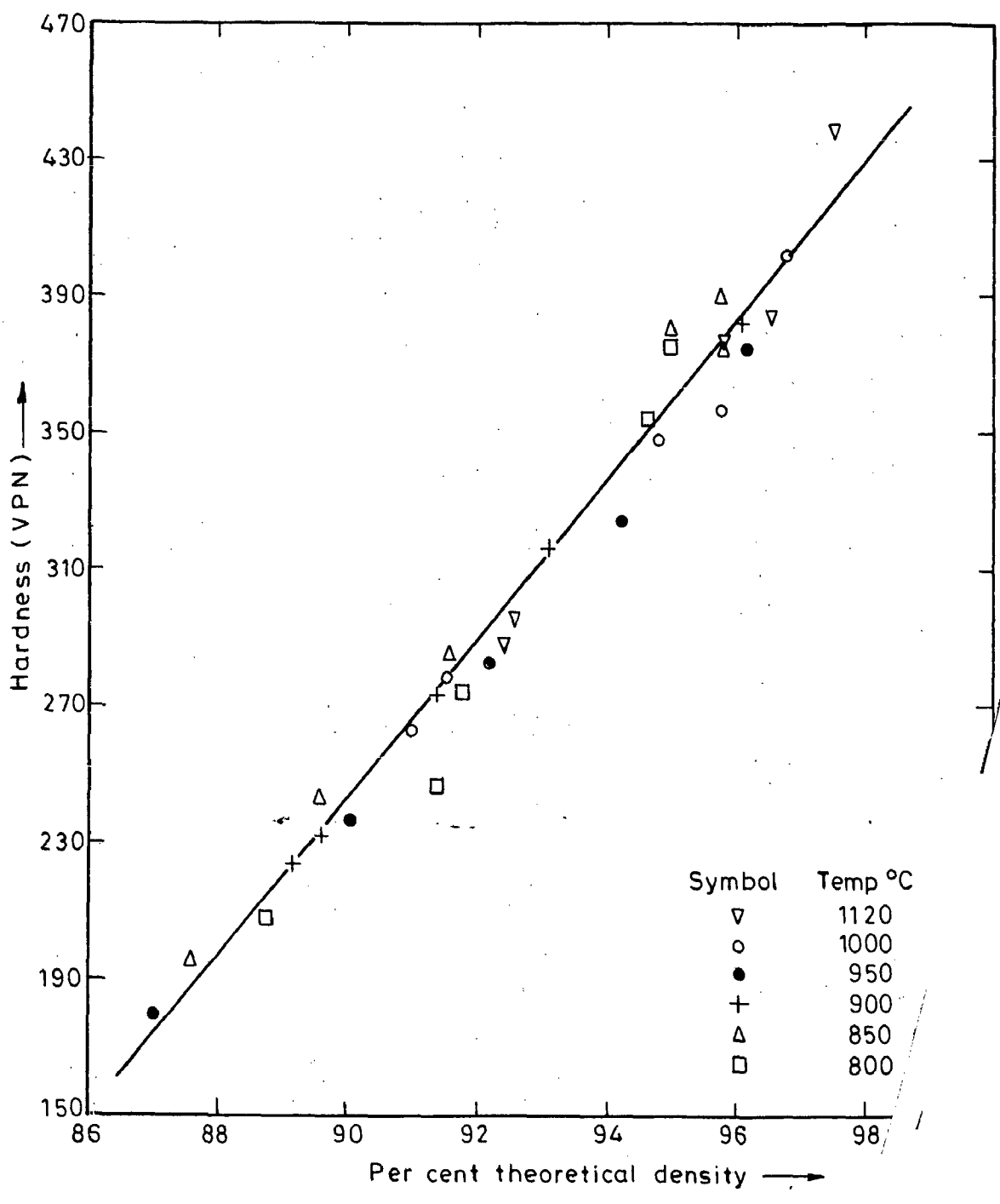


Fig.6.52-Plot of hardness v/s percent theoretical densit  
carbon steel, H/D=0.99 during hot upset forgin

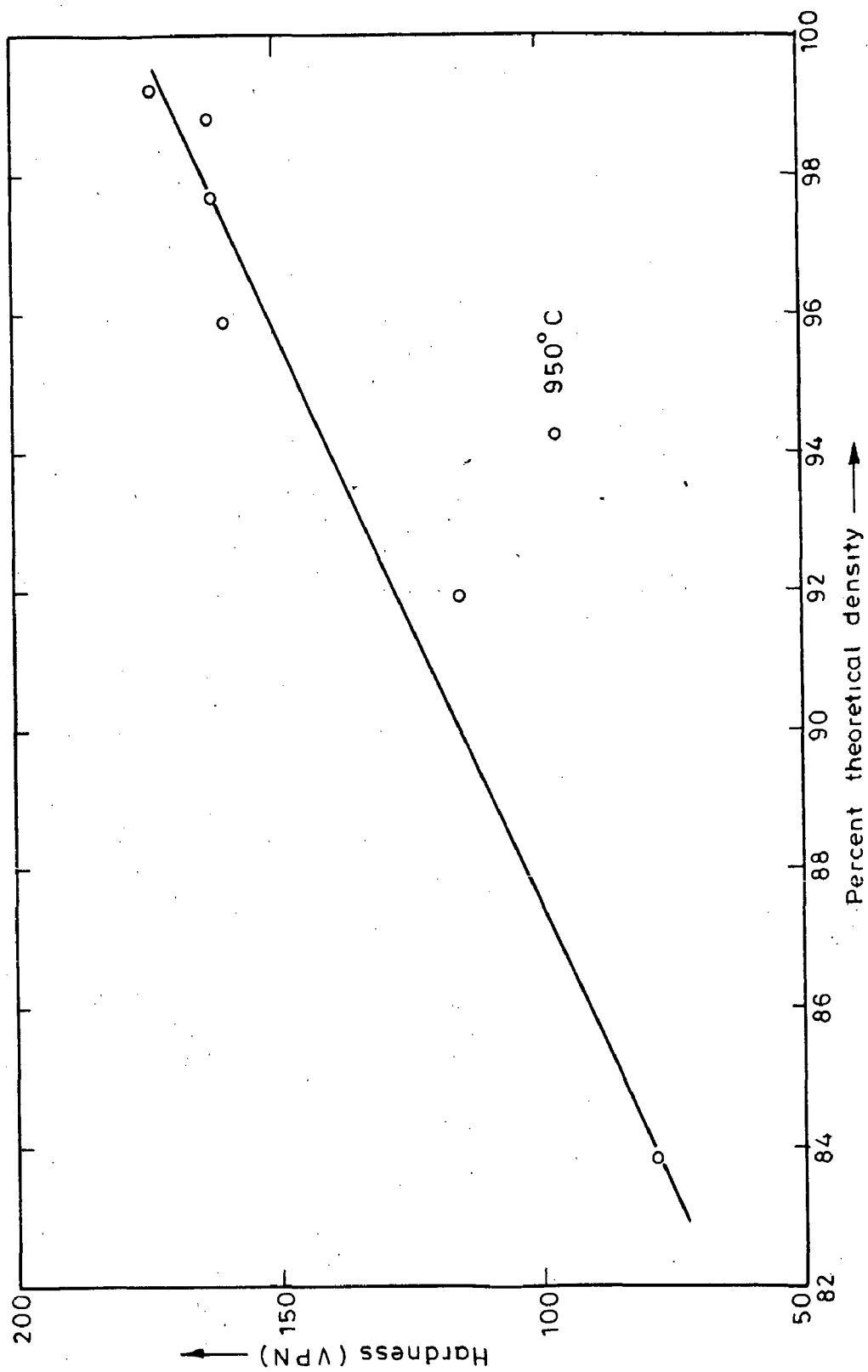


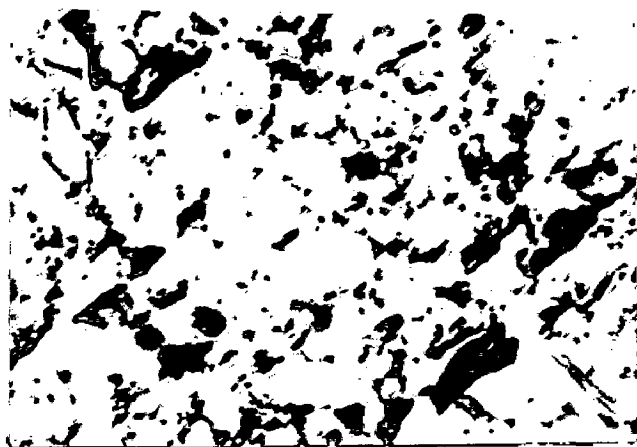
Fig.6.53 -Variation of hardness with respect to percent theoretical density for 0.45 % phosphorus steel , H/D = 0.59 during hot upset forging

Fig. 6.54 Pore Morphology of Iron Powder Sintered Preform ( $H/D = 0.99$ ) Upset Forged At  $900^{\circ}\text{C}$

- |   |   |
|---|---|
| (a) Sintered Pore structure at the centre<br>100X; enlarged 6 times.    | (b) Pore structure at 39.62 % height reduction<br>100X; enlarged 6 times. |
| (c) Pore structure at 42 % height reduction<br>100 X; enlarged 6 times. | (d) Pore structure at 53 % height reduction<br>100X; enlarged 6 times.    |

0.0 % def.

( a )



39.62 % def.

( b )

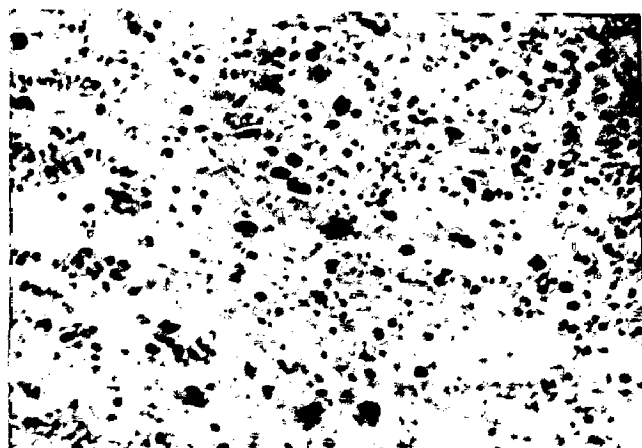
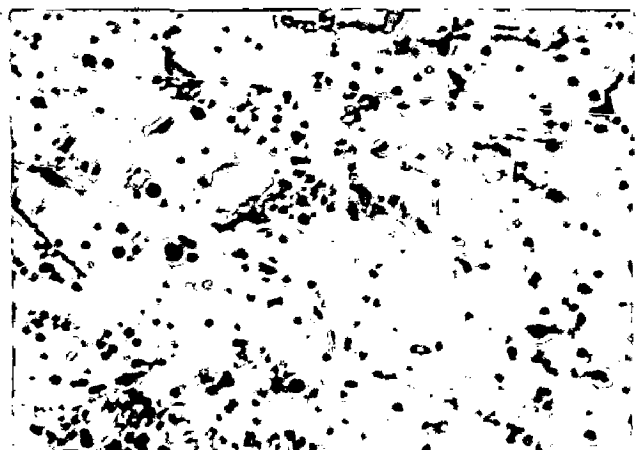


FIG. 6.54

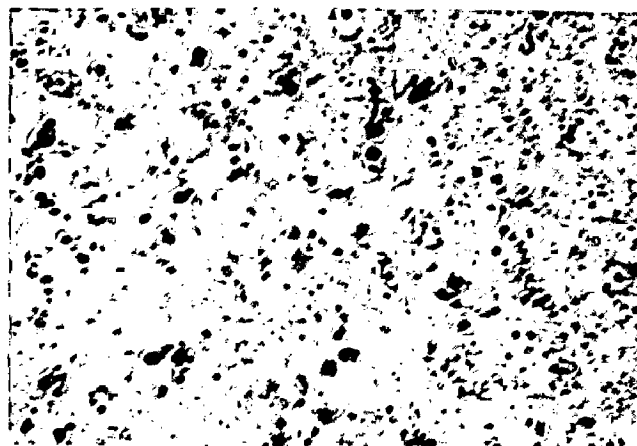
42.0 % def

( c )



53.0 % def

( d )





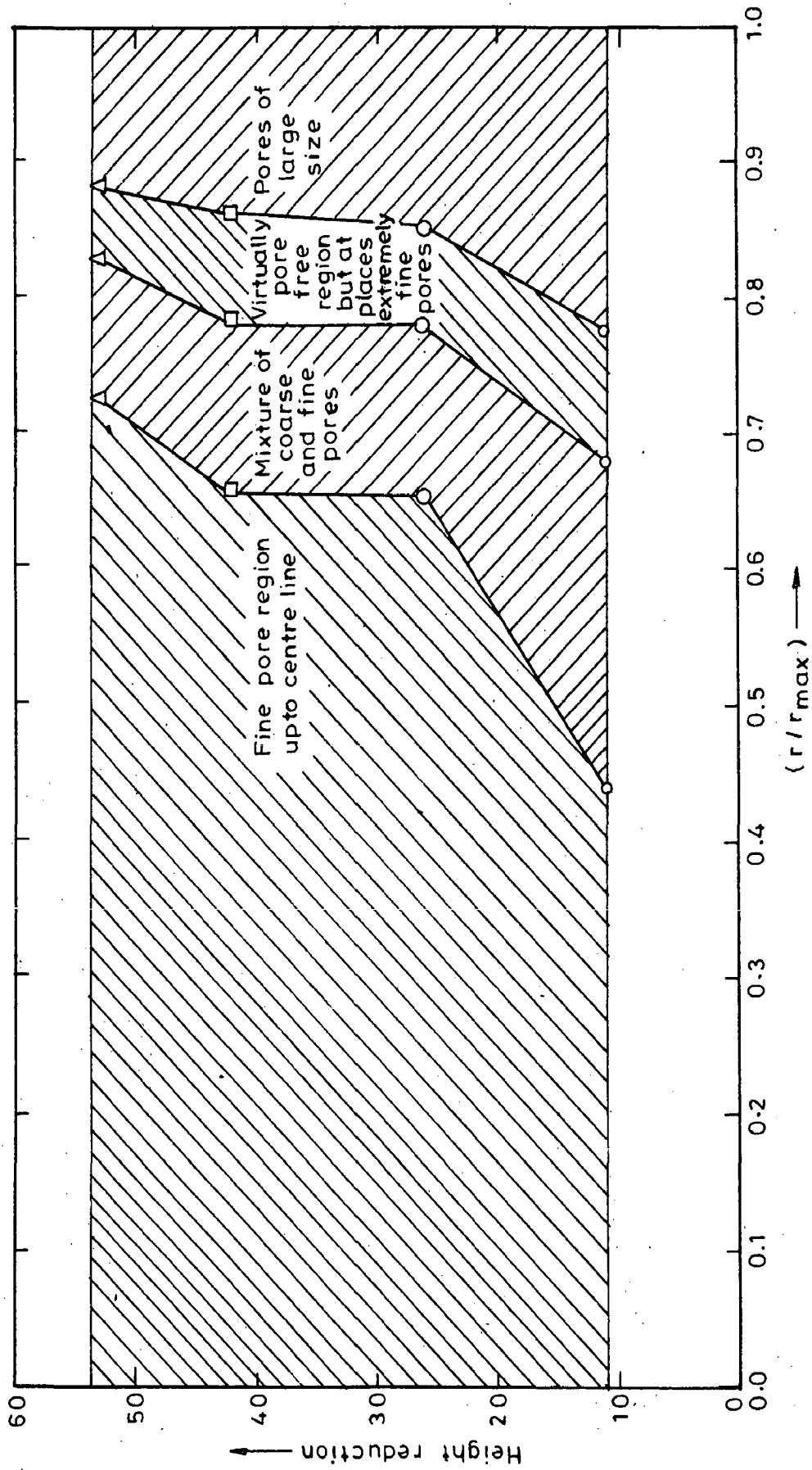


Fig.6.55-Relationship between percent deformation with coarse pores relative position

Fig. 6.56 Etched Structure of Iron Powder Sintered  
Preform (H/D=0.99) Upset Forged at 900°C

Etchant : 2 % nital

- |  |   |
|--|---|
| (a) At the centre of the sintered specimen<br>50X; enlarged<br>6 times.                | (b) Near the edge of the sintered specimen<br>50X ; enlarged<br>6 times.            |
| (c) At the edge of the sintered specimen<br>50X ; enlarged<br>6 times.                 | (d) At the centre of the 11 % height reduced specimen<br>50X : enlarged<br>6 times. |
| (e) At the centre of the 39.62 % height reduced specimen<br>50 X; enlarged<br>6 times. | (f) At the centre of the 53 % height reduced specimen<br>50X ; enlarged<br>6 times. |

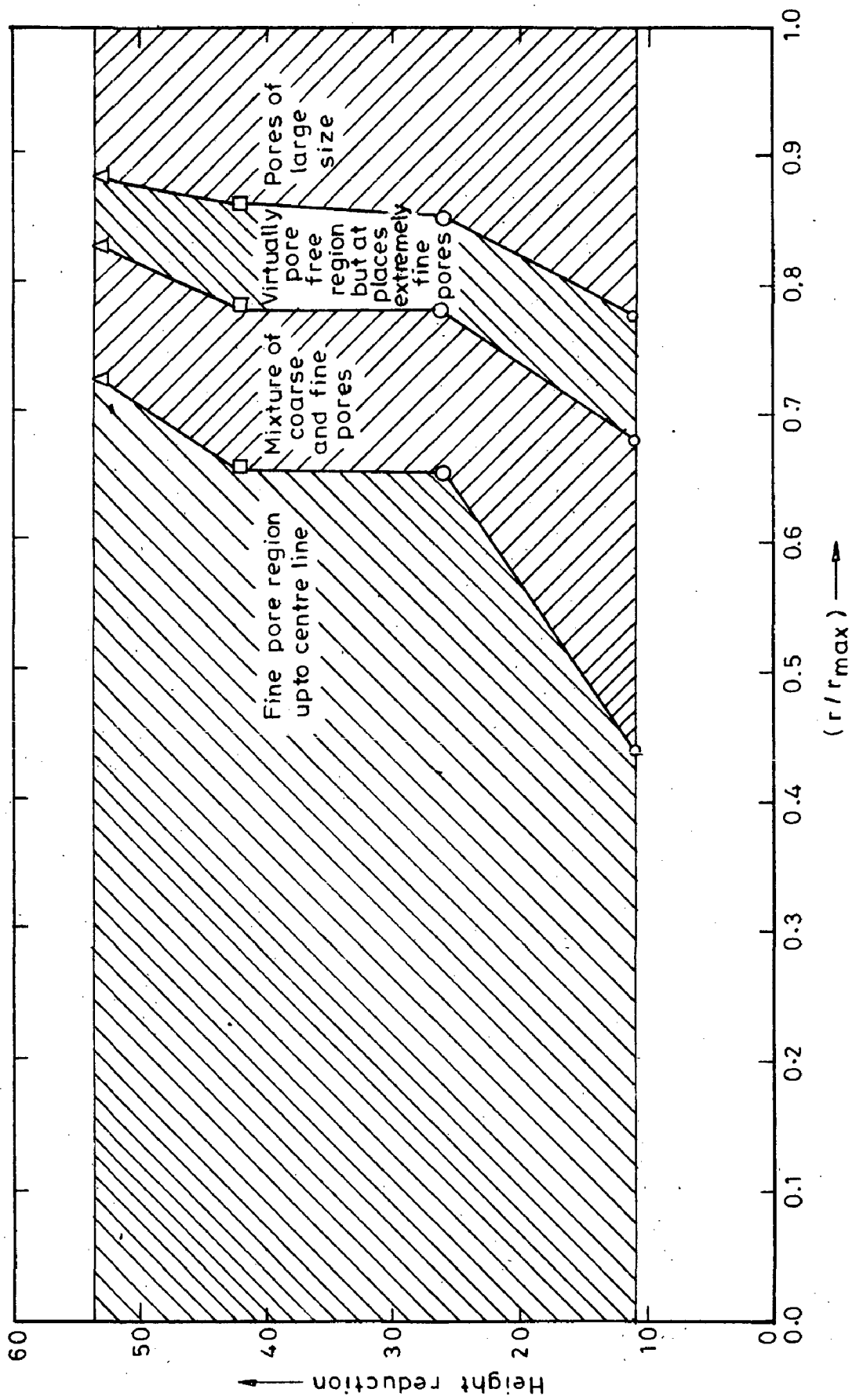
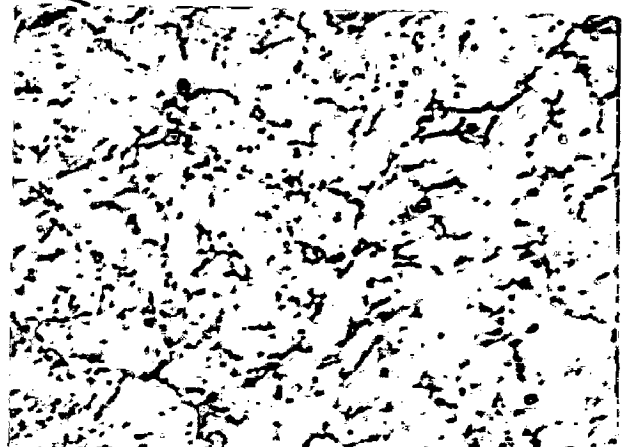
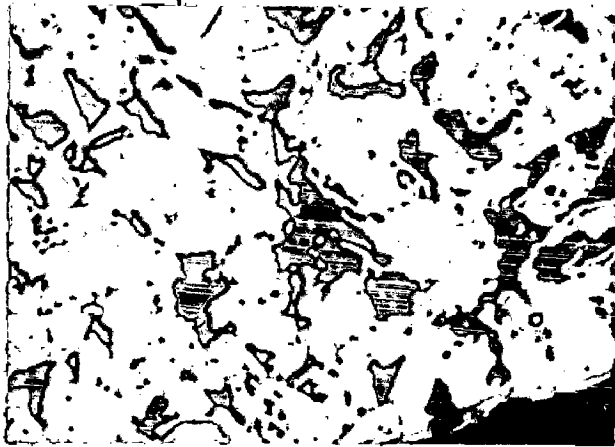
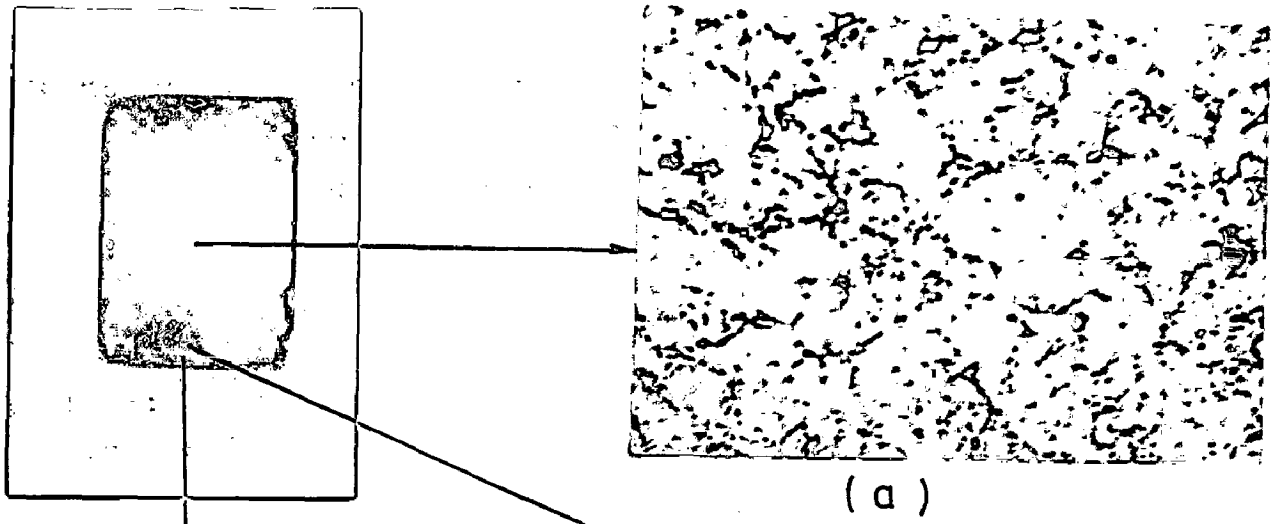


Fig.6.55-Relationship between percent deformation with coarse pores relative position

Fig. 6.56 Etched Structure of Iron Powder Sintered  
Preform (H/D=0.99) Upset Forged at 900°C

Etchant : 2 % nital

- |  |   |
|--|---|
| (a) At the centre of<br>the sintered<br>specimen<br>50X; enlarged<br>6 times.                | (b) Near the edge of<br>the sintered specimen<br>50X ; enlarged<br>6 times.               |
| (c) At the edge of the<br>sintered specimen<br>50X ; enlarged<br>6 times.                    | (d) At the centre of<br>the 11 % height<br>reduced specimen<br>50X : enlarged<br>6 times. |
| (e) At the centre of<br>the 39.62 % height<br>reduced specimen<br>50 X; enlarged<br>6 times. | (f) At the centre of<br>the 53 % height<br>reduced specimen<br>50X ; enlarged<br>6 times. |



(d)

(e)

(f)



FIG. 6.56

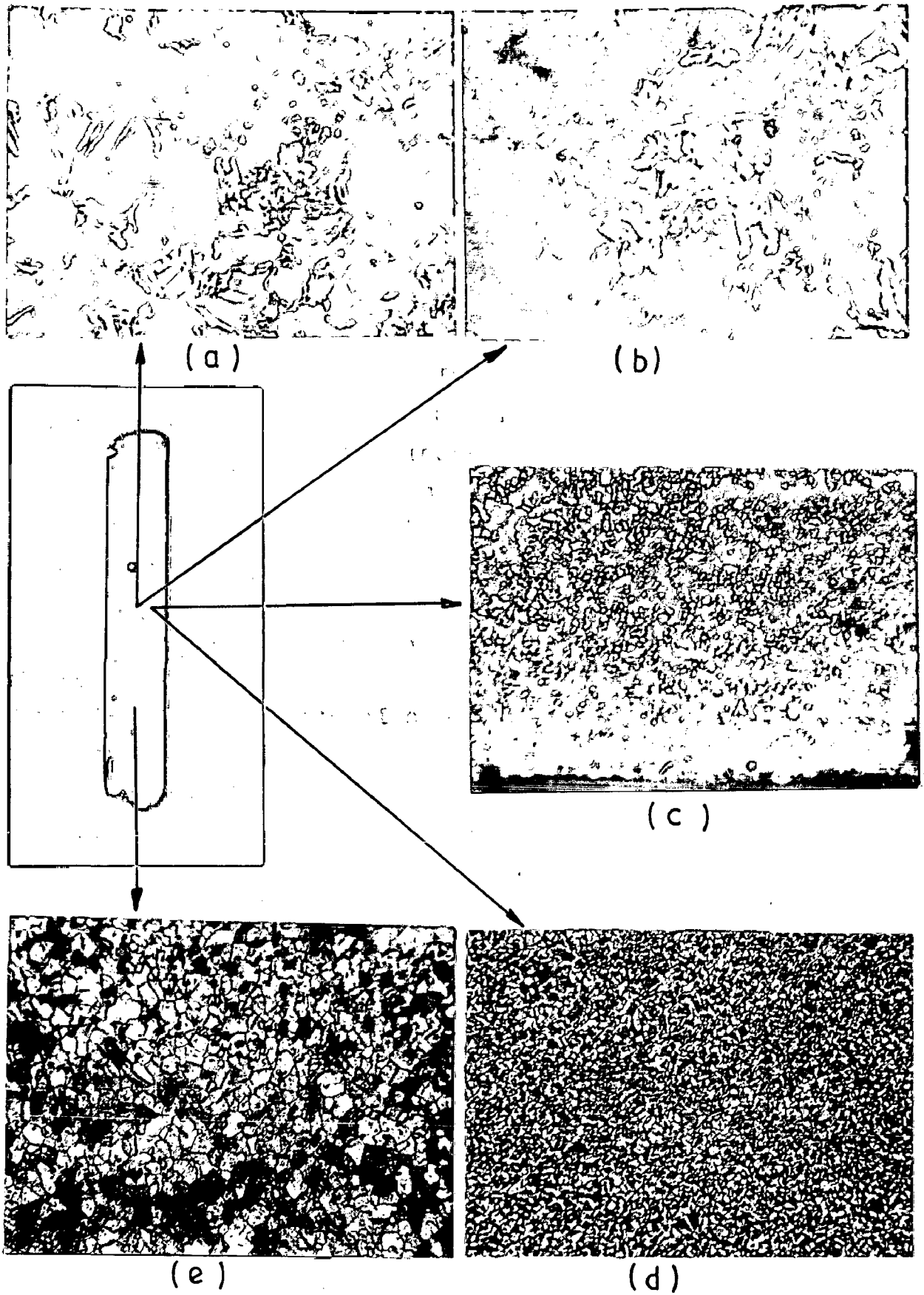


FIG. 6.57

Fig. 6.58 Morphology of 0.83 % C-Iron Powder Sintered Prefrom (H/D = 0.99) Upset Forged at 900°C.

- |  |  |
|--|--|
| <p>(a) Nearly rounded and uniformly distributed pores - at the centre of the specimen (sintered).<br/>100X ; enlarged 6 times.</p> | <p>(b) Structure at the centre showing coarse eutectoid with traces of cementite. (Height reduction nearly 50 %)<br/>Etchant : 2 % nital.<br/>500X ; enlarged 6 times.</p> |
|--|--|

Fig. 6.59 Etched Structure of 1.36 % C Iron Powder Sintered Prefrom (H/D=0.99) Upset Forged at 900°C  
Etchant : 2 % nital

Nearly 56 % Height Reduction Showing Thick Carbide Network with Fine Grain Revealing at Places Pearlite in Traces.

FIG. 6.59



FIG 658(a)

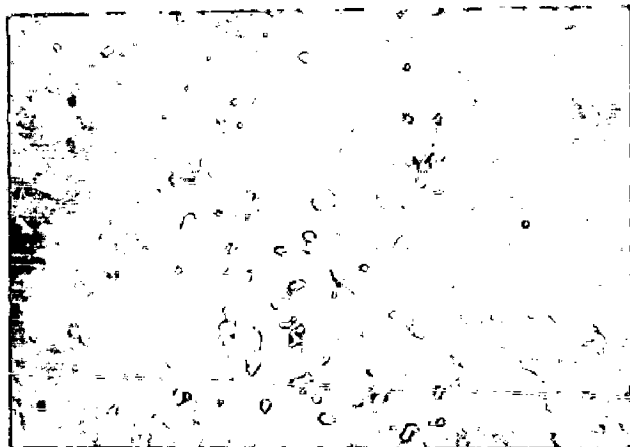


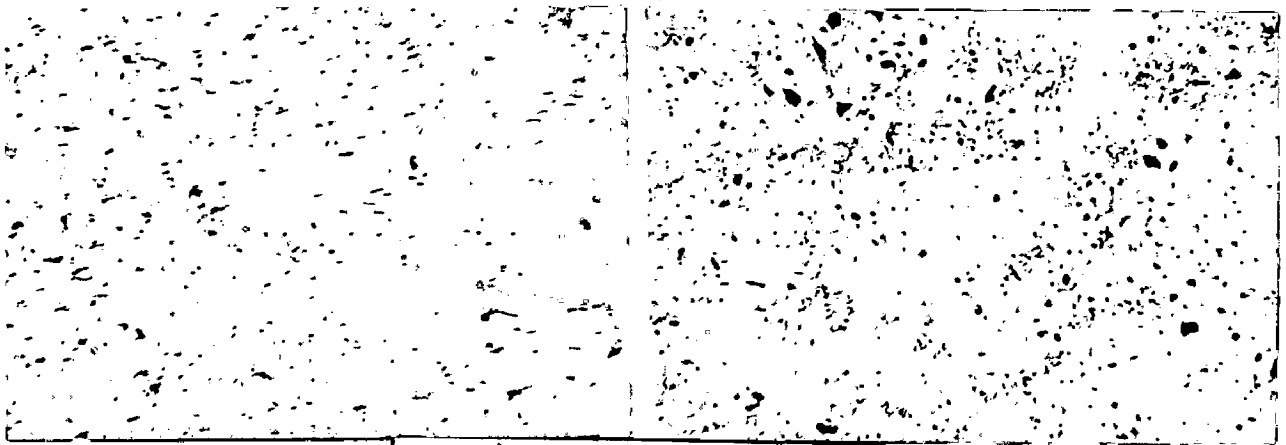
FIG. 6.58 (b)





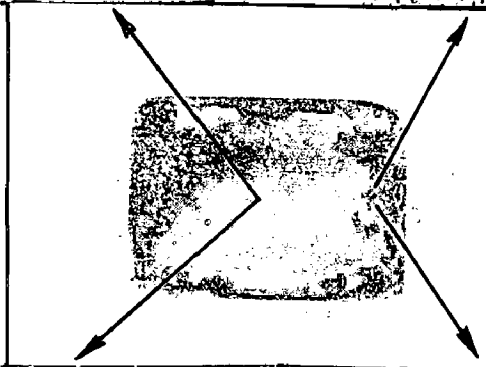
Fig. 6.60 - Morphology - 0.45 % Phosphorus Powder  
Sintered Preform (H/D=0.59) Upset Forged at 960°C

- |  |  |
|--|--|
| <p>(a) Pore structure at the centre of the sintered specimen (unetched).<br/>50X ; enlarged 6 times.</p>   | <p>(b) Pore structure at the edge of the specimen (unetched).<br/>50X ;enlarged 6 times.</p>   |
| <p>(c) Structure showing fine grains with thin boundaries and marginal porosities at the centre of the sintered specimen.<br/>100X; enlarged 6 times.<br/>Etchant : 2 % nital.</p> | <p>(d) Coarse porosities and fine grains with thick boundaries near the edge.<br/>100X; enlarged 6 times<br/>Etchant : 2 % nital.</p>  |
| <p>(e) Structure shows collapsing pores at the centre of the specimen height reduction ~55-57 %.<br/>50X; enlarged 6 times .</p>   | <p>(f) At the centre - sense of grain flow. Very thin boundaries. Pore flattening in the direction of diametrical flow.<br/>100X; enlarged 6 times.<br/>Etchant : 2 % nital.</p> |



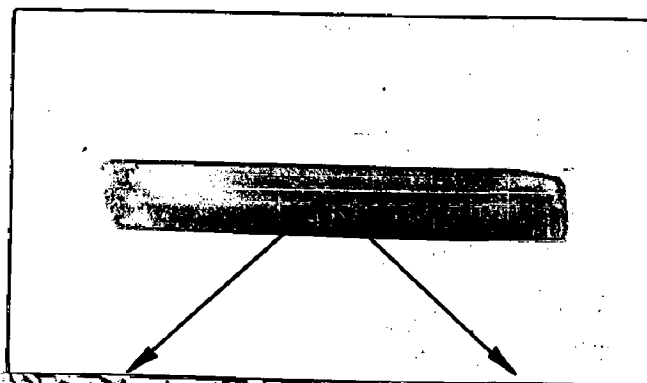
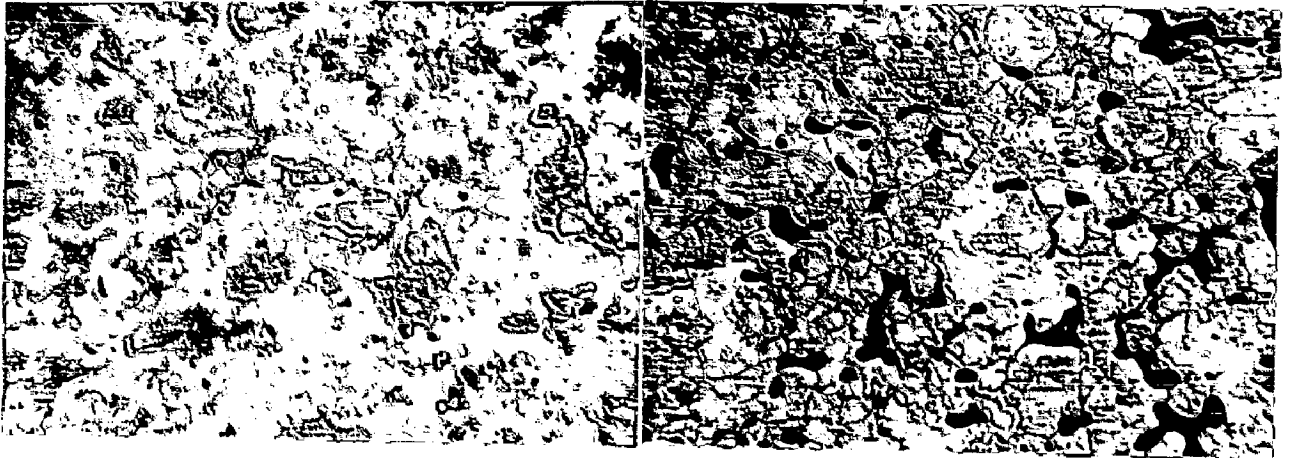
(a)

(b)



(c)

(d)



(e)

(f)

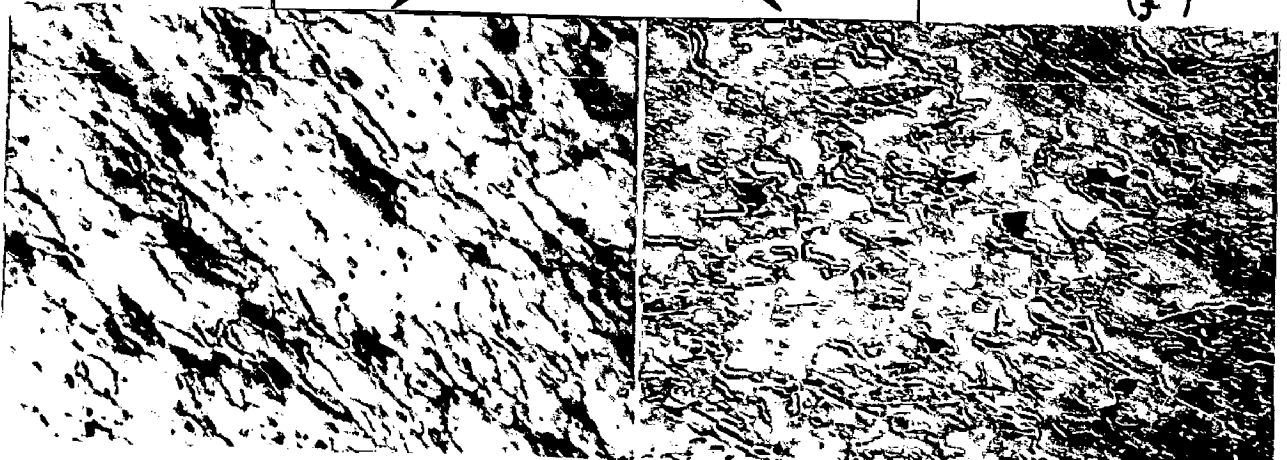


FIG. 6.60

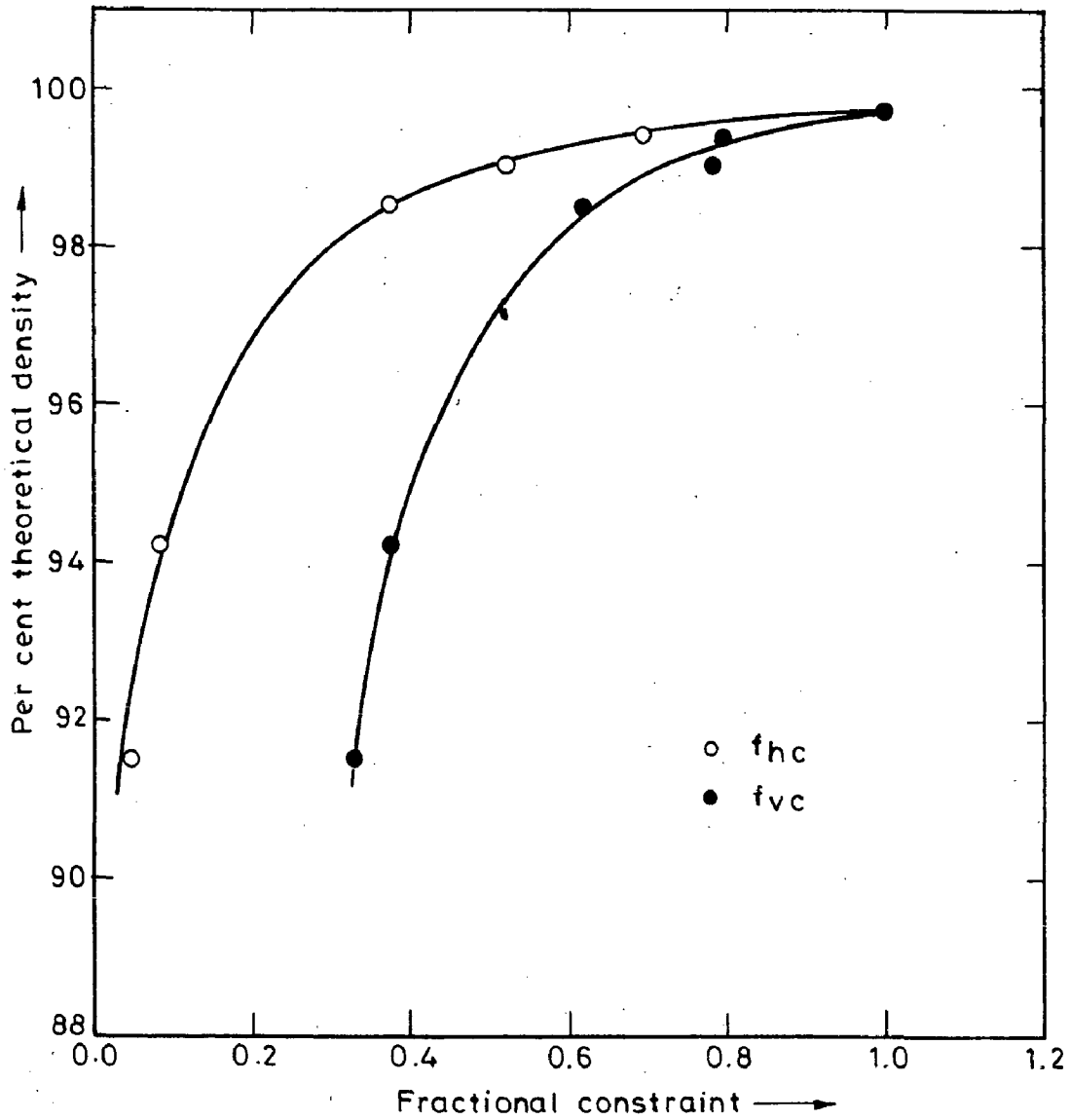


Fig.6.61-Relationship between percent theoretical density and fractional constraints (Horizontal and vertical) in forging sintered iron powder preform ( $H/D=1.18$ ) through partially open step down cylindrical die cavity at  $1120^{\circ}\text{C}$

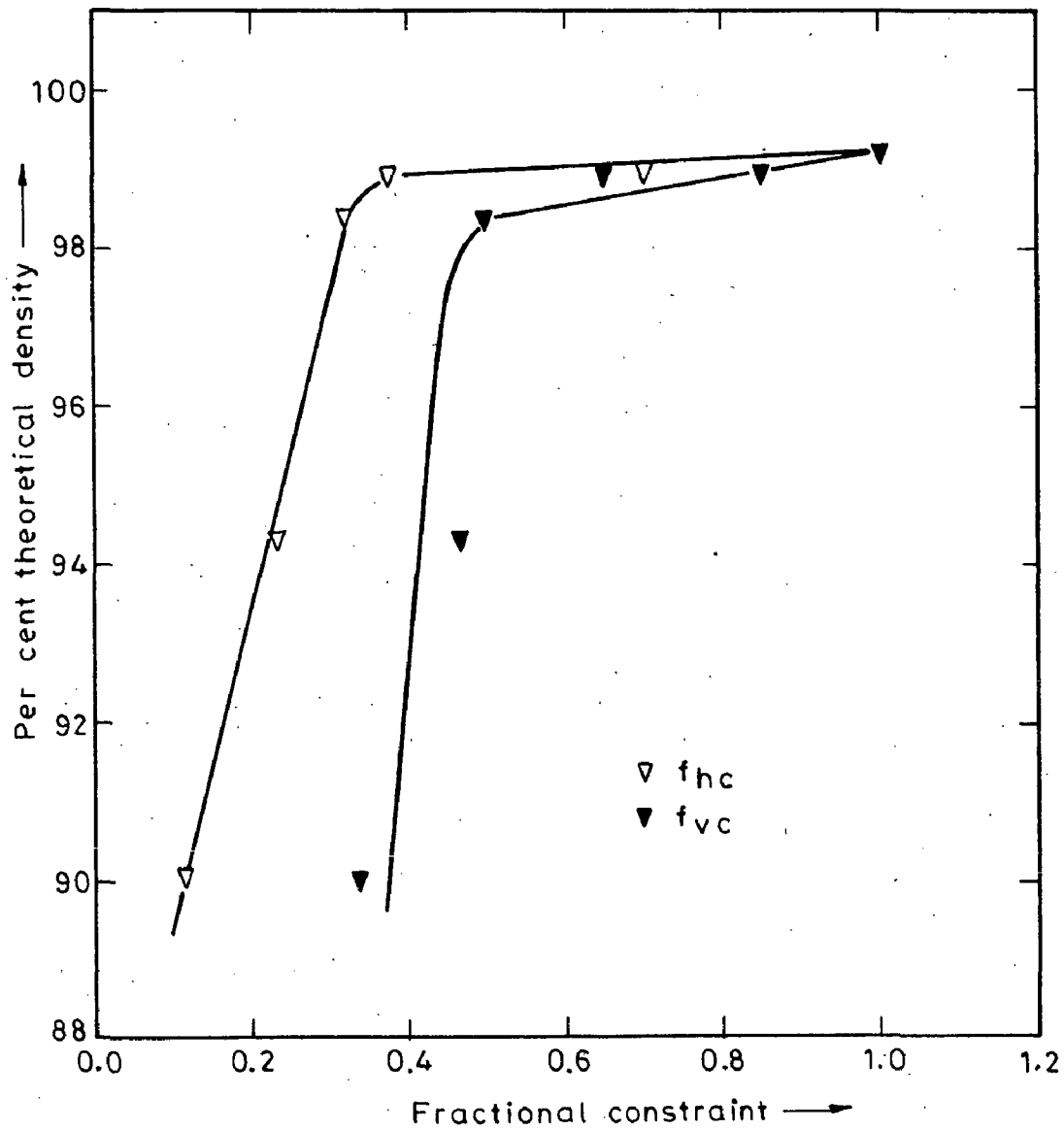


Fig.6.62-Relationship between per cent theoretical density and fractional constraints ( Horizontal and vertical ) in forging sintered 0.35% carbon steel preform (  $H/D=1.18$  ) through partially open step-down cylindrical die cavity at  $1120^{\circ}\text{C}$

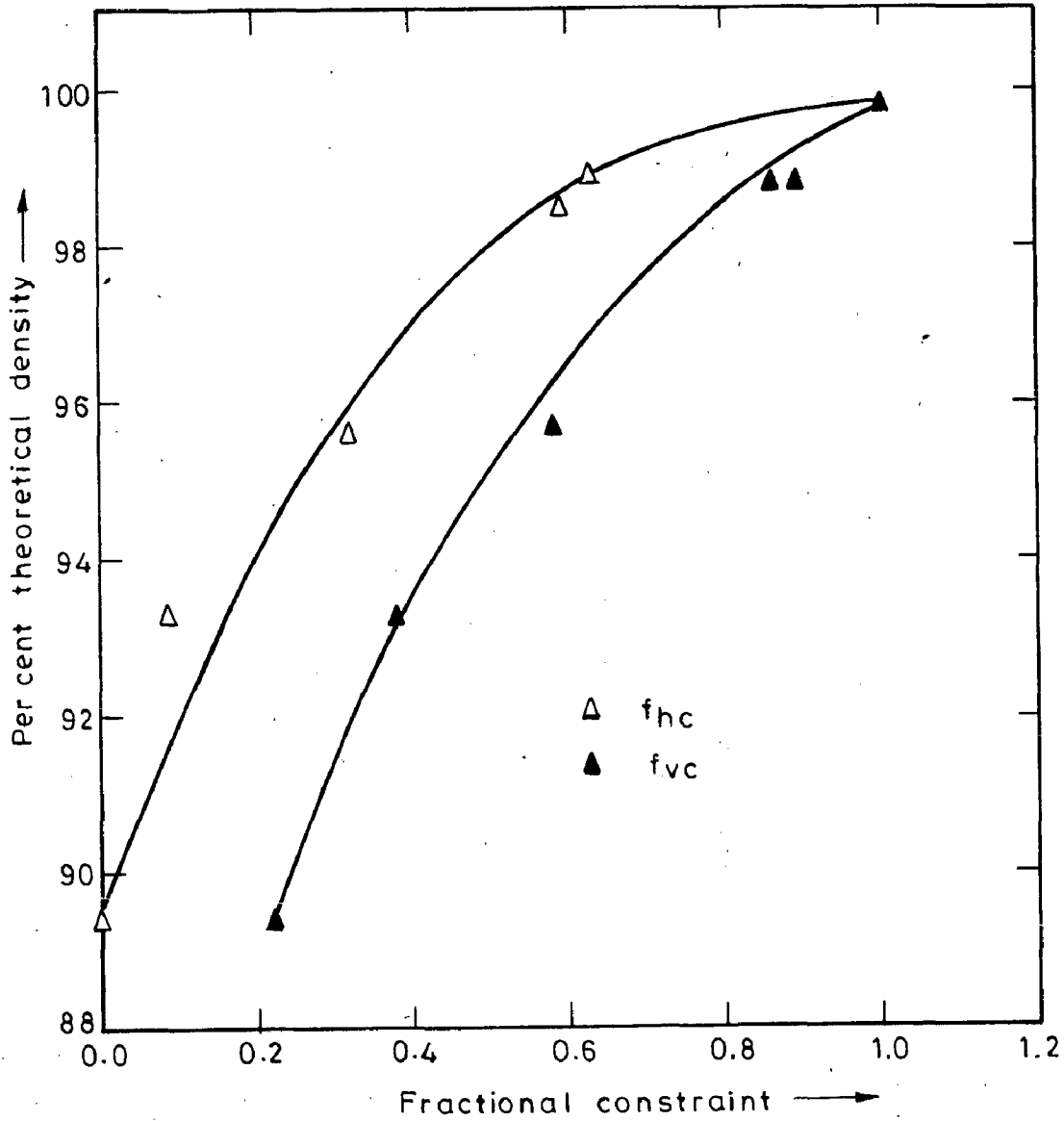


Fig.6.63-Relationship between per cent theoretical density and fractional constraints (Horizontal and vertical) in forging sintered 0.83% carbon steel preform ( $H/D=1.18$ ) through partially open step down cylindrical die cavity at  $1120^{\circ}\text{C}$

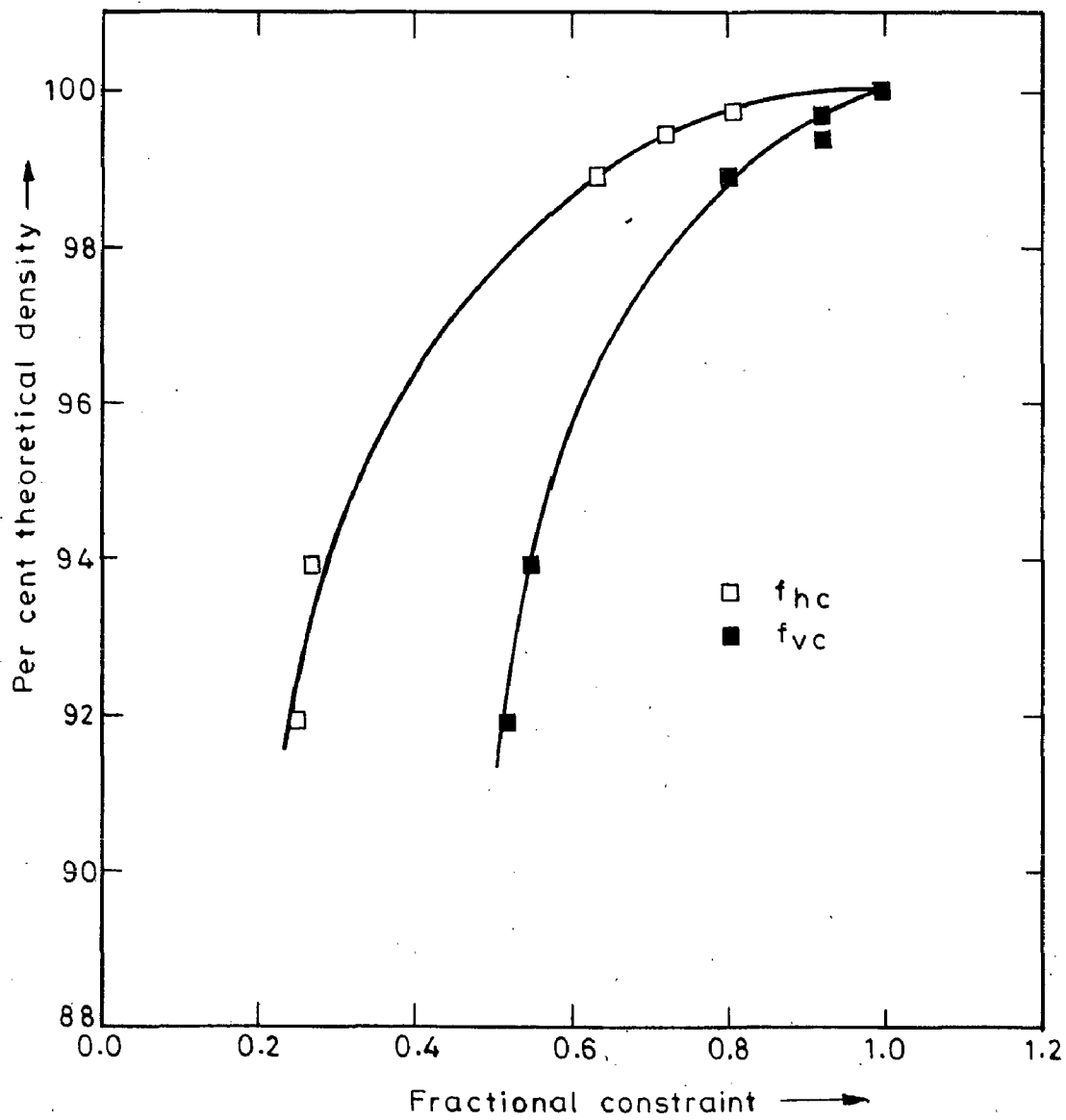


Fig.6.64-Relationship between per cent theoretical density with fractional constraints ( Horizontal and vertical ) in forging sintered 1.36% carbon steel preform ( $H/D=1.18$ ) through partially open step-down cylindrical die cavity

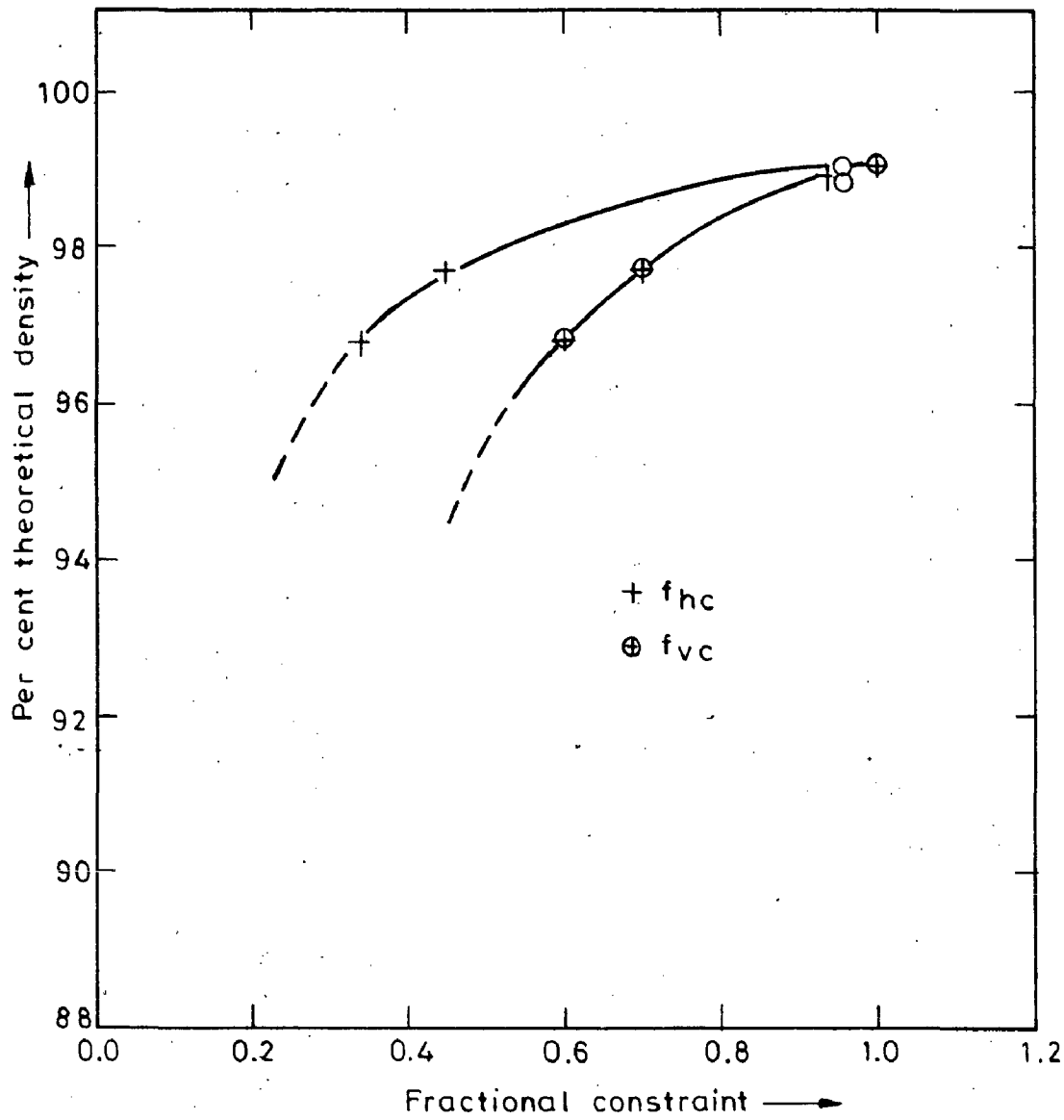


Fig.6.65-Relationship between percent theoretical density and fractional constraints (Horizontal and vertical) in forging sintered 0.45 % phosphorus steel through partially open step down cylindrical die cavity at 960°C

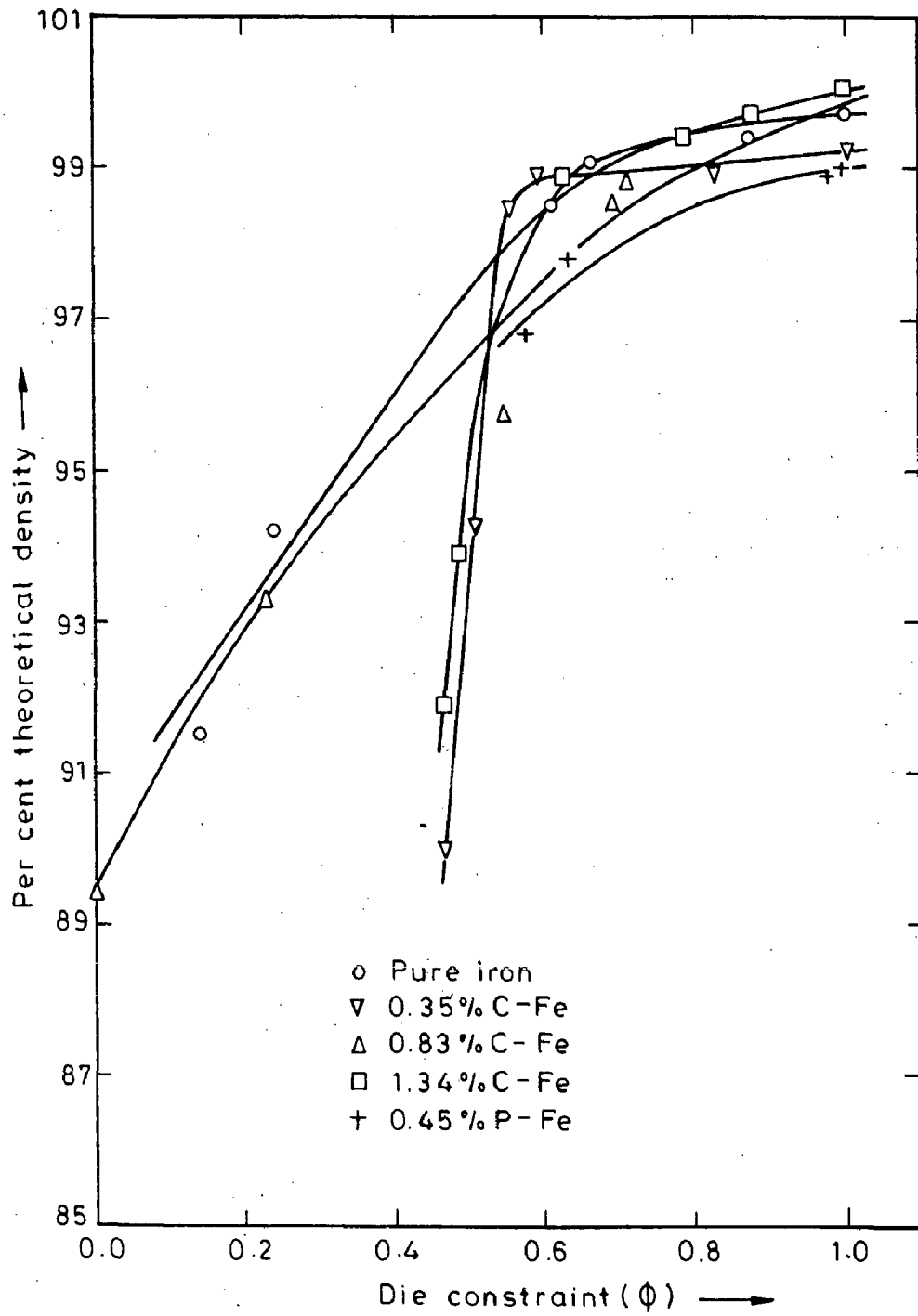


Fig.6.66-Plot of per cent theoretical density against die constraint ( $\phi$ ) in forging sintered preforms ( $H/D=1.18$ ) through partially open step down cylindrical die cavity



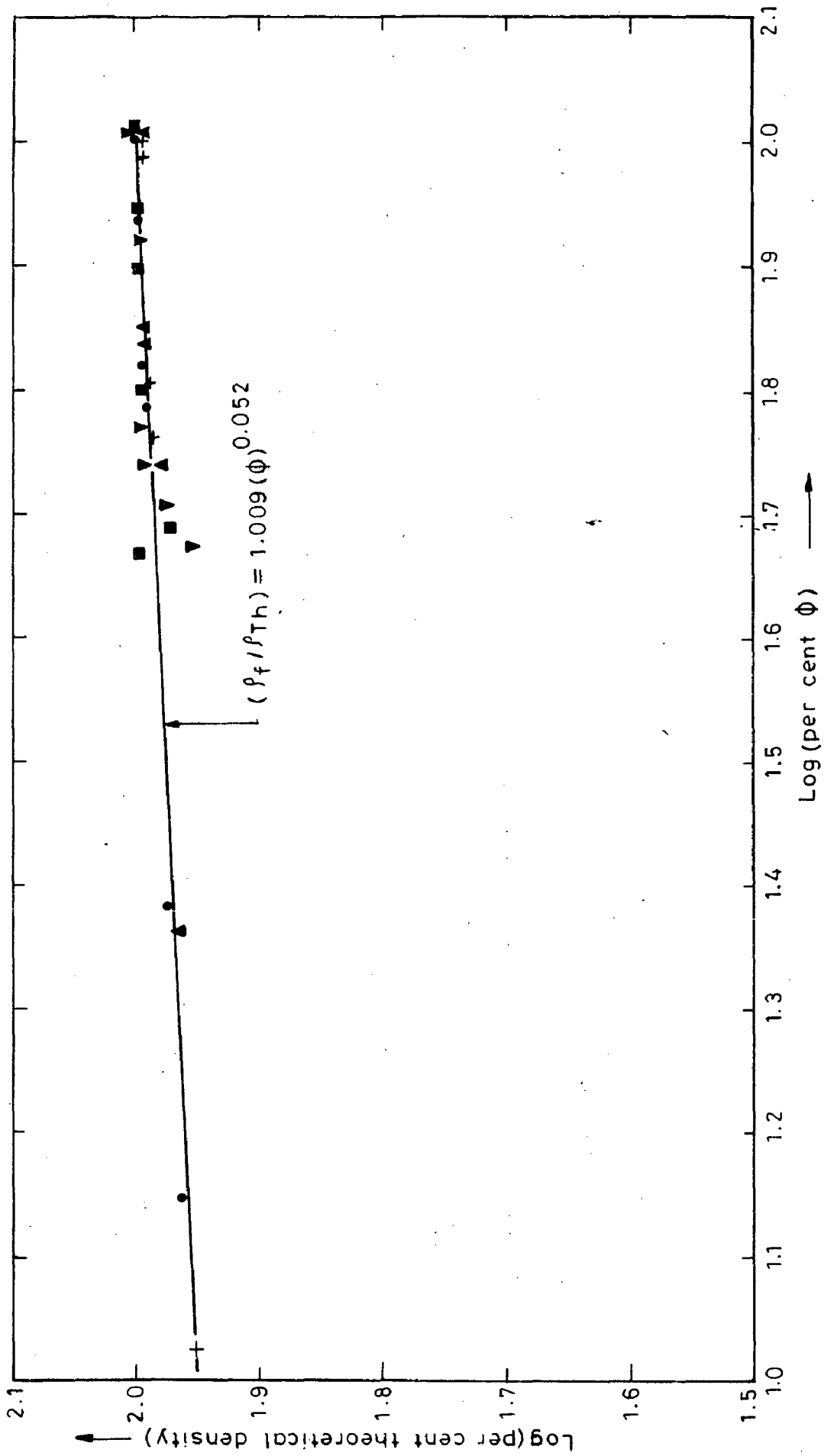


Fig. 6.67-Relationship between per cent theoretical density and  $\phi$

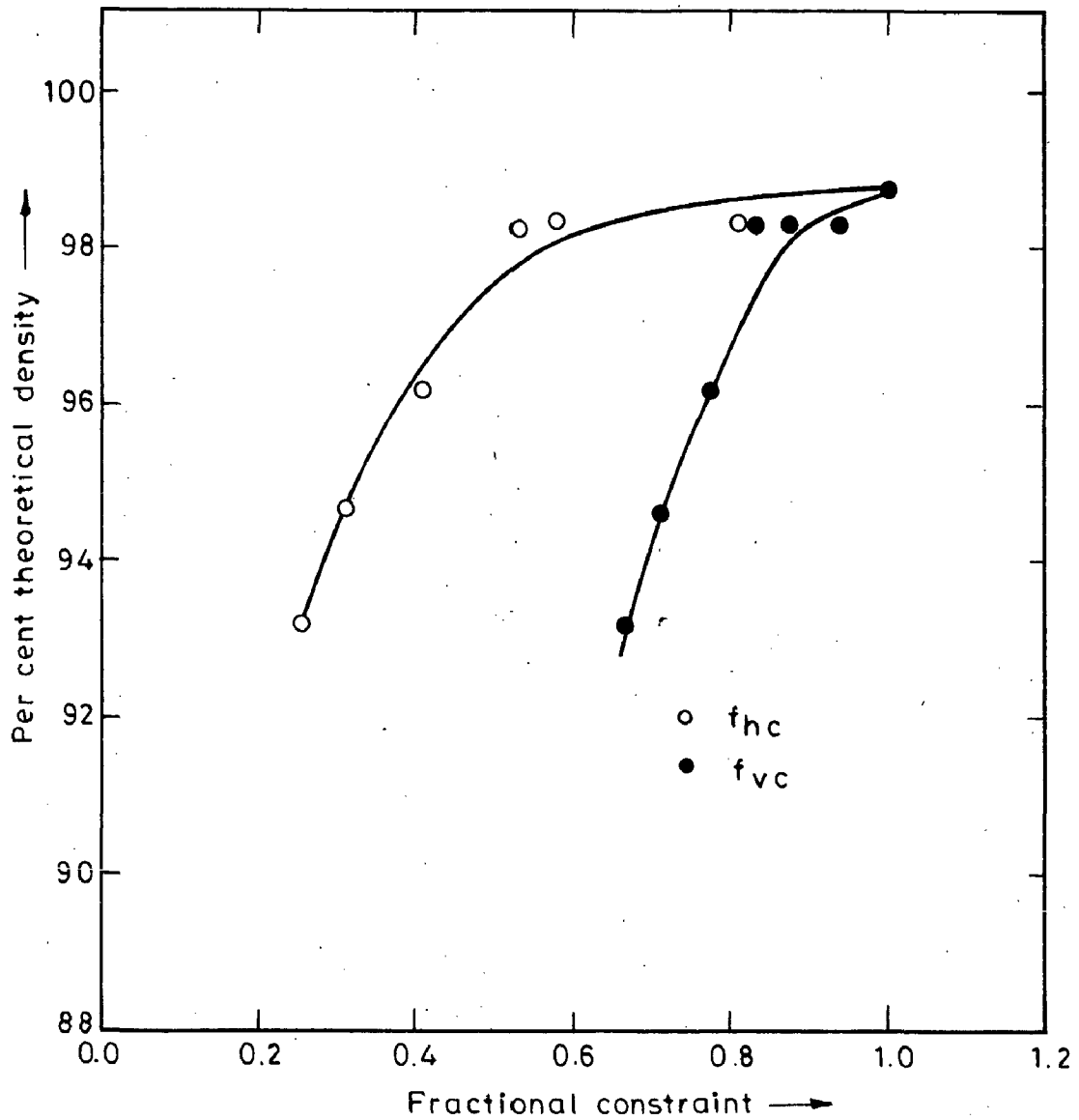


Fig.6.68-Plot of per cent theoretical density against fractional constraints in forging sintered iron powder preforms ( $H/D=1.18$ ) through partially open hemi-spherical die cavity at  $1120^{\circ}\text{C}$

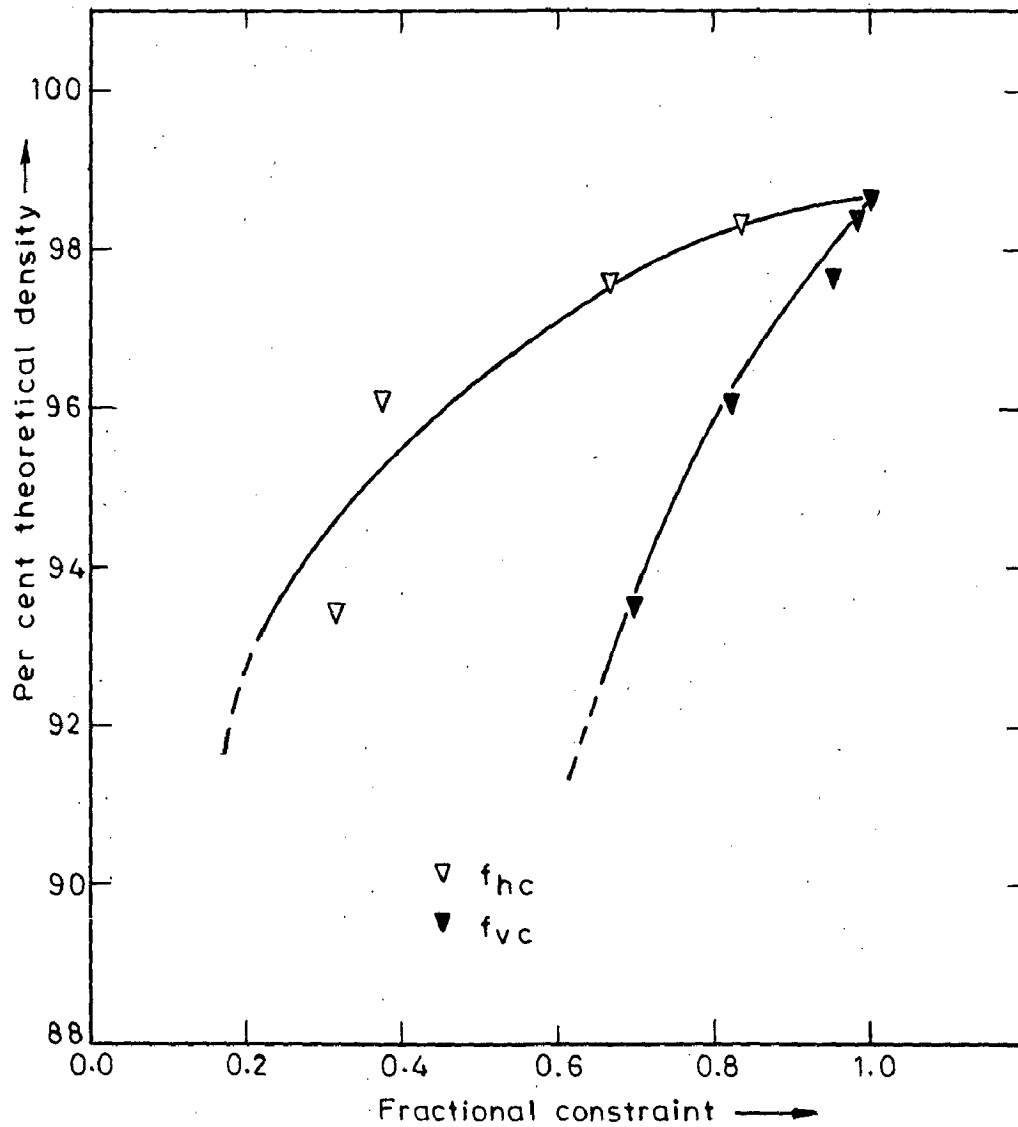


Fig.6.69-Plot of per cent theoretical density against fractional constraints ( $f_{hc}$  &  $f_{vc}$ ) in forging sintered 0.35% C steel preforms ( $H/D=1.18$ ) through partially open step down cylindrical die cavity at  $1120^{\circ}\text{C}$

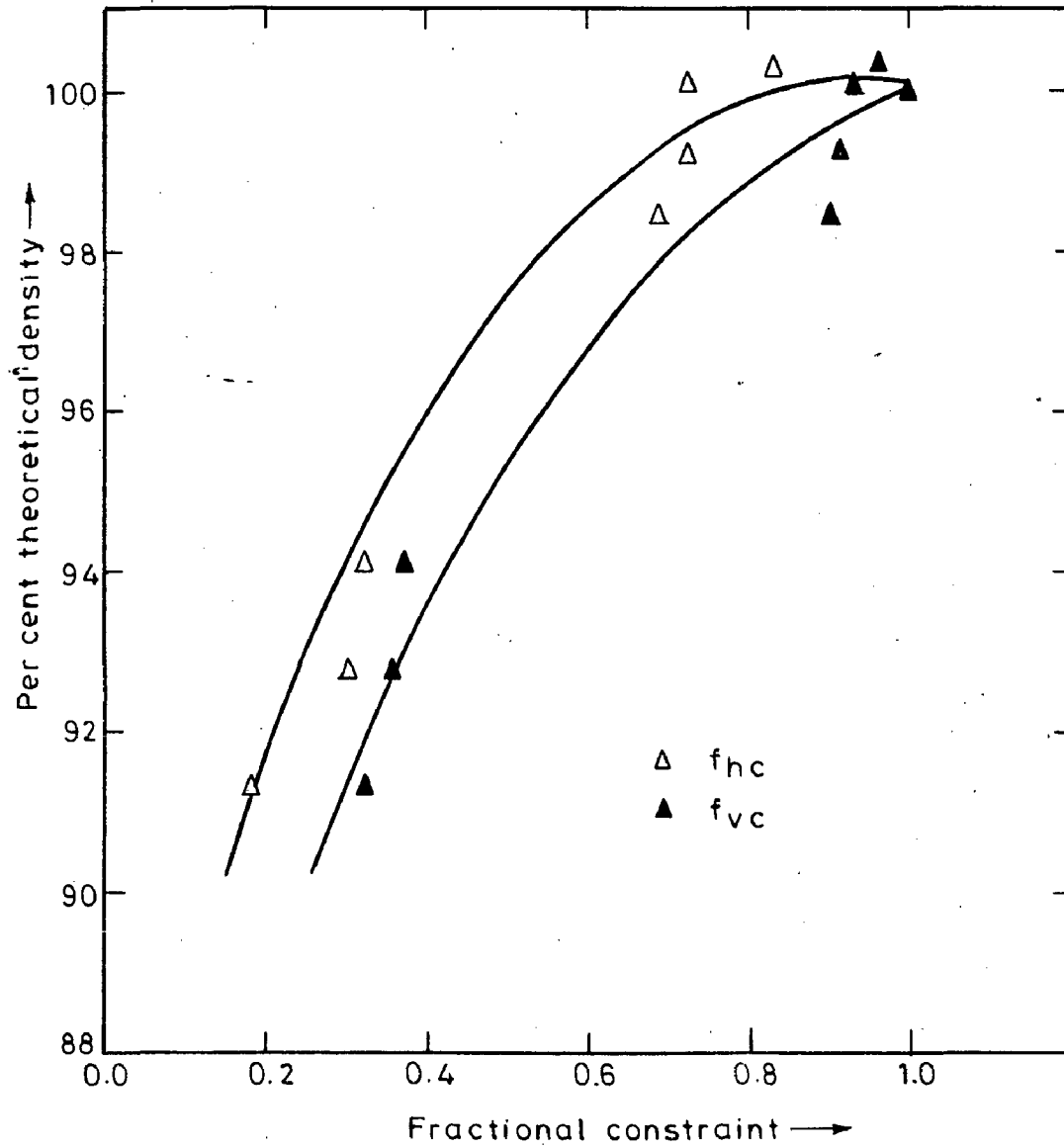


Fig.6.70-Relationship between per cent theoretical density and fractional constraint ( $f_{hc}$  &  $f_{vc}$ ) in forging sintered 0.83 carbon-steel preforms ( $H/D=1.18$ ) through partially open hemi-spherical die cavity at  $1120^{\circ}\text{C}$

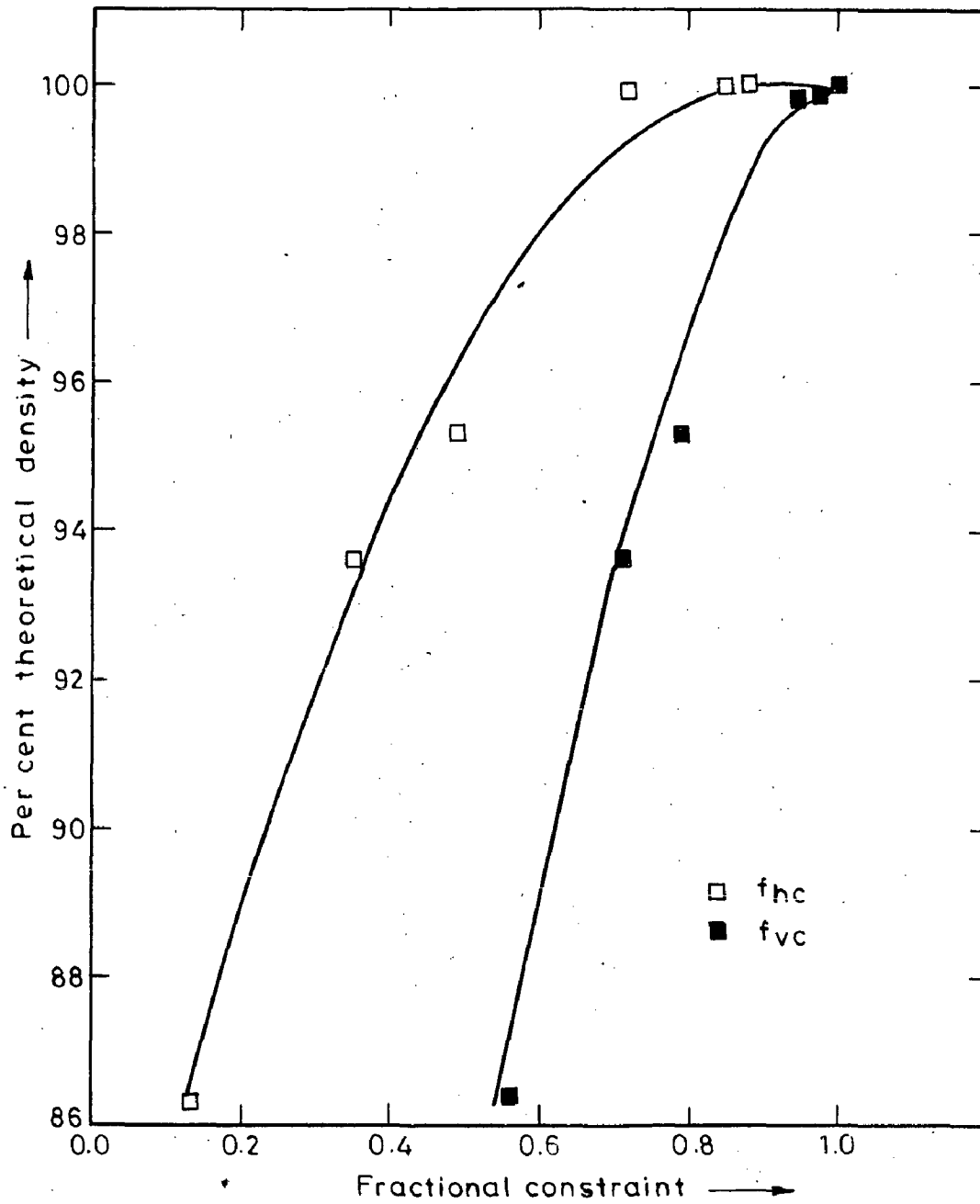


Fig.6.71-Relationship between per cent theoretical density and fractional constraint ( $f_{hc}$  &  $f_{vc}$ ) in forging sintered 1.36% carbon steel preforms ( $H/D=1.18$ ) through partially open hemi-spherical die cavity at  $1120^{\circ}\text{C}$

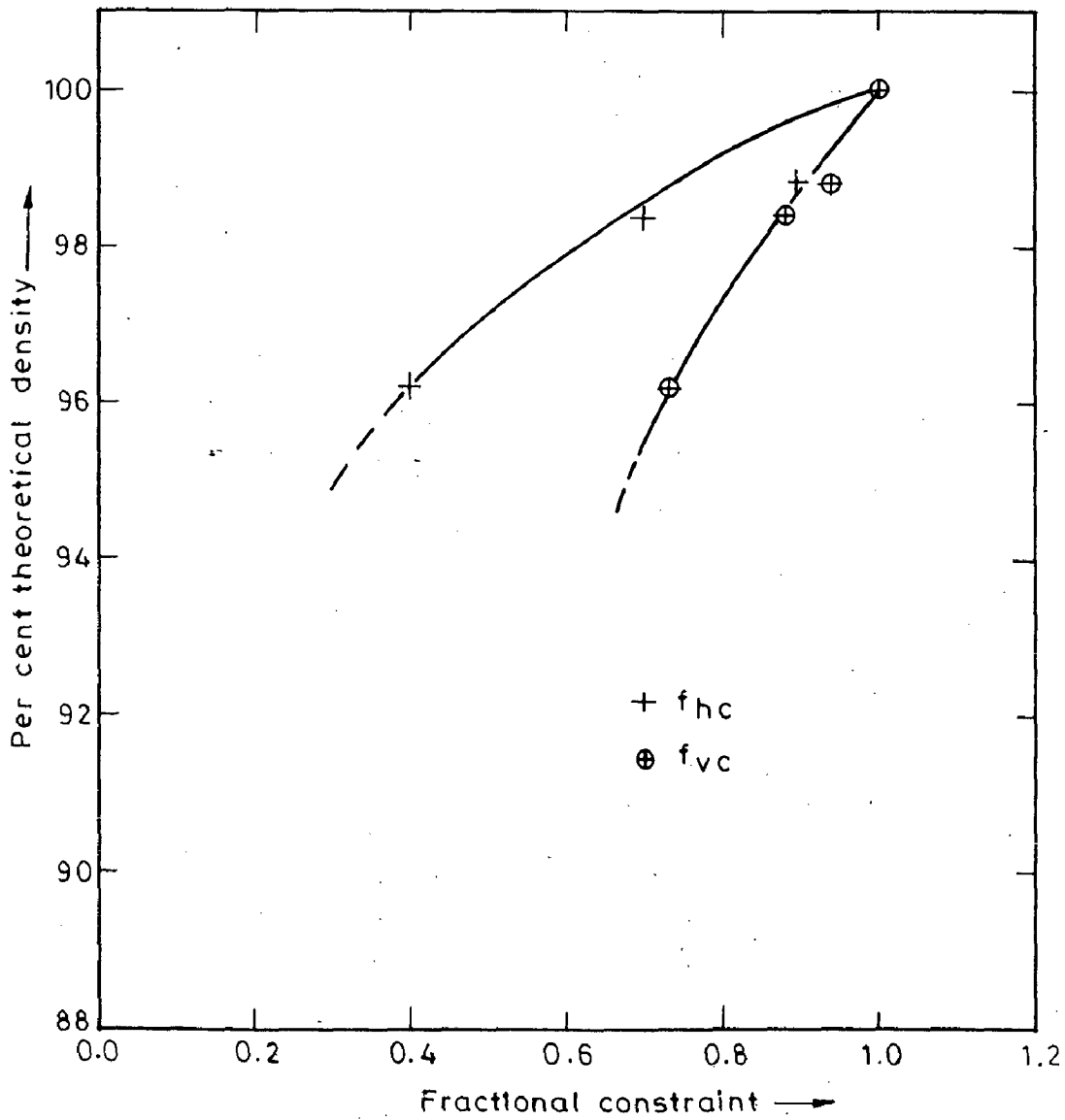


Fig.6.72-Relationship between per cent theoretical density and fractional ( $f_{hc}$  &  $f_{vc}$ ) in forging sintered 0.45% P steel through partially open hemi-spherical die cavity at 960°C

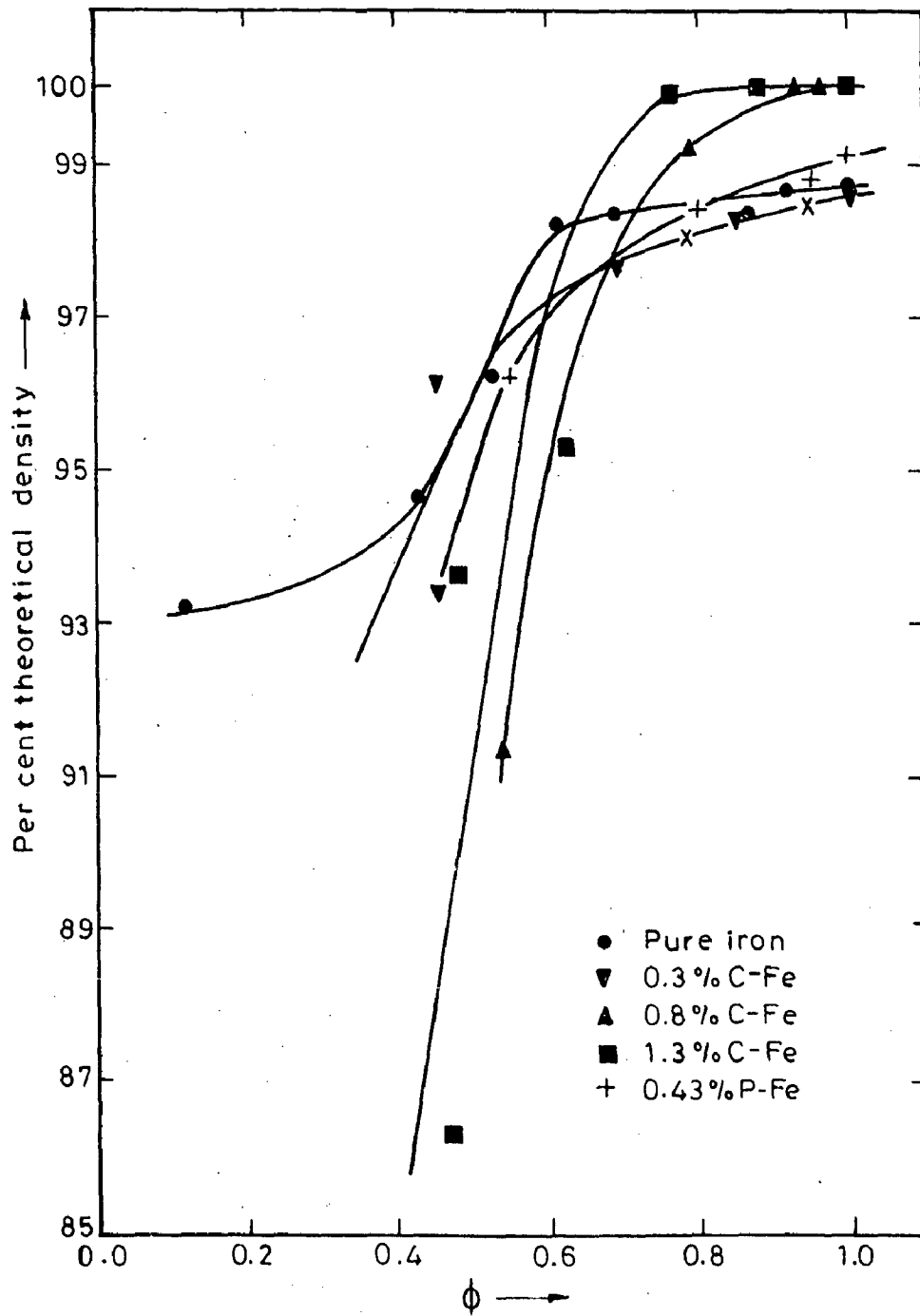


Fig.6.73-Plot of per cent theoretical density against die constraint ( $\phi$ ) in forging sintered preforms ( $H/D=1.18$ ) through partially open hemi-spherical die cavity

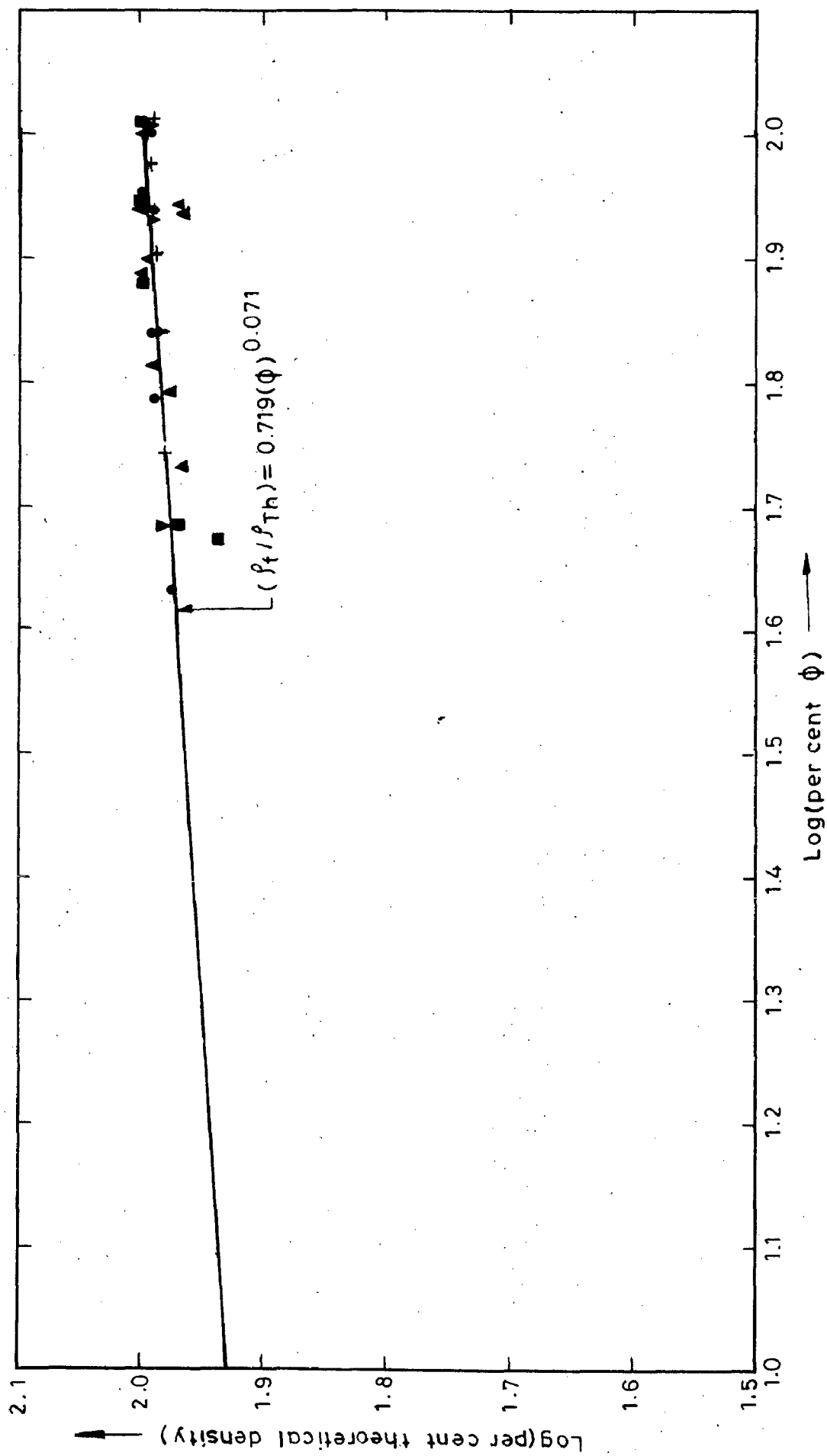


Fig.6.74-Relationship between per cent theoretical density and  $\phi$



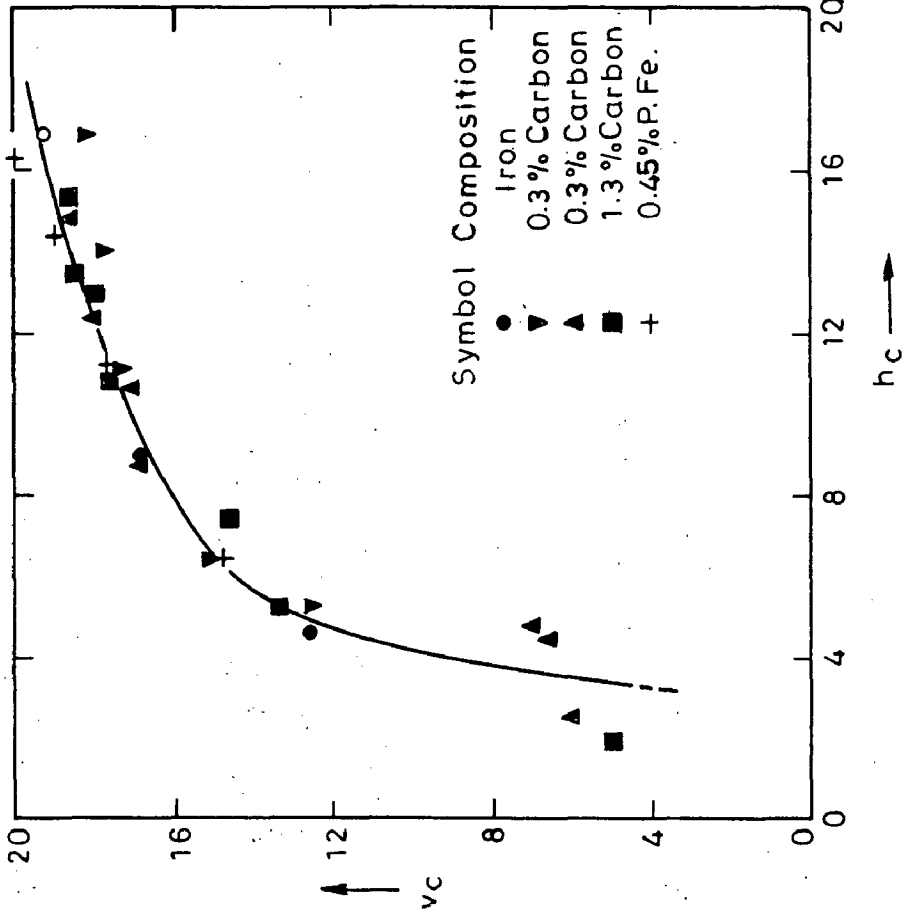
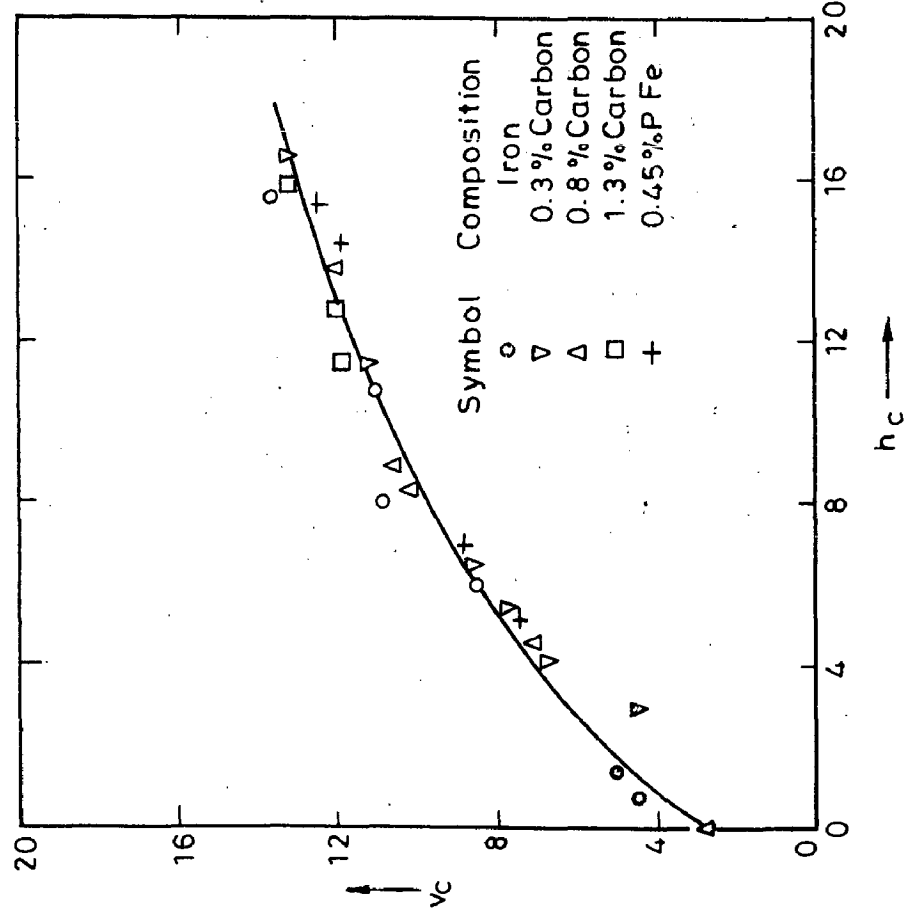


Fig.6.75(a)-Relationship between  $v_c$  and  $h_c$  in partially open step down cylindrical die cavity during forging iron and iron based alloy powder preforms ( $H/D=1.18$ )

Fig.6.75(b)-Relationship between  $v_c$  and  $h_c$  for partially open hemi-spherical die cavity during forging iron and iron based alloy powder preforms ( $H/D=1.18$ )

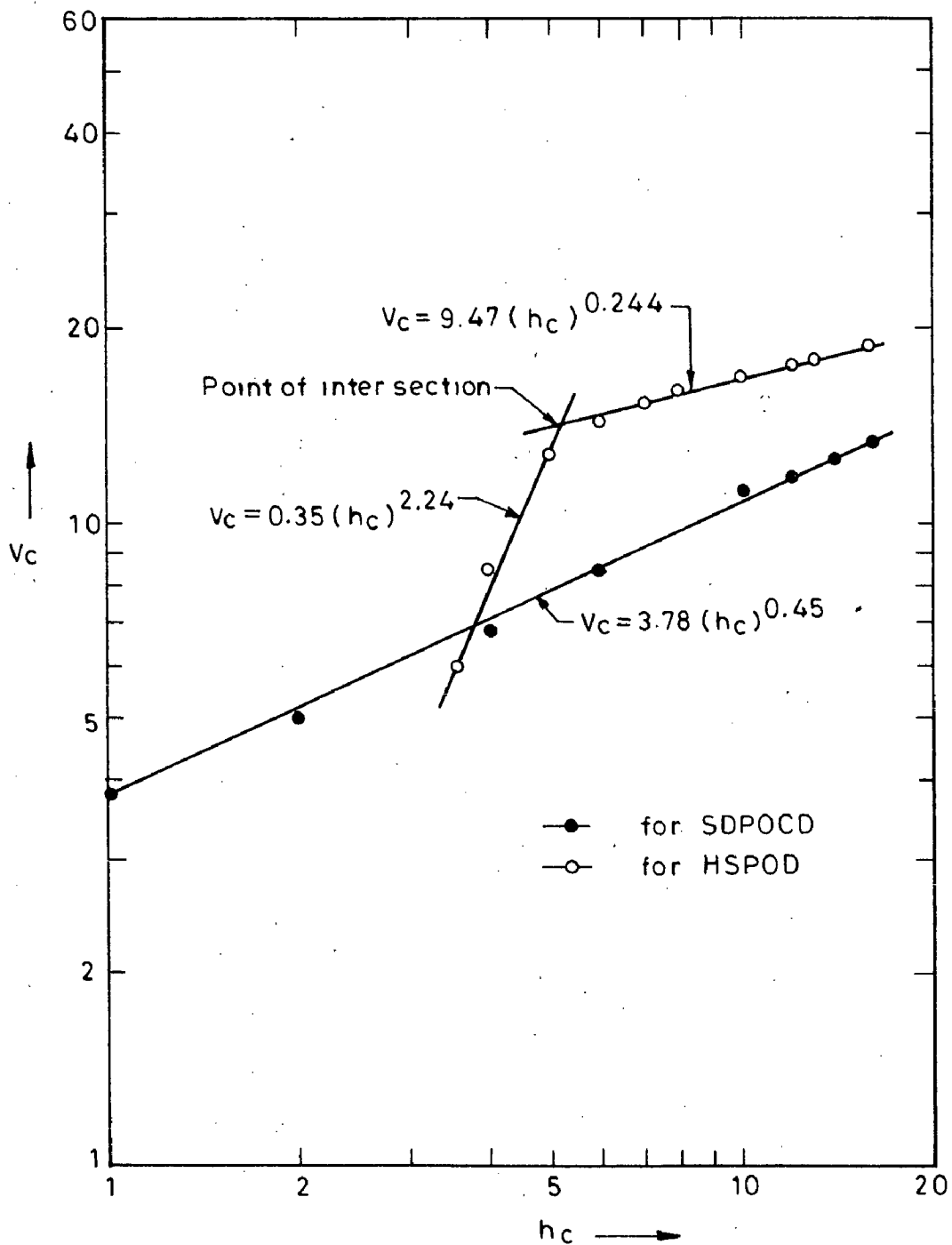


Fig.6.76-Log - log plot of vertical constraint v/s horizontal constraint during forging of iron and iron based alloy powder preforms ( $H/D=1.18$ ) through two partially open step down cylindrical and hemispherical dies

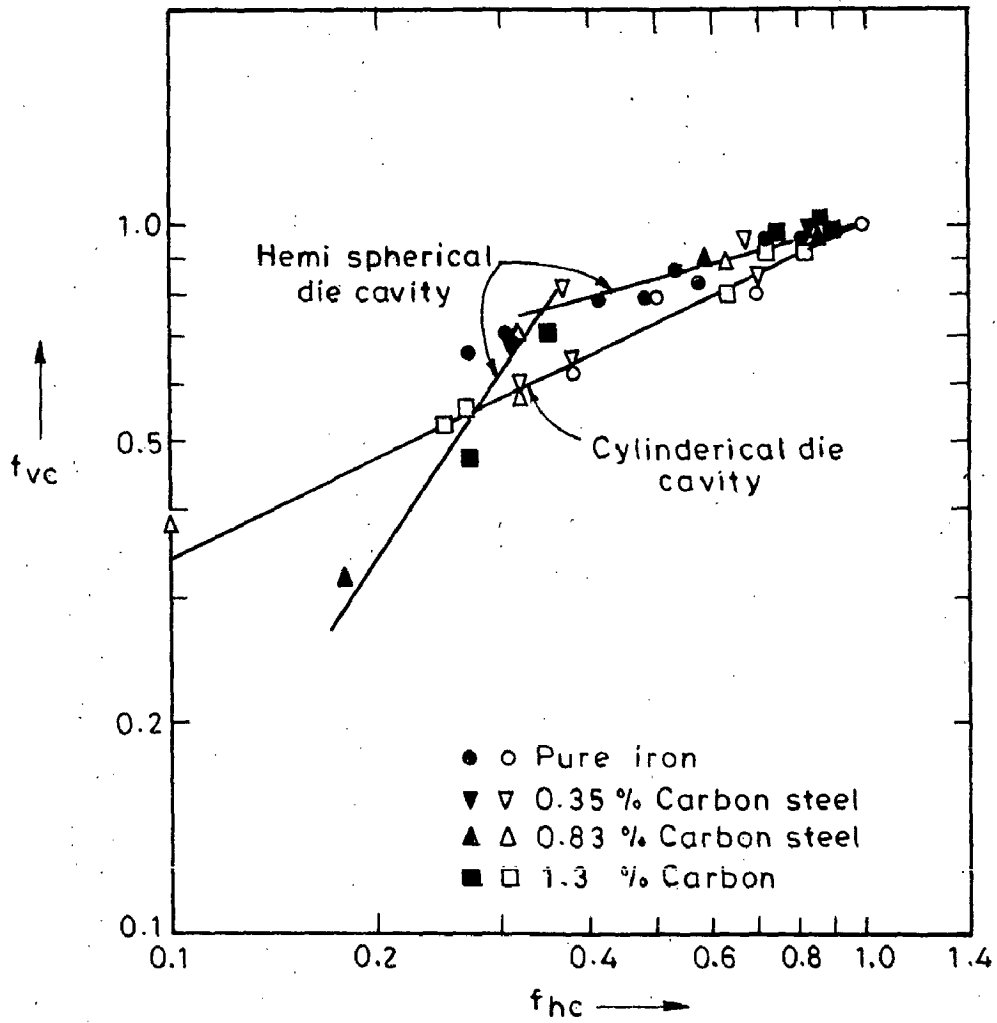


Fig.6.77-Log-log plot between  $v_c$  and  $h_c$  for partially open step-down cylindrical and hemi-spherical dies

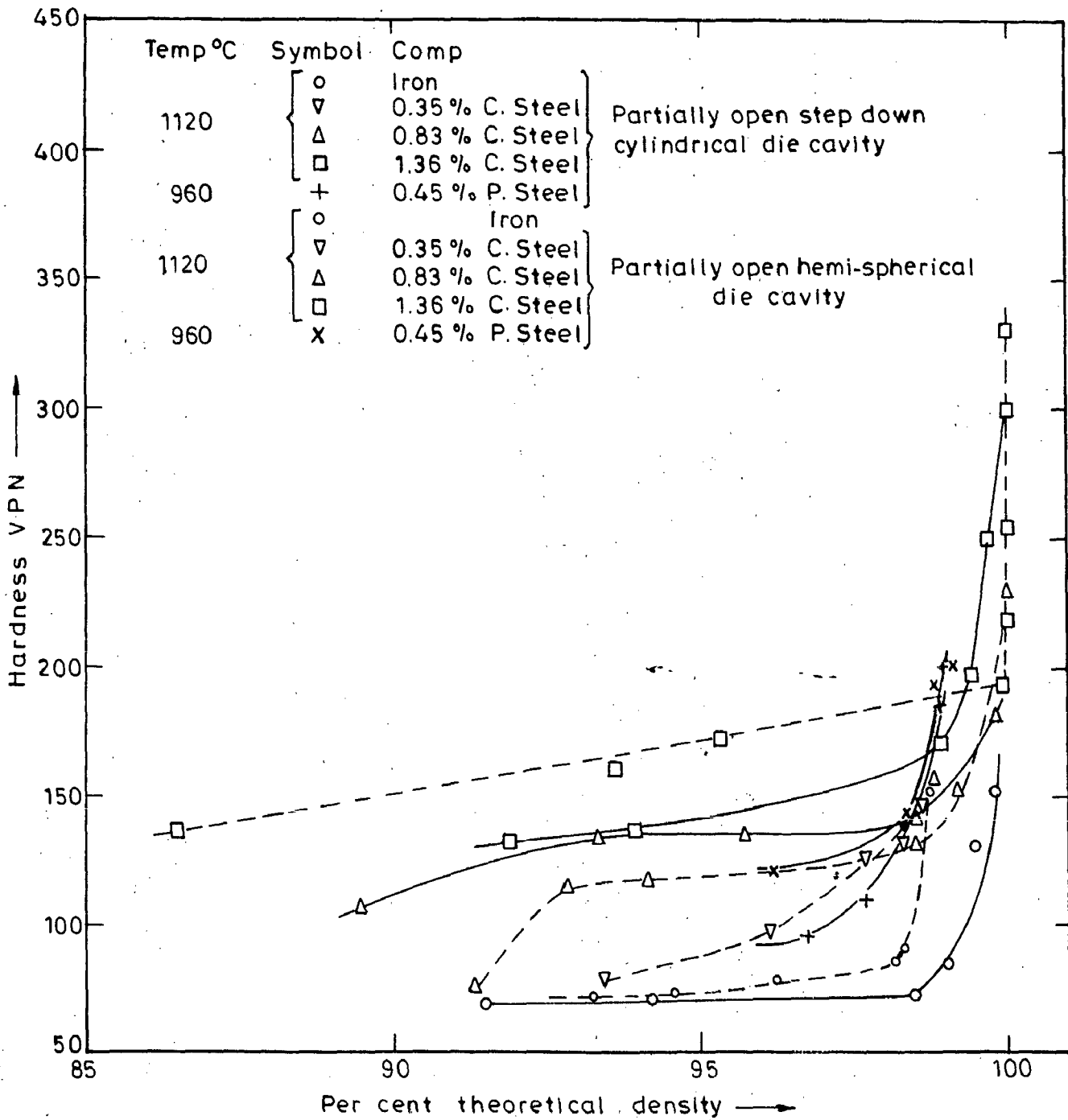


Fig.6.78-Plot of hardness versus per cent theoretical density of partially open die forgings for all compositions of steel

Fig. 6.79 - Pore Morphology Iron Powder Sintered Preform (H/D=1.18) Forged Through Hemi-Spherical Die Cavity at 1120°C

- |  |   |
|--|---|
| (a) Pore flattening in the horizontal direction.<br>50X; enlarged 6 times.   | (b) Pore flattening in the horizontal direction with a little bend.<br>50X; enlarged 6 times. |
| (c) Pore flattening but bending visible.<br>50X; enlarged 6 times.           | (d) Centre from the top - Bending of pores in the upward direction.<br>50X; enlarged 6 times. |
| (e) Pores - showing the tendency to flow downward.<br>50X; enlarged 6 times. | (f) Pore - Direction completely changed.<br>50X ; enlarged 6 times.                           |
| (g) Pore direction becomes vertical.<br>50X ; enlarged 6 times.              |   |

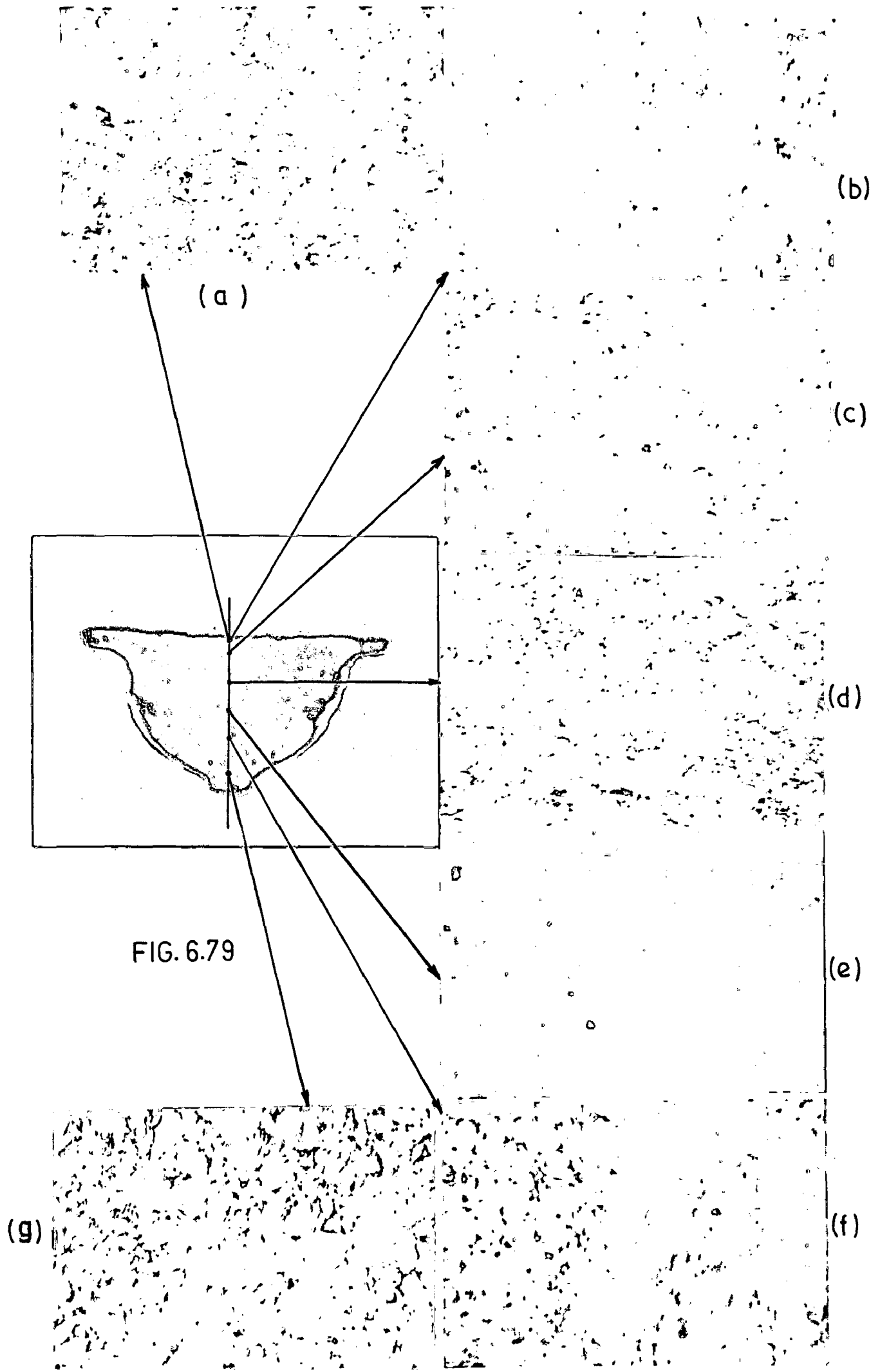


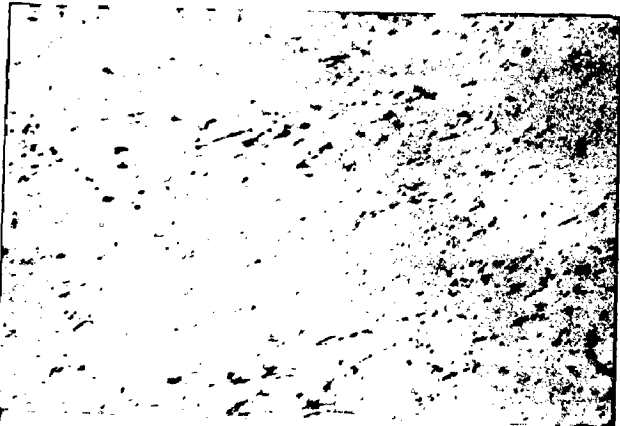
FIG. 6.79

Fig. 6.79 - Pore Morphology - Iron Powder Sintered  
 Preform ( $H/D = 1.18$ ) Forged Through the Hemi-Spherical  
 Die Cavity at  $1120^{\circ}\text{C}$

- (h) Flattened pores direction is inclined a little to the central axis of the component.  
 50X; enlarged 6 times.
- (i) Porosity exceptionally low but flattening in the horizontal direction.  
 50X ; enlarged 6 times.
- (j) Angle of porosity changes inclination towards the central axis.  
 50X ; enlarged 6 times.
- (k) Pores showing well defined directionality.  
 50X ; enlarged 6 times.
- (l) Porosity changes direction-takes the bend as the die geometry.  
 50X ; enlarged 6 times.
- (m) Grain flow visible.  
 50X; enlarged 6 times.  
 Etchant : 2 % nital.
- (n) Grain flow explicitly visible.  
 100X; enlarged 6 times .  
 Etchant : 2 % nital.



(h)



(i)



(j)

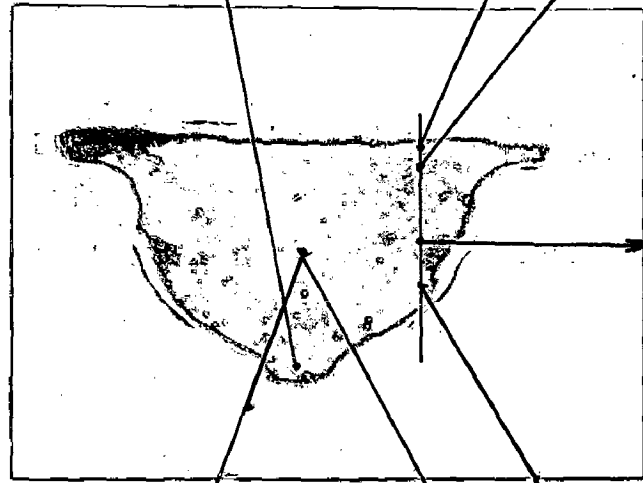
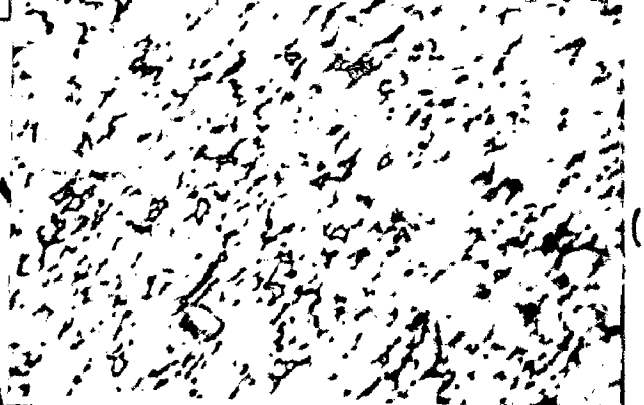


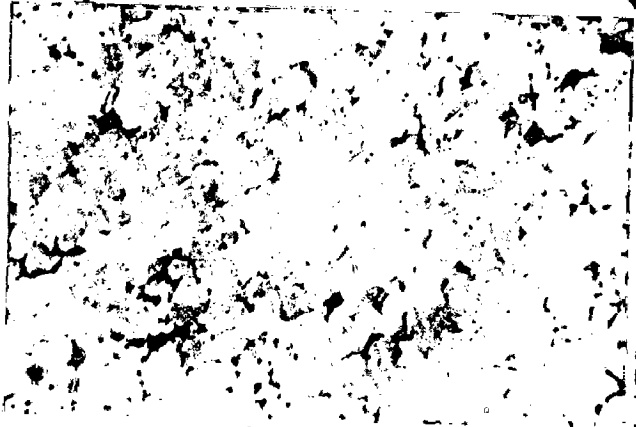
FIG. 6.79



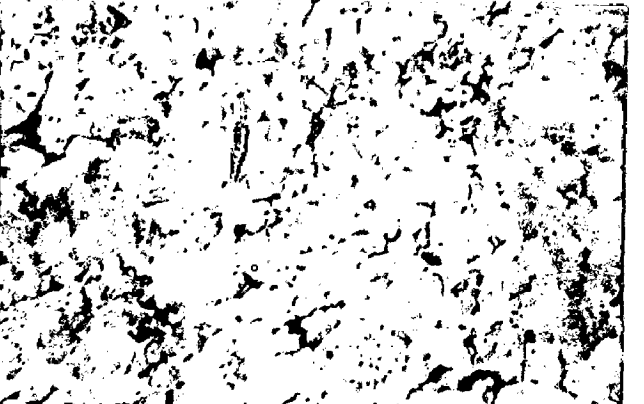
(k)



(l)



(n)



(m)



Fig. 6.80- Showing Flow of Pearlite and Ferrite In 0.35 % Carbon Steel Sintered Powder Preform (H/D = 1.18), Forged Through the Hemi-Spherical Die Cavity at 1120°C.

Fig. 6.81 - Pore Morphology - 0.83 % Carbon Steel Sintered Powder Preform (H/D = 1.18), Forged Through the Hemi-Spherical Die Cavity at 1120°C. At the Centre of the Specimen 100X ; enlarged 6 times.

Fig. 6.82 - 1.36 % Carbon Steel Sintered Powder Preform (H/D = 1.18), Forged Through the Hemi-Spherical Die Cavity at 1120°C. At the Centre of the Specimen 100X; enlarged 6 times.

FIG. 6.80



FIG. 6.81

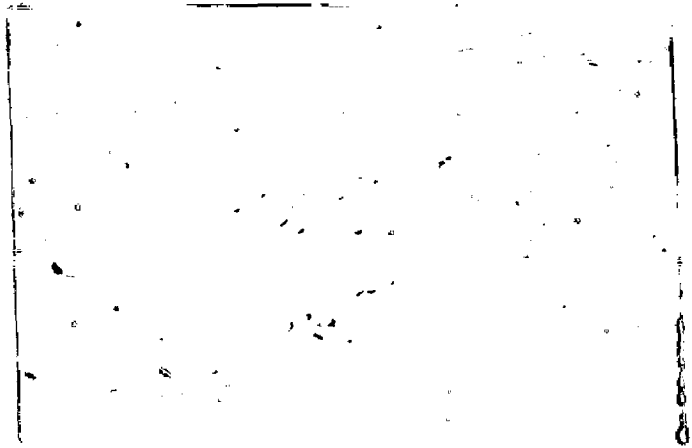


FIG. 6.82

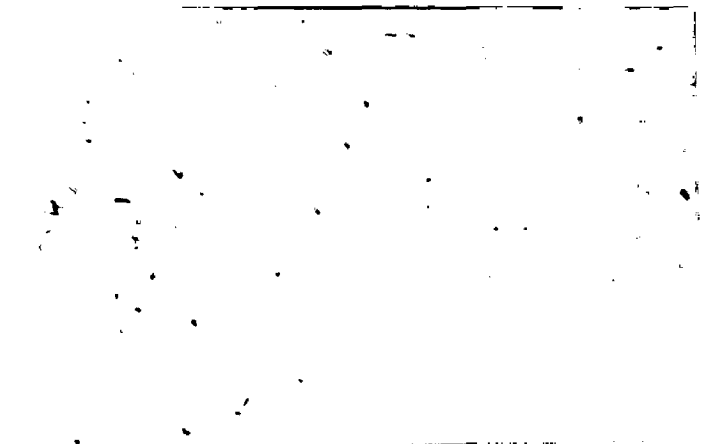


Fig. 6.83 - Microstructure - 0.45 % Phosphorous Sintered Powder Preform (H/D=1.18) Forged Through Hemi-Spherical Die Cavity at 960°C

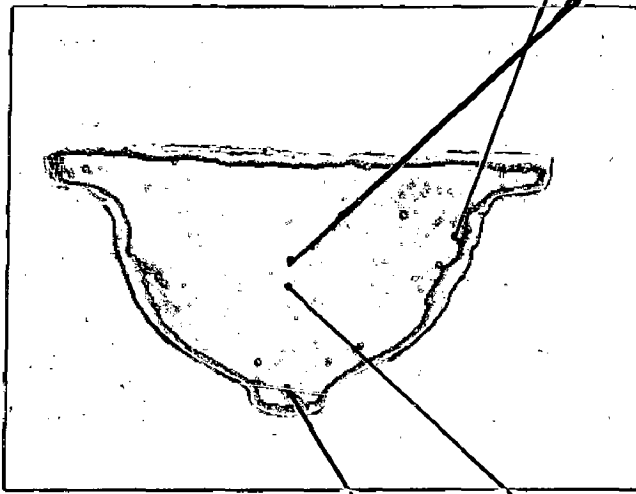
- |  |  |
|--|--|
| (a) Porosity at the edge - thin layer different than pure iron. 100X; enlarged 6 times.                                      | (b) Pin point porosity at the centre of the specimen. 100 X ; enlarged 6 times.                                |
| (c) Deformed grain boundaries, fine in nature with localized large size pores. 100 X; enlarged 6 times. Etchant : 1 % nital. | (d) Deformed fine grain boundaries. Large size pores are scanty. 100X ; enlarged 6 times. Etchant : 1 % nital. |



(a)



(b)



(c)



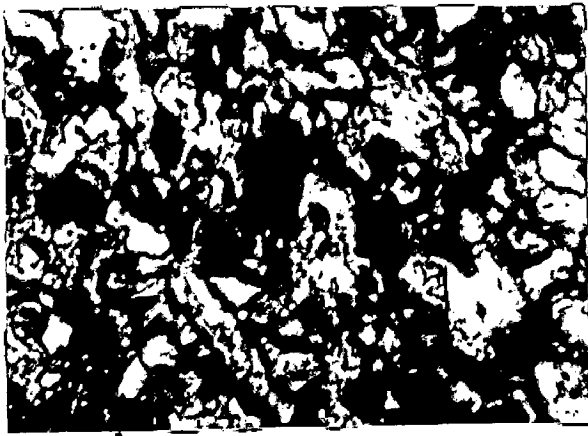
(d)

FIG. 6.83

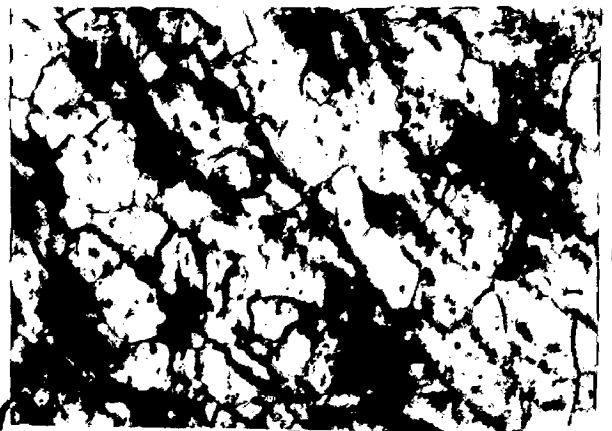
Fig. 6.84 - Microstructures Showing Different Nature at Different Location of the Forged Component of Pure Iron Through Partially Open Step Down Cylindrical Die Cavity at 1120°C

Etchant : 2 % nital.

- |   |   |
|---|---|
| (a) Microstructure in dead metal zone dark region - showing undeformed pores and absence of grain flow. 100X; enlarged 6 times. | (b) Microstructure showing the transition boundary of DMZ and the deformed region sense of recrystallization. 100X; enlarged 6 times. |
| (c) Microstructure shows pores in the form of streaks associated with coarse grains. 100X ; enlarged 6 times.                   | (d) Medium size grains pores still in the form of streaks. 100 X; enlarged 6 times.   |
| (e) Recrystallized fine grains with low order of porosity. 100X; enlarged 6 times.  | (f) Close to third confinement rounded pores with recrystallize equiaxed grains. 100X; enlarged 6 times.                              |
| (g) Extensive pore flattening close to the first confinement. 100X; enlarged 6 times.   |   |



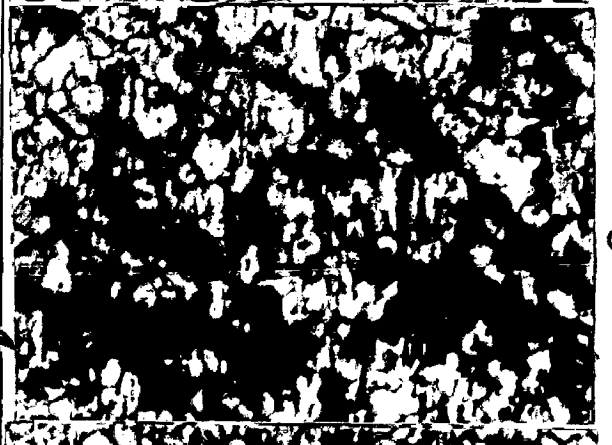
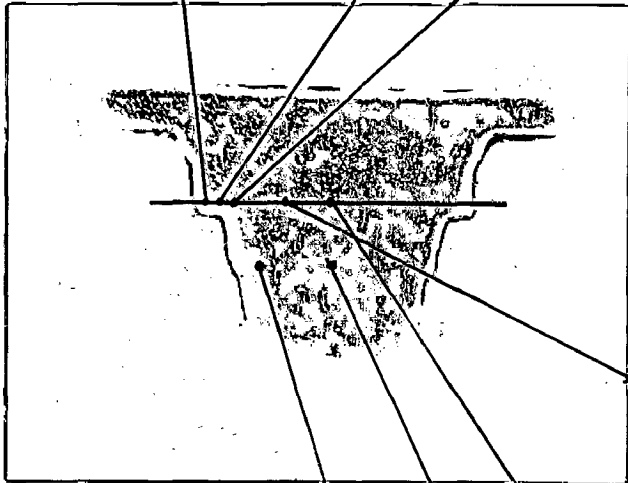
(a)



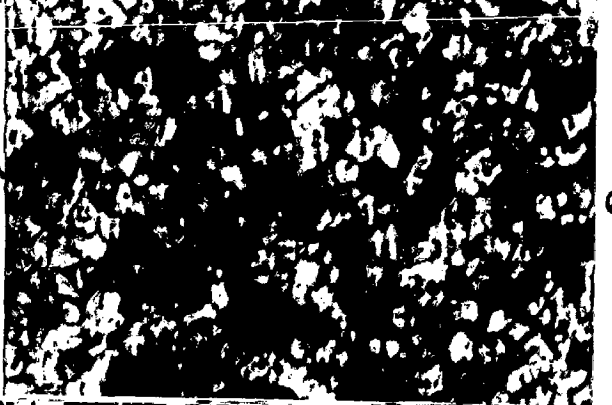
b



c



d



e



(g)

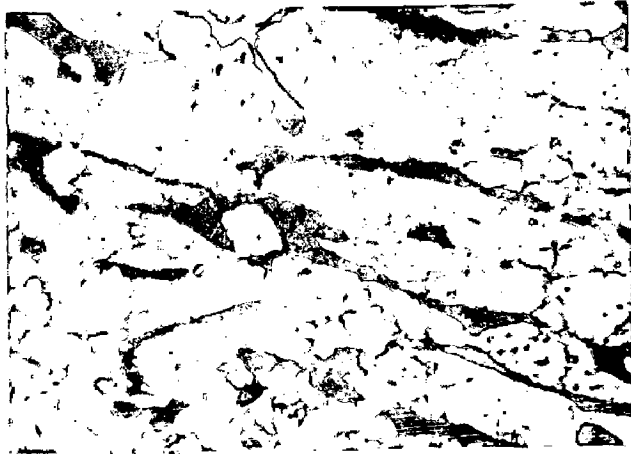


f

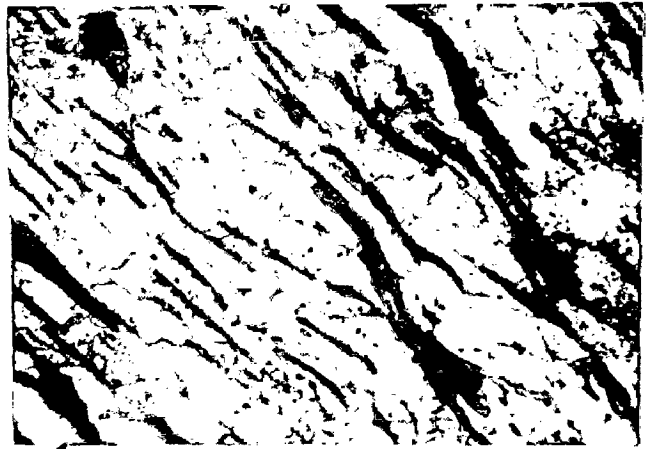
FIG. 6.84

Fig. 6.85 - Microstructure Revealing Different Modes of Pore Flattening and Grain Deformation at Different Locations of a Component Forged Through Partially Open Step Down Cylindrical Die Cavity at 1120°C  
Etchant : 2 % nital

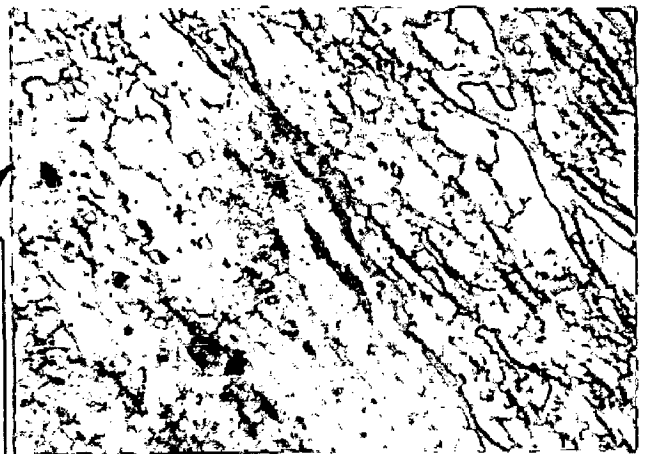
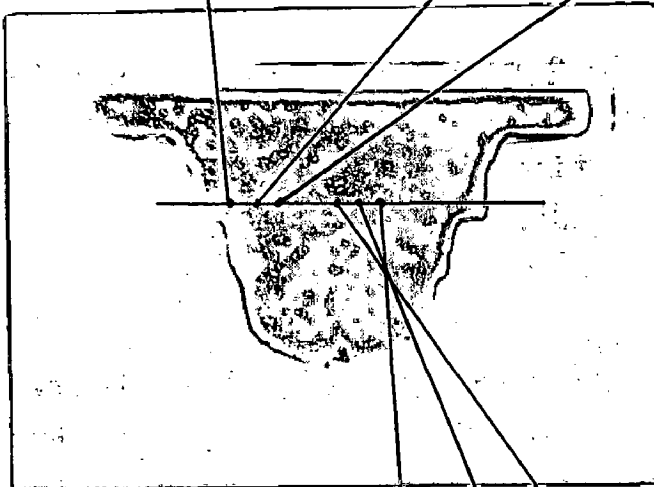
- |  |   |
|--|---|
| (a) Heavy pore flattening with fine grain size showing effect of recrystallization. 100X ; enlarged 6 times.   | (b) Heavy pore flattening with directionality. Grain elongation is clearly seen. 100X ; enlarged 6 times. |
| (c) Microstructure showing half region consisting of extensive pore and grain flattening. Other half showing no evidence of pore flattening but grain flattening is visible. 100 X ; enlarged 6 times. | (d) Fine recrystallized grains with practically no porosity. 100X ; enlarged 6 times.                     |
| (e) Uniform, recrystallized grains with little porosity. 100X; enlarged 6 times.   | (f) Grain coarsening associated with low order of porosity. 100 X ; enlarged 6 times.                     |



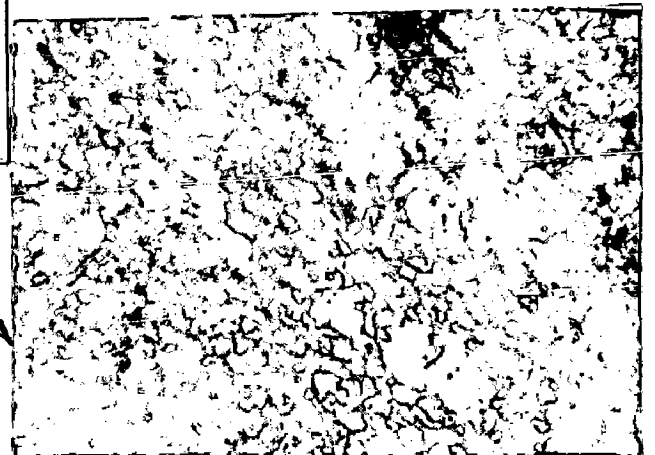
(a)



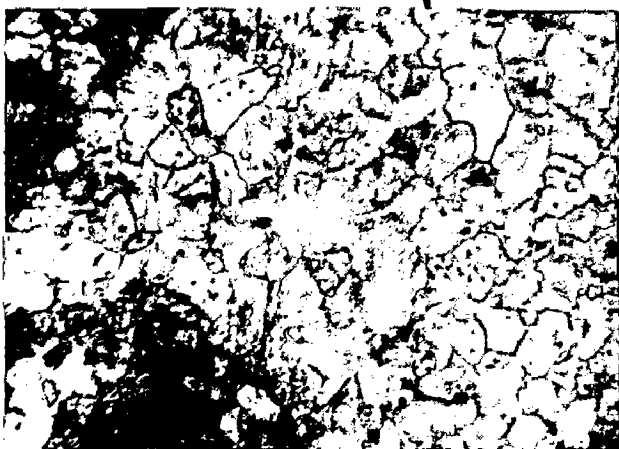
(b)



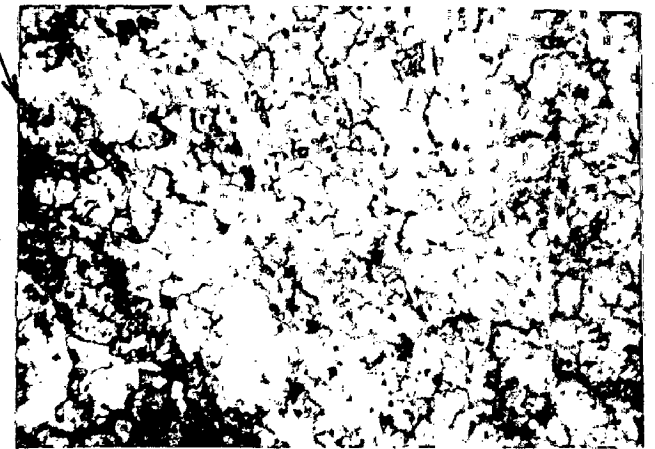
(c)



(d)



(f)



(e)

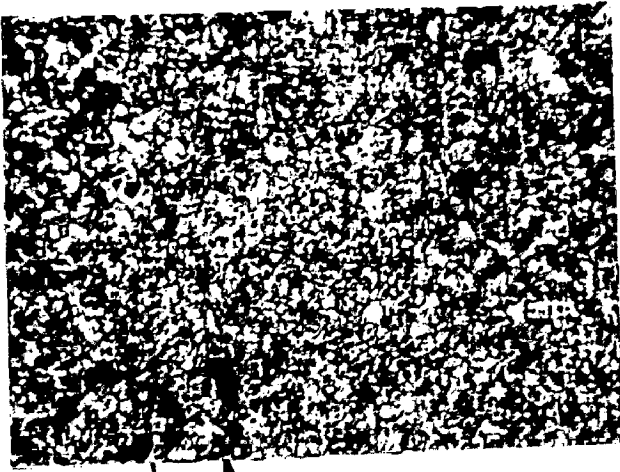
FIG. 6.85



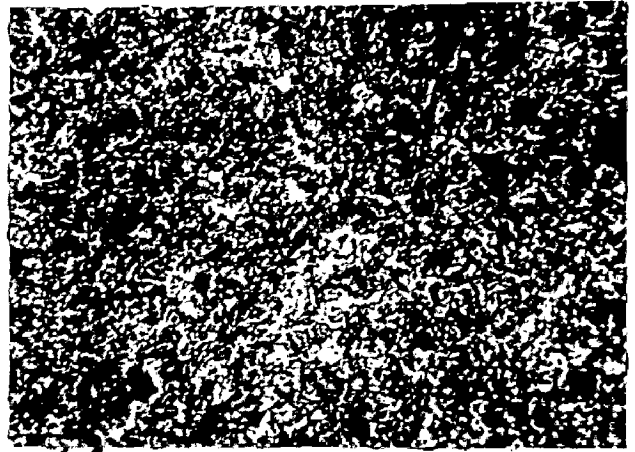
Fig. 6.85 - Microstructure Revealing Different Modes of Pore Flattening and Grain Deformation at Different Locations of a Component Forged Through Partially Open Step Down Cylindrical Die Cavity at 1120°C

Etchant : 2 % nital

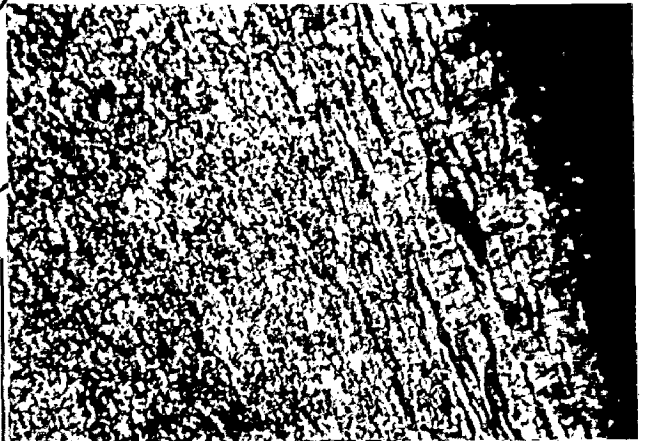
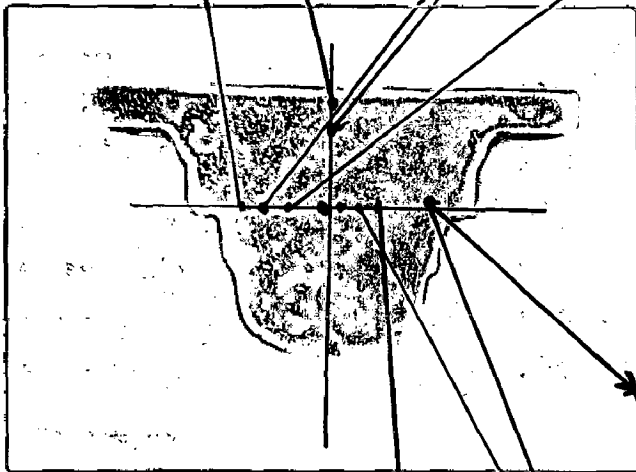
- |   |  |
|---|--|
| <p>(g) Completely recrystallized structure with a fine grain size.<br/>100X ; enlarged 6 times.</p> | <p>(h) Pearlitic structure is seen with no sign of grain identity<br/>100X; enlarged 6 times.</p>      |
| <p>(i) Elongated pores with well defined directionality<br/>100X ; enlarged.</p>                    | <p>(j) One side showing low order of porosity compared to other side.<br/>100X ; enlarged 6 times.</p> |
| <p>(k) Shows grain flow explicitly.<br/>100X ; enlarged 6 times.</p>                                | <p>(l) Equiaxed grains are seen.<br/>100X ; enlarged 6 times.</p>                                      |



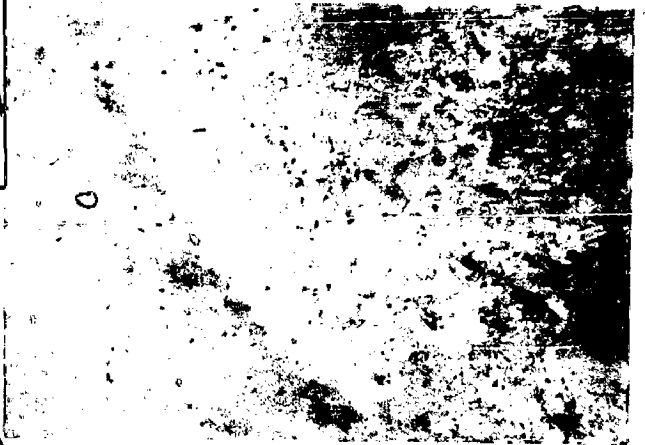
(g)



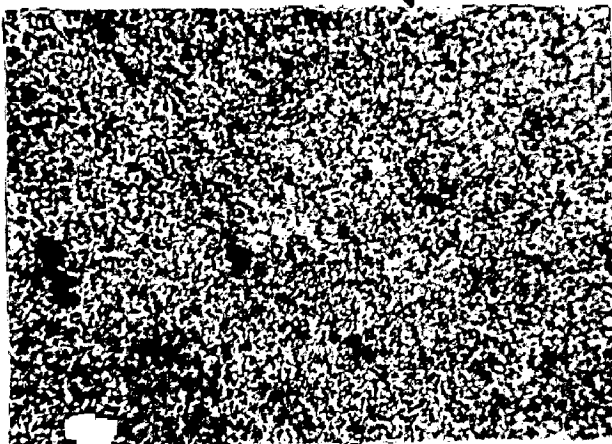
(h)



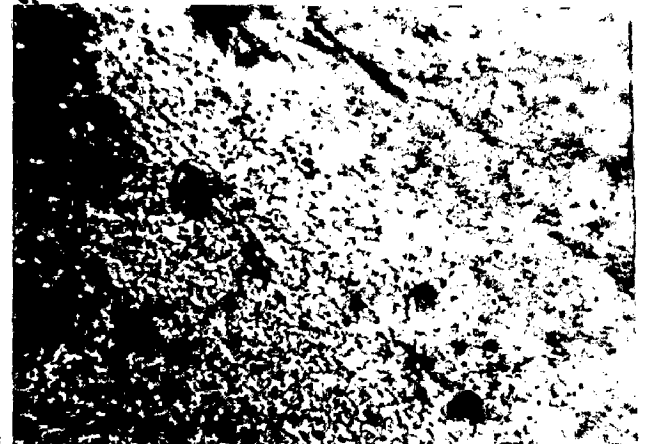
(i)



(j)



(l)



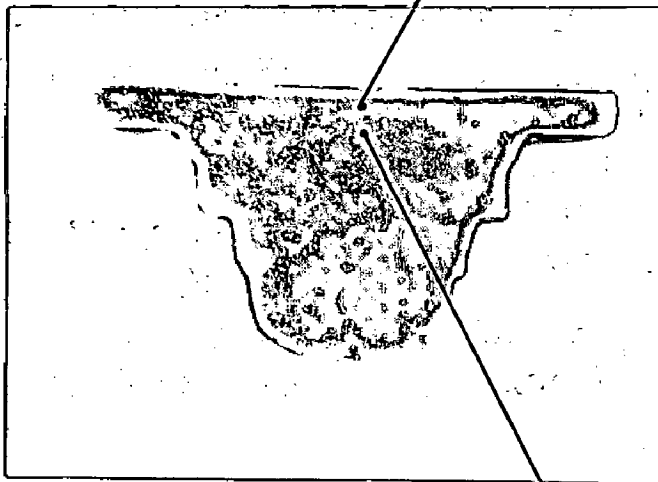
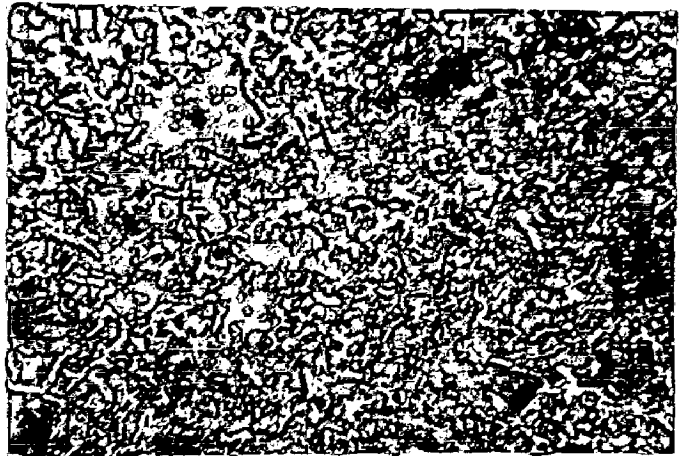
(k)

FIG. 6.85

Fig. 6.86 - Microstructures of 0.83 % Carbon Steel Sintered Preform Deformed at 1120°C Through Partially Open Step Down Cylindrical Die Cavity  
Etchant : 2 % nital

- (a) Fine grain structure with low level of porosity. Completely pearlitic structure is seen.  
100X ; enlarged 6 times.
  
- (b) Finer grain structure than 6.86(a) with scanty porosity. Completely pearlitic structure showing evidence of cementite network.  
100X ; enlarged 6 times.

(a)



(b)

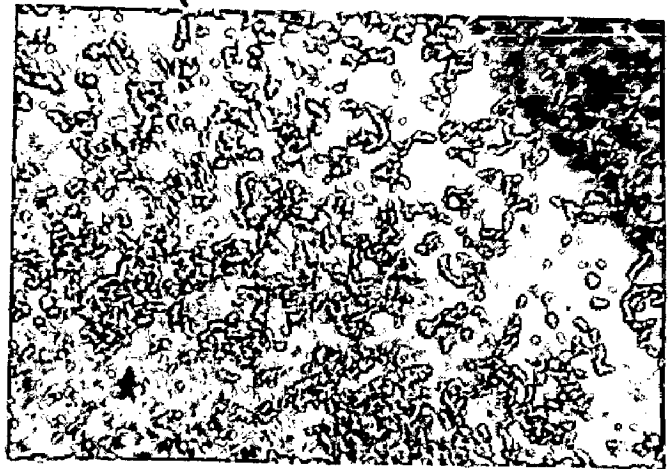
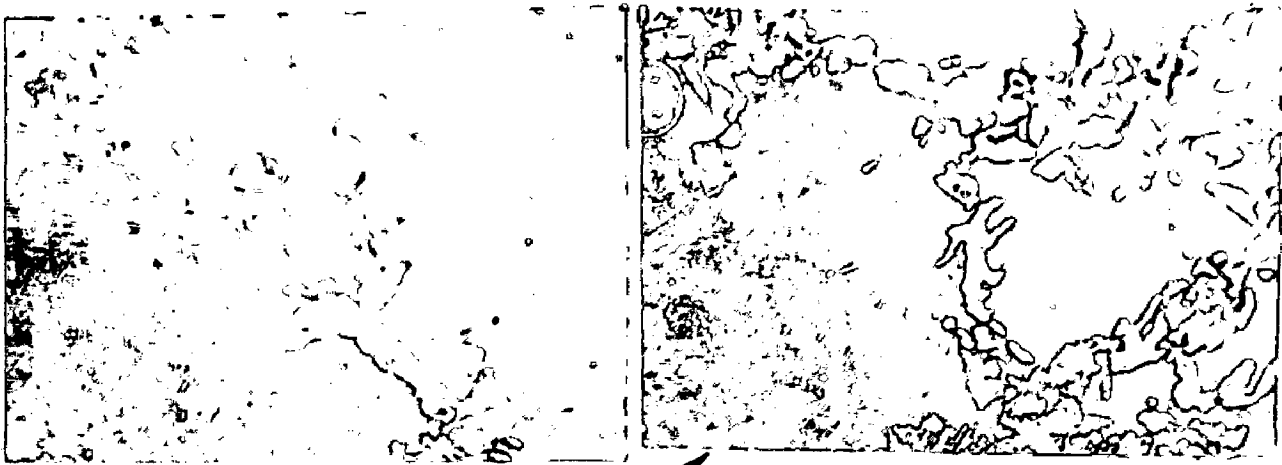


FIG. 6.86

Fig. 6.87 - Microstructures Taken on the Second Stage of Confinement in a Component (1.36 % Carbon Steel) Forged Through the Partially Open Step Down Cylindrical Die at 1120°C

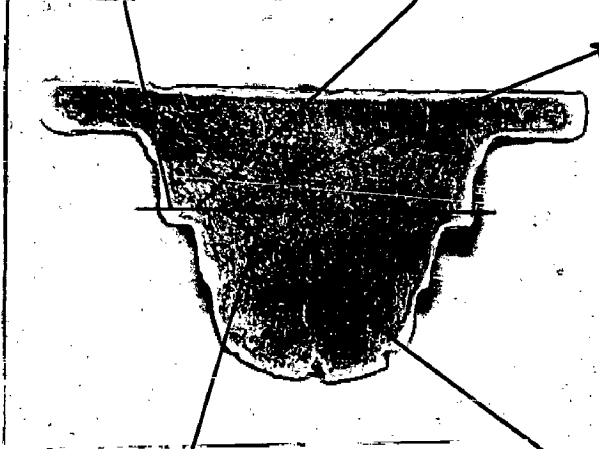
Etchant : 2 % nital

- |   |   |
|---|---|
| (a) Shows decarburized structure.<br>100X ; enlarged 6 times.   | (b) Ferrite network with low pearlitic structure.<br>100X ; enlarged 6 times. |
| (c) Fragmented ferrite 15 - 20 % rest being pearlitic structure.<br>100X ; enlarged 6 times.                                | (d) Completely pearlitic structure.<br>100X ; enlarged 6 times.               |
| (e) Coarse cementite network with a very fine grain size. Other half shows pearlitic structure.<br>100X ; enlarged 6 times. |   |

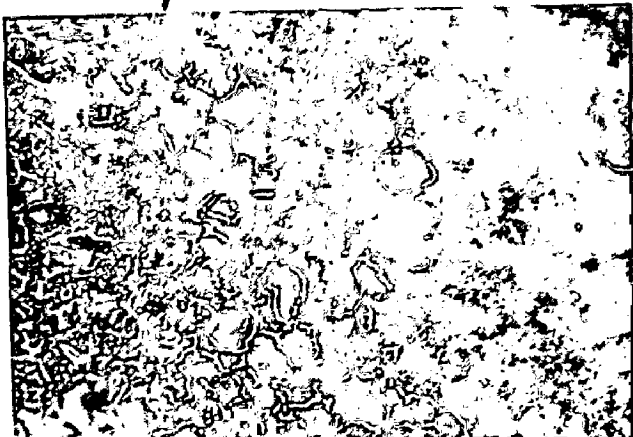


(a)

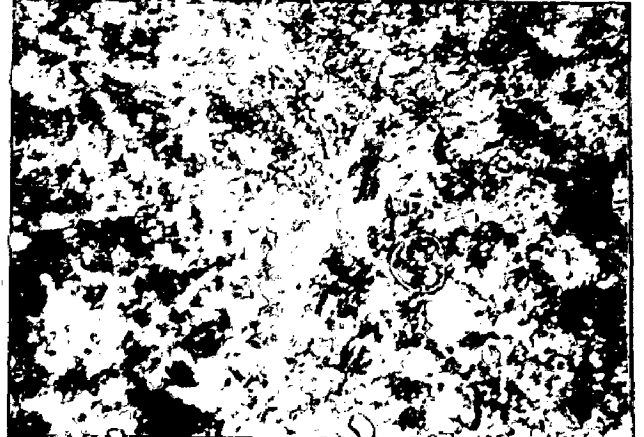
(b)



(c)



(e)



(d)

FIG. 6.87

Fig. 6.87 - Microstructure Taken at the Second Stage of Confinement in a Component (1.36 % Carbon Steel) Forged Through Partially Open Step Down Cylindrical Die Cavity at 1120°C

Etchant : 2 % nital

(f) Coarse grains of cementite with coarse network. 100X ; enlarged 6 times.

(g) Coarse grained structure - cementite plates entering into the grains. 100 X ; enlarged 6 times.

(h) Shows thin network of cementite 100X; enlarged 6 times.

(i) Shows increase in the cementite plates.

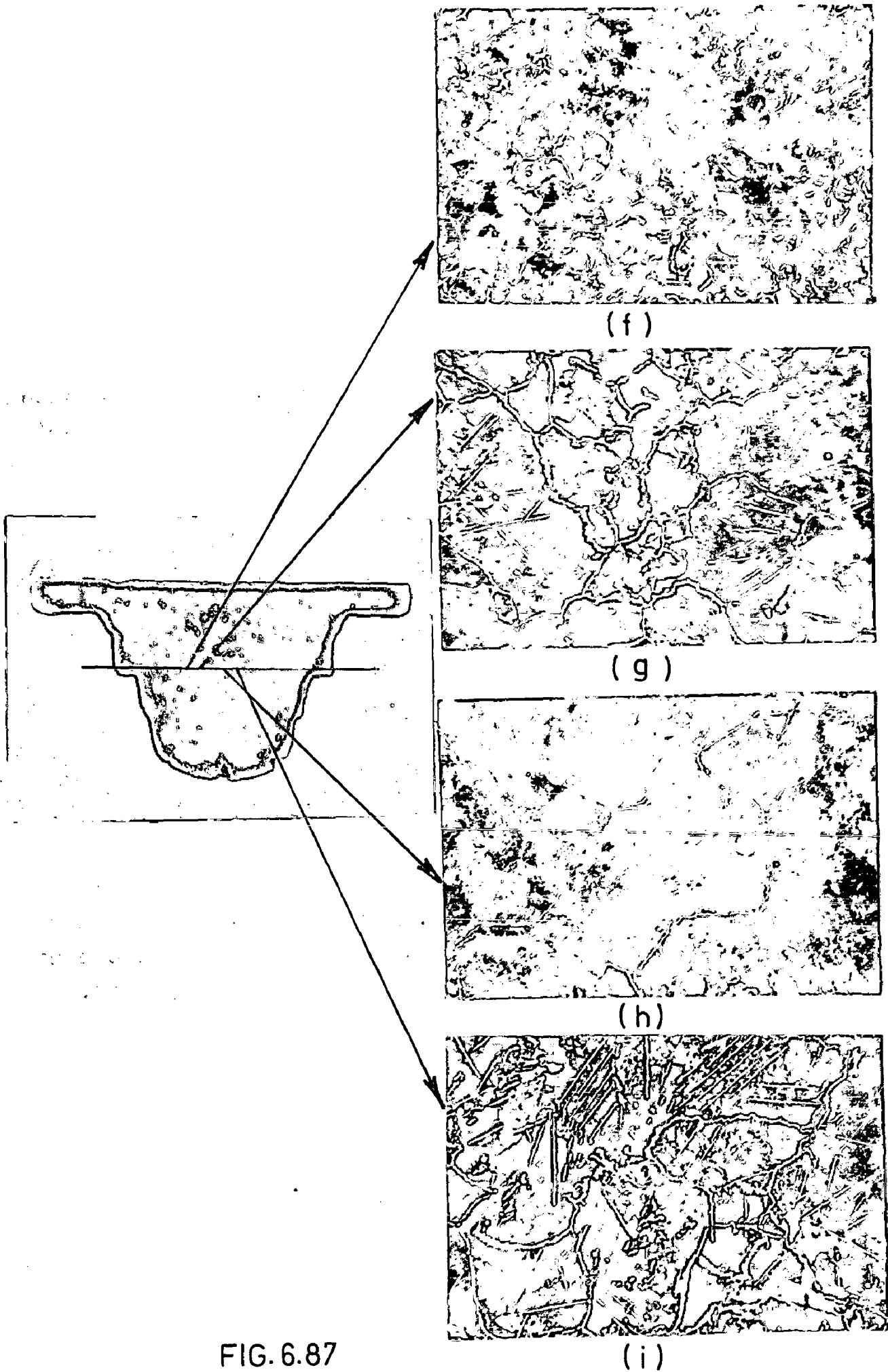
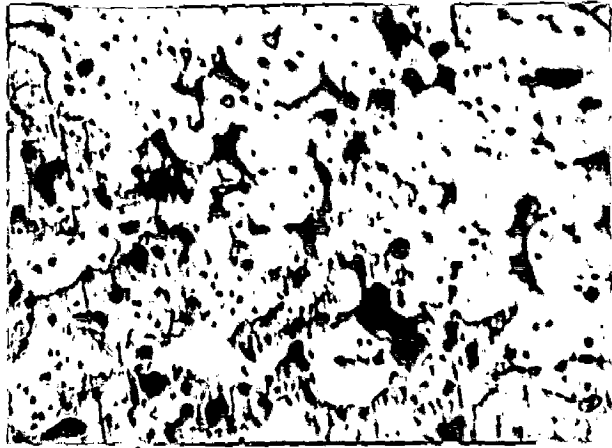


FIG. 6.87

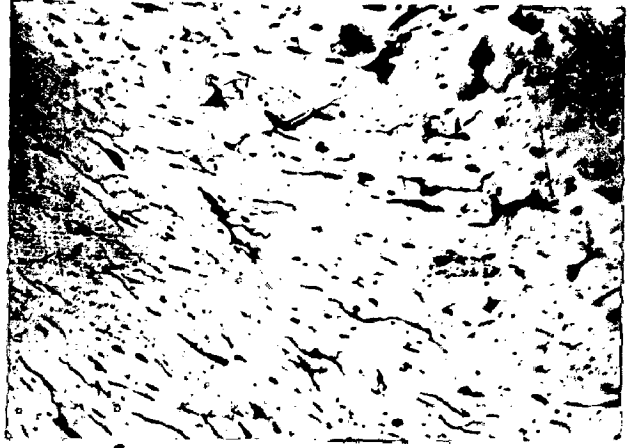


Fig. 6.88 - Microstructures Showing Pore Morphology and Structural Details at Different Locations of the Specimen Prepared from the Component Forged Through Partially Open Step Down Cylindrical Die Cavity at  $1120^{\circ}\text{C}$  for 0.45 % Phosphorus Steel

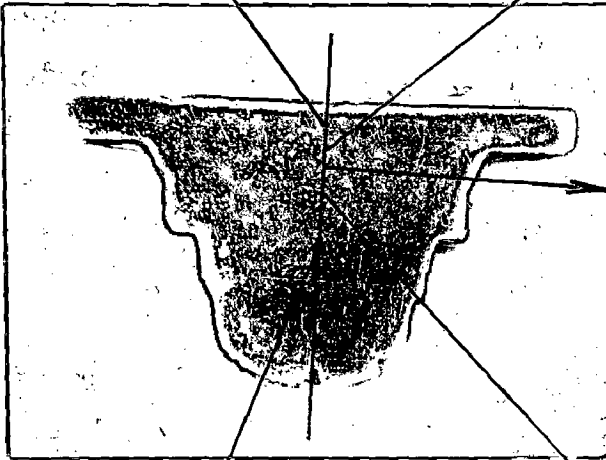
- (a) Pore morphology in the dead metal zone. 100X ; enlarged 6 times.
- (b) Pores showing very high order of collapsibility. 100 X ; enlarged 6 times.
- (c) Reduced size of the pore in length and slight increase in width. 100X ; enlarged 6 times.
- (d) Length of the pore still reduced compared to (c) and width further increased. 100X ; enlarged 6 times.
- (e) Pores lack the sense of directionality. 100X ; enlarged 6 times.



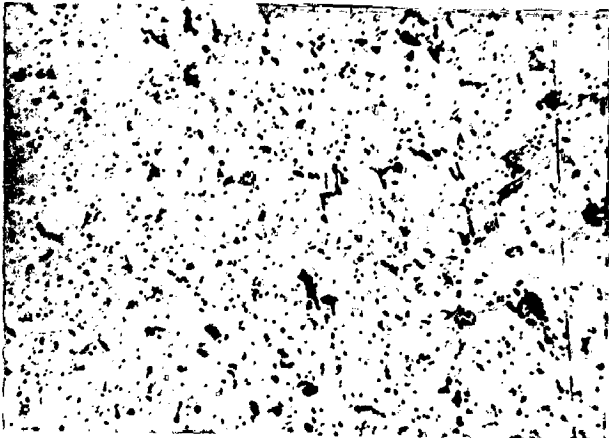
(a)



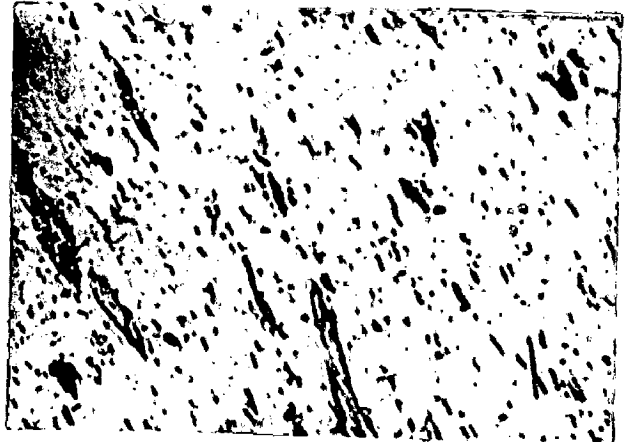
(b)



(c)



(e)



(d)

FIG. 6.88

Fig. 6.88 - Microstructures showing Pore Morphology and Structural Details at Different Locations of the Specimen Prepared from the Component Forged Through Partially Open Step Down Cylindrical Die Cavity at 1120°C for 0.45 % Phosphorus Steel

Etchant : 2 % nital

- |  |  |
|--|--|
| (f) Pore flow and grain flow is clearly seen. 100X ; enlarged 6 times.                                       | (g) Pore collapsibility is seen explicitly. 100X ; enlarged 6 times.                       |
| (h) Thin grain boundaries pore collapsibility in a different form than (f) and (g). 100X ; enlarged 6 times. | (i) Pore size extensively reduced and its amount too, is reduced. 100X ; enlarged 6 times. |
| (j) Shows heavily deformed porosity. Very thin, but, explicit grain boundaries. 100 X ; enlarged 6 times.    |  |

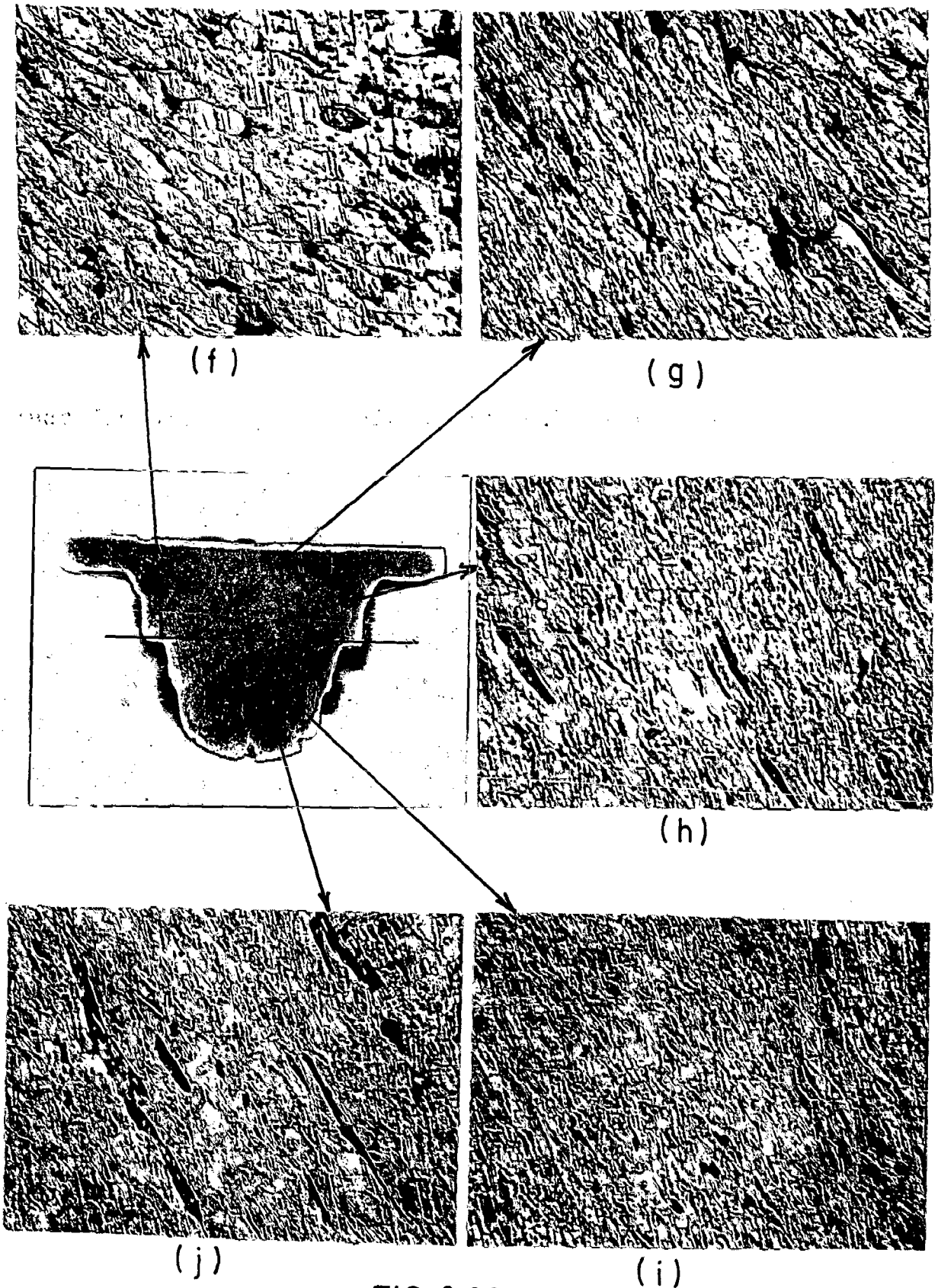


FIG. 6.88

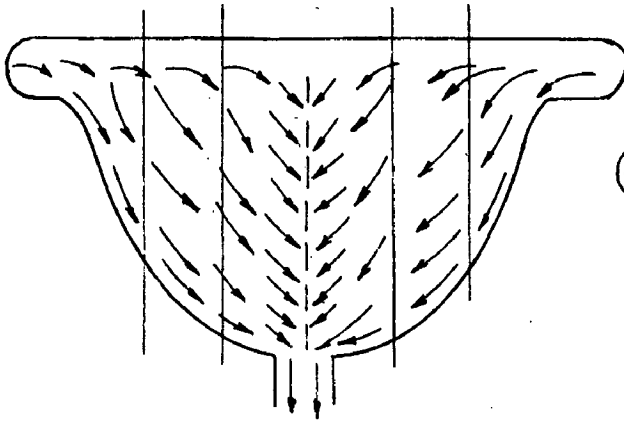


Fig.6.89(a)-Pore shape changes schematic representation as obtained from metallographic structures

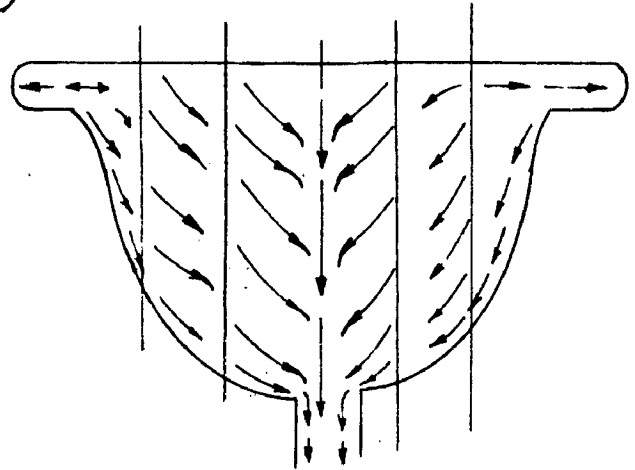


Fig.6.89(b)-Qualitative flow of metal derived from mode of shearing pore

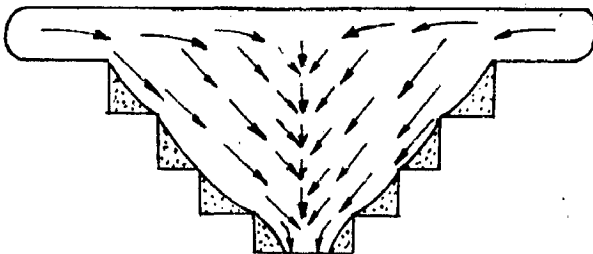

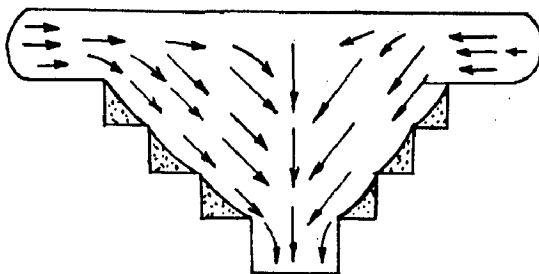


Fig.6.90(a)-Pore shape change-schematic representation as obtained from metallographic structures

 Hydrostatic zone  
or  
Dead metal zone




 Hydrostatic zone  
or  
Dead metal zone

Fig.6.90(b)-Qualitative flow of metal derived from mode of shearing pore.

Fig. 6.91 - Shows the Components Produced Through Partially Open Step Down Cylindrical Die Cavity at  $1120^{\circ}\text{C}$  of Iron and Iron Carbon Alloys

- (a) Iron powder sintered forged component show circumferential cracks as superficial.
- (b) 0.35 % carbon steel shows heavy to moderate circumferential cracking.
- (c) 0.83 % carbon steel shows moderate surface cracks.

FIG. 6.91

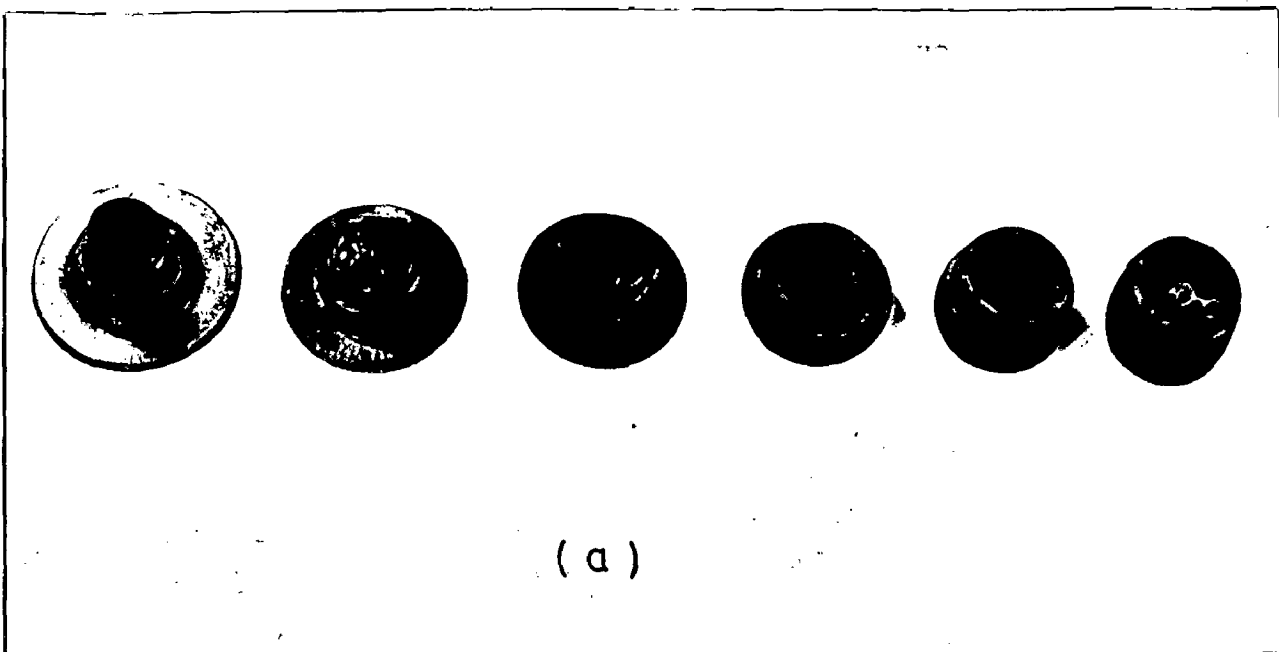
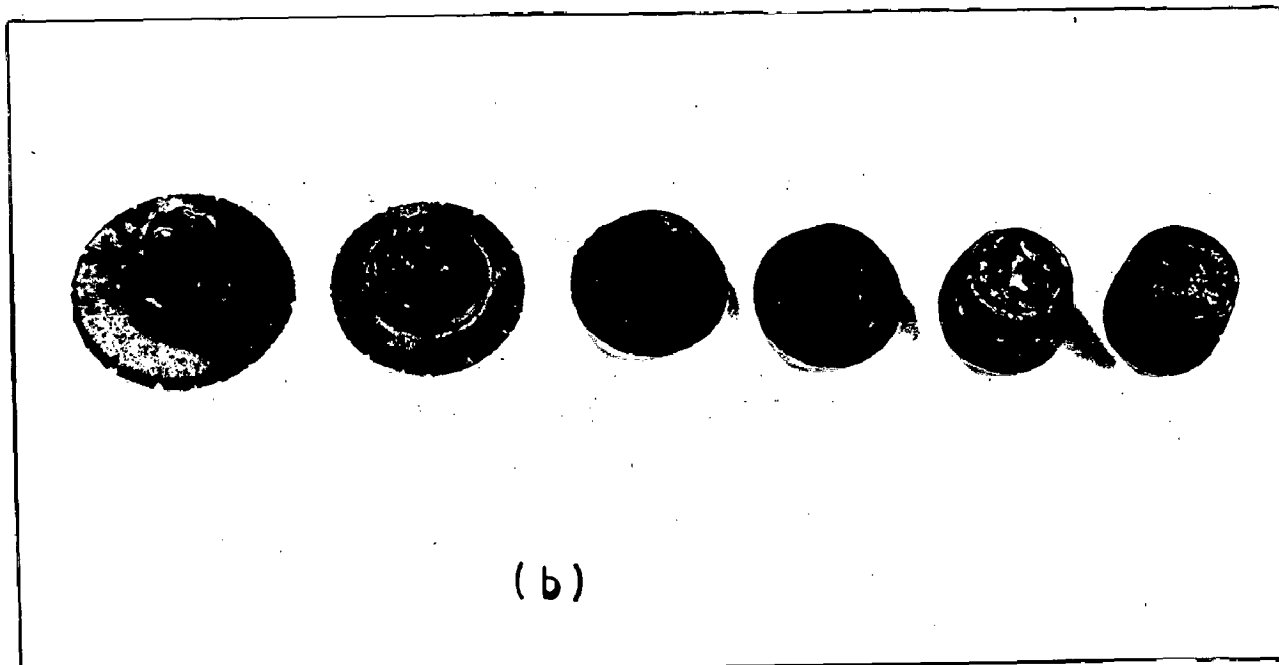
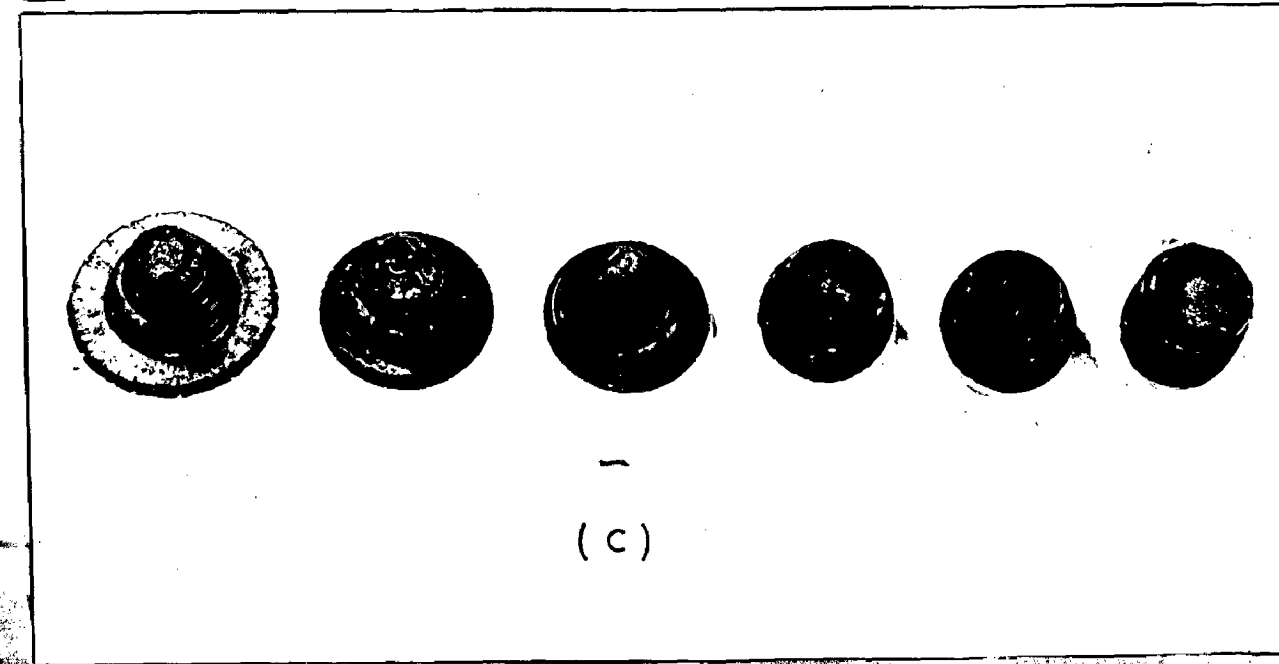


FIG.  
6.91  
(a)



(b)



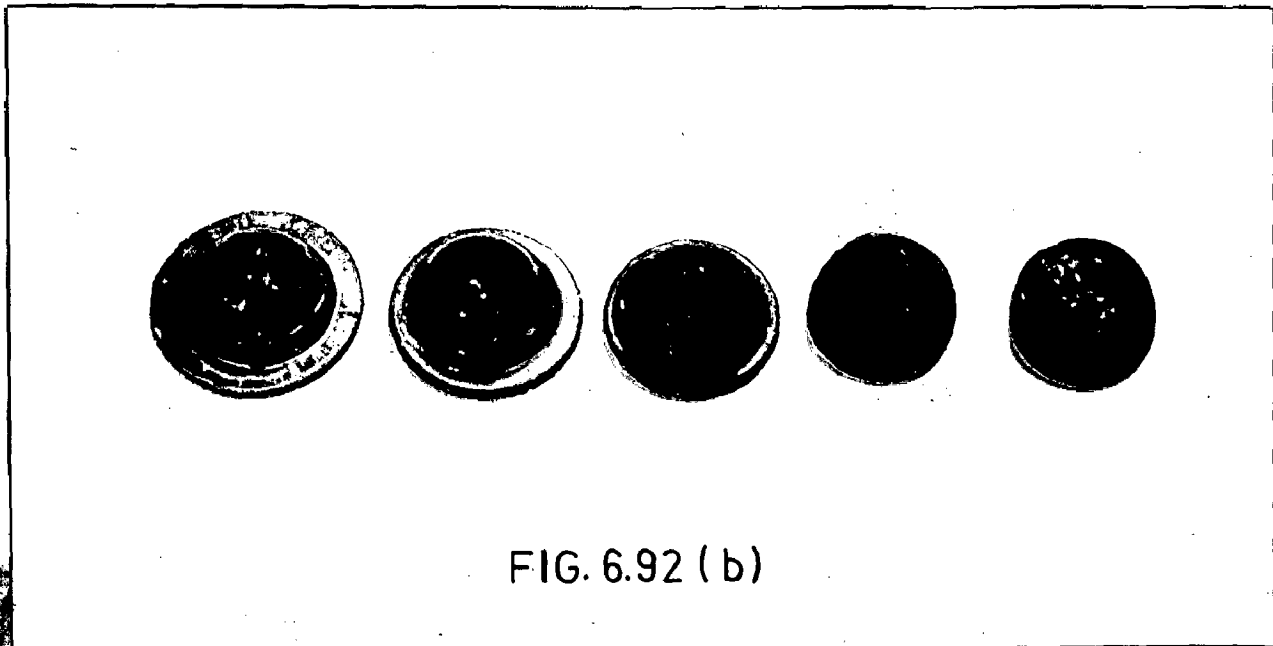
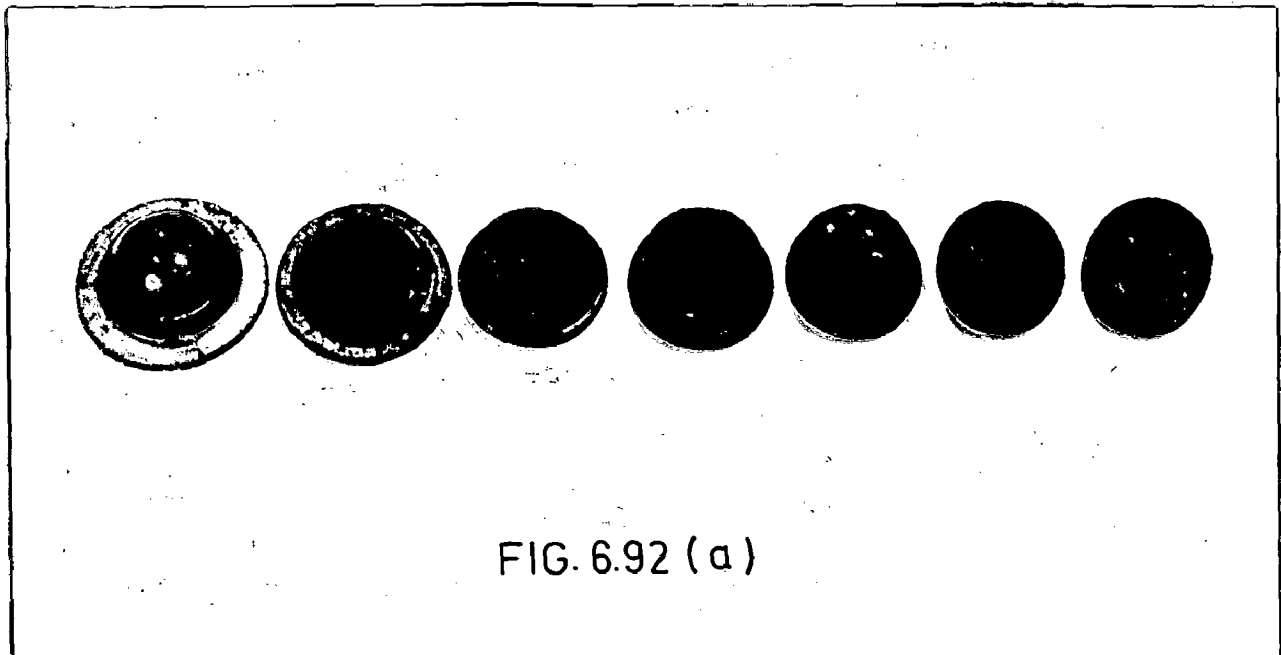
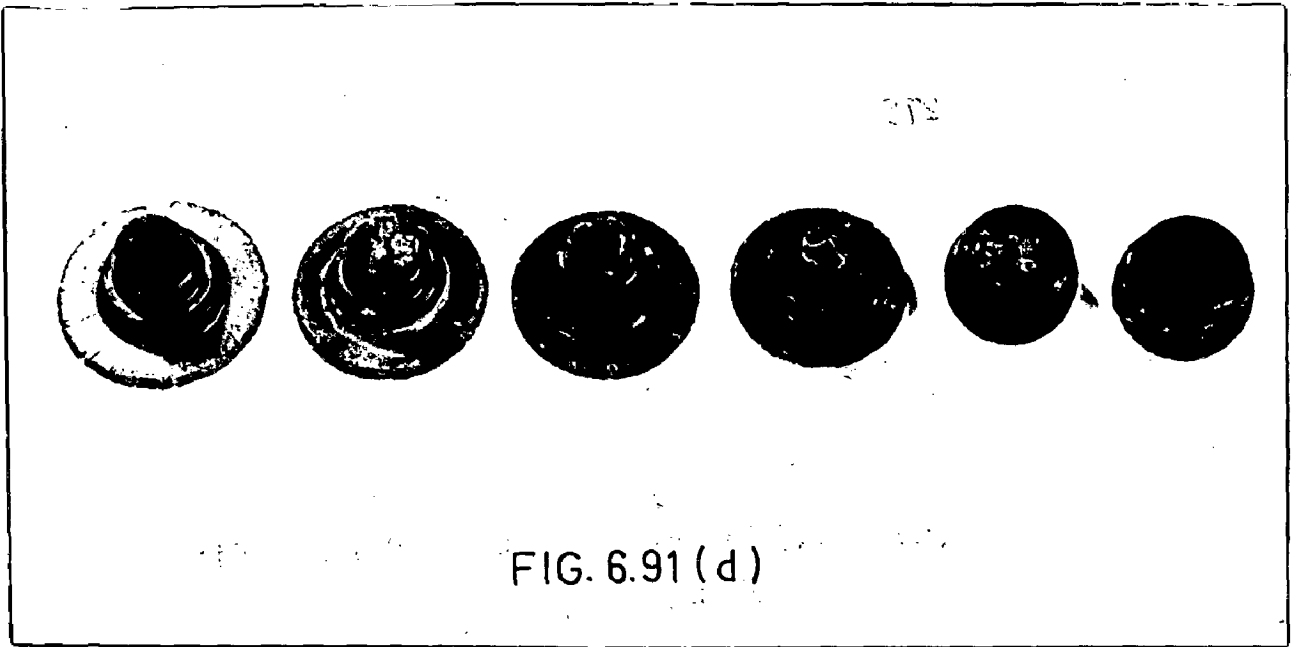
(c)

- (d) 1.36 % carbon steel shows medium to moderate level surface cracks.

Fig. 6.92 - Showing Components Produced Through Partially Open Hemi-Spherical Die Cavity at 1120°C of Iron and Iron Carbon Alloys

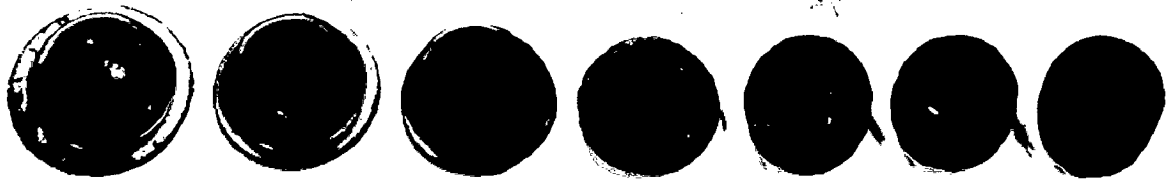
- (a) Superficial circumferential cracks - sintered iron powder preform forging.
- (b) Circumferential cracks are only superficial - sintered 0.35 % carbon alloy preform forged.





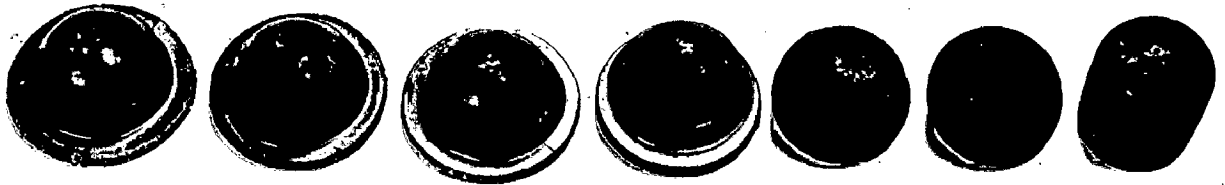
- (c) 0.83 % carbon steel shows only superficial circumferential cracks in the last deformation.
- (d) 1.36 % carbon steel shows medium to moderate circumferential cracks.

Fig. 6.93 - Forged Powder Products in Various Shapes of 0.45 % Phosphorus Steel at 960°C



(c)

FIG. 6.92 (c)



(d)

FIG. 6.92 (d)

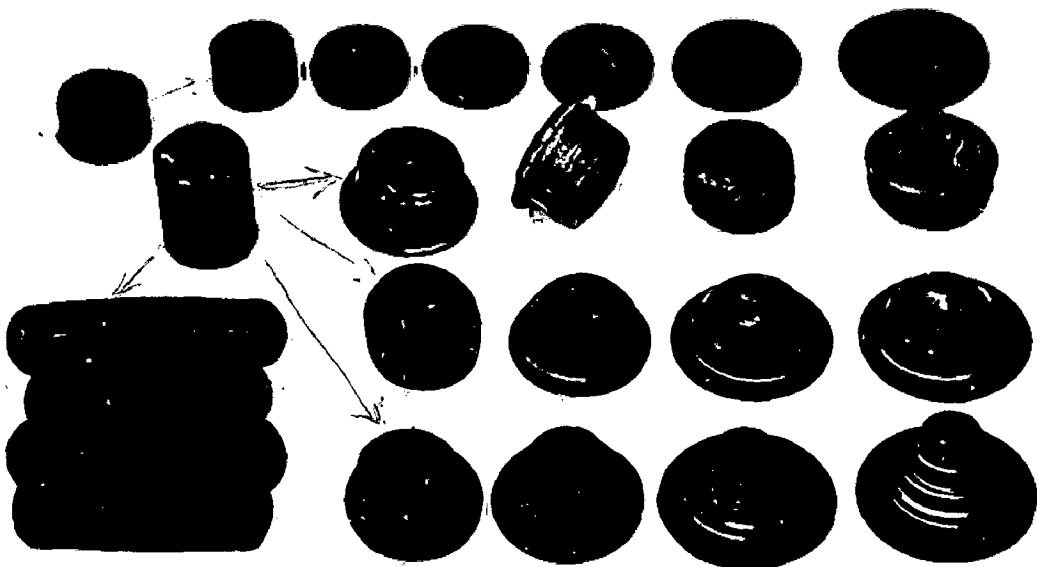


Fig  
6.93

FIG. 6.93

Fig. 6.94 - Microstructure Showing Iron Grains with the Mode of Pore Deformation Through Closed Die Forging at  $1120^{\circ}\text{C}$ .

100X ; enlarged 6 times.

Etchant : 2 % nital.

Fig. 6.95 - Microstructure Showing ~ 50 % Coarse Pearlite and ~ 50 % Ferrite. Forged Component Through Closed Die at  $1120^{\circ}\text{C}$  of 0.35 % Carbon Steel.

100X ; enlarged 6 times.

Etchant : 2 % nital.

Fig. 6.96 - Microstructure Showing Very Fine eutectoid Structure of 0.83 % Carbon Steel Forged Through Closed Die at  $1120^{\circ}\text{C}$

500X ; enlarged 6 times.

Etchant : 2 % nital.

Fig. 6.97 - Microstructure Taken at the Centre of the Polished and Etched Specimen of 1.36 % Carbon Forged Through Closed Die at  $1120^{\circ}\text{C}$ .

Etchant ; 2 % nital.

(a) Cementite network and cementite plates are seen.

100X ; enlarged 6 times.

(b) Same as in (a).

500X ; enlarged 6 times.

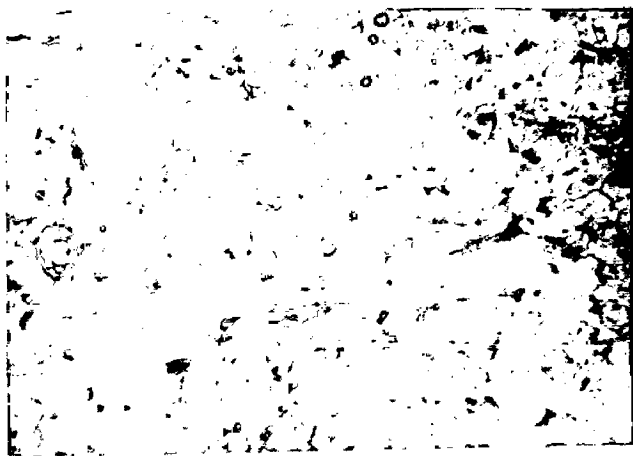


FIG. 6.94



FIG. 6.95

FIG. 6.96

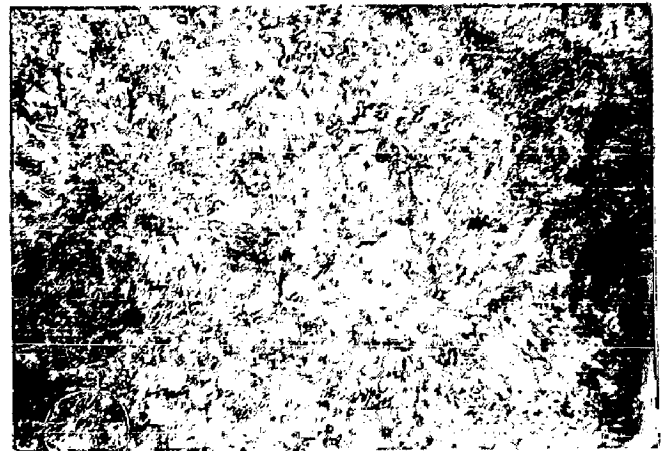
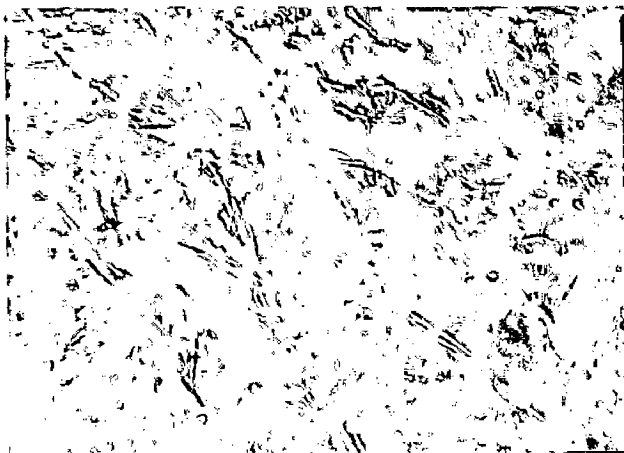


FIG. 6.97



(b)



(a)

Fig. 6.98 - Microstructural Details of Closed Die Forging of 0.45 % Phosphorus Steel at 960°C.

Etchant : 2 % nital

- (a) Pore morphology at the centre showing pore flattening in the diametrical direction.  
100X ; enlarged 6 times.
  
- (b) Polished and etched structure at the centre.  
Revealing fine grain boundaries and associated with pore orientation.  
100X ; enlarged 6 times.
  
- (c) Polished and etched microstructure near to repressing point showing in it porosities inter-connected with grain boundaries.

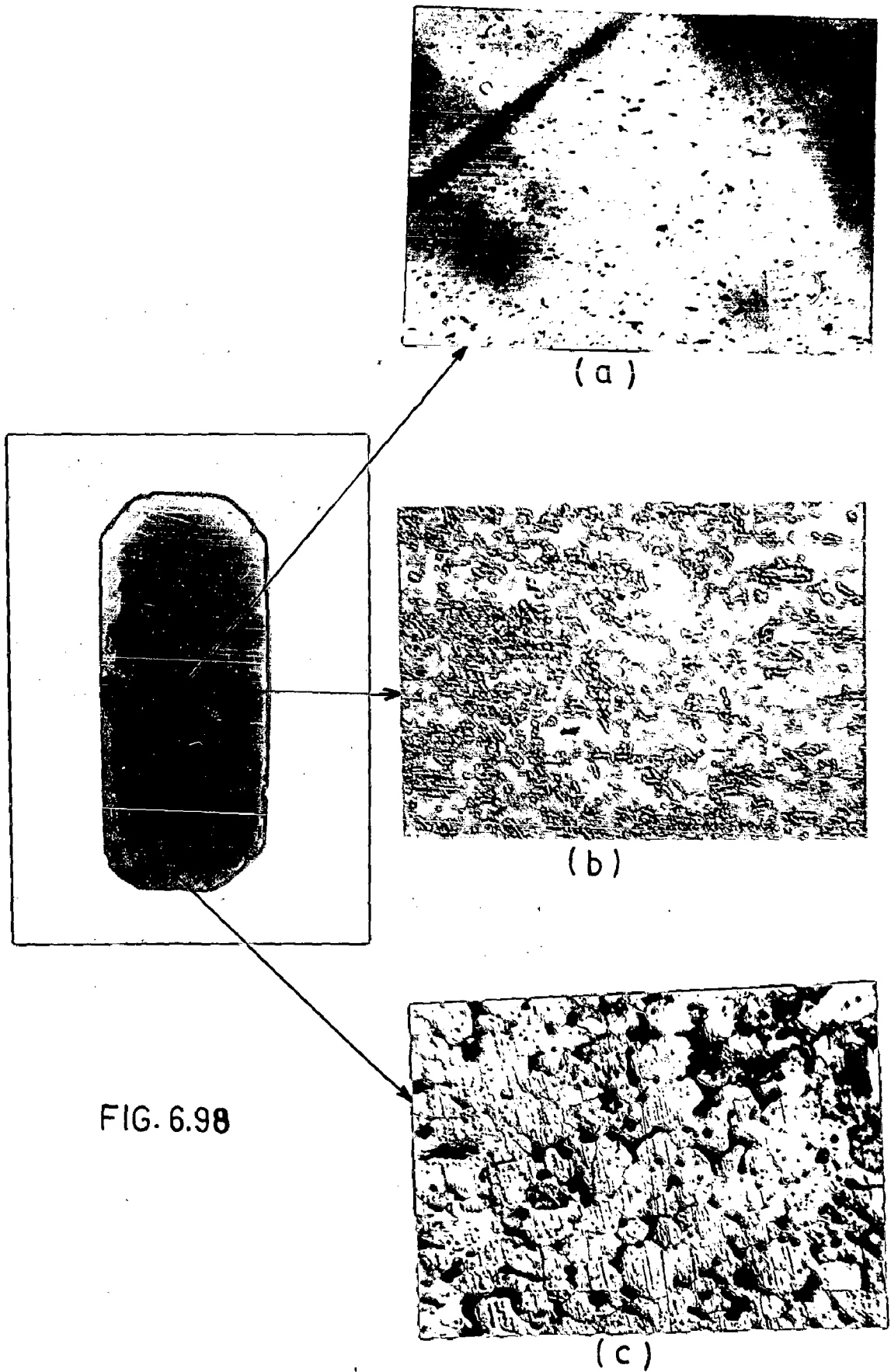


FIG. 6.98

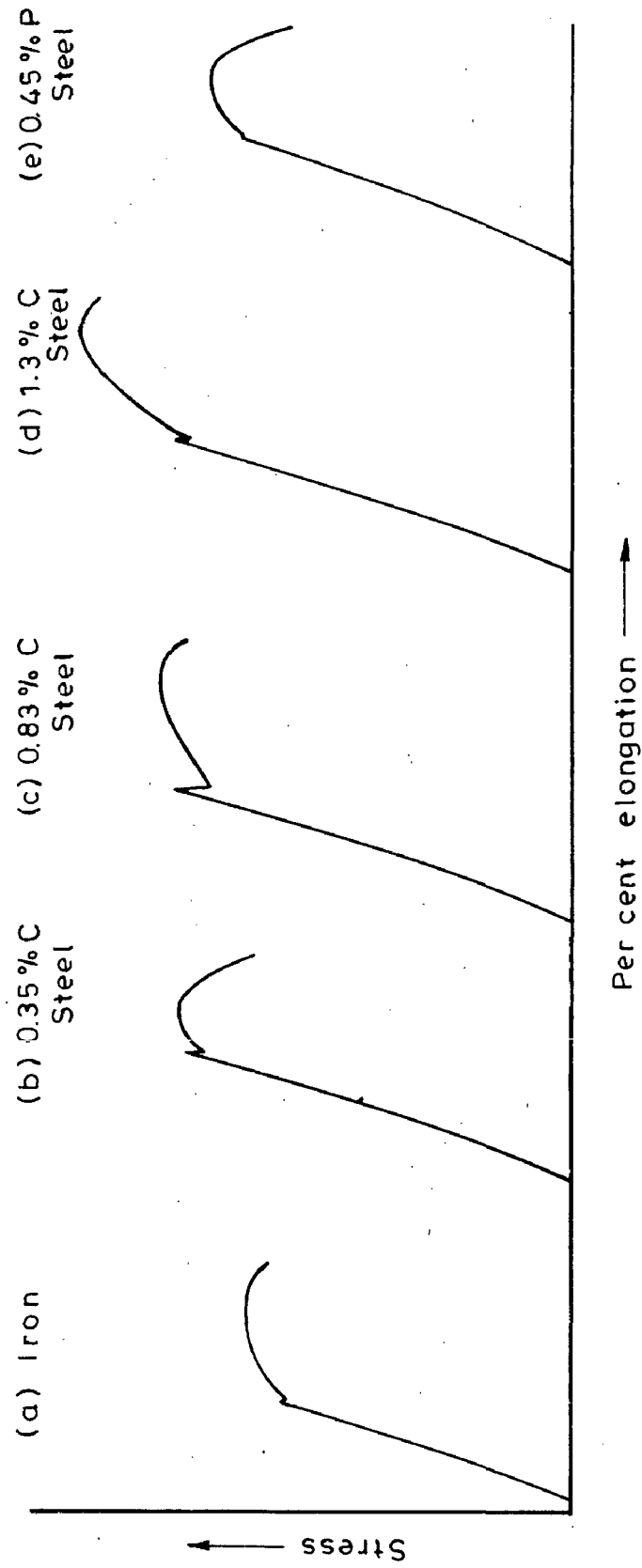


Fig.6.99(a to e)-Stress versus per cent elongation for various forged steels



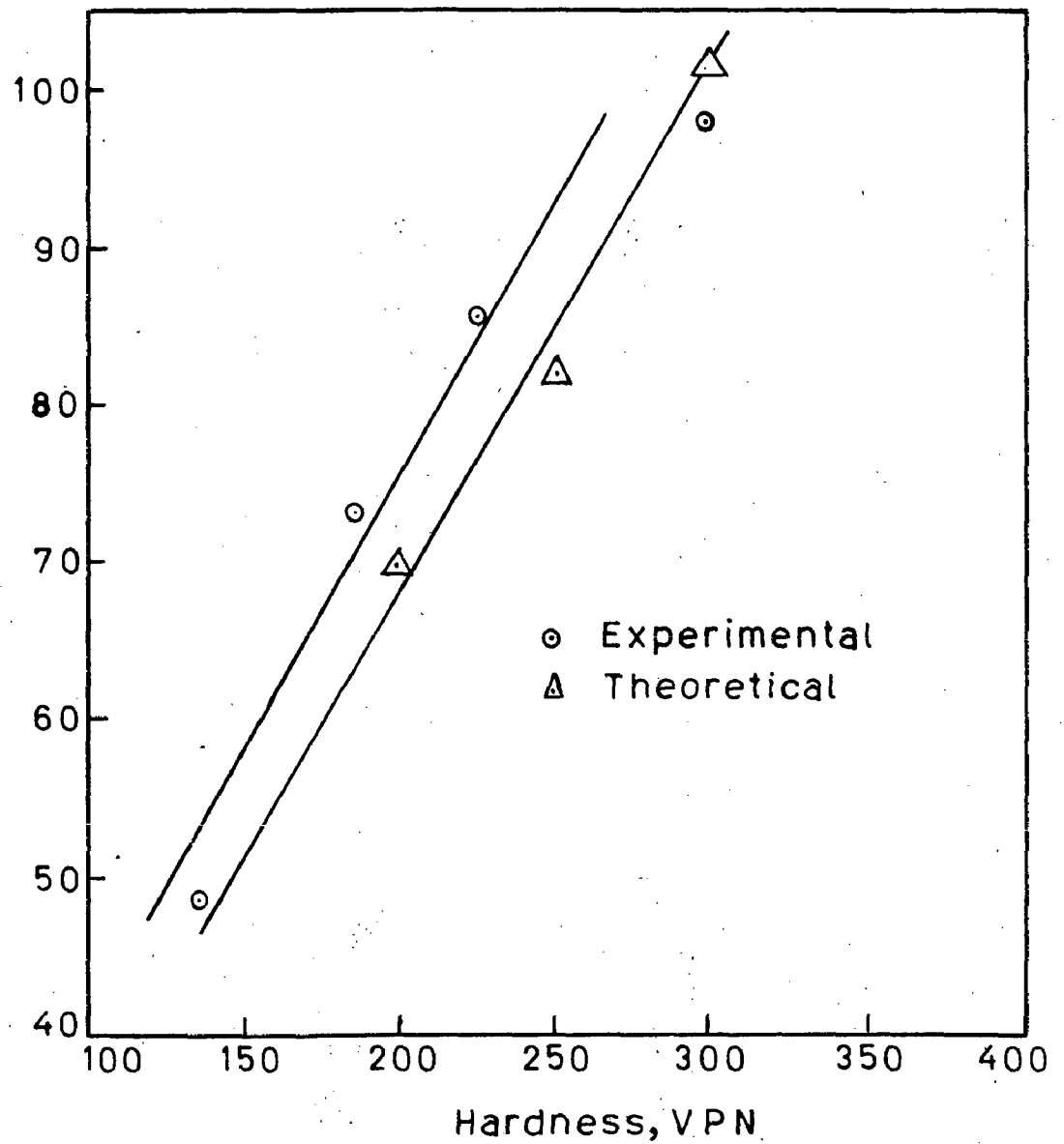


Fig.6.99 (f) - Plot of tensile strength vs. hardness for carbon steels

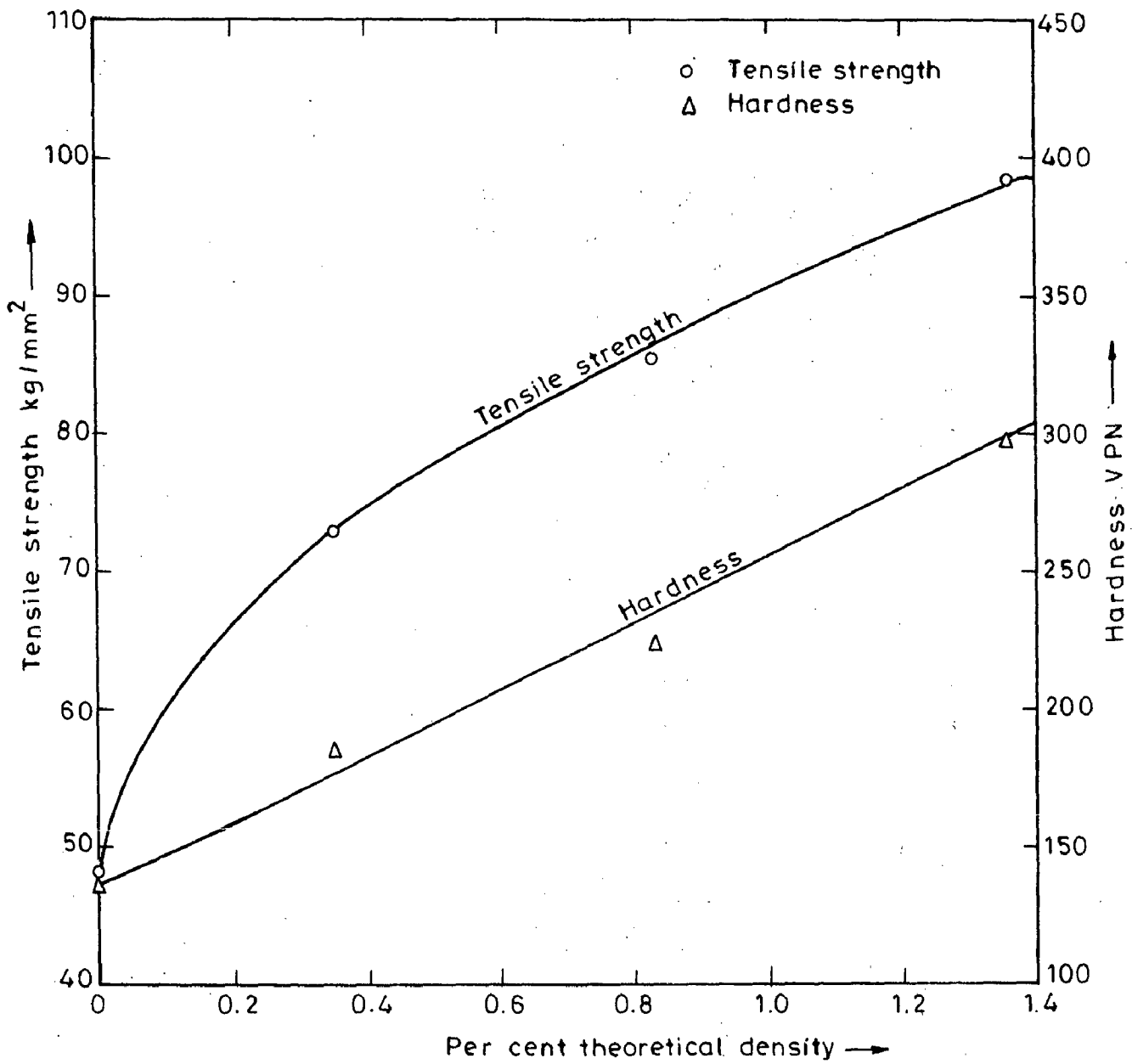


Fig. 6.99 (g)-Plot of hardness and tensile strength against composition of  $90^\circ$  turned upset forging

Fig. 6.100 - Scanning Electron Micrograph of Tensile Fracture Surface of Forged Sintered Iron.

Fig. 6.101(a) - Scanning Electron Micrograph of Tensile Fracture Surface of Forged Sintered 0.35 % Carbon Steel.

Fig. 6.101(b) - Scanning Electron Micrograph of Tensile Fracture Surface of Forged Sintered 0.35 % Carbon Steel.

Fig. 6.102 - Scanning Electron Micrograph of Tensile Fracture Surface of Forged Sintered 0.83 % Carbon Steel.

Fig. 6.103 - Scanning Electron Micrograph of Tensile Fracture Surface of Forged Sintered 1.36 % Carbon Steel.

Fig. 6.104 - Scanning Electron Micrograph of Tensile Fracture Surface of Forged Sintered 0.45 % Phosphorus Steel.

FIG. 6.100

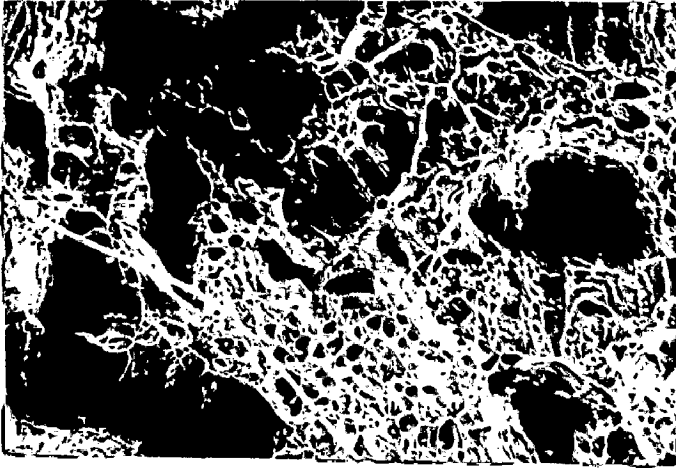


FIG. 6.101 (a)

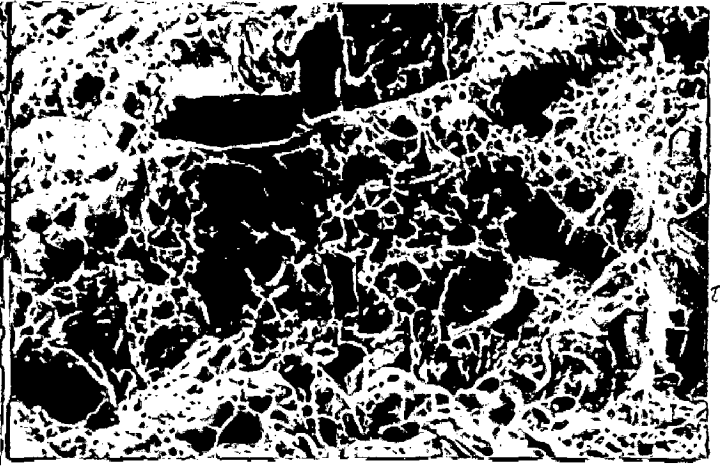
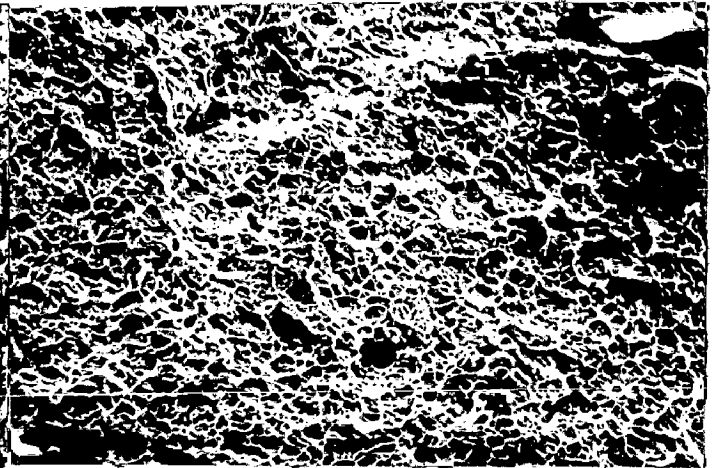
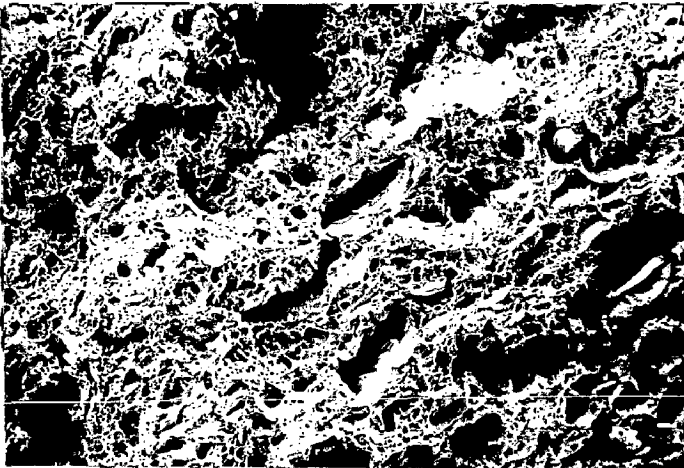


FIG. 6.100

FIG. 6.101 (a)

FIG. 6.101 (b)

FIG. 6.102



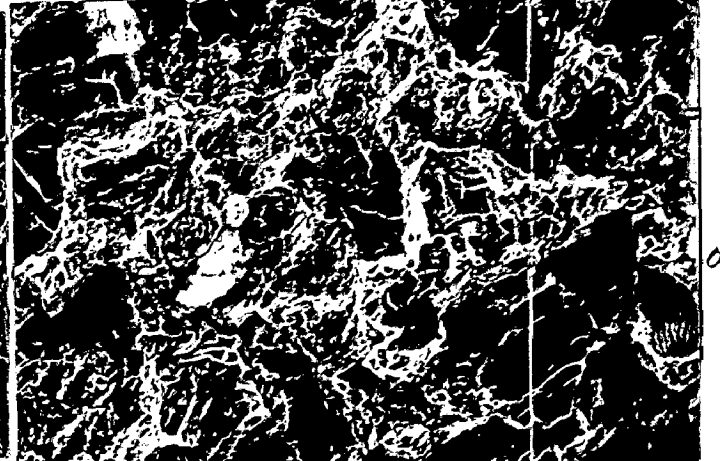
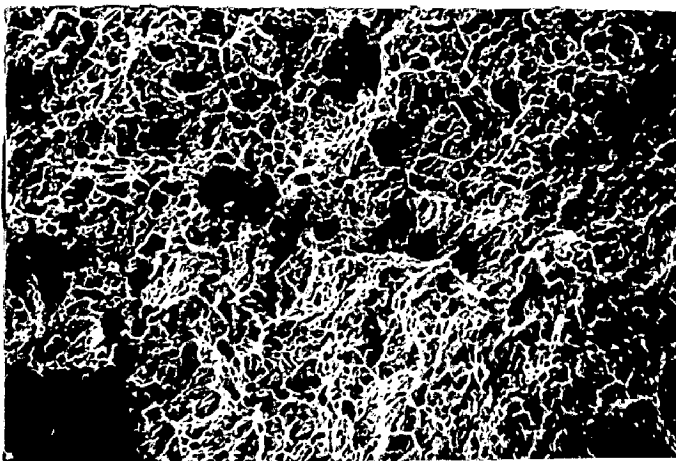
0.35

FIG. 6.101 (b)

FIG. 6.102

FIG. 6.103

FIG. 6.104



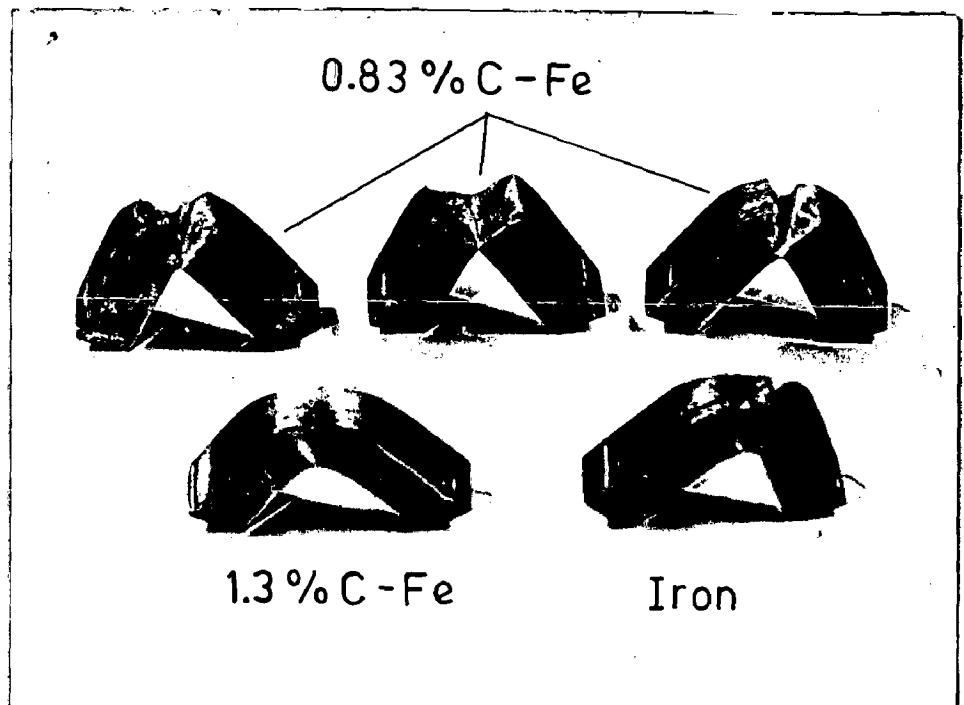
1.36

0.4

FIG. 103

FIG. 104

FIG. 6.105



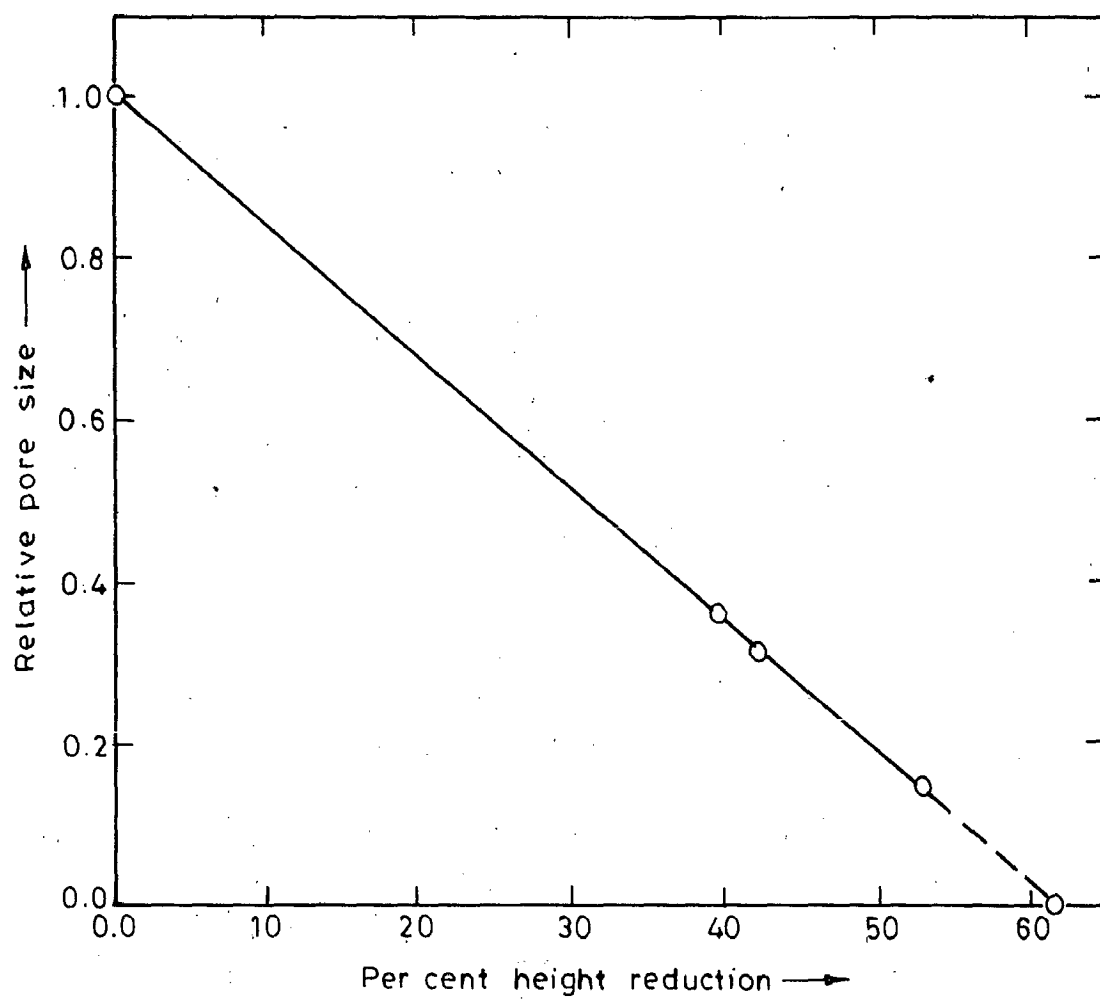


Fig. 6.106—Plot of relative pore size with respect to per cent deformation for iron powder sintered preform ( $H/D=0.99$ ) during hot upsetting at  $900^{\circ}\text{C}$

## CHAPTER - 7

### CONCLUSIONS

The main conclusions, emerging out of the present investigation, are given below :

- (1) Per cent theoretical density with respect to height strain for sintered preforms of iron and iron based alloy powders during upsetting at different temperatures and H/D ratios, can be related and expressed by a second order polynomial as follows :

$$\left( \frac{\rho_f}{\rho_{Th}} \right) = a_1 + a_2 \ln \left( \frac{H_o}{H_t} \right) + a_3 \left( \ln \frac{H_o}{H_t} \right)^2$$

where  $a_1$ ,  $a_2$  and  $a_3$  are temperature, composition and preform geometry (initial H/D ratio) dependent constants.

- (2) Lower initial H/D ratio, at any forging temperature, shows better densification as compared to higher H/D ratio for all compositions of steel studied.
- (3) Addition of carbon (upto 0.35 %) as an alloying element enhanced densification whereas higher carbon contents (0.83 and 1.3 % carbon) show poor level of densification.

- (4) 100 % dense product can not be produced by hot upsetting irrespective of the alloy composition, H/D ratio and temperature of forging employed.
- (5) Diameter strain versus height strain plots for powder preform upset forging always falls below the theoretical line for all temperatures of forging and all H/D ratios studied. Composition does not alter the position of the curve whereas H/D ratio does it. Higher H/D ratio tends to deviate more from the theoretical line than that of lower H/D ratios.
- (6) Poisson ratio versus percent theoretical density can be expressed in the form of a second order polynomial for H/D = 1.17 for pure iron as
- $$\nu = a_1 + a_2 \left( \frac{\rho_f}{\rho_{Th}} \right) + a_3 \left( \frac{\rho_f}{\rho_{Th}} \right)^2$$
- (7) Effect of alloying and H/D ratio on poisson ratio with respect to per cent theoretical density is not very significant. Both these parameters do not alter the nature of the curve but, however, shift the position of the curve. Higher H/D ratio shifts the curve to higher  $\nu$  values. Carbon upto 0.83 % does not show any significant shift



but 1.3 %C shows fairly pronounced upward shifting of the curve.

- (8) Variation in  $\rho$  with respect to per cent theoretical density shows three distinct stages, namely, (a) sharp rise in the density range of 87 to 90 % theoretical, (b) nearly steady state in the range 90 to 96 and, (c) again a sharp rise from 96 onwards to nearly 100 % theoretical density.
- (9) Hardness of forged components at various levels can be expressed as a linear function. Temperature of forging has a moderate effect over hardness values. Addition of carbon as an alloying element shows improved hardness values with respect to per cent theoretical density. However, in case of lower H/D ratio, temperature of forging shows distinct effect as it shifts the curves upward compared to that of lower temperature of forging. Whereas, at higher H/D ratio the above effect diminishes.
- (10) Circumferential cracks are delayed during hot upsetting, as carbon addition is enhanced upto 0.83 % carbon, whereas 1.36 % carbon shows cracks limit much earlier than 0.83 % carbon steel.

- (11) 0.83 % carbon and 0.45 % phosphorus steels show better forgeability.
- (12) Upsetting results of phosphorus steel shows more or less an ideal behaviour. Poission ratio plot with respect to per cent theoretical density approximates to the theoretical value at higher level of deformation.
- (13) Densification behaviour of iron, iron carbon and iron phosphorus system at their respective temperatures of forging (1120°C and 960°C respectively) can be expressed with a dimensionless geometrical parameter  $\bar{\Phi}$  in case of partially open dies is as follows :
- $$\left( \frac{\rho_f}{\rho_{Th}} \right) = C \bar{\Phi}^n$$
- (14) Hardness variation with respect to per cent theoretical density is initially gradual upto 98.5 % and this is followed by sudden rise upto 100 % theoretical density in case of partially open dies confirming the formation of metallurgically sound product.
- (15) Effect of forging parameters on microstructural features of the forged products and the sintered preforms have also been linked with

the bulk parameters such as level of deformation.

- (16) Pore shape, size, and its orientation have been linked with respect to deformation level in case of upsetting.
- (17) Pore shape, size, and its orientation in the forged products at various points in partially open die forging have been determined to establish the mode of metal flow.
- (18) Products produced through closed die forgings showed hardness values comparable with that of the wrought products.
- (19) Microstructural details of the closed die forgings showed the evidence of pore closure by flattening of the pores. 100 % theoretical density could not be achieved in closed die forgings.
- (20) Flow of grains, recrystallization and shearing of pores exhibit combined beneficial effect on densification.
- (21) In partially open die forgings lower order of fractional horizontal constraints are required compared to vertical fractional constraints in order to obtain same level of densification.

Table - A.1  
Compressibility Data for Iron Powder

Sl. No.	Load Kg	Pressure Kg/cm <sup>2</sup>	Total Height mm	Powder Height mm	Volume cm <sup>3</sup>	Density gm/cm <sup>3</sup>
1	0.00	0.00	118.70	40.30	8.513	3.935
2	1,750	828.44	113.10	34.70	7.330	4.570
3	2,500	1183.49	112.15	33.75	7.129	4.699
4	3,750	1775.23	109.80	31.40	6.633	5.051
5	5,000	2366.98	108.30	29.90	6.316	5.304
6	7,500	3550.46	106.30	27.90	5.894	5.684
7	10,000	4733.95	104.70	26.30	5.556	6.030
8	12,500	5917.44	103.50	25.00	5.281	6.343
9	15,000	7100.93	102.40	24.00	5.070	6.608

Compact Weight = 33.500 gms, Compact Dia. = 16.40 mm,  
Ejection Pressure = 2023.81 Kg/cm<sup>2</sup>

Table - A.2

## Tabulation of Mixing Behaviour of Iron Powder with Graphite

Time of Mixing mins.	Iron Powder		0.3 % Graphite Mixed		0.8 % Graphite Mixed		1.3 % Graphite Mixed	
	F.R.	A.D.	F.R.	A.D.	F.R.	A.D.	F.R.	A.D.
60	6.73	3.621	7.00	3.709	7.48	3.681	8.15	3.424
120	6.73	3.622	7.08	3.841	8.08	3.712	8.55	3.537
180	6.74	3.621	7.08	3.805	8.73	3.733	7.65	3.494
240	6.73	3.621	7.05	3.800	10.18	3.659	8.45	3.526
300	6.73	3.621	7.25	3.838	8.90	3.718	9.80	3.562
360	6.73	3.623	7.43	3.762	9.90	3.673	9.35	3.566
420	6.73	3.621	7.95	3.804	9.08	3.757	10.28	3.585
480	6.73	3.622	8.03	3.820	9.25	3.727	11.18	3.637
540	6.73	3.621	8.55	3.721	9.73	3.674	10.23	3.633
600	6.73	3.621	8.03	3.800	9.03	3.693	9.93	3.642

Table - A.3

Compressibility Data for 0.43 % Graphite Admixed Iron Powder

Sl. No.	Load Kg	Pressure Kg/cm <sup>2</sup>	Total Height mm	Powder Height mm	Volume cm <sup>3</sup>	Density gm/cm <sup>3</sup>
1	0.00	0.00	121.60	45.50	9.553	3.973
2	1,250	595.24	116.80	40.70	8.545	4.441
3	1,500	714.29	114.60	38.50	8.083	4.695
4	2,500	1190.48	112.40	36.10	7.579	5.008
5	3,500	1666.67	111.90	35.80	7.516	5.049
6	5,000	2380.95	108.90	32.80	6.886	5.511
7	6,500	3095.24	107.60	31.50	6.613	5.739
8	7,500	3571.43	106.50	30.40	6.383	5.946
9	10,000	4761.90	104.60	28.50	5.984	6.342
10	11,500	5476.19	103.80	27.70	5.812	6.530
11	12,500	5952.38	103.40	27.30	5.732	6.621

Compact Weight = 37.629 gms , Compact Dia. = 16.35 mm,  
Ejection Pressure = 1190.48 Kg/cm<sup>2</sup>

Table - A.4

## Compressibility Data for 1.14 % Graphite Admixed Iron Powder

Sl. No.	Load Kg	Pressure Kg/cm <sup>2</sup>	Total Height mm	Powder Height mm	Volume cm <sup>3</sup>	Density gm/cm <sup>3</sup>
1	0.00	0.00	123.20	46.00	9.660	3.895
2	1,250	595.24	116.30	39.10	8.211	4.583
3	2,500	1190.48	113.60	36.40	7.644	4.923
4	3,750	1785.71	111.40	34.20	7.182	5.239
5	5,000	2380.95	109.70	32.50	6.825	5.513
6	6,500	3095.24	107.90	30.70	6.447	5.837
7	7,500	3571.43	107.00	29.80	6.258	6.013
8	10,000	4761.90	105.20	28.00	5.880	6.340
9	12,500	5952.38	103.60	26.40	5.544	6.787

Compact Weight = 37.629 gms, Compact Dia. = 16.35 mm ,  
Ejection Pressure = 1071.43 Kg/cm<sup>2</sup>

Table - A.5

## Compressibility Data for 1.86 % Graphite Admixed Iron Powder

Sl.No.	Load Kg	Pressure Kg/cm <sup>2</sup>	Total Height mm	Powder Height mm	Volume cm <sup>3</sup>	Density gm/cm <sup>3</sup>
1	0.00	0.00	122.40	45.70	9.595	3.789
2	1,000	476.19	116.00	39.30	8.251	4.406
3	2,000	952.38	113.40	36.70	7.705	4.718
4	2,500	1190.48	112.20	35.50	7.453	4.878
5	3,500	1666.67	111.30	34.60	7.264	5.005
6	5,000	2380.95	108.30	31.60	6.634	5.480
7	6,000	2857.14	106.80	30.10	6.320	5.752
8	7,500	3571.43	105.50	28.80	6.047	6.012
9	8,500	4047.62	104.70	28.00	5.879	6.184
10	10,000	4761.90	103.40	26.70	5.606	6.485
11	11,500	5476.19	103.10	26.40	5.543	6.559
12	12,500	5952.38	102.40	25.70	5.396	6.737
13	13,500	6428.57	102.00	25.30	5.312	6.844

Compact Weight = 36.355 gms., Compact Dia. = 16.35 mm,

Ejection Pressure = 952.38 Kg/cm<sup>2</sup>



Table - A.6

## Compressibility Data for 0.45 % Phosphorus - Iron Alloy Powder

Sl. No.	Load Kg	Pressure Kg/cm <sup>2</sup>	Total Height mm	Powder Height mm	Volume cm <sup>3</sup>	Density gm/cm <sup>3</sup>
1	0.00	0.00	121.40	43.70	9.177	3.062
2	1,000	476.19	112.15	34.45	7.235	3.884
3	2,500	1190.48	109.20	31.50	6.615	4.249
4	3,500	1666.67	107.40	29.70	6.237	4.506
5	5,000	2380.95	105.60	27.90	5.859	4.797
6	7,500	3571.43	103.60	25.90	5.439	5.167
7	8,750	4166.67	102.80	25.10	5.271	5.332
8	10,000	4761.90	102.10	24.40	5.124	5.484
9	12,500	5952.38	100.80	23.10	4.851	5.793
10	15,000	7142.86	99.80	22.10	4.641	6.056

Compact Weight = 28.100 gms. , Compact Dia. = 16.35 mm ,  
Ejection Pressure = 1428.57 Kg/cm<sup>2</sup>

Table B<sub>1</sub>Upsetting of Sintered Iron Powder Preforms ( $H/D = 0.57$ ) at 800 °C

$H_t$ , mm	$D_t$ , mm	$\%(\frac{\Delta H}{H_0})$	$\%(\frac{\Delta D}{D_0})$	$\ln(\frac{D_t}{D_0})$	$\ln(\frac{H_0}{H_t})$	$\lambda = \frac{\ln(\frac{D_t}{D_0})}{\ln(\frac{H_0}{H_t})}$	$\frac{H_t}{D_t}$	$\rho_f$ , gm/cm <sup>3</sup>	$(\frac{\rho_f}{\rho_{Th}})$	VPN
12.90	27.06	14.00	2.50	0.025	0.151	0.164	0.48	7.120	0.907	76.34
12.40	27.55	17.33	4.36	0.043	0.190	0.224	0.45	7.198	0.917	76.70
12.30	27.78	18.00	5.23	0.051	0.198	0.257	0.44	7.214	0.919	77.21
12.15	27.83	19.00	5.42	0.053	0.211	0.250	0.44	7.332	0.934	77.75
10.50	28.85	30.00	9.28	0.089	0.357	0.249	0.36	7.450	0.949	94.35
8.80	31.65	41.33	19.89	0.181	0.533	0.340	0.28	7.677	0.978	105.94
8.50	31.98	43.33	21.14	0.192	0.568	0.338	0.27	7.685	0.979	-
7.70	33.75	48.67	27.84	0.246	0.667	0.368	0.23	-	-	-
5.60	38.85	62.67	47.16	0.386	0.985	0.392	0.14	-	-	-
3.80	48.15	74.67	82.39	0.601	1.373	0.438	0.08	-	-	-

 $H_0 = 15.00$  mm ;  $D_0 = 26.40$  mm

Table-B<sub>2</sub>Upsetting of Sintered Iron Powder Preforms ( $H/D = 0.57$ ) at 850 °C

$H_t$ , mm	$D_t$ , mm	$\% \left( \frac{\Delta H}{H_0} \right)$	$\% \left( \frac{\Delta D}{D_0} \right)$	$\ln \left( \frac{D_t}{D_0} \right)$	$\ln \left( \frac{H_0}{H_t} \right)$	$\lambda = \frac{\ln \left( \frac{D_t}{D_0} \right)}{\ln \left( \frac{H_0}{H_t} \right)}$	$\left( \frac{H_t}{D_t} \right)$	$\rho_f$ , gm/cm <sup>3</sup>	$\left( \frac{\rho_f}{\rho_{Th}} \right)$	VPN
12.80	27.43	14.67	3.90	0.038	0.159	0.241	0.47	7.191	0.916	76.33
12.30	27.76	18.00	5.15	0.050	0.198	0.253	0.44	7.246	0.923	78.61
11.20	28.80	25.33	9.09	0.087	0.292	0.298	0.39	7.458	0.950	89.33
9.80	29.84	34.67	13.03	0.122	0.426	0.288	0.33	7.615	0.970	92.54
9.10	30.80	39.33	16.67	0.154	0.500	0.308	0.30	7.701	0.981	108.48
8.10	32.53	46.00	23.22	0.209	0.616	0.418	0.25	7.779	0.991	115.75
7.50	33.50	50.00	26.89	0.238	0.693	0.344	0.22	-	-	-
5.40	39.30	64.00	48.86	0.398	1.022	0.389	0.14	-	-	-
5.10	41.00	66.00	55.30	0.440	1.079	0.408	0.12	-	-	-
3.30	51.48	78.00	95.00	0.669	1.514	0.441	0.06	-	-	-

 $H_0 = 15.00$  mm ;  $D_0 = 26.40$  mm

Table-B<sub>3</sub>

Upsetting of Sintered Iron Powder Preforms (H/D = 0.57) at 900 °C

H <sub>t</sub> , mm	D <sub>t</sub> , mm	%( $\frac{\Delta H}{H_0}$ )	%( $\frac{\Delta D}{D_0}$ )	$\ln(\frac{D_t}{D_0})$	$\ln(\frac{H_0}{H_t})$	$\ln(\frac{D_t}{D_0})$ $\lambda = \frac{\ln(\frac{D_t}{D_0})}{\ln(\frac{H_0}{H_t})}$	$\frac{H_t}{(D_t)^2}$	$\rho_f$ gm/cm <sup>3</sup>	$(\frac{\rho_f}{\rho_{Th}})$	VPN
12.70	27.33	15.33	3.52	0.035	0.166	0.208	0.46	7.198	0.917	77.18
12.25	27.70	18.33	4.92	0.048	0.203	0.237	0.44	7.246	0.923	81.82
12.10	27.78	19.33	5.23	0.051	0.215	0.237	0.44	7.261	0.925	85.02
9.85	30.00	34.33	13.64	0.128	0.421	0.304	0.33	7.575	0.965	110.10
8.50	32.03	43.33	21.33	0.193	0.568	0.340	0.27	7.740	0.986	113.84
8.35	32.30	44.33	22.35	0.202	0.586	0.344	0.26	7.772	0.990	123.63
8.10	32.80	46.00	24.24	0.217	0.616	0.352	0.25	7.787	0.992	123.99
7.20	34.90	52.00	32.20	0.279	0.734	0.380	0.21	-	-	-
6.10	37.63	59.33	42.54	0.354	0.900	0.394	0.16	-	-	-

H<sub>0</sub> = 15.00 mm ; D<sub>0</sub> = 26.40 mm

Table-B4

Upsetting of Sintered Iron Powder Preforms ( $H/D = 0.57$ ) at  $950^\circ\text{C}$ 

$H_t$ , mm	$D_t$ , mm	$\%(\frac{\Delta H}{H_0})$	$\%(\frac{\Delta D}{D_0})$	$\ln(\frac{D_t}{D_0})$	$\ln(\frac{H_0}{H_t})$	$\lambda = \frac{\ln(\frac{D_t}{D_0})}{\ln(\frac{H_0}{H_t})}$	$(\frac{H_t}{D_t})$	$\rho_f$ gm/cm <sup>3</sup>	$(\frac{\rho_f}{\rho_{Th}})$	VPN
13.4	26.78	10.67	1.44	0.014	0.113	0.127	0.50	7.081	0.902	73.74
12.70	27.18	15.33	2.95	0.029	0.166	0.175	0.45	7.206	0.918	74.53
11.25	28.45	25.00	7.77	0.075	0.288	0.260	0.40	7.403	0.943	97.38
10.00	30.15	33.33	14.20	0.133	0.405	0.328	0.33	7.575	0.965	111.12
9.55	30.19	36.33	14.36	0.134	0.452	0.297	0.32	7.630	0.972	132.30
9.40	30.73	37.33	16.40	0.152	0.467	0.325	0.31	7.677	0.978	133.00
9.20	31.20	38.67	18.18	0.167	0.489	0.342	0.29	7.685	0.979	-
8.60	32.35	42.67	22.54	0.203	0.556	0.365	0.27	7.748	0.987	-
5.3	40.95	64.67	55.11	0.439	1.040	0.422	0.13	-	-	-
3.2	50.08	78.67	89.70	0.640	1.545	0.414	0.06	-	-	-

 $H_0 = 15.00$  mm ;  $D_0 = 26.40$  mm

Table-B5

Upsetting of Sintered Iron Powder Preforms ( $H/D = 0.57$ ) at 1000 °C

$H_t$ , mm	$D_t$ , mm	$\%(\frac{\Delta H}{H_0})$	$\%(\frac{\Delta D}{D_0})$	$\ln(\frac{D_t}{D_0})$	$\ln(\frac{H_0}{H_t})$	$\ln(\frac{D_t}{D_0}) = \frac{\ln(\frac{D_t}{D_0})}{\ln(\frac{H_0}{H_t})}$	$(\frac{H_t}{D_t})$	$\rho_f$ gm/cm <sup>3</sup>	$(\frac{\rho_f}{\rho_{Th}})$	VPN
14.10	26.48	6.00	0.30	0.003	0.062	0.049	0.53	6.908	0.880	73.82
13.20	27.03	12.00	2.39	0.024	0.128	0.184	0.49	7.112	0.906	78.14
12.15	27.79	19.00	5.27	0.051	0.211	0.244	0.44	7.293	0.929	91.29
9.75	30.06	35.00	13.86	0.130	0.431	0.301	0.32	7.630	0.972	112.65
9.30	30.65	38.00	16.10	0.149	0.478	0.312	0.30	7.685	0.979	114.89
8.80	31.05	41.33	17.61	0.162	0.533	0.304	0.28	7.724	0.984	118.68
8.10	31.20	46.00	18.18	0.167	0.616	0.271	0.26	7.803	0.994	-
7.50	32.35	50.00	22.54	0.203	0.693	0.293	0.23	-	-	-
5.3	40.95	64.67	55.11	0.439	1.040	0.422	0.13	-	-	-
3.2	50.08	78.67	89.70	0.640	1.545	0.414	0.06	-	-	-

 $H_0 = 15.00$  mm ;  $D_0 = 26.40$  mm

Table-B<sub>6</sub>Upsetting of Sintered Iron Powder Preforms ( $H/D = 0.57$ ) at 1120 °C

$H_t$	$D_t$	$\%(\frac{\Delta H}{H_0})$	$\%(\frac{\Delta D}{D_0})$	$\ln(\frac{D_t}{D_0})$	$\ln(\frac{H_0}{H_t})$	$\lambda = \frac{\ln(\frac{D_t}{D_0})}{\ln(\frac{H_0}{H_t})}$	$(\frac{H_t}{D_t})$	$\rho_f$	$(\frac{\rho_f}{\rho_{Th}})$	VPN
15.00	26.40	00.00	0.00	0.00	0.00	-	0.57	6.672	0.850	79.31
13.00	26.70	13.33	1.14	0.011	0.143	0.079	0.49	7.222	0.920	90.40
9.99	28.70	33.40	8.71	0.084	0.406	0.206	0.35	7.669	0.977	107.68
9.10	29.98	39.33	13.56	0.127	0.500	0.254	0.30	7.772	0.990	114.58
8.45	31.05	43.67	17.61	0.162	0.574	0.283	0.27	7.811	0.995	120.85
6.50	33.78	56.67	27.95	0.247	0.836	0.295	0.19	-	-	131.29

 $H_0 = 15.00$  mm ;  $D_0 = 26.40$  mm

Table B7

Upsetting of Sintered Iron Powder Preforms ( $H/D = 0.99$ ) at 800 °C

$H_t$ , mm	$D_t$ , mm	$\%(\frac{\Delta H}{H_0})$	$\%(\frac{\Delta D}{D_0})$	$\ln(\frac{D_t}{D_0})$	$\ln(\frac{H_0}{H_t})$	$\ln(\frac{D_t}{D_0})$ $\lambda = \frac{\ln(\frac{D_t}{D_0})}{(\frac{H_0}{H_t})}$	$(\frac{H_t}{D_t})$	$\rho_f$ gm/cm <sup>3</sup>	$(\frac{\rho_f}{\rho_{Th}})$	VPN
22.08	27.60	14.62	4.55	0.044	0.158	0.278	0.80	6.932	0.883	-
21.68	27.80	16.92	5.30	0.052	0.185	0.272	0.78	7.010	0.893	67.34
18.12	29.23	30.00	10.72	0.102	0.357	0.283	0.62	7.253	0.924	69.49
16.65	30.28	36.54	14.70	0.137	0.455	0.305	0.55	7.379	0.940	88.13
15.36	31.35	41.15	18.75	0.172	0.530	0.324	0.49	7.481	0.953	89.59
15.26	31.36	41.54	18.79	0.172	0.537	0.319	0.48	7.482	0.953	90.74
13.98	32.50	46.54	23.11	0.208	0.626	0.330	0.43	7.536	0.960	97.89
10.66	35.55	59.16	34.66	0.298	0.901	0.329	0.30	7.709	0.982	-
9.67	40.30	62.95	52.65	0.423	1.000	0.423	0.24	7.732	0.985	-
9.07	41.30	65.25	56.44	0.447	1.076	0.416	0.22	7.740	0.986	-

 $H_0 = 26.10$  mm ;  $D_0 = 26.40$  mm



Table-B<sub>8</sub>

Upsetting of Sintered Iron Powder Preforms (H/D = 0.99) at 850 °C

H <sub>t</sub> , mm	D <sub>t</sub> , mm	$\% \left( \frac{\Delta H}{H_0} \right)$	$\% \left( \frac{\Delta D}{D_0} \right)$	$\ln \left( \frac{D_t}{D_0} \right)$	$\ln \left( \frac{H_0}{H_t} \right)$	$\ln \left( \frac{D_t}{D_0} \right) = \frac{\ln \left( \frac{D_t}{D_0} \right)}{\ln \left( \frac{H_0}{H_t} \right)}$	$\left( \frac{H_t}{D_t} \right)$	$\rho_f$ gm/cm <sup>3</sup>	$\left( \frac{\rho_f}{\rho_{Th}} \right)$	VPN
22.72	27.05	13.08	2.46	0.024	0.140	0.174	0.84	7.015	0.894	62.28
19.48	28.65	25.38	8.52	0.082	0.293	0.281	0.68	7.220	0.920	70.98
16.95	29.73	34.62	12.61	0.119	0.425	0.283	0.57	7.343	0.935	72.61
15.07	31.40	41.54	18.94	0.173	0.537	0.321	0.48	7.556	0.963	80.65
14.46	32.13	43.85	21.70	0.196	0.577	0.339	0.45	7.557	0.963	83.28
12.24	34.98	53.06	32.50	0.281	0.757	0.372	0.35	7.618	0.971	86.87
9.40	39.15	63.85	48.30	0.394	1.017	0.387	0.24	7.667	0.977	98.98
8.10	43.70	68.97	65.53	0.504	1.166	0.432	0.19	-	-	-
7.60	44.35	70.88	67.99	0.519	1.234	0.420	0.17	-	-	-

H<sub>0</sub> = 26.10 mm ; D<sub>0</sub> = 26.40 mm

Table-B<sub>9</sub>

Upsetting of Sintered Iron Powder Preforms (H/D = 0.99) at 900 °C

H <sub>t</sub> , mm	D <sub>t</sub> , mm	$\% \left( \frac{\Delta H}{H_0} \right)$	$\% \left( \frac{\Delta D}{D_0} \right)$	$\ln \left( \frac{D_t}{D_0} \right)$	$\ln \left( \frac{H_0}{H_t} \right)$	$\ln \left( \frac{D_t}{D_0} \right) = \frac{\ln \left( \frac{D_t}{D_0} \right)}{\ln \left( \frac{H_0}{H_t} \right)}$	$\left( \frac{H_t}{D_t} \right)$	$\rho_f$ gm/cm <sup>3</sup>	$\left( \frac{\rho_f}{\rho_{Th}} \right)$	VPN
23.10	26.70	11.49	1.14	0.011	0.122	0.093	0.87	6.900	0.879	-
19.20	28.68	26.44	8.64	0.083	0.307	0.270	0.67	7.238	0.922	55.28
15.70	30.85	39.85	16.86	0.156	0.508	0.307	0.51	7.497	0.955	67.49
15.10	31.60	42.15	19.70	0.180	0.547	0.329	0.48	7.535	0.960	67.85
14.90	31.75	42.91	20.27	0.185	0.561	0.329	0.47	7.560	0.963	-
12.20	35.08	53.26	32.88	0.284	0.760	0.374	0.35	7.694	0.980	-
9.40	40.58	63.98	53.71	0.430	1.021	0.421	0.23	-	-	78.53
9.00	41.13	65.52	55.80	0.443	1.065	0.416	0.22	-	-	-

H<sub>0</sub> = 26.10 mm ; D<sub>0</sub> = 26.40 mm

Table-B<sub>10</sub>Upsetting of Sintered Iron Powder Preforms ( $H/D = 0.99$ ) at 950 °C

$H_t$ , mm	$D_t$ , mm	$\%(\frac{\Delta H}{H_0})$	$\%(\frac{\Delta D}{D_0})$	$\ln(\frac{D_t}{D_0})$	$\ln(\frac{H_0}{H_t})$	$\ln(\frac{D_t}{D_0}) = \frac{\ln(\frac{D_t}{D_0})}{\ln(\frac{H_0}{H_t})}$	$(\frac{H_t}{D_t})$	$\rho_f$ gm/cm <sup>3</sup>	$(\frac{\rho_f}{\rho_{Th}})$	VPN
23.10	26.83	11.49	1.63	0.016	0.122	0.132	0.86	6.947	0.885	75.01
21.20	27.40	18.77	3.79	0.037	0.208	0.179	0.77	7.104	0.905	80.86
20.50	27.98	21.46	5.98	0.058	0.242	0.240	0.73	7.159	0.912	95.49
15.90	30.63	39.08	16.02	0.149	0.496	0.300	0.52	7.497	0.955	102.22
15.60	31.20	40.23	18.18	0.167	0.515	0.324	0.50	7.512	0.957	102.83
14.60	32.03	44.06	21.33	0.193	0.581	0.333	0.46	7.600	0.968	107.54
14.40	32.13	44.83	21.70	0.196	0.595	0.330	0.45	7.614	0.970	141.20

 $H_0 = 26.10$  mm ;  $D_0 = 26.40$  mm

Table-B11

Upsetting of Sintered Iron Powder Preforms ( $H/D = 0.99$ ) at  $1000\text{ }^{\circ}\text{C}$

$H_t$ , mm	$D_t$ , mm	$\%(\frac{\Delta H}{H_0})$	$\%(\frac{\Delta D}{D_0})$	$\ln(\frac{D_t}{D_0})$	$\ln(\frac{H_0}{H_t})$	$\ln(\frac{D_t}{D_0}) = \frac{\ln(\frac{D_t}{D_0})}{\ln(\frac{H_0}{H_t})}$	$(\frac{H_t}{D_t})$	$\rho_f$ gm/cm <sup>3</sup>	$(\frac{\rho_f}{\rho_{Th}})$	VPN
20.70	27.88	20.69	5.61	0.055	0.232	0.235	0.74	7.144	0.910	71.09
20.00	28.23	23.37	6.93	0.067	0.266	0.252	0.71	7.191	0.916	74.50
18.40	29.15	29.50	10.42	0.099	0.350	0.283	0.63	7.340	0.935	82.40
14.90	31.85	42.91	20.64	0.188	0.561	0.335	0.47	7.607	0.969	101.75
13.60	33.28	47.89	26.06	0.232	0.652	0.355	0.41	7.693	0.980	102.34
13.10	34.05	49.81	28.98	0.254	0.689	0.369	0.38	7.716	0.983	104.64
12.90	34.43	50.57	30.42	0.266	0.705	0.377	0.37	7.724	0.984	112.00
12.60	34.74	51.72	31.59	0.275	0.728	0.377	0.36	7.716	0.983	113.20

$H_0 = 26.10\text{ mm}$  ;  $D_0 = 26.40\text{ mm}$

Table-B<sub>12</sub>

Upsetting of Sintered Iron Powder Preforms (H/D = 0.99) at 1120 °C

H <sub>t</sub> , mm	D <sub>t</sub> , mm	% ( $\frac{\Delta H}{H_0}$ )	% ( $\frac{\Delta D}{D_0}$ )	$\ln\left(\frac{D_t}{D_0}\right)$	$\ln\left(\frac{H_0}{H_t}\right)$	$\ln\left(\frac{D_t}{D_0}\right) = \frac{\ln\left(\frac{D_t}{D_0}\right)}{\ln\left(\frac{H_0}{H_t}\right)}$	$\left(\frac{H_t}{D_t}\right)$	$\rho_f$ gm/cm <sup>3</sup>	$\left(\frac{\rho_f}{\rho_{Th}}\right)$	VPN
26.10	26.40	00.00	00.00	00.00	00.00	-	0.97	6.672	0.850	-
21.30	27.08	18.39	2.58	0.025	0.203	0.125	0.79	7.175	0.914	78.75
19.50	28.10	25.29	6.44	0.062	0.292	0.214	0.69	7.332	0.934	85.03
13.90	31.98	46.74	21.14	0.192	0.630	0.304	0.43	7.732	0.985	90.35
11.60	34.88	55.56	32.12	0.279	0.811	0.343	0.33	7.826	0.997	109.20
9.80	38.03	62.45	44.05	0.365	0.980	0.372	0.26	-	-	112.40
6.40	42.98	75.48	62.80	0.487	1.406	0.347	0.15	-	-	-

H<sub>0</sub> = 26.10 mm ; D<sub>0</sub> = 26.40 mm

Table-B<sub>13</sub>

Upsetting of Sintered Iron Powder Preforms ( $H/D = 1.17$ ) at 800 °C

$H_t$ , mm	$D_t$ , mm	$\%(\frac{\Delta H}{H_0})$	$\%(\frac{\Delta D}{D_0})$	$\ln(\frac{D_t}{D_0})$	$\ln(\frac{H_0}{H_t})$	$\ln(\frac{D_t}{D_0}) / \ln(\frac{H_0}{H_t})$	$(\frac{H_t}{H_0})^3$	$\rho_f$ gm/cm <sup>3</sup>	$(\frac{\rho_f}{\rho_{Th}})$	VPN
28.24	27.15	8.90	2.84	0.028	0.093	0.301	1.04	6.688	0.852	58.64
26.48	27.30	14.58	3.41	0.034	0.158	0.212	0.97	6.853	0.873	75.93
25.16	27.95	18.84	5.87	0.057	0.209	0.273	0.90	6.924	0.882	79.77
22.04	29.00	28.90	9.85	0.094	0.341	0.275	0.76	7.167	0.913	88.46
19.63	30.20	36.68	14.39	0.134	0.457	0.294	0.65	7.403	0.943	93.94
17.98	31.55	42.00	19.51	0.178	0.545	0.327	0.57	7.481	0.953	101.70
15.78	32.88	49.10	24.54	0.220	0.675	0.325	0.48	7.5	0.958	107.51
14.52	34.58	53.16	30.98	0.270	0.758	0.356	0.42	7.552	0.962	107.86

$H_0 = 31.00$  mm ;  $D_0 = 26.40$  mm

Table-B14

Upsetting of Sintered Iron Powder Preforms ( $H/D = 1.17$ ) at 850 °C

$H_t$ , mm	$D_t$ , mm	$\%(\frac{\Delta H}{H_0})$	$\%(\frac{\Delta D}{D_0})$	$\ln(\frac{D_t}{D_0})$	$\ln(\frac{H_0}{H_t})$	$\lambda = \frac{\ln(\frac{D_t}{D_0})}{\ln(\frac{H_0}{H_t})}$	$(\frac{H_t}{D_t})$	$\rho_f$ gm/cm <sup>3</sup>	$(\frac{\rho_f}{\rho_{Th}})$	VPN
27.03	27.03	12.81	2.39	0.024	0.137	0.172	1.00	6.947	0.885	73.53
22.82	28.53	26.39	8.07	0.078	0.306	0.254	0.80	7.379	0.940	74.21
20.90	29.85	32.58	13.07	0.123	0.394	0.312	0.70	7.418	0.945	81.18
19.51	30.48	37.06	15.45	0.144	0.463	0.310	0.64	7.442	0.948	85.51
18.39	30.65	40.68	16.10	0.149	0.522	0.286	0.60	7.630	0.972	91.71
16.56	31.85	46.58	20.64	0.188	0.627	0.299	0.52	7.834	0.998	95.19
15.13	32.90	51.19	24.62	0.220	0.717	0.307	0.46	7.842	0.999	108.55
12.38	38.68	60.06	46.52	0.382	0.918	0.416	0.32	7.850	1.000	113.60
12.29	39.63	60.35	50.11	0.406	0.925	0.439	0.31	7.850	1.000	120.20
10.76	41.38	65.29	56.74	0.449	1.058	0.425	0.26	7.850	1.000	121.93

 $H_0 = 31.00$  mm ;  $D_0 = 26.40$  mm

Table-B<sub>15</sub>

Upsetting of Sintered Iron Powder Preforms ( $H/D = 1.17$ ) at 900 °C

$H_t$ , mm	$D_t$ , mm	$\%(\frac{\Delta H}{H_0})$	$\%(\frac{\Delta D}{D_0})$	$\ln(\frac{D_t}{D_0})$	$\ln(\frac{H_0}{H_t})$	$\lambda) = \frac{\ln(\frac{D_t}{D_0})}{\ln(\frac{H_0}{H_t})}$	$(\frac{H_t}{D_t})$	$\rho_f$ , gm/cm <sup>3</sup>	$(\frac{\rho_f}{\rho_{Th}})$	VPN
28.49	26.88	8.10	1.82	0.018	0.084	0.214	1.06	6.735	0.858	74.62
26.59	27.13	14.22	2.77	0.027	0.153	0.178	0.98	6.877	0.876	74.97
24.10	28.35	22.26	7.39	0.071	0.252	0.283	0.85	7.096	0.904	76.28
22.85	28.93	26.29	9.58	0.092	0.305	0.300	0.79	7.128	0.908	76.43
21.71	29.34	29.97	11.14	0.106	0.356	0.297	0.74	7.269	0.926	77.89
17.06	32.18	44.97	21.89	0.198	0.597	0.332	0.53	7.528	0.959	86.49
14.34	34.15	53.74	29.36	0.257	0.771	0.334	0.42	7.599	0.968	92.73
10.80	40.50	65.16	53.41	0.428	1.054	0.406	0.27	7.716	0.983	100.98
10.50	41.90	66.13	58.71	0.462	1.083	0.427	0.25	7.732	0.985	109.11
10.30	42.00	66.77	59.09	0.464	1.102	0.421	0.25	7.740	0.986	122.32

$H_0 = 31.00$  mm ;  $D_0 = 26.40$  mm



Table-B<sub>16</sub>Upsetting of Sintered Iron Powder Preforms ( $H/D = 1.17$ ) at 950 °C

$H_t$ , mm	$D_t$ , mm	$\% \left( \frac{\Delta H}{H_0} \right)$	$\% \left( \frac{\Delta D}{D_0} \right)$	$\ln \left( \frac{D_t}{D_0} \right)$	$\ln \left( \frac{H_0}{H_t} \right)$	$\ln \left( \frac{D_t}{D_0} \right) = \frac{\ln \left( \frac{D_t}{D_0} \right)}{\ln \left( \frac{H_0}{H_t} \right)}$	$\left( \frac{H_t}{D_t} \right)$	$\rho_f$ gm/cm <sup>3</sup>	$\left( \frac{\rho_f}{\rho_{Th}} \right)$	VPN
27.32	27.05	11.87	2.46	0.024	0.126	0.193	1.01	6.822	0.869	71.35
26.26	27.35	15.29	3.60	0.035	0.166	0.213	0.96	6.939	0.884	89.16
22.89	28.98	26.16	9.77	0.093	0.303	0.308	0.79	7.191	0.916	93.93
22.20	29.60	28.39	12.12	0.114	0.334	0.343	0.75	7.285	0.928	94.62
20.05	29.93	35.32	13.37	0.125	0.436	0.288	0.67	7.403	0.943	97.90
18.20	31.38	41.29	18.86	0.173	0.533	0.324	0.58	7.481	0.953	115.90
16.51	32.38	46.74	22.65	0.204	0.630	0.324	0.51	7.567	0.964	116.30
13.20	36.35	57.42	37.69	0.320	0.854	0.374	0.36	7.662	0.976	121.00
11.70	38.83	62.26	47.08	0.386	0.974	0.396	0.30	7.717	0.983	122.20
10.80	40.80	65.16	54.54	0.435	1.054	0.413	0.26	7.740	0.986	129.60

 $H_0 = 31.00$  mm ;  $D_0 = 26.40$  mm

Table-B<sub>17</sub>Upsetting of Sintered Iron Powder Preforms ( $H/D = 1.17$ ) at 1000 °C

$H_t$ , mm	$D_t$ , mm	$\%(\frac{\Delta H}{H_0})$	$\%(\frac{\Delta D}{D_0})$	$\ln(\frac{D_t}{D_0})$	$\ln(\frac{H_0}{H_t})$	$\ln(\frac{D_t}{D_0})$ $\ln(\frac{H_0}{H_t})$	$(\frac{H_t}{D_t})$	$\rho_f$ gm/cm <sup>3</sup>	$(\frac{\rho_f}{\rho_{Th}})$	VPN
25.37	27.58	18.16	4.47	0.044	0.200	0.219	0.92	7.081	0.902	86.27
23.39	28.53	24.55	8.07	0.078	0.282	0.275	0.82	7.246	0.923	87.18
22.41	29.10	27.71	10.23	0.097	0.324	0.301	0.77	7.285	0.928	91.58
20.84	29.35	32.77	11.17	0.106	0.397	0.267	0.71	7.410	0.944	101.29
19.05	31.23	38.55	18.30	0.168	0.487	0.345	0.61	7.473	0.952	103.35
17.36	32.15	44.00	21.78	0.197	0.580	0.340	0.54	7.560	0.963	113.40
14.26	35.65	54.00	35.04	0.300	0.777	0.387	0.40	7.677	0.978	117.30
14.25	36.53	54.03	38.37	0.325	0.777	0.418	0.39	7.693	0.980	119.00
13.67	36.95	55.90	39.96	0.336	0.819	0.411	0.37	7.700	0.981	121.60
12.93	38.03	58.29	44.05	0.365	0.874	0.410	0.34	7.732	0.985	132.50

 $H_0 = 31.00$  mm ;  $D_0 = 26.40$  mm

Table-B<sub>18</sub>Upsetting of Sintered Iron Powder Preforms ( $H/D = 1.17$ ) at 1120 °C

$H_t$ , mm	$D_t$ , mm	$\% \left( \frac{\Delta H}{H_0} \right)$	$\% \left( \frac{\Delta D}{D_0} \right)$	$\ln \left( \frac{D_t}{D_0} \right)$	$\ln \left( \frac{H_0}{H_t} \right)$	$\lambda = \frac{\ln \left( \frac{D_t}{D_0} \right)}{\ln \left( \frac{H_0}{H_t} \right)}$	$\left( \frac{H_t}{D_t} \right)$	$\rho_f$ gm/cm <sup>3</sup>	$\left( \frac{\rho_f}{\rho_{Th}} \right)$	VPN
26.11	27.2	15.77	3.03	0.030	0.172	0.174	0.96	7.104	0.905	88.49
25.28	27.78	18.45	5.23	0.051	0.204	0.250	0.91	7.324	0.933	92.12
20.87	28.98	32.68	9.77	0.093	0.396	0.235	0.72	7.434	0.947	93.73
14.36	31.90	53.68	20.83	0.189	0.770	0.246	0.45	7.693	0.980	138.32
12.21	39.40	60.61	49.24	0.400	0.931	0.430	0.31	7.818	0.996	147.80
8.42	40.10	72.84	51.89	0.418	1.303	0.321	0.21	7.834	0.998	151.36

 $H_0 = 31.00$  mm ;  $D_0 = 26.40$  mm

Table-B<sub>19</sub>

Upsetting of Sintered 0.43 % Graphite Admixed  
Iron Powder Preforms(H/D = 0.57) at 800 °C

H <sub>t</sub> , mm	D <sub>t</sub> , mm	$\% \left( \frac{\Delta H}{H_0} \right)$	$\% \left( \frac{\Delta D}{D_0} \right)$	$\ln \left( \frac{D_t}{D_0} \right)$	$\ln \left( \frac{H_0}{H_t} \right)$	$\lambda = \frac{\ln \left( \frac{D_t}{D_0} \right)}{\ln \left( \frac{H_0}{H_t} \right)}$	$\left( \frac{H_t}{D_t} \right)$	$\rho_f$ gm/cm <sup>3</sup>	$\left( \frac{\rho_f}{\rho_{Th}} \right)$	VPN
15.00	26.40	0.00	0.00	0.000	0.000	-	0.57	6.728	0.857	65.39
12.30	27.65	18.00	4.73	0.046	0.198	0.234	0.44	7.293	0.929	135.78
11.55	28.20	23.00	6.82	0.066	0.261	0.253	0.41	7.363	0.938	141.61
11.40	28.23	24.00	6.93	0.067	0.274	0.245	0.40	7.390	0.941	140.32
9.40	30.73	37.33	16.40	0.152	0.467	0.325	0.31	7.653	0.975	164.21
8.30	32.85	44.67	24.43	0.219	0.592	0.369	0.25	7.716	0.983	171.44
8.10	32.88	46.00	24.55	0.220	0.616	0.356	0.25	7.754	0.988	179.43

H<sub>0</sub> = 15.00 mm ; D<sub>0</sub> = 26.40 mm

Table-B20

Upsetting of Sintered 0.43 % Graphite Admixed  
Iron Powder Preforms (H/D = 0.57) at 850 °C

H <sub>t</sub> , mm	D <sub>t</sub> , mm	$\%(\frac{\Delta H}{H_0})$	$\%(\frac{\Delta D}{D_0})$	$\ln(\frac{D_t}{D_0})$	$\ln(\frac{H_0}{H_t})$	$\lambda = \frac{\ln(\frac{D_t}{D_0})}{\ln(\frac{H_0}{H_t})}$	$(\frac{H_t}{D_t})$	$\rho_f$ gm/cm <sup>3</sup>	$(\frac{\rho_f}{\rho_{Th}})$	VPN
15.00	26.40	0.00	0.00	0.000	0.000	-	0.57	6.821	0.869	72.01
12.40	27.63	17.33	4.66	0.046	0.173	0.263	0.45	7.265	0.925	128.34
10.80	28.48	28.00	7.88	0.076	0.280	0.271	0.38	7.499	0.955	145.48
10.40	29.58	30.66	12.04	0.110	0.307	0.359	0.35	7.556	0.963	153.97
9.60	30.30	36.00	14.77	0.138	0.360	0.383	0.32	7.629	0.972	176.53
8.40	32.45	44.00	22.92	0.206	0.440	0.469	0.26	7.731	0.985	181.64

H<sub>0</sub> = 15.00 mm ; D<sub>0</sub> = 26.40 mm

Table-B21

Upsetting of Sintered 0.43 % Graphite Admixed  
Iron Powder Preforms (H/D = 0.57) at 900 °C

H <sub>t</sub> , mm	D <sub>t</sub> , mm	$\% \left( \frac{\Delta H}{H_0} \right)$	$\% \left( \frac{\Delta D}{D_0} \right)$	$\ln \left( \frac{D_t}{D_0} \right)$	$\ln \left( \frac{H_0}{H_t} \right)$	$\lambda = \frac{\ln \left( \frac{D_t}{D_0} \right)}{\ln \left( \frac{H_0}{H_t} \right)}$	$\left( \frac{H_t}{D_t} \right)$	$\rho_f$ gm/cm <sup>3</sup>	$\left( \frac{\rho_f}{\rho_{Th}} \right)$	VPN
15.00	26.40	0.00	0.00	0.000	0.000	-	0.57	6.806	0.867	75.03
11.40	28.15	24.00	6.62	0.064	0.274	0.234	0.40	7.402	0.943	145.91
11.30	23.58	24.67	8.26	0.079	0.283	0.280	0.40	7.445	0.948	147.33
10.00	30.28	33.33	14.70	0.137	0.405	0.339	0.33	7.601	0.968	165.55
9.80	30.35	34.67	14.96	0.139	0.426	0.327	0.32	7.655	0.975	175.00
9.10	31.33	39.33	18.67	0.171	0.500	0.342	0.29	7.709	0.982	179.47
7.60	34.13	49.33	29.28	0.257	0.680	0.378	0.22	7.772	0.990	197.99
7.50	34.23	50.00	29.66	0.260	0.693	0.375	0.22	7.803	0.994	191.83

H<sub>0</sub> = 15.00 mm ; D<sub>0</sub> = 26.40 mm

Table-B22

Upsetting of Sintered 0.43 % Graphite Admixed  
Iron Powder Preforms (H/D = 0.57) at 950 °C

$H_t$ , mm	$D_t$ , mm	$\% \left( \frac{\Delta H}{H_0} \right)$	$\% \left( \frac{\Delta D}{D_0} \right)$	$\ln \left( \frac{D_t}{D_0} \right)$	$\ln \left( \frac{H_0}{H_t} \right)$	$\lambda = \frac{\ln \left( \frac{D_t}{D_0} \right)}{\ln \left( \frac{H_0}{H_t} \right)}$	$\left( \frac{H_t}{D_t} \right)$	$\rho_f$ gm/cm <sup>3</sup>	$\left( \frac{\rho_f}{\rho_{Th}} \right)$	VPN
15.00	26.40	0.00	0.00	0.000	0.000	-	0.57	6.727	0.857	62.50
11.80	27.25	21.33	3.22	0.032	0.240	0.132	0.43	7.395	0.942	145.79
10.90	27.80	27.33	5.30	0.052	0.319	0.162	0.39	7.536	0.960	163.00
9.65	30.62	35.67	15.98	0.148	0.441	0.336	0.32	7.693	0.980	183.70
8.60	31.70	42.67	20.08	0.183	0.556	0.329	0.27	7.787	0.992	194.00
7.90	32.50	47.33	23.11	0.208	0.641	0.324	0.24	7.795	0.993	196.35
7.33	33.15	57.13	25.57	0.228	0.716	0.318	0.22	7.811	0.995	201.00
7.10	34.15	52.67	29.36	0.257	0.748	0.344	0.21	7.834	0.998	207.84

$H_0 = 15.00$  mm ;  $D_0 = 26.40$  mm

Table-B<sub>23</sub>

Upsetting of Sintered 0.43 % Graphite Admixed  
Iron Powder Preforms (H/D = 0.57) at 1000 °C

H <sub>t</sub> , mm	D <sub>t</sub> , mm	$\% \left( \frac{\Delta H}{H_0} \right)$	$\% \left( \frac{\Delta D}{D_0} \right)$	$\ln \left( \frac{D_t}{D_0} \right)$	$\ln \left( \frac{H_0}{H_t} \right)$	$\lambda = \frac{\ln \left( \frac{D_t}{D_0} \right)}{\ln \left( \frac{H_0}{H_t} \right)}$	$\left( \frac{H_t}{D_t} \right)$	$\rho_f$ gm/cm <sup>3</sup>	$\left( \frac{\rho_f}{\rho_{Th}} \right)$	VPN
15.00	26.40	0.00	0.00	0.000	0.000	-	0.57	6.727	0.857	70.19
12.70	27.23	15.33	3.14	0.031	0.166	0.186	0.47	7.293	0.929	150.38
11.50	27.98	23.33	5.98	0.058	0.266	0.218	0.41	7.458	0.950	163.09
10.60	28.55	29.33	8.14	0.078	0.347	0.224	0.37	7.567	0.964	172.80
9.80	30.23	34.67	14.51	0.135	0.426	0.318	0.32	7.677	0.978	190.87
7.40	34.70	50.67	31.44	0.273	0.707	0.387	0.21	7.779	0.991	203.41
6.20	37.95	58.67	43.75	0.363	0.884	0.411	0.16	7.819	0.996	208.34

H<sub>0</sub> = 15.00 mm ; D<sub>0</sub> = 26.40 mm



○

Table-B 24

Upsetting of Sintered 0.43 % Graphite Admixed Iron Powder Preforms (H/D = 0.57) at 1120 °C

H <sub>t</sub> , mm	D <sub>t</sub> , mm	% ( $\frac{\Delta H}{H_0}$ )	% ( $\frac{\Delta D}{D_0}$ )	$\ln(\frac{D_t}{D_0})$	$\ln(\frac{H_0}{H_t})$	$\ln(\frac{D_t}{D_0}) = \frac{\ln(\frac{D_t}{D_0})}{\ln(\frac{H_0}{H_t})}$	$(\frac{H_t}{D_t})$	$\rho_f$ gm/cm <sup>3</sup>	$(\frac{\rho_f}{\rho_{Th}})$	VPN
15.00	26.40	0.00	0.00	0.000	0.000	-	0.57	6.837	0.871	90.23
13.40	26.70	10.67	1.14	0.011	0.113	0.100	0.50	7.136	0.909	125.46
11.40	28.33	24.00	7.31	0.071	0.274	0.257	0.40	7.473	0.952	170.39
10.30	29.26	31.33	10.83	0.103	0.376	0.274	0.35	7.630	0.972	187.50
8.90	30.50	40.67	15.33	0.144	0.522	0.277	0.29	7.748	0.987	200.79
8.40	30.85	44.00	16.86	0.156	0.580	0.269	0.27	7.803	0.994	214.07
7.80	33.05	48.00	25.19	0.225	0.654	0.344	0.24	7.819	0.996	215.31
7.25	34.15	51.67	29.36	0.257	0.727	0.354	0.21	7.834	0.998	221.03

H<sub>0</sub> = 15.00 mm ; D<sub>0</sub> = 26.40 mm

Table-B25

Upsetting of Sintered 0.43 % Graphite Admixed  
Iron Powder Preforms (H/D = 0.98) at 800 °C

$H_t$ , mm	$D_t$ , mm	$\%(\frac{\Delta H}{H_0})$	$\%(\frac{\Delta D}{D_0})$	$\ln(\frac{D_t}{D_0})$	$\ln(\frac{H_0}{H_t})$	$\ln(\frac{D_t}{D_0}) = \frac{\ln(\frac{D_t}{D_0})}{\ln(\frac{H_0}{H_t})}$	$(\frac{H_t}{D_t})$	$\rho_f$ , gm/cm <sup>3</sup>	$(\frac{\rho_f}{\rho_{Th}})$	VPN
26.00	26.40	0.00	0.00	0.000	0.000	-	0.98	6.727	0.857	85.00
21.90	27.33	15.77	3.52	0.035	0.172	0.201	0.80	6.979	0.889	110.23
18.00	29.46	30.77	11.59	0.110	0.368	0.298	0.61	7.324	0.933	147.89
16.60	30.23	36.15	14.51	0.135	0.449	0.302	0.55	7.418	0.945	165.32
12.80	33.80	50.77	28.03	0.247	0.709	0.349	0.38	7.646	0.974	188.18
11.80	34.98	54.62	32.50	0.281	0.790	0.356	0.34	7.654	0.975	208.78
11.00	36.65	57.69	38.82	0.328	0.860	0.381	0.30	7.701	0.981	216.34

$H_0 = 26.00$  mm ;  $D_0 = 26.40$  mm

Table-B26

Upsetting of Sintered 0.43 % Graphite Admixed  
Iron Powder Preforms (H/D = 0.98) at 850 °C

H <sub>t</sub> , mm	D <sub>t</sub> , mm	$\% \left( \frac{\Delta H}{H_0} \right)$	$\% \left( \frac{\Delta D}{D_0} \right)$	$\ln \left( \frac{D_t}{D_0} \right)$	$\ln \left( \frac{H_0}{H_t} \right)$	$\ln \left( \frac{D_t}{D_0} \right) = \frac{\ln \left( \frac{D_t}{D_0} \right)}{\ln \left( \frac{H_0}{H_t} \right)}$	$\left( \frac{H_t}{D_t} \right)$	$\rho_f$ gm/cm <sup>3</sup>	$\left( \frac{\rho_f}{\rho_{Th}} \right)$	VPN
26.00	26.40	0.00	0.00	0.000	0.000	-	0.98	6.732	0.858	77.23
21.70	27.15	16.54	2.76	0.028	0.181	0.156	0.80	7.049	0.898	125.39
18.80	28.48	27.69	7.86	0.076	0.324	0.237	0.66	7.261	0.925	148.01
15.30	30.60	41.15	15.91	0.148	0.530	0.279	0.50	7.544	0.961	187.50
13.00	33.10	50.00	25.38	0.226	0.693	0.328	0.39	7.646	0.974	192.32
10.20	37.55	60.77	42.23	0.352	0.936	0.375	0.29	7.701	0.981	200.19
9.60	38.90	63.08	47.35	0.388	0.996	0.388	0.26	7.732	0.985	215.01

H<sub>0</sub> = 26.00 mm ; D<sub>0</sub> = 26.40 mm

Table-B<sub>27</sub>

Upsetting of Sintered 0.43 % Graphite Admixed  
Iron Powder Preforms (H/D = 0.98) at 900 °C

H <sub>t</sub> , mm	D <sub>t</sub> , mm	$\% \left( \frac{\Delta H}{H_0} \right)$	$\% \left( \frac{\Delta D}{D_0} \right)$	$\ln \left( \frac{D_t}{D_0} \right)$	$\ln \left( \frac{H_0}{H_t} \right)$	$\lambda = \frac{\ln \left( \frac{D_t}{D_0} \right)}{\ln \left( \frac{H_0}{H_t} \right)}$	$\left( \frac{H_t}{D_t} \right)$	$\rho_f$ gm/cm <sup>3</sup>	$\left( \frac{\rho_f}{\rho_{Th}} \right)$	VPN
26.00	26.40	0.00	0.00	0.000	0.000	-	0.98	6.731	0.857	68.33
20.00	28.15	23.08	6.63	0.064	0.262	0.245	0.71	7.214	0.919	151.87
17.00	29.38	34.62	11.28	0.107	0.425	0.252	0.58	7.442	0.948	178.36
16.20	29.98	37.69	13.56	0.127	0.473	0.269	0.54	7.512	0.957	192.69
14.30	31.75	45.00	20.26	0.185	0.598	0.309	0.45	7.630	0.972	205.16
9.40	37.60	63.85	42.42	0.354	1.017	0.348	0.25	7.756	0.988	222.50
7.30	45.30	71.92	71.59	0.540	1.270	0.425	0.16	7.764	0.989	230.17

H<sub>0</sub> = 26.00 mm ; D<sub>0</sub> = 26.40 mm

Table-B 28

Upsetting of Sintered 0.43 % Graphite Admixed Iron Powder Preforms (H/D = 0.98) at 950 °C

H <sub>t</sub> , mm	D <sub>t</sub> , mm	% ( $\frac{\Delta H}{H_0}$ )	% ( $\frac{\Delta D}{D_0}$ )	$\ln(\frac{D_t}{D_0})$	$\ln(\frac{H}{H_t})$	$\ln(\frac{D_t}{D_0})$ - $\frac{\ln(\frac{D_t}{D_0})}{\ln(\frac{H}{H_t})}$	$(\frac{H_t}{D_t})$	$\rho_f$ gm/cm <sup>3</sup>	$(\frac{\rho_f}{\rho_{Th}})$	VPN
26.00	26.40	0.00	0.00	0.000	0.000	-	0.98	6.727	0.857	70.13
22.40	26.95	13.85	2.08	0.021	0.149	0.138	0.83	7.049	0.898	116.97
18.40	28.43	29.23	7.69	0.074	0.346	0.214	0.65	7.379	0.940	163.49
17.10	29.35	34.23	11.17	0.106	0.419	0.253	0.58	7.481	0.953	186.73
16.60	29.63	36.15	12.23	0.115	0.449	0.257	0.56	7.505	0.956	186.31
14.50	31.55	44.23	19.51	0.178	0.584	0.305	0.46	7.638	0.973	203.11
12.00	33.75	53.85	27.84	0.246	0.773	0.318	0.36	7.740	0.986	220.33

H<sub>0</sub> = 26.00 mm ; D<sub>0</sub> = 26.40 mm

Table-B29

Upsetting of Sintered 0.43 % Graphite Admixed  
Iron Powder Preforms (H/D = 0.98) at 1000 °C

H <sub>t</sub> mm	D <sub>t</sub> mm	$\% \left( \frac{\Delta H}{H_0} \right)$	$\% \left( \frac{\Delta D}{D_0} \right)$	$\ln \left( \frac{D_t}{D_0} \right)$	$\ln \left( \frac{H_0}{H_t} \right)$	$\lambda = \frac{\ln \left( \frac{D_t}{D_0} \right)}{\ln \left( \frac{H_0}{H_t} \right)}$	$\left( \frac{H_t}{D_t} \right)$	$\rho_f$ gm/cm <sup>3</sup>	$\left( \frac{\rho_f}{\rho_{Th}} \right)$	VPN
26.00	26.40	0.00	0.00	0.000	0.000	-	0.98	6.730	0.857	75.33
19.80	27.90	23.85	5.68	0.055	0.272	0.203	0.71	7.300	0.930	152.39
18.10	29.67	30.38	12.39	0.117	0.362	0.323	0.61	7.434	0.947	183.03
16.40	30.28	36.92	14.70	0.137	0.461	0.297	0.54	7.575	0.965	195.52
13.60	32.00	47.69	21.21	0.192	0.648	0.297	0.42	7.709	0.982	208.19
11.80	34.58	54.62	30.98	0.270	0.790	0.342	0.34	7.771	0.990	215.91
8.00	42.15	69.23	59.66	0.468	1.179	0.397	0.19	7.787	0.992	221.64
6.80	45.60	73.85	72.73	0.547	1.341	0.408	0.15	7.810	0.995	213.57

H<sub>0</sub> = 26.00 mm ; D<sub>0</sub> = 26.40 mm

Table-B<sub>30</sub>

Upsetting of Sintered 0.43% Graphite Admixed  
Iron Powder Preforms (H/D = 0.98) at 1120 °C

H <sub>t</sub> , mm	D <sub>t</sub> , mm	% ( $\frac{\Delta H}{H_0}$ )	% ( $\frac{\Delta D}{D_0}$ )	$\ln(\frac{D_t}{D_0})$	$\ln(\frac{H_0}{H_t})$	$\lambda = \frac{\ln(\frac{D_t}{D_0})}{(\frac{H_0}{H_t})}$	$(\frac{H_t}{D_t})$	$\rho_f$ gm/cm <sup>3</sup>	$(\frac{\rho_f}{\rho_{Th}})$	VPN
26.00	26.40	0.00	0.00	0.000	0.000	-	0.98	6.728	0.857	80.99
22.70	27.78	12.69	5.23	0.051	0.136	0.375	0.82	7.081	0.902	133.19
20.80	28.98	20.00	9.77	0.093	0.223	0.418	0.72	7.191	0.916	135.79
17.60	29.50	32.31	11.74	0.111	0.390	0.285	0.60	7.536	0.960	195.37
15.65	31.15	39.81	17.99	0.165	0.508	0.326	0.50	7.638	0.973	208.21
14.30	32.05	45.00	21.40	0.194	0.598	0.324	0.45	7.709	0.982	222.50
12.40	34.78	52.31	31.74	0.276	0.740	0.373	0.36	7.795	0.993	227.83
9.60	41.25	63.08	56.25	0.446	0.996	0.448	0.23	7.819	0.996	231.01

H<sub>0</sub> = 26.00 mm ; D<sub>0</sub> = 26.40 mm

Table-B31

Upsetting of Sintered 1.14 % Graphite Admixed  
Iron Powder Preforms ( $H/D_0 = 0.57$ ) at 800 °C

$H_t$ , mm	$D_t$ , mm	$\% \left( \frac{\Delta H}{H_0} \right)$	$\% \left( \frac{\Delta D}{D_0} \right)$	$\ln \left( \frac{D_t}{D_0} \right)$	$\ln \left( \frac{H_0}{H_t} \right)$	$\lambda = \frac{\ln \left( \frac{D_t}{D_0} \right)}{\ln \left( \frac{H_0}{H_t} \right)}$	$\left( \frac{H_t}{D_t} \right)$	$\rho_f$ gm/cm <sup>3</sup>	$\left( \frac{\rho_f}{\rho_{Th}} \right)$	VPN
15.00	26.40	0.00	0.00	0.000	0.000	-	0.57	6.735	0.858	110.12
12.70	27.75	15.33	0.050	0.166	0.166	0.300	0.46	6.971	0.888	153.67
12.10	27.88	19.33	0.055	0.215	0.215	0.254	0.43	7.049	0.898	165.32
10.70	29.48	28.67	0.110	0.338	0.338	0.326	0.36	7.269	0.926	215.13
9.90	30.25	34.00	0.136	0.416	0.416	0.327	0.33	7.355	0.937	237.50
7.90	33.75	47.33	0.246	0.641	0.641	0.383	0.23	7.536	0.960	278.14
6.80	36.10	54.67	0.313	0.791	0.791	0.396	0.19	7.591	0.967	287.50

$H_0 = 15.00$  mm ;  $D_0 = 26.40$  mm



Table-B 32

Upsetting of Sintered 1.14 % Graphite Admixed  
Iron Powder Preforms (H/D = 0.57) at 850 °C

H <sub>t</sub> , mm	D <sub>t</sub> , mm	% $\frac{\Delta H}{H_0}$	% $\left(\frac{\Delta D}{D_0}\right)$	$\ln\left(\frac{D_t}{D_0}\right)$	$\ln\left(\frac{H_0}{H_t}\right)$	$\lambda = \frac{\ln\left(\frac{D_t}{D_0}\right)}{\ln\left(\frac{H_0}{H_t}\right)}$	$\left(\frac{H_t}{D_t}\right)$	$\rho_f$ gm/cm <sup>3</sup>	$\left(\frac{\rho_f}{\rho_{Th}}\right)$	VPN
15.00	26.40	0.00	0.00	0.000	0.000	-	0.57	6.727	0.857	127.33
12.50	27.08	16.67	2.58	0.025	0.182	0.140	0.46	7.010	0.893	162.73
11.90	27.55	20.67	4.36	0.043	0.232	0.184	0.43	7.128	0.908	200.73
9.95	29.13	33.67	10.34	0.098	0.410	0.240	0.34	7.355	0.937	238.47
9.00	30.63	40.00	16.02	0.149	0.511	0.291	0.29	7.465	0.951	285.43
7.95	32.73	47.00	23.98	0.215	0.635	0.338	0.24	7.551	0.962	300.00
7.00	34.10	53.33	29.17	0.256	0.762	0.336	0.21	7.591	0.967	310.29

H<sub>0</sub> = 15.00 mm ; D<sub>0</sub> = 26.40 mm

Table-B33

Upsetting of Sintered 1.14 % Graphite Admixed  
Iron Powder Preforms (H/D = 0.57) at 900 °C

H <sub>t</sub> , mm	D <sub>t</sub> , mm	$\% \left( \frac{\Delta H}{H_0} \right)$	$\% \left( \frac{\Delta D}{D_0} \right)$	$\ln \left( \frac{D_t}{D_0} \right)$	$\ln \left( \frac{H_0}{H_t} \right)$	$\ln \left( \frac{D_t}{D_0} \right) = \frac{\ln \left( \frac{D_t}{D_0} \right)}{\ln \left( \frac{H_0}{H_t} \right)}$	$\left( \frac{H_t}{D_t} \right)$	$\rho_f$ gm/cm <sup>3</sup>	$\left( \frac{\rho_f}{\rho_{Th}} \right)$	VPN
15.00	26.40	0.00	0.00	0.000	0.000	-	0.57	6.727	0.857	115.00
11.90	27.78	20.67	5.23	0.051	0.232	0.220	0.43	7.144	0.910	212.50
10.60	28.98	29.33	9.77	0.093	0.347	0.269	0.37	7.348	0.936	270.78
10.20	29.25	32.00	10.80	0.103	0.386	0.266	0.35	7.379	0.940	272.13
10.00	29.30	33.33	10.98	0.104	0.405	0.257	0.34	7.418	0.945	282.73
9.90	29.50	34.00	11.74	0.111	0.416	0.267	0.34	7.434	8.947	287.50
9.10	30.90	39.33	17.04	0.157	0.500	0.315	0.29	7.505	0.956	300.62
7.10	33.50	52.67	26.89	0.238	0.748	0.318	0.21	7.630	0.972	326.19
5.60	39.45	62.67	49.43	0.401	0.985	0.408	0.14	7.654	0.975	330.11

H<sub>0</sub> = 15.00 mm ; D<sub>0</sub> = 26.40 mm

Table-B34

Upsetting of Sintered 1.14 % Graphite Admixed  
Iron Powder Preforms (H/D = 0.57) at 950 °C

H <sub>t</sub> , mm	D <sub>t</sub> , mm	% ( $\frac{\Delta H}{H_0}$ )	% ( $\frac{\Delta D}{D_0}$ )	$\ln(\frac{D_t}{D_0})$	$\ln(\frac{H_0}{H_t})$	$\ln(\frac{D_t}{D_0}) = \frac{\ln(\frac{D_t}{D_0})}{\ln(\frac{H_0}{H_t})}$	$(\frac{H_t}{D_t})$	$\rho_f$ gm/cm <sup>3</sup>	$(\frac{\rho_f}{\rho_{Th}})$	VPN
15.00	26.40	0.00	0.00	0.000	0.000	-	0.57	6.735	0.858	114.17
13.40	26.93	10.67	2.01	0.020	0.113	0.176	0.50	6.884	0.877	153.00
11.40	28.20	24.00	6.82	0.066	0.274	0.241	0.40	7.261	0.925	240.18
10.50	29.83	30.00	12.99	0.112	0.357	0.342	0.35	7.398	0.942	291.98
9.20	30.88	38.67	16.97	0.157	0.489	0.321	0.30	7.544	0.961	313.49
8.70	31.65	42.00	19.89	0.181	0.545	0.333	0.27	7.560	0.963	315.13
8.60	31.88	42.67	20.76	0.189	0.556	0.339	0.27	7.567	0.964	314.27
6.30	37.60	58.00	42.42	0.354	0.868	0.407	0.17	7.654	0.975	332.11

H<sub>0</sub> = 15.00 mm ; D<sub>0</sub> = 26.40 mm

Table-B35

Upsetting of Sintered 1.14% Graphite Admixed  
Iron Powder Preforms (H/D = 0.57) at 1000 °C

H <sub>t</sub> , mm	D <sub>t</sub> , mm	$\% \left( \frac{\Delta H}{H_0} \right)$	$\% \left( \frac{\Delta D}{D_0} \right)$	$\ln \left( \frac{D_t}{D_0} \right)$	$\ln \left( \frac{H_0}{H_t} \right)$	$\lambda = \frac{\ln \left( \frac{D_t}{D_0} \right)}{\ln \left( \frac{H_0}{H_t} \right)}$	$\left( \frac{H_t}{D_t} \right)$	$\rho_f$ gm/cm <sup>3</sup>	$\left( \frac{\rho_f}{\rho_{Th}} \right)$	VPN
15.00	26.40	0.00	0.00	0.000	0.000	-	0.57	6.727	0.857	115.03
12.60	26.78	16.00	1.44	0.014	0.174	0.082	0.47	7.089	0.903	208.19
11.10	28.35	26.00	7.39	0.071	0.301	0.237	0.39	7.230	0.921	242.79
10.00	29.48	33.33	11.67	0.110	0.405	0.272	0.34	7.481	0.953	310.15
7.90	32.93	47.33	24.73	0.221	0.641	0.345	0.24	7.630	0.972	340.34
7.50	33.65	50.00	27.46	0.243	0.693	0.350	0.22	7.646	0.974	343.94
6.70	36.45	55.33	38.07	0.323	0.806	0.400	0.18	7.662	0.976	341.78

H<sub>0</sub> = 15.00 mm ; D<sub>0</sub> = 26.40 mm

Table-B37

Upsetting of Sintered 1.14 % Graphite Admixed Iron Powder Preforms (H/D = 0.98) at 800 °C

H <sub>t</sub> , mm	D <sub>t</sub> , mm	$\%(\frac{\Delta H}{H_0})$	$\%(\frac{\Delta D}{D_0})$	$\ln(\frac{D_t}{D_0})$	$\ln(\frac{H_0}{H_t})$	$\ln(\frac{D_t}{D_0}) / \ln(\frac{H_0}{H_t})$	$(\frac{H_t}{D_t})$	$\rho_f$ gm/cm <sup>3</sup>	$(\frac{\rho_f}{\rho_{Th}})$	VPN
26.00	26.40	0.00	0.00	0.000	0.000	-	0.98	6.523	0.831	
20.90	27.05	19.62	2.46	0.024	0.218	0.112	0.77	6.861	0.874	145.32
18.50	29.00	28.85	9.85	0.094	0.340	0.276	0.64	7.057	0.899	165.76
15.80	30.05	39.23	13.82	0.129	0.498	0.260	0.53	7.277	0.927	226.33
12.90	32.08	50.38	21.52	0.195	0.701	0.278	0.40	7.418	0.945	255.82
12.60	32.55	51.54	23.30	0.209	0.724	0.289	0.39	7.426	0.946	265.93
8.90	38.55	65.77	46.02	0.379	1.072	0.553	0.23	7.505	0.956	278.00

H<sub>0</sub> = 26.00 mm ; D<sub>0</sub> = 26.40 mm.

Table-B 38

Upsetting of Sintered 1.14 % Graphite Admixed  
Iron Powder Preforms (H/D = 0.98) at 850 °C

H <sub>t</sub> , mm	D <sub>t</sub> , mm	%( $\frac{\Delta H}{H_0}$ )	%( $\frac{\Delta D}{D_0}$ )	$\ln(\frac{D_t}{D_0})$	$\ln(\frac{H_0}{H_t})$	$\lambda = \frac{\ln(\frac{D_t}{D_0})}{\ln(\frac{H_0}{H_t})}$	$(\frac{H_t}{D_t})$	$\rho_f$ gm/cm <sup>3</sup>	$(\frac{\rho_f}{\rho_{Th}})$	VPN
26.00	26.4	0.00	0.00	0.000	0.000	-	0.98	6.531	0.832	101.00
21.50	27.19	17.31	2.99	0.029	0.190	0.155	0.79	6.830	0.870	141.00
19.25	28.02	25.96	6.14	0.060	0.301	0.198	0.69	7.010	0.893	188.31
16.70	29.57	35.77	12.01	0.113	0.443	0.256	0.56	7.230	0.921	235.00
15.40	30.18	40.77	14.31	0.134	0.524	0.255	0.51	7.316	0.932	258.89
12.25	32.77	52.88	24.13	0.216	0.753	0.287	0.37	7.473	0.952	283.17
11.55	34.55	55.58	30.87	0.269	0.811	0.332	0.33	7.489	0.954	289.38
10.40	36.63	60.00	38.75	0.328	0.916	0.358	0.28	7.528	0.959	290.97
8.60	39.51	66.92	49.66	0.403	1.106	0.365	0.22	7.552	0.962	295.39

H<sub>0</sub> = 26.00 mm ; D<sub>0</sub> = 26.40 mm.

Table-B<sub>39</sub>

Upsetting of Sintered 1.14 % Graphite Admixed Iron Powder Preforms (H/D = 0.98) at 900 °C

H <sub>t</sub> , mm	D <sub>t</sub> , mm	% ( $\frac{\Delta H}{H_0}$ )	% ( $\frac{\Delta D}{D_0}$ )	$\ln\left(\frac{D_t}{D_0}\right)$	$\ln\left(\frac{H_0}{H_t}\right)$	$\lambda = \frac{\ln\left(\frac{D_t}{D_0}\right)}{\ln\left(\frac{H_0}{H_t}\right)}$	$\left(\frac{H_t}{D_t}\right)$	$\rho_f$ gm/cm <sup>3</sup>	$\left(\frac{\rho_f}{\rho_{Th}}\right)$	VPN
26.0	26.40	0.00	0.00	0.000	0.900	-	0.98	6.516	0.830	102.50
23.28	26.93	10.46	2.01	0.020	0.111	0.179	0.86	6.712	0.855	125.13
20.20	27.59	22.31	4.51	0.044	0.252	0.175	0.73	6.947	0.885	168.32
17.75	28.90	31.73	9.47	0.090	0.382	0.237	0.61	7.167	0.913	215.03
14.20	30.76	45.38	16.52	0.153	0.605	0.253	0.46	7.418	0.945	262.18
10.85	33.67	58.27	27.54	0.243	0.874	0.278	0.32	7.552	0.962	300.08
9.50	35.83	63.46	35.72	0.303	1.007	0.303	0.27	7.575	0.965	303.29
8.30	39.65	68.56	50.19	0.407	1.142	0.356	0.20	7.583	0.966	320.11

H<sub>0</sub> = 26.00 mm ; D<sub>0</sub> = 26.40 mm.

Table-B 40

Upsetting of Sintered 1.14 % Graphite Admixed  
Iron Powder Preforms ( $H/D = 0.98$ ) at 950 °C

$H_t$ , mm	$D_t$ , mm	$\% \left( \frac{\Delta H}{H_0} \right)$	$\% \left( \frac{\Delta D}{D_0} \right)$	$\ln \left( \frac{D_t}{D_0} \right)$	$\ln \left( \frac{H_0}{H_t} \right)$	$\lambda = \frac{\ln \left( \frac{D_t}{D_0} \right)}{\ln \left( \frac{H_0}{H_t} \right)}$	$\left( \frac{H_t}{D_t} \right)$	$\rho_f$ gm/cm <sup>3</sup>	$\left( \frac{\rho_f}{\rho_{Th}} \right)$	VPN
26.00	26.40	0.00	0.00	0.000	0.000	-	0.98	6.539	0.833	108.33
21.90	26.75	15.77	1.33	0.013	0.172	0.077	0.82	6.830	0.870	150.93
20.65	27.15	20.58	2.84	0.028	0.230	0.122	0.76	6.932	0.883	181.23
18.50	28.06	28.85	6.29	0.061	0.340	0.179	0.66	7.120	0.907	206.11
16.40	29.11	36.92	10.27	0.098	0.455	0.215	0.56	7.301	0.930	250.32
14.40	30.60	44.62	15.91	0.148	0.591	0.250	0.47	7.426	0.946	260.18
12.90	31.69	50.38	20.04	0.183	0.701	0.261	0.41	7.497	0.955	288.7
10.75	35.11	58.65	32.99	0.285	0.883	0.323	0.31	7.599	0.968	316.17
9.50	37.55	63.46	42.23	0.352	1.007	0.350	0.25	7.607	0.969	314.64
8.20	41.95	68.46	58.90	0.463	1.154	0.401	0.20	7.622	0.971	319.00

$H_0 = 26.00$  mm ;  $D_0 = 26.40$  mm.



Table-B<sub>41</sub>

Upsetting of Sintered 1.14 % Graphite Admixed  
Iron Powder Preforms (H/D = 0.98) at 1000 °C

H <sub>t</sub> , mm	D <sub>t</sub> , mm	% ( $\frac{\Delta H}{H_0}$ )	% ( $\frac{\Delta D}{D_0}$ )	$\ln\left(\frac{D_t}{D_0}\right)$	$\ln\left(\frac{H_0}{H_t}\right)$	$\lambda = \frac{\ln\left(\frac{D_t}{D_0}\right)}{\ln\left(\frac{H_0}{H_t}\right)}$	$\left(\frac{H_t}{D_t}\right)$	$\rho_f$ gm/cm <sup>3</sup>	$\left(\frac{\rho_f}{\rho_{Th}}\right)$	VPN
26.00	26.40	0.00	0.00	0.000	0.000	-	0.98	6.523	0.831	145.10
22.40	26.93	13.85	2.01	0.020	0.149	0.133	0.83	6.806	0.867	152.50
20.45	27.59	21.35	4.51	0.044	0.240	0.184	0.74	6.994	0.891	185.00
17.60	28.78	32.31	9.02	0.086	0.390	0.221	0.61	7.214	0.919	225.00
15.25	29.96	41.35	13.48	0.126	0.534	0.237	0.51	7.410	0.944	276.10
12.90	32.00	50.38	21.21	0.192	0.701	0.274	0.40	7.536	0.960	300.00
10.20	36.78	60.77	39.32	0.332	0.936	0.354	0.28	7.638	0.973	310.00
8.70	40.65	66.54	53.98	0.432	1.095	0.394	0.21	7.654	0.975	330.00

H<sub>0</sub> = 26.00 mm ; D<sub>0</sub> = 26.40 mm.

Table-B<sub>42</sub>

Upsetting of Sintered 1.14 % Graphite Admixed  
Iron Powder Preforms (H/D = 0.98) at 1120 °C

H <sub>t</sub> , mm	D <sub>t</sub> , mm	$\% \left( \frac{\Delta H}{H_0} \right)$	$\% \left( \frac{\Delta D}{D_0} \right)$	$\ln \left( \frac{D_t}{D_0} \right)$	$\ln \left( \frac{H_0}{H_t} \right)$	$\lambda = \frac{\ln \left( \frac{D_t}{D_0} \right)}{\ln \left( \frac{H_0}{H_t} \right)}$	$\left( \frac{H_t}{D_t} \right)$	$\rho_f$ gm/cm <sup>3</sup>	$\left( \frac{\rho_f}{\rho_{Th}} \right)$	VPN
26.00	26.40	0.00	00.00	0.000	0.000	-	0.98	6.532	0.831	151.98
20.00	28.15	23.08	6.63	0.064	0.262	0.245	0.71	7.034	0.896	169.80
19.80	28.23	23.85	6.93	0.067	0.272	0.246	0.70	7.057	0.899	211.83
19.00	28.50	26.92	7.95	0.077	0.314	0.244	0.67	7.136	0.909	218.66
14.50	31.70	44.23	20.08	0.183	0.584	0.313	0.46	7.481	0.953	298.50
13.50	32.75	48.08	24.05	0.216	0.655	0.329	0.41	7.536	0.960	308.00
11.60	35.20	55.38	33.33	0.288	0.807	0.356	0.33	7.630	0.972	319.23
8.20	41.75	68.46	58.14	0.458	1.154	0.397	0.20	7.685	0.979	332.66

H<sub>0</sub> = 26.00 mm ; D<sub>0</sub> = 26.40 mm.

Table-B<sub>43</sub>

Upsetting of Sintered 1.86% Graphite Admixed  
Iron Powder Preforms (H/D = 0.57) at 800 °C

H <sub>t</sub> , mm	D <sub>t</sub> , mm	$\%(\frac{\Delta H}{H_0})$	$\%(\frac{\Delta D}{D_0})$	$\ln(\frac{D_t}{D_0})$	$\ln(\frac{H_0}{H_t})$	$\ln(\frac{D_t}{D_0}) / \ln(\frac{H_0}{H_t})$	$(\frac{H_t}{D_t})$	$\rho_f$ gm/cm <sup>3</sup>	$(\frac{\rho_f}{\rho_{Th}})$	VPN
15.00	26.40	0.00	0.00	0.000	0.000	-	0.57	6.516	0.830	-
12.40	28.03	17.33	6.17	0.060	0.190	0.315	0.44	7.018	0.894	185.67
10.50	29.58	30.00	12.04	0.114	0.357	0.319	0.35	7.277	0.927	224.17
8.70	32.64	42.00	23.64	0.212	0.545	0.389	0.27	7.448	0.949	243.00
8.35	33.14	44.33	25.55	0.227	0.586	0.388	0.25	7.458	0.950	251.83
7.25	35.53	51.67	34.58	0.297	0.727	0.409	0.20	7.536	0.960	268.83
6.70	38.00	55.33	43.94	0.364	0.806	0.452	0.18	7.590	0.967	275.67

H<sub>0</sub> = 15.00 mm ; D<sub>0</sub> = 26.40 mm.

Table-B  
44

Upsetting of Sintered 1.86 % Graphite Admixed  
Iron Powder Preforms (H/D = 0.57) at 850 °C

H <sub>t</sub> , mm	D <sub>t</sub> , mm	% ( $\frac{\Delta H}{H_0}$ )	% ( $\frac{\Delta D}{D_0}$ )	$\ln(\frac{D_t}{D_0})$	$\ln(\frac{H_0}{H_t})$	$\lambda = \frac{\ln(\frac{D_t}{D_0})}{\ln(\frac{H_0}{H_t})}$	( $\frac{H_t}{D_t}$ )	$\rho_f$ gm/cm <sup>3</sup>	( $\frac{\rho_f}{\rho_{Th}}$ )	VPN
15.00	26.40	0.00	0.00	0.000	0.000	-	0.57	6.520	0.831	-
11.50	28.50	23.33	7.95	0.077	0.266	0.288	0.40	7.167	0.913	217.33
11.00	28.00	26.67	9.93	0.090	0.310	0.290	0.38	7.245	0.923	228.21
10.60	29.53	29.33	11.86	0.112	0.347	0.323	0.36	7.293	0.929	234.79
7.90	32.28	47.33	22.27	0.201	0.641	0.314	0.24	7.521	0.958	297.96
7.60	34.53	49.33	30.80	0.268	0.680	0.395	0.22	7.544	0.961	302.17

H<sub>0</sub> = 15.00 mm ; D<sub>0</sub> = 26.40 mm.

Table-B 45

Upsetting of Sintered 1.86% Graphite Admixed  
Iron Powder Preforms (H/D = 0.57) at 900 °C

H <sub>t</sub> , mm	D <sub>t</sub> , mm	$\% \left( \frac{\Delta H}{H_0} \right)$	$\% \left( \frac{\Delta D}{D_0} \right)$	$\ln \left( \frac{D_t}{D_0} \right)$	$\ln \left( \frac{H_0}{H_t} \right)$	$\lambda = \frac{\ln \left( \frac{D_t}{D_0} \right)}{\ln \left( \frac{H_0}{H_t} \right)}$	$\left( \frac{H_t}{D_t} \right)$	$\rho_f$ gm/cm <sup>3</sup>	$\left( \frac{\rho_f}{\rho_{Th}} \right)$	VPN
15.00	26.40	0.00	0.00	0.000	0.000	-	0.57	6.539	0.833	-
11.40	28.75	24.00	8.90	0.085	0.274	0.311	0.40	7.237	0.922	232.17
8.65	32.10	42.33	21.59	0.195	0.550	0.355	0.27	7.488	0.954	283.83
7.80	33.23	48.00	25.87	0.230	0.654	0.352	0.23	7.536	0.960	307.97
6.20	38.38	58.67	45.38	0.374	0.884	0.423	0.16	7.638	0.973	338.11
5.25	41.50	65.00	57.20	0.452	1.050	0.431	0.13	-	-	347.04

H<sub>0</sub> = 15.00 mm ; D<sub>0</sub> = 26.40 mm.

Table-B  
46

Upsetting of Sintered 1.86 % Graphite Admixed  
Iron Powder Preforms (H/D = 0.57) at 950 °C

H <sub>t</sub> , mm	D <sub>t</sub> , mm	% ( $\frac{\Delta H}{H_0}$ )	% ( $\frac{\Delta D}{D_0}$ )	$\ln(\frac{D_t}{D_0})$	$\ln(\frac{H_0}{H_t})$	$\lambda = \frac{\ln(\frac{D_t}{D_0})}{\ln(\frac{H_0}{H_t})}$	$(\frac{H_t}{D_t})$	$\rho_f$ gm/cm <sup>3</sup>	$(\frac{\rho_f}{\rho_{Th}})$	VPN
15.00	26.40	0.00	0.00	0.000	0.000	-	0.57	6.522	0.871	-
13.40	27.28	10.67	3.33	0.033	0.113	0.290	0.49	6.900	0.879	202.56
12.40	27.60	17.33	4.55	0.044	0.190	0.234	0.45	7.081	0.902	218.59
9.50	30.50	36.67	15.53	0.144	0.457	0.316	0.31	7.433	0.947	278.09
8.60	31.68	42.67	20.00	0.182	0.556	0.328	0.27	7.552	0.962	300.80
7.00	35.25	53.33	33.52	0.289	0.762	0.379	0.20	7.630	0.972	334.69
5.90	38.35	60.67	45.27	0.373	0.933	0.400	0.15	-	-	350.96

H<sub>0</sub> = 15.00 mm ; D<sub>0</sub> = 26.40 mm.

Table-B<sub>47</sub>

Upsetting of Sintered 1.86 % Graphite Admixed  
Iron Powder Preforms (H/D = 0.57) at 1000 °C

H <sub>t</sub> , mm	D <sub>t</sub> , mm	% ( $\frac{\Delta H}{H_0}$ )	% ( $\frac{\Delta D}{D_0}$ )	$\ln(\frac{D_t}{D_0})$	$\ln(\frac{H_0}{H_t})$	$\lambda = \frac{\ln(\frac{D_t}{D_0})}{\ln(\frac{H_0}{H_t})}$	$(\frac{H_t}{D_t})$	$\rho_f$ gm/cm <sup>3</sup>	$(\frac{\rho_f}{\rho_{Th}})$	VPN
15.00	26.40	0.00	0.00	0.000	0.000	-	0.57	6.515	0.830	-
12.40	27.68	17.33	4.85	0.047	0.190	0.249	0.45	7.092	0.904	224.67
10.75	29.13	28.33	10.34	0.098	0.333	0.295	0.37	7.347	0.936	260.07
8.30	33.23	44.67	25.87	0.230	0.592	0.389	0.25	7.590	0.967	312.21
7.40	34.93	50.67	32.31	0.280	0.707	0.396	0.21	7.661	0.976	332.30
5.90	38.60	60.67	46.21	0.380	0.933	0.407	0.15	-	-	360.18

H<sub>0</sub> = 15.00 mm ; D<sub>0</sub> = 26.40 mm.

Table-B 48

Upsetting of Sintered 1.86 % Graphite Admixed  
Iron Powder Preforms (H/D = 0.57) at 1120 °C

H <sub>t</sub> , mm	D <sub>t</sub> , mm	% ( $\frac{\Delta H}{H_0}$ )	% ( $\frac{\Delta D}{D_0}$ )	$\ln(\frac{D_t}{D_0})$	$\ln(\frac{H}{H_t})$	$\lambda = \frac{\ln(\frac{D_t}{D_0})}{\ln(\frac{H}{H_t})}$	$(\frac{H_t}{D_t})$	$\rho_f$ gm/cm <sup>3</sup>	$(\frac{\rho_f}{\rho_{Th}})$	VPN
15.00	26.40	0.00	0.00	0.000	0.000	-	0.57	6.530	0.832	143.32
12.70	27.88	15.33	5.61	0.055	0.166	0.329	0.46	7.072	0.901	231.17
10.55	29.58	29.67	12.04	0.114	0.352	0.323	0.36	7.394	0.942	276.06
10.30	29.66	31.13	12.35	0.116	0.376	0.310	0.35	7.442	0.948	282.21
7.35	35.08	51.00	32.88	0.284	0.713	0.399	0.21	7.676	0.978	340.18
7.25	35.55	51.67	34.66	0.298	0.727	0.409	0.20	7.685	0.979	347.87
5.50	41.60	66.00	57.58	0.440	1.079	0.408	0.12	-	-	370.33

H<sub>0</sub> = 15.00 mm ; D<sub>0</sub> = 26.40 mm.



Table-B 49

Upsetting of Sintered 1.86 % Graphite Admixed  
Iron Powder Preforms ( $H/D = 0.98$ ) at 800 °C

$H_t$ , mm	$D_t$ , mm	$\%(\frac{\Delta H}{H_0})$	$\%(\frac{\Delta D}{D_0})$	$\ln(\frac{D_t}{D_0})$	$\ln(\frac{H_0}{H_t})$	$\ln(\frac{D_t}{D_0}) = \frac{\ln(\frac{D_t}{D_0})}{\ln(\frac{H_0}{H_t})}$	$(\frac{H_t}{D_t})$	$\rho_f$ gm/cm <sup>3</sup>	$(\frac{\rho_f}{\rho_{Th}})$	VPN
26.00	26.40	0.00	0.00	0.000	0.000	-	0.98	6.531	0.832	-
18.90	29.40	27.31	11.36	0.108	0.319	0.337	0.64	6.970	0.888	208.50
16.95	30.63	34.81	16.02	0.149	0.428	0.347	0.55	7.080	0.902	247.06
15.20	31.39	41.54	18.90	0.173	0.534	0.324	0.48	7.191	0.916	273.97
10.00	38.33	61.54	45.19	0.373	0.956	0.390	0.26	7.425	0.946	354.01
8.60	41.33	66.92	56.55	0.448	1.106	0.405	0.21	7.458	0.950	376.16

$H_0 = 26.00$  mm ;  $D_0 = 26.40$  mm

Table-B<sub>50</sub>  
 Upsetting of Sintered 1.86 % Graphite Admixed  
 Iron Powder Preforms (H/D = 0.98) at 850 °C

H <sub>t</sub> , mm	D <sub>t</sub> , mm	% ( $\frac{\Delta H}{H_0}$ )	% ( $\frac{\Delta D}{D_0}$ )	$\ln(\frac{D_t}{D_0})$	$\ln(\frac{H_0}{H_t})$	$\lambda = \frac{\ln(\frac{D_t}{D_0})}{\ln(\frac{H_0}{H_t})}$	$(\frac{H_t}{D_t})$	$\rho_f$ gm/cm <sup>3</sup>	$(\frac{\rho_f}{\rho_{Th}})$	VPN
26.00	26.40	0.00	0.00	0.000	0.000	-	0.97	6.516	0.830	-
20.70	27.85	20.38	5.49	0.053	0.228	0.235	0.74	6.876	0.876	195.50
18.30	29.21	29.62	10.64	0.101	0.351	0.288	0.63	7.040	0.897	243.09
16.00	30.80	38.46	16.67	0.154	0.486	0.317	0.52	7.191	0.916	288.96
9.80	38.68	62.31	46.52	0.382	0.976	0.391	0.25	7.456	0.950	309.16
8.80	40.10	66.15	51.89	0.418	1.083	0.386	0.22	7.510	0.957	390.01

H<sub>0</sub> = 26.00 mm ; D<sub>0</sub> = 26.40 mm

Table-B  
51

Upsetting of Sintered 1.86 % Graphite Admixed  
Iron Powder Preforms ( $H/D = 0.99$ ) at  $900^\circ\text{C}$

$H_t$ , mm	$D_t$ , mm	$\%(\frac{\Delta H}{H_0})$	$\%(\frac{\Delta D}{D_0})$	$\ln(\frac{D_t}{D_0})$	$\ln(\frac{H_0}{H_t})$	$\gamma = \frac{\ln(\frac{D_t}{D_0})}{\ln(\frac{H_0}{H_t})}$	$(\frac{H_t}{D_t})$	$\rho_f$ gm/cm <sup>3</sup>	$(\frac{\rho_f}{\rho_{Th}})$	VPN
26.00	26.40	0.00	0.00	0.000	0.000	-	0.97	6.522	0.831	-
19.30	28.90	25.77	9.47	0.090	0.298	0.304	0.67	7.000	0.892	223.89
19.00	29.10	26.92	10.23	0.097	0.314	0.310	0.65	7.034	0.896	232.03
16.90	30.45	35.00	15.34	0.143	0.431	0.331	0.56	7.175	0.914	273.17
14.30	32.50	45.00	23.11	0.208	0.598	0.348	0.44	7.308	0.931	316.18
9.50	40.35	63.35	52.84	0.424	1.007	0.421	0.24	7.543	0.961	381.97

$H_0 = 26.00$  mm ;  $D_0 = 26.40$  mm

Table-B 52

Upsetting of Sintered 1.86 % Graphite Admixed  
Iron Powder Preforms (H/D = 0.98) at 950 °C

$H_t$ , mm	$D_t$ , mm	$\% \left( \frac{\Delta H}{H_0} \right)$	$\% \left( \frac{\Delta D}{D_0} \right)$	$\ln \left( \frac{D_t}{D_0} \right)$	$\ln \left( \frac{H_0}{H_t} \right)$	$\lambda = \frac{\ln \left( \frac{D_t}{D_0} \right)}{\ln \left( \frac{H_0}{H_t} \right)}$	$\left( \frac{H_t}{D_t} \right)$	$\rho_f$ gm/cm <sup>3</sup>	$\left( \frac{\rho_f}{\rho_{Th}} \right)$	VPN
26.00	26.40	0.00	0.00	0.000	0.000	-	0.97	6.516	0.830	-
22.10	27.60	15.00	4.55	0.044	0.163	0.273	0.35	7.033	0.869	178.51
18.80	29.18	27.69	10.53	0.100	0.324	0.309	0.64	7.064	0.900	237.33
16.50	30.55	36.54	15.72	0.146	0.455	0.321	0.54	7.237	0.922	283.04
14.00	32.93	46.15	24.73	0.221	0.619	0.357	0.43	7.395	0.942	323.91
9.50	39.88	63.46	51.06	0.413	1.007	0.410	0.24	7.567	0.964	391.83

$H_0 = 26.00$  mm ;  $D_0 = 26.40$  mm

Table-B53

Upsetting of Sintered 1.86 % Graphite Admixed  
Iron Powder Preforms (H/D = 0.98) at 1000 °C

$H_t$ , mm	$D_t$ , mm	$\% \left( \frac{\Delta H}{H_0} \right)$	$\% \left( \frac{\Delta D}{D_0} \right)$	$\ln \left( \frac{D_t}{D_0} \right)$	$\ln \left( \frac{H_0}{H_t} \right)$	$\lambda = \frac{\ln \left( \frac{D_t}{D_0} \right)}{\ln \left( \frac{H_0}{H_t} \right)}$	$\left( \frac{H_t}{D_t} \right)$	$\rho_f$ gm/cm <sup>3</sup>	$\left( \frac{\rho_f}{\rho_{Th}} \right)$	VPN
26.00	26.40	0.00	0.00	0.000	0.000	-	0.97	6.530	0.832	-
18.20	29.48	30.00	11.67	0.110	0.357	0.309	0.62	7.143	0.910	263.66
17.40	29.60	33.08	12.12	0.114	0.402	0.285	0.59	7.200	0.917	278.33
13.50	33.28	48.08	26.06	0.232	0.655	0.354	0.41	7.441	0.948	348.00
11.50	36.20	55.77	37.12	0.316	0.816	0.387	0.32	7.528	0.959	376.06
9.80	38.78	62.31	46.89	0.385	0.976	0.394	0.25	7.602	0.968	402.12

$H_0 = 26.00$  mm ;  $D_0 = 26.40$  mm

Table-B  
54

Upsetting of Sintered 1.86 % Graphite Admixed  
Iron Powder Preforms (H/D = 0.98) at 1120 °C

$H_t$ , mm	$D_t$ , mm	$\% \left( \frac{\Delta H}{H_0} \right)$	$\% \left( \frac{\Delta D}{D_0} \right)$	$\ln \left( \frac{D_t}{D_0} \right)$	$\ln \left( \frac{H_0}{H_t} \right)$	$\ln \left( \frac{D_t}{D_0} \right) = \frac{\ln \left( \frac{D_t}{D_0} \right)}{\ln \left( \frac{H_0}{H_t} \right)}$	$\left( \frac{H_t}{D_t} \right)$	$\rho_f$ gm/cm <sup>3</sup>	$\left( \frac{\rho_f}{\rho_{Th}} \right)$	VPN
26.00	26.40	0.00	0.00	0.000	0.000	-	0.97	6.520	0.831	-
22.05	27.34	15.19	3.56	0.035	0.165	0.212	0.81	6.877	0.876	-
17.10	30.18	34.23	14.23	0.134	0.419	0.319	0.57	7.251	0.924	288.07
16.70	30.44	35.76	15.30	0.142	0.443	0.321	0.55	7.263	0.925	295.89
14.50	31.78	44.23	20.34	0.185	0.584	0.318	0.46	7.410	0.944	-
12.20	35.41	53.08	34.13	0.294	0.757	0.388	0.34	7.518	0.958	376.12
11.70	35.83	55.00	35.72	0.305	0.799	0.383	0.33	7.569	0.964	384.37
7.70	43.70	70.38	65.53	0.504	1.217	0.414	0.18	7.656	0.975	438.12

$H_0 = 26.00$  mm ;  $D_0 = 26.40$  mm

Table-B<sub>55</sub>

Upsetting of 0.43 P-Fe Alloy Powder Preforms  
(H/D = 0.59) at 960 °C

H <sub>t</sub> , mm	D <sub>t</sub> , mm	$\% \left( \frac{\Delta H}{H_0} \right)$	$\% \left( \frac{\Delta D}{D_0} \right)$	$\ln \left( \frac{D_t}{D_0} \right)$	$\ln \left( \frac{H_0}{H_t} \right)$	$\ln \left( \frac{D_t}{D_0} \right) = \frac{\ln \left( \frac{D_t}{D_0} \right)}{\ln \left( \frac{H_0}{H_t} \right)}$	$\left( \frac{H_t}{D_t} \right)$	$\rho_f$ gm/cm <sup>3</sup>	$\left( \frac{\rho_f}{\rho_{Th}} \right)$	VPN
15.50	26.25	0.00	0.00	0.000	0.000	-	0.59	6.582	0.838	78.25
12.40	27.80	20.00	5.90	0.057	0.223	0.257	0.45	7.212	0.919	115.12
9.30	31.48	40.00	19.92	0.182	0.511	0.355	0.30	7.527	0.959	159.76
8.50	32.80	45.16	24.95	0.223	0.601	0.371	0.26	7.669	0.977	161.87
6.30	38.10	59.35	45.14	0.373	0.900	0.414	0.17	7.756	0.988	162.50
5.20	42.05	66.45	60.19	0.471	1.092	0.431	0.13	7.787	0.992	173.89

H<sub>0</sub> = 15.50 mm ; D<sub>0</sub> = 26.25 mm

Table - C<sub>1</sub>

Data of Partially Open Step Down Cylindrical Die on Forging of Sintered Iron Powder Preforms (H/D = 1.18) at 1120°C.

$h$ , mm	$D_t$ , mm	$h_c$ cm <sup>2</sup>	$V_c$ , cm <sup>2</sup>	$f_{hc}$	$f_{vc}$	$\Phi = \left(\frac{f_{hc}}{f_{vc}}\right)$	$f_{fc}$ , cm/cm <sup>3</sup>	$\left(\frac{f_{fc}}{f_{th}}\right)$	VPN
19.10	28.23	0.70	4.49	0.05	0.33	0.14	7.185	0.915	68.25
14.90	25.73	1.38	5.17	0.09	0.38	0.24	7.396	0.942	70.50
9.10	33.05	5.94	8.57	0.38	0.62	0.61	7.728	0.985	73.59
6.70	36.20	8.02	10.80	0.52	0.79	0.66	7.768	0.990	84.65
5.50	40.80	10.80	10.96	0.70	0.80	0.87	7.805	0.994	130.30
3.60	47.60	15.53	13.74	1.00	1.00	1.00	7.822	0.997	150.67

$H_o = 31.75$  mm ;  $D_o = 26.40$  mm.



Table - C<sub>2</sub>

Data of Partially Open Step Down Cylindrical Die on Forging of Sintered  
0.43 % Graphite Admixed Iron Powder Preforms (H/D = 1.18) at 1120°C

h, mm	D <sub>t</sub> , mm	h <sub>c</sub> , cm <sup>2</sup>	v <sub>c</sub> , cm <sup>3</sup>	f <sub>hc</sub>	f <sub>vc</sub>	$\phi = \left(\frac{f_{hc}}{f_{vc}}\right)$	f <sub>fc</sub> gm/cm <sup>3</sup>	$\left(\frac{f_{fc}}{f_{Th}}\right)$	VPN
21.40	26.90	2.86	4.49	0.16	0.34	0.47	7.065	0.900	83.60
14.80	30.00	4.00	6.24	0.24	0.47	0.51	7.401	0.943	98.62
8.90	32.70	5.32	7.76	0.32	0.59	0.55	7.726	0.984	103.44
7.80	34.60	6.32	8.63	0.38	0.65	0.59	7.766	0.989	116.33
4.70	42.00	11.58	11.23	0.70	0.85	0.83	7.772	0.990	121.74
3.50	48.90	16.51	13.26	1.00	1.00	1.00	7.789	0.992	122.08

H<sub>0</sub> = 31.75 mm ; D<sub>0</sub> = 26.40 mm.

Table C<sub>3</sub>

Data of Partially Open Step Down Cylindrical Die on Forging of Sintered  
1.14 % Graphite Admixed Iron Powder Preforms (H/D = 1.18) at 1120°C

h, mm	D <sub>t</sub> , mm	h <sub>c</sub> , cm <sup>2</sup>	v <sub>c</sub> , cm <sup>2</sup>	f <sub>hc</sub>	f <sub>vc</sub>	$\Phi = \left( \frac{f_{hc}}{f_{vc}} \right)$	$\rho_{fc}$ , gm/cm <sup>3</sup>	$\left( \frac{\rho_{fc}}{\rho_{Th}} \right)$	VPN
21.60	26.50	0.00	2.67	0.00	0.22	0.00	7.016	0.894	106.66
18.20	30.75	1.37	4.49	0.09	0.38	0.23	7.322	0.933	138.90
17.30	31.03	4.48	6.95	0.32	0.58	0.55	7.510	0.957	140.16
7.40	37.00	8.23	10.22	0.59	0.86	0.69	7.735	0.985	146.42
6.90	37.65	8.86	10.59	0.63	0.89	0.71	7.757	0.988	156.86
4.50	45.50	13.99	11.93	1.00	1.00	1.00	7.833	0.998	181.75

H<sub>0</sub> = 31.75 mm ; D<sub>0</sub> = 26.40 mm.

Table C4

Data of Partially Open Step Down Cylindrical Die on Forging of Sintered  
1.86 % Graphite Admixed Iron Powder Preforms ( $H/D = 1.18$ ) at  $1120^{\circ}\text{C}$

$h$ , mm	$D_t$ , mm	$h_c$ , $\text{cm}^2$	$V_c$ , $\text{cm}^2$	$f_{hc}$	$f_{vc}$	$\bar{\phi} = \left(\frac{f_{hc}}{f_{vc}}\right)$	$\rho_{fc}$ , $\text{gm}/\text{cm}^3$	$\left(\frac{\rho_{fc}}{\rho_{Th}}\right)$	VPN
14.30	29.85	3.92	6.83	0.25	0.52	0.47	7.214	0.919	131.98
12.70	30.60	4.28	7.14	0.27	0.55	0.49	7.371	0.939	135.73
6.20	39.50	9.98	10.50	0.63	0.80	0.63	7.767	0.989	170.28
5.30	41.70	11.39	11.94	0.72	0.92	0.79	7.829	0.994	197.00
5.00	43.80	12.80	12.00	0.81	0.92	0.88	7.806	0.997	250.50
3.90	48.00	15.83	13.05	1.00	1.00	1.00	7.850	1.000	299.50

$H_o = 31.75$  mm ;  $D_o = 26.40$  mm.

Table - C<sub>5</sub>

Data of Partially Open Step Down Cylindrical Die on Forging of Sintered  
0.45 % P-Fe Alloy Powder Preforms (H/D = 1.18) at 960°C

h, mm	D <sub>t</sub> , mm	h <sub>c</sub> , cm <sup>2</sup>	v <sub>c</sub> , cm <sup>2</sup>	f <sub>hc</sub>	f <sub>vc</sub>	$\phi = \left(\frac{f_{hc}}{f_{vc}}\right)$	$\rho_{fc}$ , gm/cm <sup>3</sup>	$\left(\frac{\rho_{fc}}{\rho_{Th}}\right)$	VPN
11.20	32.63	5.28	7.45	0.34	0.60	0.58	7.598	0.968	95.76
8.40	35.77	6.97	8.76	0.45	0.70	0.64	7.670	0.977	110.07
4.30	46.00	14.35	11.87	0.93	0.95	0.98	7.761	0.989	183.42
4.10	47.37	15.35	12.46	1.00	1.00	1.00	7.774	0.990	200.47

H<sub>0</sub> = 31.75 mm ; D<sub>0</sub> = 26.40 mm

Table - C<sub>6</sub>

Data of Partially Open Hemi-Spherical Die on Forging of Sintered Iron Powder Preforms (H/D = 1.18) at 1120°C.

h, mm	D <sub>t</sub> , mm	h <sub>c</sub> , cm <sup>2</sup>	v <sub>c</sub> , cm <sup>2</sup>	f <sub>hc</sub>	f <sub>vc</sub>	$\Phi = \left(\frac{f_{hc}}{f_{vc}}\right)$	Pfc, gm/cm <sup>3</sup>	$\left(\frac{Pfc}{\rho_{th}}\right)$	VPN
12.60	28.65	4.64	12.64	0.27	0.66	0.12	7.317	0.932	71.70
10.30	29.60	5.17	13.70	0.31	0.71	0.43	7.426	0.946	72.70
7.70	30.50	7.02	14.92	0.41	0.78	0.53	7.533	0.962	77.30
6.30	34.80	9.05	16.80	0.53	0.87	0.61	7.706	0.982	85.08
6.00	36.00	9.80	16.00	0.58	0.83	0.69	7.717	0.983	87.70
4.40	42.40	13.79	18.01	0.81	0.94	0.87	7.731	0.985	144.80
3.40	46.90	16.94	19.22	1.00	1.00	1.00	7.744	0.987	151.48

H<sub>0</sub> = 31.75 mm ; D<sub>0</sub> = 26.40 mm.

Table - C<sub>7</sub>

Data of Partially Open Hemi-Spherical Die on Forging of Sintered  
0.43 % Graphite Admixed Iron Powder Preforms (H/D = 1.18) at 1120°C.

h, mm	D <sub>t</sub> , mm	h <sub>c</sub> , cm <sup>2</sup>	v <sub>c</sub> , cm <sup>2</sup>	f <sub>hc</sub>	f <sub>vc</sub>	$\Phi = \left(\frac{f_{hc}}{f_{vc}}\right)$	$\rho_{fc}$ , gm/cm <sup>3</sup>	$\left(\frac{\rho_{fc}}{\rho_{Th}}\right)$	VPN
10.80	31.45	5.19	12.59	0.31	0.69	0.45	7.335	0.934	77.72
7.80	32.00	6.41	14.65	0.38	0.80	0.48	7.545	0.961	96.06
5.20	38.20	11.08	17.47	0.66	0.95	0.69	7.660	0.976	125.12
4.30	42.80	14.06	17.91	0.83	0.98	0.85	7.716	0.983	132.00
3.10	46.80	16.87	18.31	1.00	1.00	1.00	7.737	0.986	146.58

H<sub>o</sub> = 31.75 mm ; D<sub>o</sub> = 26.40 mm.

Table - C<sub>8</sub>

Data of Partially Open Hemi-Spherical Die on Forging of Sintered  
1.14% Graphite Admixed Iron Powder Preforms (H/D = 1.18) at 1120°C.

h, mm	D <sub>t</sub> , mm	h <sub>c</sub> , cm <sup>2</sup>	v <sub>c</sub> , cm <sup>2</sup>	f <sub>hc</sub>	f <sub>vc</sub>	$\Phi = \left(\frac{f_{hc}}{f_{vc}}\right)$	$\rho_{fc}$ , gm/cm <sup>3</sup>	$\left(\frac{\rho_{fc}}{\rho_{Th}}\right)$	VPN
20.20	27.05	2.61	6.07	0.18	0.32	0.54	7.168	0.913	75.20
18.00	28.80	4.49	6.60	0.30	0.35	0.86	7.284	0.928	114.92
16.50	29.35	4.77	6.89	0.32	0.37	0.87	7.387	0.941	116.55
6.50	34.10	8.78	16.91	0.59	0.90	0.65	7.725	0.984	132.10
4.40	37.40	10.65	17.02	0.72	0.91	0.79	7.789	0.992	152.00
3.90	37.50	10.71	17.52	0.72	0.93	0.77	7.861	1.001	161.94
3.20	39.70	12.38	18.06	0.83	0.96	0.86	7.877	1.003	230.00
2.40	44.00	14.87	18.76	1.00	1.00	1.00	7.850	1.000	241.50

H<sub>0</sub> = 31.75 mm ; D<sub>0</sub> = 26.40 mm

Table - C<sub>9</sub>

Data of Partially Open Hemi-Spherical Die on Forging of Sintered  
1.86% Graphite Admixed Iron Powder Preforms (H/D = 1.18) at 1120°C.

h, mm	D <sub>t</sub> , mm	h <sub>c</sub> , cm <sup>2</sup>	v <sub>c</sub> , cm <sup>2</sup>	f <sub>hc</sub>	f <sub>vc</sub>	$\bar{\phi} = \left( \frac{f_{hc}}{f_{vc}} \right)$	ρ <sub>fc</sub> , gm/cm <sup>3</sup>	$\left( \frac{\rho_{fc}}{\rho_{th}} \right)$	VPN
23.90	26.50	1.99	5.11	0.13	0.27	0.47	6.773	0.863	138.56
10.00	31.00	5.28	13.29	0.35	0.71	0.48	7.334	0.936	159.38
9.10	31.45	7.42	14.61	0.49	0.79	0.62	7.482	0.953	170.86
4.50	37.50	11.04	17.61	0.72	0.95	0.76	7.839	0.999	192.35
4.00	41.30	13.06	18.02	0.85	0.97	0.88	7.850	1.000	218.00
3.90	42.00	13.52	18.52	0.88	0.99	0.89	7.850	1.000	254.86
3.40	44.60	15.29	18.59	1.00	1.00	1.00	7.850	1.000	331.00

H<sub>0</sub> = 31.75 mm ; D<sub>0</sub> = 26.40 mm.



Table - C<sub>10</sub>

Data of Partially Open, Hemi-Spherical Die on Forging of Sintered  
0.45 % P-Fe Alloy Powder Preforms (H/D = 1.18) at 960°C

$(H_t/H_o)$ h, mm	$D_t$ , mm	$h_c$ , cm <sup>2</sup>	$v_c$ cm <sup>2</sup>	$f_{hc}$	$f_{vc}$	$\Phi = \left(\frac{f_{hc}}{f_{yc}}\right)$	$\rho_{fc}$ , gm/cm <sup>3</sup>	$\left(\frac{\rho_{fc}}{\rho_{Th}}\right)$	VPN
8.90	31.93	6.45	14.74	0.40	0.73	0.55	7.556	0.962	120.82
4.90	38.50	11.31	17.71	0.70	0.88	0.80	7.728	0.984	142.27
4.00	43.47	14.51	19.00	0.90	0.94	0.95	7.753	0.988	193.83
3.30	45.83	16.71	20.17	1.00	1.00	1.00	7.779	0.991	199.25

APPENDIX - DPROCEDURE OF CERAMIC COATING

Basic purpose of applying ceramic coating over the entire surface of the compact was to ensure against oxidation and decarburization during sintering and upto transferring it to the forging press.

5 gms of STAHLGUARD-PM2 was thoroughly mixed in 16 ml. of aqueous solution [99] in a plastic bottle by a wooden stirrer. Slurry, so prepared was applied over the entire surface of the compacts and then coating was allowed to dry under room temperature conditions for a period of six hours. After this, compacts were re-coated using the same slurry in the direction perpendicular to the previous coating. Final coatings were dried again under the similar conditions for a period of twelve hours.

APPENDIX 'E'MODEL CALCULATIONS FOR UPSET FORGING

Initial height of the preform and diameter were taken as 15 and 26.40 mm respectively. After having deformed the sintered sample at 800°C of forging temperature, the following measurements were taken :

- (1) Forged height,  $H_t$ , (average height)
- (2) Forged diameter,  $D_t$  (average dia)
- (3) Mass of the Machined preform
- (4) Volume of the preform by water immersion technique.

The following other parameters were calculated:

- (1) per cent height reduction
- (2) per cent diameter increase  
[Degree of diametrical flow]
- (3) true diameter strain
- (4) true height strain
- (5) Poisson's Ratio,
- (6) forged aspect ratio,  $H_t/D_t$
- (7) the relative density.
- (8) forged density, and
- (9) the hardness, VPN

Measured Parameters

$$H_o = 15.00 \text{ mm}$$

$$D_o = 26.40 \text{ mm}$$

$$H_t = 10.50 \text{ mm}$$

$$D_t = 28.85 \text{ mm}$$

Above values are average of 3 to 4 observations in different directions.

### Calculated Quantities

(1) Per cent Height Reductions,  $\left(\frac{\Delta H}{H_0}\right) \times 100$

$$= \frac{15.00 - 10.50}{15.00} \times 100$$

$$= 30 \%$$

(2) Per cent Diametrical Deformation

$$100 \times \left(\frac{\Delta D}{D_0}\right) = \frac{28.85 - 26.40}{26.40} \times 100$$

$$= 9.28 \%$$

(3) True Height Strain

$$= \ln\left(\frac{H_0}{H_t}\right) = \ln\left(\frac{15}{10.5}\right) = 0.357$$

(4) True Diameter Strain

$$= \ln\left(\frac{D_t}{D_0}\right) = \ln\left(\frac{28.85}{26.40}\right)$$

$$= 0.089$$

(5) Poisson's Ratio ;  $= \ln\left(\frac{D_t}{D_0}\right) / \ln\left(\frac{H_0}{H_t}\right)$

$$= \frac{0.089}{0.357} = 0.249$$

$$(6) \quad \text{Final Aspect Ratio} = \left( \frac{H_t}{D_t} \right) = \frac{10.50}{28.85} = 0.36.$$

Density was calculated using Archimedes principle and relative density was calculated assuming theoretical density to be 7.85 gm/CC.

### Evaluation of Coefficients of Second Order Polynomial

Observations of all the plots corresponding to theoretical density vs height strain (expressed in ln terms) appear to be parabolic in nature for all temperatures of upset forging. Therefore, the curves drawn using least square method were evaluated for parabolic behaviour as follows :

$$\ln\left(\frac{\rho_f}{\rho_{Th}}\right) = a_0 + a_1 \ln\left(\frac{H_0}{H_t}\right) + a_2 \left[ \ln\left(\frac{H_0}{H_t}\right) \right]^2 \quad \dots(E.1)$$

The values of constants were chosen in a manner so that

$$P = \left\{ \ln\left(\frac{\rho_f}{\rho_{Th}}\right) - a_0 - a_1 \ln\left(\frac{H_0}{H_t}\right) - a_2 \left[ \ln\left(\frac{H_0}{H_t}\right) \right]^2 \right\}^2 \quad \dots(E.2)$$

is minimum.

Differentiating (2) partially with respect to  $a_0$ ,  $a_1$ ,  $a_2$  respectively, the following necessary conditions were obtained :

$$\sum \left[ \ln\left(\frac{\rho_f}{\rho_{Th}}\right) - a_0 - a_1 \ln\left(\frac{H_0}{H_t}\right) - a_2 \left\{ \ln\left(\frac{H_0}{H_t}\right) \right\}^2 \right] = 0$$

$$\sum \ln\left(\frac{H_0}{H_t}\right) \left[ \ln\left(\frac{\rho_f}{\rho_{Th}}\right) - a_0 - a_1 \ln\left(\frac{H_0}{H_t}\right) - a_2 \left\{ \ln\left(\frac{H_0}{H_t}\right) \right\}^2 \right] = 0$$

$$\sum \left( \left[ \ln\left(\frac{H_0}{H_t}\right) \right]^2 \left\{ \ln\left(\frac{\rho_f}{\rho_{Th}}\right) - a_0 - a_1 \ln\left(\frac{H_0}{H_t}\right) - a_2 \ln\left(\frac{H_0}{H_t}\right) \right\}^2 \right) = 0$$

Therefore the normal equations are :

$$\left[ \left( \frac{\rho_f}{\rho_{Th}} \right) \right] - n a_0 - \left[ \left\{ \ln\left(\frac{H_0}{H_t}\right) \right\} \left\{ \ln\left(\frac{H_0}{H_t}\right) \right\} \right] a_2 = 0 \dots (E.3)$$

$$\begin{aligned} \left\{ \ln\left(\frac{H_0}{H_t}\right) \right\} \left\{ \frac{\rho_f}{\rho_{Th}} \right\} - \left[ \ln\left(\frac{H_0}{H_t}\right) \right] a_0 - \left\{ \ln\left(\frac{H_0}{H_t}\right) \right\} \left\{ \ln\left(\frac{H_0}{H_t}\right) \right\} a_1 \\ - \left[ \left\{ \ln\left(\frac{H_0}{H_t}\right) \right\} \left\{ \ln\left(\frac{H_0}{H_t}\right) \right\} \left\{ \ln\left(\frac{H_0}{H_t}\right) \right\} \right] a_2 = 0 \\ \dots (E.4) \end{aligned}$$

$$\begin{aligned} \left[ \left\{ \ln\left(\frac{H_0}{H_t}\right) \right\} \left\{ \ln\left(\frac{H_0}{H_t}\right) \right\} \left\{ \frac{\rho_f}{\rho_{Th}} \right\} \right] - \left\{ \ln\left(\frac{H_0}{H_t}\right) \right\} \left\{ \ln\left(\frac{H_0}{H_t}\right) \right\} a_0 \\ - \left\{ \ln\left(\frac{H_0}{H_t}\right) \right\} \left\{ \ln\left(\frac{H_0}{H_t}\right) \right\} \left\{ \ln\left(\frac{H_0}{H_t}\right) \right\} a_1 \\ - \left[ \left\{ \ln\left(\frac{H_0}{H_t}\right) \right\} \left\{ \ln\left(\frac{H_0}{H_t}\right) \right\} \left\{ \ln\left(\frac{H_0}{H_t}\right) \right\} \left\{ \ln\left(\frac{H_0}{H_t}\right) \right\} \right] a_2 = 0 \\ \dots (E.5) \end{aligned}$$

The solutions of the above equations i.e. E.3 to E.5 provides the most suitable values of  $a_0$ ,  $a_1$  and  $a_2$ .

Sample Calculation

System chosen ; 0.3 %C-Fe alloy, H/D=0.57 and Forging Temperature = 800°C

Data (from plot)

x [ =ln(H <sub>0</sub> /H <sub>t</sub> ) ]	0.1	0.2	0.3	0.4	0.5	0.6	0.7
y [=(P <sub>f</sub> /P <sub>Th</sub> )]	0.894	0.925	0.946	0.963	0.977	0.985	0.987

Assuming that  $y = b_0 + b_1x + b_2x^2$ , where to simplify the arithmetic the value of x is taken as equal to  $10x-4$  and tabulated the working as follows :

x	y	x <sup>2</sup>	x <sup>3</sup>	x <sup>4</sup>	xy	xy <sup>2</sup>	y( Calc. )	d	d <sup>2</sup>	
0.1	-3	0.894	9	-27	81	-2.682	8.046	0.8949	-0.0009	0.81x10 <sup>-6</sup>
0.2	-2	0.925	4	-08	16	-1.850	3.700	0.9231	0.0019	3.61x10 <sup>-6</sup>
0.3	-1	0.946	1	-01	01	-0.946	0.946	0.9462	-0.0002	0.04x10 <sup>-6</sup>
0.4	0	0.963	0	00	00	0.000	0.000	0.9641	-0.0011	1.21x10 <sup>-6</sup>
0.5	1	0.977	1	01	01	0.977	0.977	0.9769	0.0001	0.01x10 <sup>-6</sup>
0.6	2	0.985	4	08	16	1.970	3.940	0.9846	0.0004	0.16x10 <sup>-6</sup>
0.7	3	0.987	9	27	81	2.961	8.883	0.9871	-0.0001	0.01x10 <sup>-6</sup>
Sum	0	6.677	28	0	196	0.430	26.492			5.85x10 <sup>-6</sup>

Hence the normal equations are

$$\begin{aligned}
 7b_0 + 28b_2 &= 6.667 \\
 28b_1 &= 0.430 \\
 28b_0 + 196b_2 &= 26.492
 \end{aligned}$$

which on simplification yields  $b_0 = -0.96414$ ,  $b_1 = 0.01537$  and  $b_2 = -0.0025714$

$$\begin{aligned}
\text{Therefore, } y &= 0.96414 + 0.015357 X - 0.0025714 X^2 \\
&= 0.96414 + 0.015357(10x-4) - 0.0025714(10x-4)^2 \\
&= 0.86156 + 0.35928.x - 0.25714 x^2
\end{aligned}$$

which gives for equation

$$y = a_0 + a_1x + a_2x^2, \quad a_0 = 0.86156, \quad a_1 = 0.35928, \quad a_2 = 0.25714.$$

The mean square error ( $\alpha^2$ ) is estimated as

$$\alpha^2 = [dd]/(n-3) = \frac{5.85 \times 10^{-6}}{4} = 1.4625 \times 10^{-6}.$$

If the standard errors of  $a_0$ ,  $a_1$  and  $a_2$  be denoted by  $\alpha_0$ ,  $\alpha_1$  and  $\alpha_2$  respectively, then we have

$$\frac{\alpha_0^2}{\begin{vmatrix} 28 & 0 \\ 0 & 196 \end{vmatrix}} = \frac{\alpha_1^2}{\begin{vmatrix} 7 & 28 \\ 28 & 196 \end{vmatrix}} = \frac{\alpha_2^2}{\begin{vmatrix} 7 & 0 \\ 0 & 28 \end{vmatrix}} = \frac{\alpha^2}{\begin{vmatrix} 7 & 0 & 28 \\ 0 & 28 & 0 \\ 28 & 0 & 196 \end{vmatrix}}$$

$$\text{Therefore, } \frac{\alpha_0^2}{112} = \frac{\alpha_1^2}{12} = \frac{\alpha_2^2}{4} = \frac{1.4625 \times 10^{-6}}{336}$$

$$\begin{aligned}
\text{Therefore, } \alpha_0 &= \pm 6.982 \times 10^{-4}, \quad \alpha_1 = \pm 2.285 \times 10^{-4}, \\
\alpha_2 &= \pm 1.319 \times 10^{-4}
\end{aligned}$$

Hence,

$$\begin{aligned}
y &= (0.86156 \pm 6.982 \times 10^{-4}) + (0.35928 \pm 2.285 \times 10^{-4})x \\
&\quad - (0.25714 \pm 1.319 \times 10^{-4})x^2.
\end{aligned}$$



Model Calculations In Partially Open Step-Down  
Cylindrical Die Cavity Forgings

Diameters of the step down cylindrical die cavity in order of decreasing magnitude is given as below :

$$D_1 = 29.80 \text{ mm}$$

$$D_2 = 26.60 \text{ mm}$$

$$D_3 = 19.80 \text{ mm, and}$$

$$D_4 = 17.20 \text{ mm}$$

Step depths are as follows :

$$2.5 \text{ mm, } 7.5 \text{ mm and } 12.5 \text{ mm}$$

Therefore,

$$\pi D_1 = 9.362 \text{ cm}$$

$$\pi D_2 = 8.357 \text{ cm}$$

$$\pi D_3 = 6.220 \text{ cm}$$

$$\pi D_4 = 5.341 \text{ cm}$$

$$\text{or, } \pi D_1 h_1 = 2.340 \text{ cm}^2; \quad h_1 = 2.50 \text{ mm}$$

$$\pi D_2 h_2 = 4.178 \text{ cm}^2; \quad h_2 = 5.00 \text{ mm}$$

$$\pi D_3 h_3 = 3.110 \text{ cm}^2; \quad h_3 = 5.00 \text{ mm}$$

$$\pi D_4 h_4 = 4.112 \text{ cm}^2; \quad h_4 = 6.8 \text{ mm.}$$

The total vertical constraint is assumed to be the total vertical surface area coming in contact with the die and similarly the total horizontal area is evaluated on the basis of the horizontal surface area of deforming preform with that of the die cavity.

Therefore, the total vertical constraint

$$v_c = 13.741 \text{ cm}^2 .$$

Horizontal constraint,

$$h_c = [(4.76)^2 - (1.72)^2] \times \frac{\pi}{4} = 15.53 \text{ cm}^2$$

These constrain were calculated at the full load of the press (100 ton capacity Friction Screw Press).

Therefore, fractional vertical and horizontal constraints are calculated as follows :

$$f_{vc} = \frac{v_c}{v_c} = 1.00$$

$$f_{hc} = \frac{h_c}{h_c} = 1.00$$

$$\text{Hence, } \phi = \left(\frac{v_c}{v_c}\right) / \left(\frac{h_c}{h_c}\right) = 1.00.$$

In another case where deformation was done to a lower order, there the values of  $v_c$  and  $h_c$  were 10.964 and 10.804  $\text{cm}^2$  respectively. Therefore,

$$f_{vc} = \frac{10.964 \text{ cm}^2}{13.741 \text{ cm}^2} = 0.788, \text{ and}$$

$$f_{hc} = \frac{10.804}{15.53} = 0.696$$

$$\text{Therefore, } \phi = \frac{f_{hc}}{f_{vc}} = \frac{0.696}{0.798} = 0.872$$

The theoretical density of each forged component was calculated following Archemedian Principle. Per cent theoretical density was plotted against the parameter  $\phi$ .

Similarly the values of  $\phi$  with respect to density achieved were calculated for partially open hemi-spherical die cavity.

REFERENCES

1. Bockstiegel, G. and Blande, C.-A.; " The Influence of Slag Inclusions and Pores on Impact Strength and Fatigue Strength of Powder Forged Iron and Steel" , Powder Metallurgy International, Vol. 8, pp 155-160, 1976.
2. Huppmann, W.J. and Hirschvogel, M.; " Powder Forging Review 233", International Metals Reviews, Vol. No.5, pp 209-239, 1978.
3. Skelly, H.M.; " A Survey of Powder Forging Literature, 1960-1974," Minerals Research Program, Physical Metallurgy Research Laboratories, CANMET REPORT 76-38, September, 1976.
4. Henry, Otto H. and Cardiano, J.J. ; "Hot Pressing of Iron Powders" , Metals Technology T.P. 1919, p 10, Oct. 1945.
5. Tormyn, H., Steel, Vol. 108, p 76, 1941.
6. Koehring, R.P.; " Powder Metallurgy" , (ed. by J. Wulff), Cleveland, Ohio, American Society for Metals, p 304, 1942.
7. Wassermann, G. ; Z. Metallkd., Vol. 38, p 129, 1947.
8. Halter, R.F.; " Pilot Production System for Hot Forging of P/M Preforms" , New Perspectives in Powder Metallurgy, Vol. 6 (Ed. by Hausner, H.H. et. al.), Published by MPIF, New York, USA, 1973, pp 69-82.
9. Anon; " Where Powder Metallurgy is Growing Application Outlook for Forging P/M Preforms" , Metal Progress, Vol. 99, No.4, pp 54-60, 1971.

10. Mocarski, S. and Eloff, P.C.; " Equipment Considerations for Forging Powder Preforms" , International Journal of Powder Metallurgy, Vol.7, No.2, pp 15-25, 1971.
11. Hirshhorn, J.S. and Bargainnier, R.B.; " The Forging of Powder Metallurgy Preforms" , Journal of Metals, Vol. 22, No. 9, pp 21-29, 1970.
12. Jones, P.K.; " The Technical and Economic Advantages of Powder - Forged Products", New Perspective in Powder Metallurgy, Vol. 6 (Ed. by Hausner, H.H. et. al.), Published by MPIF, New York, USA, 1973, pp 19-34.
13. Durdaller, C.G.; " The Hoeganaes Powder Forging Laboratory" , ibid, pp 35-43.
14. Di Benedetto, J. et.al.; " Forging of Steel Powder Products" , ibid, pp 104-130.
15. Bargainnier, R.B. and Hirschhorn, J.S.; " Forging Studies of a Ni-Mo P/M Steel" , ibid, pp 229-266.
16. Robert, A.H.; " Forgings From P/M Preforms" , ibid, pp 83-101.
17. McIntire, Hoy.O. and McCall, James, L.; " Metallographic Principles, Diffusion Structures of Sintered Powder Metallurgy Alloys" , Metals Hand Book, 8th Edition, Vol. 8, ASM, Metals Park, Ohio 44073, pp 207-210, 1973.
18. Antes, H.W.; " Cold Forging Iron and Steel Powder Preforms" , Modern Developments in Powder Metallurgy, Proc. 1970 Int. Powder Met. Conf., Sponsored by MPIF and APMI, Ed. by H.H. Hausner, Vol.4, Processes Plenum Press, 415-424, 1971.
19. Krishnamoorthy, G.M.; " Influence of Iron Powder Type on the Properties of Sintered Iron At Various Density Levels" , Powder Metallurgy, Vol. 14, No.27, pp 124-143, 1971.

20. Marx, J.B., Davies, R. and Guest, T.L.; "Some Consideration of the Hot Forging of Powder Preforms" , Proc., 11th Int., MTDR Conf., Birmingham, England, Sept. 1970, Vol.B, Ed. by S.A. Tobias and F. Koenigsberger, Pergamon Press, 1st ed., pp 729-744, 1971.
21. Mocarski, S., DeAngelis, L.E. and Winqvist, L.A.; "Influence of Controlled Atmosphere on Magnetic Properties of Forged Powder Metal Preforms" , Proc. 1970, Int. Powder Met. Conf., Sponsored by MPIF and APMI, Ed. by H.H. Hausner, Vol. 4, Processes, Plenum Press, pp 167-189, 1971.
22. Alves, A.L. ; " Powder Forging Technique And Physical Properties" , ibid, pp 135-165, 1971.
23. Kuhn, H.A., Hagerty, M.M., Gaigher, H.L. and Lawley, A.; " Deformation Characteristics of Iron-Powder Compacts" , ibid, pp 463-473, 1971.
24. Moyer, Kenneth, H. ; " The Effect of Preform Density on the Impact Properties of Atomized Iron P/M Forgings" , Fall Powder Met. Conf. Proc., Detroit, Mich. Sponsored by MPIF, APMI and ASM, pp 53-63, 1971.
25. Anon ; " Sintered Iron Powder Cold Forging Technique Perfected" , Technocrat (Japan), Vol.4, No. 11, p 8, 1971.
26. Antes, H.W.; " Forming Metal Powders", Manufacturing Eng. Trans., Vol. II, pp 137-145, 1973.
27. Bockstiegel, G.; " Some Technical And Economic Aspects of P/M Hot Forging", Hoeganaes AB PM Iron Powder Information, No. PM 73-7, Hoeganaes, Sweden, p 46, 1973.

28. Anon ; " Powder Metallurgy Offers Many Routes To Lower Cost" , Metal Progress, Vol. 102, No. 3, pp 57-58, 1972.
29. Moyer, Kenneth H. ; " The Effect of Flow On Impact Properties of Hot Forged Iron Powder Preforms" , National Powder Metallurgy Conf., Proc., ed. by Allan S. Bufferd, MPIF, New York, pp 6-40, 1972.
30. Durdaller, Neil. ; " Status of New Advances In P/M Technology: Iron P/M Forging", Progress In Powder Met., Vol. 27, Part 1: In Ordnance, pp 135-141, June 1971.
31. Davies, R. and Dixon, R.H.T.; " The Forging of Powder Preforms Using Petro-Forge Machines" , Powder Met., Vol. 14, No. 28, pp 207-234, Autumn 1971.
32. Anon ; " Forging Gives Bigger Muscles to Powder Metal Products", Products Engineering, Vol. 43, No.9, 40-41, Sept. 1972.
33. Anon; " Powdered Steel: A Tough Customer", Metallurgia, Vol. 83, No.496/7, pp 63-64, 1971.
34. Moyer, K.H., " Cold Forging of 316L Powder Preforms" , Paper presented at 1971 Western Metal and Tool Conference and Exposition, under auspices of ASM and SME, 8-11 March, 1971, Las Angeles, California, Paper W71-5.3.
35. Anon ; " Where Powder Metallurgy is Growing Application Outlook for Forging P/M Preforms" , Metal Progress, Vol. 99; No. 4, pp 54-60, 1971.
36. Pietrocini, T.W., " Hot Densification of P/M Alloy 8360" , Precision Metal, Vol. 29, No. 1, 58-60, 1971.

37. Cook, J.P. ; " Degradation of P/M Forging Preforms During Interim Exposures in Air" , Fall Powder Metallurgy Conf. Proc., Oct. 20-21, 1970, Cleveland, Ohio. Sponsored by MPIF and APMI. Published by MPIF, pp 237-259, 1971.
38. Bargainnier, R.B. and Hirschhorn, J.S., " Forging Studies of a Ni-Mo P/M Steel" , *ibid*, pp 191-235.
39. Knopp, W.V., " Furnace Heating vs Induction Heating of P/M Preforms" , *ibid*, pp 104-118.
40. Pietrocini, T.W. and Gustafson, D.A., " Fatigue and Toughness of Hot Formed Cr-Ni-Mo and Ni-Mo Prealloyed Steel Powders", *Int. J. Powder Metallurgy*, Vol. 6, No. 4, pp 19-25, 1970.
41. Hirschhorn, J.S., " Forgings from Powder Preforms" , Tech. Paper No.EM70-509. Soc. Mfg. Engrs., Dearborn, Mich., U.S.A. Pamphlet, 12 pp, 1970.
42. Huseby, R.A. and Scheil, M.A., " Forgings from P/M Preforms", *Modern Developments in Powder Metallurgy*, Proc. 1970 Int. Powder Met. Conf., Sponsored by MPIF and APMI, Ed. by Hausner, H.H., Vol.4, Processes, Plenum Press, pp 395-413, 1971.
43. Smith, T.J. and Weber, E.P., " Forging of 410 Stainless Steel Made by Powder Metallurgy", Proc. New and Exotic P/M Materials Clinic Conference, Spring 1967, Cleveland.
44. Westerman, R.E. and Sump, K.R., " Properties of Prealloyed Steel Powder Metallurgy Products" , Battelle Mem. Inst. Pacific Northwest Labs., ADA 727660, AMSWE RE-71-22, May 1971.
45. Huseby, R.A., " New Prealloyed Steel Powders for Forging Preforms" , *Metal Progress*, Vol. 100, pp 84-86, 1971.

46. Dower, R.J. and Miles, G.I.; " High-Velocity Extrusion Forging of Billets Compacted from Iron and Steel Powders", Powder Metallurgy, Vol. 13, No. 26, pp 85-99, 1970.
47. Knopp, W.V.; " Properties of Hot-Forged P/M Steels", Fall Powder Metallurgy Conf. Proc., Oct. 14-16, 1969, Philadelphia, Pa. Sponsored by MPIF and APMI. Published by MPIF, New York, pp 11-24, 1970.
48. Kobrin, C.L.; " Forging Powder Preforms Combine Strength, Economy" , Iron Age Metal working International, Vol. 6, No. 11, pp 38-39, 1967.
49. Roll, K.H.; " Projecting Powder-Metal Progress" , Machine Design, Vol. 40, No.2, pp 30-32, 1968.
50. Carlson, E.E.; " New High-Strength Ferrous P/M Materials", Progress in Powder Metallurgy, Vol. 125, pp 63-69, 1969.
51. Mocarski, S. et.al.; " Properties of Magnetically Soft Parts Made by Hot Forging of P/M Preforms", Modern Developments in Powder Metallurgy, Proc. 1970, Int. Powder Met. Conf., Sponsored by MPIF and APMI, Ed. by Hausner, H.H., Vol. 4, Processes, Plenum Press, pp 451-462, 1971.
52. Ishimaru, Y. et.al., " On the Properties of Forged P/M Alloys" , ibid, pp 441-449.
53. Anon ; " P/M Forgings Poised for Production" , Materials Engineering (Metals News), Vol. 72, No.2, p 24, 1970.
54. Woulds, M.J. et.al., " Hot Forging of Sintered Stainless Steel" , Fall Powder Met.Conf. Proc., Detroit, Mich. Sponsored by MPIF, APMI and ASM, pp 65-82, Oct. 19-21, 1971.



55. Kawakita, T. et.al.; " Properties of Forged Super-High Density Sintered Steel" , New Perspectives in Powder Metallurgy, Vol. 6 - Forging of Powder Metallurgy Preforms, Ed. by Hausner, H.H. et.al., Published by MPIF, pp 349-356, 1973.
56. Anon ; " Prealloy Mn-Mo Steel Powder Introduced for P/M Forging" , Materials Eng. Vol. 14, No.7, p 52, 1971.
57. Kaufman, S.M. and Mocarski, S.; " The Effect of Small Amounts of Residual Porosity on the Mechanical Properties of P/M Forgings", Int. J. Powder Met., Vol. 7, No. 3, pp 19-30, 1971.
58. Smith, Y.E. and Pathak, R.; " New Hardenability Data for Application in Low Alloy Ferrous Powder Forging" , Fall Powder Met.Conf. Proc., Detroit, Mich. Sponsored by MPIF, APMI and ASM, pp 19-33, Oct. 19-21, 1971.
59. Olsson, L.R., Lampe, V. and Fischmeister, H.F.; " Direct Forging of High-Alloy Steel Powders To Bar Stock" , Powder Metallurgy, Vol. 17, No. 34, pp 347-362, Autumn 1974.
60. Mocarski, S.; " Influence of Process Variables On The Properties of Modified 8600 And Manganese-Nickel-Molybdenum Low-Alloy Hot Formed P/M Steels" , Modern Developments In Powder Metallurgy, ed. H.H. Hausner And Walter, E. Smith, Vol. 7, P/M Forging And Copper P/M Proc. 1973, Inter. P/M Conf. MPIF, pp 303-321, 1974.
61. Wick, C.H.; " Forging Powder Metal Preforms: A New Production Technique" , Machinery, Vol. 76, No.12, pp 50-52, 1970.

62. Moyer, Kenneth, H.; " A Comparison of Deformed Iron-Carbon Alloy Powder Preforms With Commercial Iron-Carbon Alloys" , Metals Eng. Quarterly (ASM), Vol.14, No. 4, pp 235-254, 1974.
63. Davies, R. and Marx, J.B.; " Production of Components By Forging Of Powder Preforms", 13th International Machine Tool Design And Research Conf., University of Birmingham, Birmingham, England, pp 18-22 Sept. 1972.  
(From: Boulger, F.W. And Byrer, T.G. Review of Metals Technology, Metals and Ceramics Information Centre, Metal Working, " A Review of Selected Developments", Battelle Columbus Laboratories, Columbus, Ohio, May 11, 1973).
64. Cross; Allen; " Forgings From Sintered Aluminium" , Precision Metal Moulding; Vol. 23, No. 8, pp 23-25 and 46-47, Aug. 1965.
65. Joyce, J.F. ; " Review of Powder Metallurgy Methods On Extrusion And Forgings", Light Metal Age, Vol.29, No.7, 8 and 10, Sept. 1971.
66. Matthew, Paul, E.; " Cubraloy, A New Development In Aluminium Bronze Powder Metallurgy" , Fall Powder Met. Conf. Proc. Detroit, Mich. Sponsored by MPFI, APMI and ASM, pp 205-216, 1971.
67. Buchovecky, K.E. and Rearick, M.R.; " Aluminium P/M Forging", *ibid*, pp 163-174, 1971.
68. Buchovecky, Kalman E. and Rearick, Milton R. ; " Aluminium P/M Forgings" , Metal Progress; Vol. 101, No. 2, pp 74-78, 1972.
69. Anon ; " Al-Alloy P/M Forgings Make More Advances", Materials Eng., Vol. 75, No.5, p-12, 1972.

70. Greenspan, J.; " Some Effects of Powder Particles Size on the Physical Behaviour of Press Forged Beryllium, Europaisches Symposium uber Pulvermetallurgie, Stuttgart, Vol. 1, pp 1-19, May 1968.
71. Witt, R.H.; " Close Tolerance Airframe From Sintered Preforms", Abstract Bulletin: TMS And ASM, Fall Meeting, Cleveland, Ohio, 1970.
72. Haller, John ; " Hot Forging of Metal Powder Preforms", Industrial Heating, Vol. 37, No. 1, p 34, p 36, p 38, 1970.
73. Abkowitz, S.; Siergieij, J.M. and Regan, R.D.; " Titanium P/M Preforms, Parts And Composites, Modern Developments In Powder Metallurgy, Proc. 1970 Int. Powder Met. Conf., Sponsored by MPIF and APMI, Ed. by H.H. Hausner, Vol4, Processes, Plenum Press, pp 501-511, 1971.
74. Goetzel, C.G. ; " Tensile Properties of Titanium Alloy Forgings Made From Spark-Sintered Preforms, ASM Metals Eng. Quart., Vol. 11, No.2, pp 53-61, May 1971.
75. Malim, Thomas H.; " Now, Titanium Parts From Powder", Iron Age, Vol. 208, No.21, p-60, p-18, Nov. 1971.
76. Peebles, Roger B. ; " Titanium Powder Metallurgy for Forgings; Final Report, Mar. 30, 1968 - June 30, 1971", Air Force Materials Laboratory NTIS, AD 736477, p 283, 1971.
77. Blakeslee, H.W.; " Powder Metallurgy In Aerospace Research", A Survey Prepared Under Contract for NASA by Franklin, Institute Research Laboratories, Philadelphia, Pa. U.S.A., 1971.
78. Anon ; " Metal News: Titanium P/M Forgings For Air Craft Appear Practical" , Materials Engineering, Vol. 76, No. 5, p 22, Oct. 1972.

79. Abkowitz, S.; "Titanium P/M Preforms, Parts And Composites", Titanium Science And Technology, Proc. , 2nd Int.Conf. held at Cambridge, Mass., 2-5 May, 1972; Ed. by R.I. Jaffee and H.M. Burte, Plenum Press, Vol. 1, pp 381-398, 1973.
80. Pavlov, V.A., Zhivou, L.I., Scherbina, V.V., Lyashenko, A.P., Petrykina, R. Ya., and Litvin, V.M.; "Hot Die Forming of Compacted Titanium Powder", Sov. Powder Metall. Met. Ceram., Vol.12, No. 8, pp 615-618, 1973.
81. Anon ; "Forgeable Tungsten Ingots Of Large Size Produced By New Powder Metallurgy Process", Industrial Heating, Vol. 27, No.7, p 1446, p 1448, p 1450, 1960.
82. Parikh, N.M. et.al.; "Final Report on Improved Production of Powder Metallurgy Items", Technical Report No.AFML-TR-65-103. Prepared under Contract AF 33(657)-9140 by IIT Research Inst., Chicago, Ill., Mar. 1965.
83. Hirschhorn, J.S., "Powder Metallurgy Research - Contemporary Trends", J. of Metals, Vol. 19, No.9, pp 25-30, 1967.
84. Joyce, J.F.; Preliminary Information From TRW Inc., Cleveland, Ohio on U.S. Air Force Contract AF33(615)-5411, Abstracted in DMIC Review of Recent Developments, Powder Metallurgy, Battelle Memorial Inst., Columbus, Ohio, Nov. 1, 1968.
85. Allen, M.M. et.al., "Application of Powder Metallurgy to Superalloy Forgings", Metals Eng. Quarterly (ASM), Vol. 10, No. 1, pp 20-30, 1970.
86. Anon.; "Metals Here And There", Precision Metal, Vol. 29, No.6, p 32, 1971.

87. Anon ; " Powder Metallurgy: A Sleeping Giant", Iron Age, Vol. 208, No. 15, pp 63-67, 1971.
88. Clare , L.P., " Where High-Temperature P/M Metals Are Being Used" , Metal Progress, Vol. 101, No.5, p 84, pp 86-87, 1972.
89. Gessinger, G.H. and Cooper, P.D.; " Direct Forging of Cr-Ni-W Steel Powder" , Metal Powder Report, Vol. 29, No.3, p 67, 1974.
90. Anon ; " Advanced Forming Techniques Spur Beryllium Usage" , Iron Age, Vol. 188, pp 111-113, 1961.
91. Cieslicki, M.E., " Forging Beryllium Powder", J. Metals, Vol. 14, No.2, pp 149-153, 1962.
92. Orrell, N.G., " Beryllium Powder Forging", Perspectives in Powder Metallurgy, Vol. 1, New Methods for the Consolidation of Powders, Plenum Press, New York, pp 203-220, 1967.
93. Anon ; " Aluminium P/M Forgings", Metallurgia and Metal Forming, Vol. 40, No. 1, p 7, 1973.
94. Mott, L.H., " Progress Report On Hot Forging Prealloyed Metal Powders", Precision Metal Molding, Vol. 10, No. 10, pp 38-39, pp 89-94, 1952.
95. Brandstedt, S.B.; " Effects of Atomization Media and Consolidation Techniques Upon Physical Properties of a P/M Cobalt-Base Alloy", Modern Developments in Powder Metallurgy, Proc. 1970 Int. Powder Met. Conf., Sponsored by MPIF and APMI, Ed. by Hausner, H.H., Vol. 4, Processes. Plenum Press, pp 487-500, 1971.
96. Young, A.W.; " Tough Alloys Become Formable", Iron Age, Vol. 195, No.6, pp 65-66, 1965.
97. Wakefield, B.D., " Forging P/M Preforms Leads to Part Economy", Iron Age, Vol. 210, No.4, pp 53-54, 1972.

98. Hoefs, R.H.; " The Present Status of P/M Forging - Part 2" , Precision Metal, Vol. 31, No.6, pp 65-67, 1973.
99. Narayan, R., " Ceramic Coatings", I.I.T. Kanpur, Private Communication.
100. Lawley, A. ; " P/M Hot Forming - An Introduction And Overview", New Perspective In Powder Metallurgy, Ed. H.H. Hausner, et.al. Published by MPIF, New York, U.S.A., Vol. 6, pp 153-164, 1973.
101. Halter, R.F.; " Modern Developments In Powder Metallurgy", Ed. by H.H. Hausner, Plenum Press, New York, London, Vol. 4, p 385, 1971.
102. Halter, R.F.; " Modern Development In Powder Metallurgy"; Ed. by H.H. Hausner And W.E. Smith, MPIF, Princeton, NJ, Vol. 7, p 213, 1974.
103. Halter, R.F. and Rajan, S.S. ; " Die Wall Lubrication For P/M Parts And Preforms, Fall Powder Met. Conf. Proc. Detroit, Mich, Sponsored by MPIF, AFMI And ASM, pp 83-85, 1971.
104. Bockstiegel and H. Olsen; Powder Metallurgy. Conf. Suppl. Part 1, p 127, 1971.
105. Fischmeister, H.F.; Annual Rev. Mater. Sci. Vol.5, p 151, 1975.
106. Pilliar, R.M., Bratina, W.J. And Megrath, Modern Developments In Powder Metallurgy, ed. by H.H. Hausner and W.E. Smith, MPIF, Princeton, NJ, Vol.7, p 51, 1974.
107. Avitzur, B. And Blum, P.;"Modern Developments In Powder Metallurgy", ed. by H.H. Jausner And W.E. Smith, MPIF, Princeton, NJ, Vol. 7, p. 73, 1974.

108. Antes, H.W. and Stockl, P.L.; " The Effect of Deformation on Tensile and Impact Properties of Hot P/M Formed Nickel - Molybdenum Steels", Powder Metallurgy, Vol. 17, No. 33, pp 178-192, 1974.
109. Ferguson, B.L., Lawley, A.; Modern Developments In Power Metallurgy, ed. H.H. Hausner and W.E. Smith, MPIF, Princeton, NJ, Vol. 7, p 485, 1974.
110. Fischmeister, H.F., et al, Modern Developments In Powder Metallurgy, ed. By H.H. Hausner and P.W. Taubentlat, MPIF, Princeton, NJ, Vol. 9, p 437.
111. Maclean, M.S., Cambell, W.E. and Dower, R.J.; An Insight Into the Mechanical Properties of Powder Metal Forgings As a Function of Processing Route", Powder Metallurgy International, Vol. 7., No.3, pp 118-120, 1975.
112. Niessen, Jorg; " Production Experience In Forging P/M Parts" , New Perspectives in Powder Metallurgy, Vol. 6 (Ed. by Hausner, H.H. et.al), Published by MPIF, New York, U.S.A., 1973, pp 69-82.
113. F. and Muzik, J. ; " Successful Applications And Processing Considerations For Hoegnaes Conf. pp 1-23, October, 1978.
114. Kuhn, H.A., and Downey, C.L.; " Material Behaviour In Powder Preform Forging" , Trans. of the ASME of Engg. Materials And Tech., pp 41-46, 1973.
115. Schey, J.A. ; " Progress Report on Recent Advances In Bulk Metal Deformation Processes" , Review 223, International Metals Reviews, December, 1977.
116. Downey, C.L., Jr. And Kuhn, H.A.; " Application of Forming Limit Concept to the Design of Powder Preforms for Forging" , Trans. of the ASME of Engg. Materials and Technology, pp 121-125, April 1975.

117. Antes, H.W.; " Deformation of Porous Materials", Hoeganaes Corporation 'Report', Riverton, NJ, pp 1-22.
118. Thomson, E.G., Yang, C.T. and Kobayashi, S.; " Plastic Deformation In Metal Processing", The Macmillan Press, New York (1965).
119. Dieter, G.E., Jr. Mechanical Metallurgy; McGraw-Hill Book Co., 1961.
120. Hoffman, O. and Sach, G.; " Introduction to the Theory of Plasticity For Engineers; " McGraw Hill Book Co., 1953.
121. McAdam, G.D., Journal of Iron and Steel Institute, Vol. 168, No.4, pp 346-358, 1951.
122. Kuhn, H.A., et.al.; " Deformation Characteristics of Iron Powder Compacts", International Conf. on P/M, 1970.
123. Hill, R.; " The Mathematical Theory of Plasticity", The Clarendon Press, Oxford 1971.
124. Suh, N.P.; " A Yield Criterion for Plastic Frictional Work Hardening Granular Materials" ,Int. Journal of Powder Metallurgy, Vol.5, No.1, p 69, 1969.
125. Kuhn, H.A. and Downey, C.L.; " Def.Characteristics and Plasticity Theory of Sintered Powder Materials," Int. Journal of Powder Metallurgy, Vol. 7, No. 1, p 15, 1971.
126. Fischmeister, H.F., Aren, B., Easterling, K.E., " Deformation and Densification of Porous Preforms In Hot Forging" , Powder Metallurgy, Vol. 14, No. 27, 1971.
127. Bockstiegel, G.; " A Study of the Work of Compaction In Powder Pressing," Powder Metallurgy International, Vol.3, No. 1, 1971.



128. Koerner, R.M.; " Triaxial Compaction of Metal Powders", Powder Metallurgy International, Vol. 3, No.4, 1971.
129. Antes, H.W.; " Cold and Hot Forging P/M Preforms," SME International Meeting Philadelphia, 1971, Published as a Special SME Report, EMR 71-01, 1971.
130. Kuhn, H.A.; " Powder Preform Design for Hot Forging" , APMI-ASM Metals Congress, Oct. 1971.
131. Bockstiegel, G. and Olsen, H.; " Processing Parameters In Hot Forming of Powder Preforms" , Powder Metallurgy, Third European Powder Metallurgy Symposium, 1971, Conference Supplement Part I.
132. Moyer, K.H. ; " Effect of Preform Density on the Impact Properties of Hot Forged P/M Parts" , P/M 72, National Powder Metallurgy Conference, Chicago, 1972.
133. Moyer, K.H., ; " Effect of Preform Density on the Impact Properties of Atomized Iron P/M Forgings", Metal Engineering Congress, Oct. 1971.
134. Cundil, R.T., Marsh, E. and Ridal , K.A.; " Mechanical Properties of Sinter/Forged Low-Alloy Steels", 'Forging of Powder Metallurgy Preforms', New Perspective In Power Metallurgy, Vol. 6, (Ed. by Hausner H.H., etl.al), Published by MPIF, New York, U.S.A., 1973, pp 175. - 204.
135. Kaufman, M. and Mocarski, S.; Int. J. Powder Metall., Vol. 7, p 19, 1971.
136. Ishimaru, Y. et.al.; " Modern Developments in Powder Metallurgy" , (Ed. by Hausner, H.H.), New York,London, Plenum Press. Vol. 4, p 441, 1971.
137. Bockstiegel, G. and Blande, C.-A. ; Power Metall. Int., Vol. 8, p 155, 1976.
138. Pilliar, R.M., et.al.; Int. J. Powder Metall. Powder Technol., Vol. 13, p 99, 1977.

139. Koczak, M.J. et.al. : Powder Metall. Int., Vol.6, p 13, 1974.
140. Huppmann, W.J. : Powder Metall., Vol. 20, p 36, 1977.
141. Pilliar, R.M. et.al. ; " Modern Developments in Powder Metallurgy" , (Ed. by Hausner, H.H. and Smith, W.E.), Princeton, NJ, Metal Powder Industries Federation, Vol. 7, p 51, 1974.
142. Lindskog, P. and Grek, S.E. ; ibid, p 285.
143. Ferguson, B.L. and Lawley, A. ; ibid, p 323.
144. Hense, V.C., " Forging Powder Metal Preforms for the Automative Industry" , Presented at Metal Powder Industries Federation's, Fall Conf., Philadelphia, Pa., 1969.
145. Bockstiegel, G. ; " HFF-Bericht 9. Umformtechnisches Kolloquium 1977" , p 27, 1977.
146. Brown, G.T. ; Powder Metall., Vol. 14, p 124, 1971.
147. Huseby, R.A. and Scheil, M.A. ; " Modern Developments in Powder Metallurgy" , (Ed. by Hausner,H.H.), New York, London, Plenum Press, Vol.4, p 395, 1971.
148. Kaufman, S.M. ; Int. J. Powder Metall., Vol. 10, p 257, 1974.
149. Brown, G.T. ; " Powder Metallurgy: Promises and Problems" , Paris, Societe Francaise de Metallurgie - Materiaux et Techniques, p 96, 1975.
150. Brown, G.T. and Steed, J.A. ; " Powder Metall., Vol. 17, p 157, 1974.
151. Brown, G.T.; Met. Technol., Vol. 3, p 229, 1976.
152. Lusa, G. ; " Modern Developments in Powder Metallurgy" (Ed. by Hausner, H.H.), New York, London, Plenum Press, Vol.4, p 425, 1971.

153. Eloff, P.C. and Wilcox, L.E. ; " Modern Developments in Powder Metallurgy" , (Ed. by Hausner, H.H. and Smith, W.E.), Princeton, NJ, Metal Powder Industries Federation, Vol. 7, p 213, 1974.
154. Antes, H.W. and Stockl, P.L.; Powder Metall., Vol.17, p 178, 1974.
155. Rueckl, R.L. ; Int. J. Powder Metall. Powder Technol., Vol. 11, p 209, 1975.
156. MocarSKI, S. ; " Modern Developments in Powder Metallurgy", (Ed. by Hausner, H.H. and Smith, W.E.), Princeton, NJ, Metal Powder Industries Federation, Vol. 7, p 303, 1974.
157. Pietrocini, T.W. and Gustafson, D.A.; " Modern Developments in Powder Metallurgy" , (Ed. by Hausner, H.H.), New York, London, Plenum Press, Vol. 4, p 431, 1971.
158. Cook, J.P. ; " Progress in Powder Metallurgy" , (Ed. by Halter, R.F.), Princeton, NJ, Metal Powder Industries Federation, Vol. 30, p 173, 1974.
159. Dorofeev, Yu. G. et.al. ; Sci. Sinter., Vol. 9, p 187, 1977.
160. Ferguson, B.L., Suh, S.K., and Lawley, A., Int. J. Powder Metall. Powder Technol., Vol. 11, p 263, 1975.
161. Steed, J.A. ; Powder Metall., Vol. 18, p 201, 1975.
162. MocarSKI, S.; Int. J. Powder Metall. Powder Technol, Vol. 12, p 47, 1976.
163. Davies, R. and Negm, M. ; Powder Metall., Vol. 20, p 39, 1977.
164. Ladanyi, T.J. et. al. ; Metall. Trans., Vol. 6A, p 2037, 1975.
165. Dorofeev, Yu. G. et. al. : Sov. Powder Metall. Met. Ceram., Vol. 13, p 152, 1974.

166. Khol, R.; " Forged Powder Metal" , Machine Design, Vol. 41, No. 8, pp 142-146, 1969.
167. Brady, B.D. ; " Where Forging and Stamping in Australia Stands Today in the face of Current Technologies" , Metallurgia and Metal Forming, Vol. 41, No. 11, 324-325, Nov. 1974.
168. Eshelman, Ralph.; "P/M Parts Forge Ahead" , Automative Industries, 36-37, 15 March, 1973.
169. Happmann, W.J. and Albano-Muller, L.; " Production of Powder Forged Parts of Complex Geometry" , Sintermetallwerk Krebsoge GmbH, P/M 80.
170. Gustafson, D.A. ; " HD:P/M" and " High Density Via P/M Techniques" , Metal Progress, Vol. 101, No. 4, pp 44-45, and 48-49, April 1972.
171. Anon, " Trends in Powder Metallurgy" , Metal Progress, Vol. 103, No. 1, pp 90-92, Jan. 1973.
172. de Sablet, P. and Accary, A.; " Comparison Between Powder Metallurgy and Competitive Processes for the Mass Production of Structural Parts" , Powder Metall. Int., Vol. 9, No.3, pp 127-130, 1977.
173. McGee Sherwood, W. and Walter, G.M.; " Five Case Histories Reflect State of P/M Technology", Metal Progre Vol. 101, No.5, pp 76-77 and 79, May 1972.
174. Pietrocini, T.W.; " Hot Formed P/M - Applications" , Modern Developments in Powder Metallurgy, Ed. H.H. Hausner, and W.E. Smith, Vol. 7, pp 395-410, 1974.
175. Hirschvogel, M. and Aldinger, F.; " Hot Forging of Pure and Coated Beryllium Powders" , ibid, pp 441-445.
176. Anon ; " The Future of Forging - A Delphi Probe" , Precision Metal, Vol. 31, No. 5, pp 46-47, May 1973.
177. Jarret, M.P. and Jones, P.K.; " The Powder Forging Process and its Potentialities", Engineers' Digest, Vol. 34, No.3, pp 41-43, March 1973.

178. Balshin, M.Yu. and Kiparisov, S.S., "General Principles of Powder Metallurgy", Translated by Savin, I.V., MIR Publishers, Moscow, 1980.
179. Alves, A.L.; Powder Forging Technique and Physical Properties , Fall Powder Metallurgy Conf. Proc., Oct. 20-21, 1970, Cleveland, Ohio. Sponsored by MPIF and APMI. Published by MPIF, pp 135-165, 1971.
180. Vaccari, J.A., "P/M Forgings: a Rapidly Emerging Technology", Materials Eng., Vol. 78, No.3, pp 20-27, Sept. 1973.
181. Gale, K.; "Sintering Squeezes Out the Shapes For Profits" , The Engineer, pp 30-32, Oct., 1971.
182. Roll, K.H.; Metal Progress, Vol. 101, No.6, p 12, June 1972.
183. Zapf, G. and Niessen, J.; " Investigations of the the Effect of Temperature of Press Tool and Compact and of the Sintering State of the Compact on additional Hot Compacting or Hot Forming With Various Sintered Ferrous Materials", Third Powder Metallurgy Symposium 1971, Conf. Supplement, Part 1 Powder Metallurgy (U.K.) pp 127-149, 1971.
184. " Gould Hot Densities P/M Parts", Staff Report, Metal Progress, Vol. 103, No.5, pp 42-44, May 1973.
185. Lawley, A.;" Emerging Technologies in Powder Metallurgy", Powder Metallurgy for High-Performance Applications, Ed. by John J. Burke and Volker Weiss, Proc. 18th. Sagamore, Army Materials Research Conf., Syracuse University Press, pp 3-23, 1972.
186. Stenfanides, E.J.; " Hot Formed P/M Preformed Parts", Design News, Vol. 27, No. 23, pp 60-61, 1972.
187. Pandey, K.S., Misra, P.S. and Mehta, M.L.;" " Densification Behaviour of Iron Powder Preform During Hot Upsetting", National P/M Conf., 9-10 Mar 1982, FMAI, Hyderabad.

188. Gaigher, H.L. and Lawley, A.; " Structure Changes During the Densification of P/M Preforms", Int. J. Powder Metall. Powder Technol., Vol. 10, No. 1, pp 21-31, 1974.
189. Majumdar, P. and Davies, T.J.; " Porosity and Densification in Forged Ferrous Powders", *ibid*, Vol. 15, No.2, pp 103-113, 1979.
190. Hoefs, R.H. and Scharnick, E.C.; " Prealloyed Powders for P/M Hot Densification" , Soc. Manufacturing Eng., Dearborn, Michigan, Technical Paper No. MF 72-801, 9 pp., 1972.
191. Brown, G.T.; " Properties of Structural Powder-Metal Parts - Over-Rated or Under-Estimated?", Powder Metallurgy, Vol. 17, No. 33, pp 103-125, 1974.
192. Kahlow, K.J.; " Void Behaviour as Influenced by Pressure and Plastic Deformation" , Lehigh University, Ph.D. Dissertation, Nov. 1971.
193. Moyer, K.H.; " The Effect of Density on Impact Properties of Iron P/M Forgings", Metals Engineering Quarterly, pp 34-38, Aug. 1972.
194. (a) Clark, D.S. and Varney, W.R.; " Physical Metallurgy for Engineers", East-West Student Edition, 1968.  
(b) Lindskog, P. et.al.; " Phosphorus as an Alloying Element in Ferrous P/M", Hoganas AB PM 76-2, S-26301, Hoganas, Sweden, pp 1-32.
195. Kuhn, H.A.; " Deformation Processing of Sintered Powder Materials", Powder Metallurgy Processing, Ed. By Kuhn, H.A. and Lawley, A., Academic Press, New York, pp 99-138, 1978.
196. Nishino, Y. et.al.; " The Elimination of the Sintering Step In P/M Hot Forging Process", Modern Developments In Powder Metallurgy, Ed. by H.H. Hausner and P.W. Taubenblat, MPIF, APMI, Princeton, NJ.

197. Stassi -D'Alia, F.; " Flow and Fracture of Materials According to a New Limiting Condition of Yielding", Meccania, 3, II, 1967.
198. Hirschhorn, " Characterization of Powders", Introduction to Powder Metallurgy, APMI, Princeton, New Jersey, 1976.
199. Agrawal, B.C. and Jain, S.P.; " A Textbook of Metallurgical Analysis", Khanna Publishers, New Delhi, pp 113-120, 1976.
200. Moyer, K.H.; "Measuring Density of P/M Materials with Improved Precision", Int. J. Powder Metall. Powder Technology, 15, pp 33-42, 1979.
201. Mikheyev, M.; " Fundamentals of Heat Transfer" , Translated by Semyonov, S., Peace Publibhsers, Moscow
202. Instruction Manual, Tensometer Type 'W', Monsanto, Reg. No.291962.
203. Operating Instructions for Pendulum Impact Testing Machine, PS-30, Ser. No.423/64/63.
204. Kumar, Ashok; " Hot Extrusion of Aluminium Powder", Ph.D. Thesis, University of Roorkee, Roorkee, U.P., India, 1981.
205. Kawakita, T. and Nagasaka, Y.; " Properties of Forged Super-High Density Sintered Steel", New Perspective In Powder Metallurgy, Vol. 6, Ed. By H.H. Hausner et. al., pp 349-356, 1973.

